Interaction of steroidal molecules with C12-chain surfactant monolayers and micelles

Shao, Yanan

Awarding institution:
King's College London

KING'S COLLEGE LONDON

Interaction of steroidal molecules with C_{12}-chain surfactant monolayers and micelles

Yanan Shao

A thesis submitted in partial fulfilment of the requirements

for the degree of Doctor of Philosophy

in the

Faculty of Life Sciences & Medicine

Institute of Pharmaceutical Science

November 2019

Abstract

Many drugs have poor aqueous solubility which causes problems for their formulation as effective medicines. One way of solving this problem involves solubilizing drugs using aqueous dispersions of self-assembled surfactant micelles. It is well-established that surfactant micelles can solubilize drug, but where the drug will locate within the micelles and the factors that affect this are not fully understood. It is the locus of drug solubilization, however, that is thought to be important in determining the loading-capacity of the micelles, and it is this too that affects the drug's stability and its rate of release inside the body and so it also impacts the drug's therapeutic activity.

In order to gain a better understanding of the location of drug in surfactant micelles, a series of systematic studies have been performed to determine the extent and locus of solubilization of two poorly water-soluble steroids, 4-cholesten-3-one (4-CHOL) and adrenosterone (ADRENO) compounds in a range of C_{12}-chain surfactant of varying head group.

The solubilisation capacities of steroids in the various surfactant micelle, as well as the interfacial and solvation behaviour of the various surfactant systems were explored. In order to estimate the preferred site(s) of solubilization of the steroids within the micelles, neutron techniques (both small-angle neutron scattering (SANS) and specular neutron reflectivity (SNR)) in combination with isotopic (H/D) contrast variation were used. The NR study revealed that regardless of the nature of the head groups, steroids were solubilised within the hydrophobic chain of surfactant at the air-water interface. The SANS studies were in good agreement with the NR study, and also suggested in some cases the presence of steroids could change the shape of the micelle.

The information gained in these studies has provided for a more complete understanding of the relationship between the structure of a surfactant and the structure of the micelles likely to be formed when loaded with steroid drugs, allowing predictions to be made to guide the design of new surfactants to optimize steroid drug loading.

Acknowledgements

My sincere gratitude goes to my professors Dr. David Barlow, Professor Jayne Lawrence and Dr. Hisham Al-Obaidi, who provided me with the opportunity, resources and support to be able to complete the work for this thesis. In particular, I thank David and Jayne for the sleepless nights we were working together during the neutron experiments and for the stimulating discussions before the deadline. Without their precious support it would not have been possible to conduct this research.

Many thanks to the Institut Laue-Langevin (ILL) and the Rutherford Appleton Labs (RAL) for awarding neutron beam time. Special thanks to Dr. Richard A. Campbell for offering his expertise without hesitation on instrument setup and neutron data analysis. I would also like to thank Dr. Ann Terry, and Drs. Najet Mahmoudi, Maximilian Skoda and Becky Welbourn for their help and support provided on the ISIS neutron beamlines. Many thanks to Dr. Peixun Li who synthesized the chain-deuterated surfactants.

My deepest thanks also go to all the members of the Pharmaceutical Biophysics Group for the pleasant working environment, especially Pao, Or, Xing, Kelly and Simona.

Last but not least, I would like to thank my friends and parents for supporting me spiritually throughout the writing of this thesis and over the course of my life in general; their ceaseless love and encouragement aiding me through all the difficulties.

Table of Contents

List of Figures

List of Tables

Abbreviations

4-CHOL	4-cholesten-3-one
ACMW	air contrast matched water
ADRENO	adrenosterone
ADS	ammonium dodecyl sulfate
Brij 35	polyoxyethylene (23) lauryl ether
CMC	critical micelle concentration
DDAO	N,N-dimethyldecylamine N-oxide
DDAPS	n-dodecyl-N,N-dimethyl-3-ammonio-1-propanesulfonate
DPC	n-dodecyl phosphocholine
DTAB	dodecyl trimethylammonium bromide
EO	ethylene oxide
HLB	hydrophile−lipophile balance
LDS	lithium dodecyl sulfate
Log P	partition coefficient in octanol−water
MSR	molar solubilisation ratio
NMR	nuclear magnetic resonance
NR	neutron reflectometry
POE	polyoxyethylene
SAA	surface active agent
SANS	small−angle neutron scattering
SDS	sodium dodecyl sulfate
SL	scattering length

ρ	scattering length density
ST	surface tensiometry
Tween 20	polyoxyethylene sorbitan monolaurate
UV	ultraviolet

Chapter 1

Introduction

1.1 Background

The oral route of drug administration is generally regarded as the preferred route of administration, partly because it offers greater convenience and is more cost effective than other routes but also because it is the route that is preferred by most patients (in the UK, at least) and so leads to a higher level of patient compliance [1, 2]. The formulation of drugs for oral administration, however, regularly presents problems, the greatest challenge generally being to ensure a high bioavailability of the drug – ensuring that sufficient drug enters the patient to give the required clinical effect.

Bioavailability is the proportion of active drug that enters the systemic circulation. For drugs given intravenously by injection, bioavailability is (by definition) 100% but drugs given orally generally have a much reduced bioavailability, this decrease arising because of their poor absorption and/or extensive first-pass metabolism [3, 4]. The dose of a drug given orally, therefore, is usually much higher than that given parenterally. For example, for the steroidal drug testosterone, the initial dosing for injection is 50 – 400 mg every 2 – 4 weeks, but when the drug is given by oral administration, one tablet (30 mg) is required every 12 hours [5].

In order for an orally administrated drug to reach its required site of action, it must first dissolve in the gastrointestinal (GI) fluids of the digestive system and it must then permeate the intestinal wall and enter the bloodstream [6]. Drugs that have low aqueous solubility will dissolve only poorly in the GI tract, and they will thus have poor bioavailability, and will need to be administered at higher doses to achieve the required therapeutic plasma concentrations. For any drug with a water-solubility less than 100 μg/mL, the bioavailability achieved following oral administration is likely to be unacceptable [7].

Recent years have seen an increasing number of drug candidates developed by the pharmaceutical industries that fall into class 2 (low solubility, high permeability) and class 4 (low solubility, low permeability) on the Biopharmaceutics Classification System [8]. Such compounds are considered poorly water-soluble because they have an aqueous solubility lower than 100 μg/mL (0.01 wt%). It is reported that over 70% of the new drug candidates have poor aqueous solubility and approximately 40% of the new chemical entities are practically insoluble (Table 1.1) [9-11]. There has thus been much interest in the development of formulation strategies to improve bioavailability [12-14].

Table 1. 1 Definition of solubility of solute at 20 ºC [15]

	Solubility (wt%)
Very soluble	> 100
Freely soluble	10 – 100
Soluble	3.3 – 10
Sparingly soluble	1 – 3.3
Slightly soluble	0.1 – 1
Very slightly soluble	0.01 – 0.1
Practically insoluble	< 0.01

The various formulation strategies employed to overcome poor drug solubility have been summarized by Williams et al. [16]. These strategies include the use of buffers, the use of co-solvents, salt formation, and size reduction of the solid drug particles. However, these approaches each have their own limitations. Some drug solids are not readily amenable to effective particle size reduction, for example, and the use of buffers and salt formation are strategies that are only useful for ionized drugs [17, 18].

The use of self-assembled surfactant micelles for solubilising poorly water-soluble drugs is also considered to offer potential for drug delivery [19-21].

1.2 Surfactants

Surfactants are often called surface-active agents (SAAs) and they play important roles as wetting agents, detergents, emulsifiers, foaming agents and dispersants in drug formulation [21]. Surfactants are amphipathic, possessing both hydrophilic (water-loving) and hydrophobic (water-hating) components, and the self-assembled aggregates they form are referred to as micelles. Generally, the hydrophobic part of a surfactant consists of a long hydrocarbon chain (often referred to as the surfactant tail group) and the hydrophilic head group can be either ionic, non-ionic or zwitterionic. The most common surfactant examples are shown in Figure 1.1.

The hydrophilic regions of conventional non-ionic surfactants consist of a polyoxyethylene chain (see Figure 1.1 (IV)). The polar/hydrophilic head groups of the ionic surfactants can carry negative or positive charges and these are referred to as anionic and cationic surfactants, respectively. The negatively charged head groups of anionic surfactants associate with positively charge counterions such as sodium, lithium, potassium, or ammonium ions. In these surfactants, the sulfonate head group is one of the most common [21], and a typical example is shown in Figure 1.1 (I). In cationic surfactants, a trimethylammonium moeity in the polar head group is common, and this is most often associated with a counterion of bromide or chloride (see Figure 1.1 (II)). Surfactants that possess both positive and negative charges are referred to as zwitterionic surfactants (see Figure 1.1, (III)).

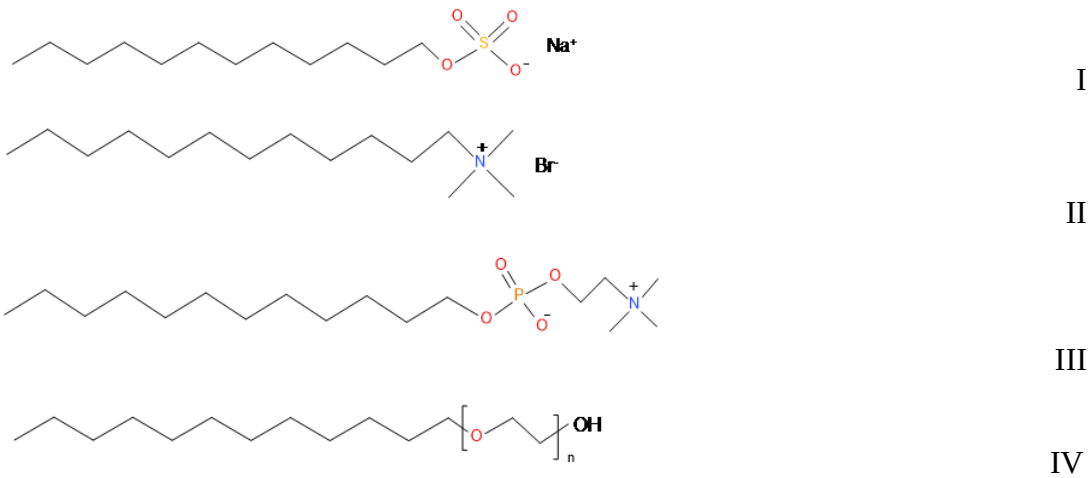

I

II

III

IV

Figure 1. 1 Examples of common I-anionic surfactant (SDS), II – cationic surfactant (DTAB), III – zwitterionic surfactant (DPC), IV – nonionic surfactant (Brij 35) molecules.

In aqueous solution, due to their amphiphilicity, surfactant molecules tend to adsorb at the water surface – at the air-water interface – with their hydrophilic head groups immersed in the water and their hydrophobic groups directed outwards into the air. The intrusion of the surfactant molecules at the water surface leads to a reduction in the surface free energy because the intermolecular forces between the surfactant and the water molecules are much lower than those between water molecules [22]. The presence of surfactant at the interface thus lowers the surface tension of the solution.

1.3 Micellisation

1.3.1 The critical micelle concentration

When surfactant molecules accumulate at the air-water interface they tend to form a monolayer across the surface. As the surfactant concentration is increased, the surfactant monomers become more closely packed at the surface and eventually, when no further molecules can be accommodated at the surface, the excess surfactant forms aggregates in the bulk. These aggregates are the surfactant micelles, and the concentration at which they begin to appear is termed the critical micelle concentration (CMC).

The experimental determination of the CMC of a surfactant can be made by monitoring the changes seen in the physical properties of the surfactant solution as a function of surfactant concentration (for a review, see Mukerjee et al. [23, 24]). One of the techniques most commonly used involves measurement of surface tension. With this technique, the concentration of a surfactant solution is increased progressively and the resulting change in surface tension is measured. At and above the CMC of a surfactant the surface tension of the solution ceases to decrease. Other forms of measurement that are used in determination of surfactant CMC are detailed by Mukerjee and Mysels [23].

1.3.2 Micelle structure

Above the CMC, the nanoscale micelle is formed as a ‘core-shell’ structure with the apolar/hydrophobic chains of the surfactant molecules forming the micelle core. The core is shielded from contact with the surrounding water by the polar/hydrophilic head

groups of the surfactant molecules. The head groups of the surfactant molecules interact with the surrounding water molecules via hydrogen bond and/or ion-dipole interactions.

The main driving force for the formation of micelles is the minimisation of the free energy of the surfactant-water system, which is otherwise increased by the disruption of the water structure caused by the presence of surfactant. The geometrical diversity seen in the size, shape and internal structure of surfactant micelles arises from the various competing forces that operate during self-assembly. These forces include the hydrophobic effect that leads to the removal of the surfactant hydrophobes from contact with water and their interaction with one another via van der Waals forces, the hydrogen bonding and electrostatic interactions that favour immersion of the surfactant head groups in the water, and the repulsive (electrostatic) interactions between the surfactant polar head groups which tend to keep the molecules apart [20].

For the structure of micelles formed by ionic surfactants (Figure 1.2, (a)), there is a Stern layer immediately surrounding the micelle core which contains both the ionic head group and (1-α)N counterions, where α is the degree of ionization (generally from 0.2 to 0.5) and N is the micelle aggregation number [22]. Surrounding the Stern layer

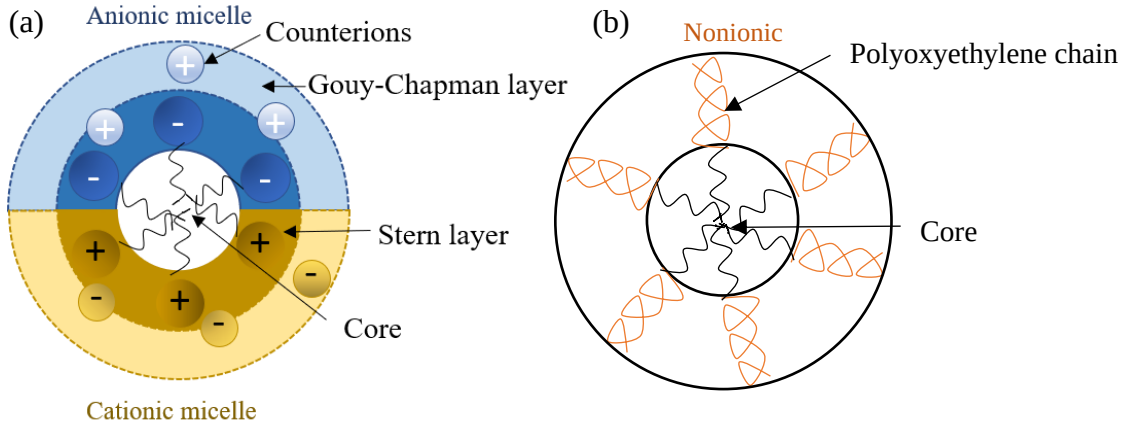

Figure 1. 2 Cross-section of surfactant micelles

there is a diffuse layer – termed the Gouy-Chapman layer – that contains the remaining αN counterions and neutralises the charge on the micelle.

In the micelles formed by non-ionic surfactants with a polyoxyethylated head group (Figure 1.2, (b)) the hydrophobic core of the micelle is surrounded by the so-called palisade layer which contains the long polyoxyethylene chains which are heavily

hydrated. The micelles formed by non-ionic surfactants are usually larger and more elongated than those formed by ionic surfactants.

Zwitterionic surfactants are of particular interest for drug solubilisation because of their high aqueous solubility and their insensitivity to the presence of salt and changes in temperature [25]. The micelles formed by zwitterionic surfactants are generally small and close to spherical [26], and since their surfaces carry both negatively charged and positively charged groups their behaviour is not like ionic or nonionic surfactant micelles but more like the micelles that are formed by ionic surfactants in salt-containing media [27]. For surfactants having a common hydrophobe, the micelles of non-ionic surfactants are formed more readily than those formed by zwitterionic and ionic surfactants [28].

Most surfactant micelles are assumed to be approximately spherical when the surfactant concentration is near the CMC [29] but their shape will invariably change with an increase in the surfactant concentration, with the addition of electrolyte, or a change in temperature. It is common for a micelle to change to a more asymmetric form when one of these conditions changes.

It should be noted here too that a surfactant micelle is not a permanent 'frozen' structure but a dynamic structure in which there is a constant exchange of surfactant molecules between the aggregate and the continuous phase. This exchange of unimers is very rapid, the lifetime of a surfactant molecule within a micelle estimated to be between 10^{-5} and 10^{-3} s [21].

1.3.3 Factors affecting the critical micelle concentration and micellar aggregation

The properties of the micellar solution of a surfactant change remarkably when the surfactant concentration is above the CMC. Efforts are thus invested in determining the CMC of a surfactant and in elucidating the factors that affect the CMC. From a pharmacological point of view, the micelles that are formed by surfactants with low CMCs are more stable in use, because they are less perturbed by their dilution within the large volume of the gastrointestinal fluids before they enter the systemic circulation [30].

Nature of the hydrophobic group

For surfactants with an alkyl chain hydrophobe, an increase in the alkyl chain length (up to 16 carbon atoms) is shown to lead to a decrease in the CMC [31]. For most ionic surfactants, an increase of one methylene group in the hydrocarbon chain results in the CMC being reduced by half [22]. For non-ionic surfactants, this effect is even more pronounced, with the addition of one methylene group to the alkyl chain decreasing the CMC to one-third of its original value [32].

As might be expected, an increased length of a surfactant hydrophobe leads to a larger micelle size, and in many cases there is a linear relationship between the log micelle weight and the hydrocarbon chain length [22, 33]. The linear relationship between micelle aggregation number and the number of carbon atoms in the alkyl chains of non-ionic surfactants was first demonstrated by Arnarson and Elworthy [34] and later confirmed by Oliver et al. [35]. Tanford [36] also pointed out that the increase in micelle aggregation number caused by increased surfactant alkyl chain length varies according to the geometry of the micelle: for a prolate ellipsoid micelle, the aggregation number is predicted to increase by 12 – 15 monomers with each additional carbon in the alkyl chain, and for oblate micelles, there is an increase of 20 – 25 monomers in the aggregation number per additional carbon atom.

Mukerjee [37] proposed that when the number of carbon atoms in a surfactant's alkyl chain exceeds 16 there is no further change in CMC because of the coiling of the hydrophobe.

For surfactants with branched hydrocarbon chain hydrophobes, the change in CMC due to increasing carbon chain length is not as high as in the equivalent straight chain surfactant [38]. It has also been shown that the introduction of a phenyl group into a surfactant hydrophobe leads to a change in the CMC equal to that caused by the addition of three and a half methylene groups, while substitution of the terminal methyl in an alkyl chain by the CF_3 group leads to a doubling of the CMC [22].

Nature of the hydrophilic group

For surfactants with alkyl chain hydrophobes longer than $C_{10}H_{21}$, the CMCs increase in the order non-ionic surfactants < zwitterionic surfactants < ionic surfactants [39]. In general, the CMCs of non-ionic surfactants are a magnitude lower than the CMCs

of ionic surfactants as a consequence of the lower electrical work required in formation of the micelles [40].

An increase in the length of the polyoxyethylene head group in a non-ionic surfactant makes the surfactant more hydrophilic, leading to an increase in CMC and to a decrease in micelle size. It is reported by Chen et al., for example, that the CMCs of nonionic surfactants $C_{10}E_4$ and $C_{10}E_8$ are 0.67 and 1.1 mM at 25 ^oC, respectively [41].

For ionic surfactants, the presence of charged groups within their polar head groups requires more electrical work to be done to form a micelle. This additional work causes an increase in the surfactant CMC, and the CMC is increased further when the charged groups are closer to the α-carbon atom in the hydrocarbon chain [42]. Stigter [42] explained that when ionic surfactants form micelles, the head groups must move from the bulk water to the vicinity of the non-polar core of the micelle, and this leads to an increase in the electrostatic self-potential of the surfactant ion, and so more work must then be done to move the (charged) head group closer to the lower dielectric medium. The CMCs of ionic surfactants are also affected by their binding of counterions, with increased binding strength leading to an increase in the polarizability of the surfactant's ionized head group and causing a decrease in its hydrated ionic radius. In general, the order of CMCs of ionic surfactants with alkyl chain hydrophobes decrease in the order: aminium salts > carboxylates > sulfonates > sulfates [43].

Anacker et al. [44] have also found that size of an ionic surfactant micelle is influenced by the distance separating its centre of charge and the counterion. These workers demonstrated, for example, that the size of micelle formed by decylammonium bromide is much larger than that formed by decyltrimethylammounium bromide due to the fact that the Br^- counterions are much closer to the N^+ of the decylammonium moiety. With a shorter distance, the repulsive electrical forces are effectively shielded and a larger micelle is allowed to form.

Electrolytes

The presence of electrolytes in a surfactant solution causes a decrease in the surfactant CMC and an increase in the micelle aggregation number, and these effects are more pronounced for ionic surfactants than for zwitterionic or nonionic surfactants [45]. The depression of the ionic surfactant CMC caused by added electrolytes arises because of

increased screening of the head group charges which allows more surfactant molecules to insert into the micelle without increasing the free energy of the system. For zwitterionic and nonionic surfactants there is very little effect of added electrolyte on micelle size [37].

Temperature

In contrast, the effect of temperature on the aggregation number of ionic surfactant micelles is much smaller than for nonionic surfactant micelles. Increased temperature leads to a slight decrease in the aggregation number of ionic surfactant micelles but leads to a significant increase in the aggregation number of nonionic surfactant micelles.

The effect of temperature on the CMC of a surfactant, however, is more complex. An increase in temperature initially leads to a decrease in CMC but then further increases in temperature cause the CMC to increase again [45]. Rosen [45] explains that the increased temperature causes a dehydration of the surfactant head group but also disrupts the structure of the water surrounding the head groups. These two opposing effects thus cause a minimum CMC of the surfactant over a particular temperature range. For ionic surfactants, the minimum CMC is generally around 25 ^{o}C, while for nonionic surfactants it is around 50 ^{o}C [46]. There are only limited data available of the effect of temperature on the CMCs of zwitterionic surfactants, but Tori reports that temperature increases over the range 6 – 60 ^{o}C cause the CMC to decrease steadily [47].

1.4 Solubilisation

An important property of surfactant micelles as regards their use in pharmacy is their ability to increase the apparent solubility of drug substances that are otherwise poorly soluble in aqueous media. Rosen defines micellar solubilisation as “the spontaneous dissolving of a substance by reversible interaction with the micelles of a surfactant in water to form a thermodynamically stable isotropic solution with the reduced thermodynamic activity of the solubilised material.” [45]. From a thermodynamic point of view, the solubilisation of drug within surfactant micelles can be considered as a normal partitioning of the drug between the micelles and water.

The increase in apparent solubility of a drug within a surfactant solution is only observed when the concentration of the surfactant is above the CMC [48]. The extent of micellar solubilisation of a given solute can be described by the molar solubilisation capacity, which is defined as the number of moles of solute solubilised per mole of surfactant. In practice, however, the solubilisation capacity is also expressed as the weight of solute solubilised per unit weight of surfactant, because it is this quantity that is important as regards formulation of the drug.

It is generally observed that an increase in surfactant concentration leads to an increase in its solubilisation capacity for a given solute [29, 49].

1.4.1 Locus of the solubilisation

The site of solubilisation of a given solute within a surfactant micelle is generally believed to be determined by the chemical structure of the solute. The locus of the solubilisation reflects the type(s) of interaction between surfactant and solubilisate molecules and is an important determinant of the extent to which the material is solubilised. Experimental data on the micellar solubilisation location have previously been obtained mainly using X-ray diffraction, absorption spectrometry, nuclear magnetic resonance spectroscopy, fluorescence depolarization, and electron spin resonance [22]. The main sites of solubilisation within micelles (Figure 1.3) are shown to be: 1) at the micelle-solvent interface; 2) between the polyoxyethylene hydrophilic head groups (in the case of nonionic surfactant micelles); 3) between the head group and the first few carbon atoms of the hydrophobic tail group; 4) more deeply within the tail region; and 5) in the micelle core.

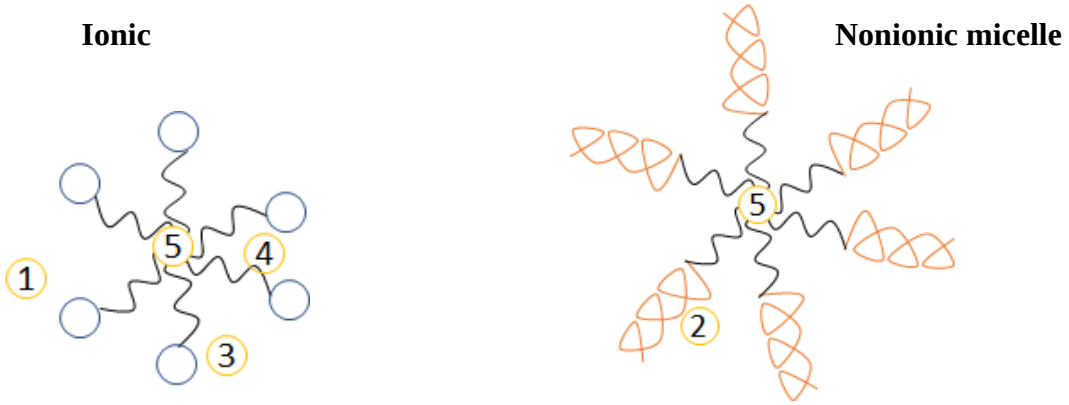

Figure 1. 3 Schematic of possible loci of solubilisation of solubilisates in micelles

The locus of solubilisation of a solute within a surfactant micelle is independent of the surfactant concentration. For both concentrated and dilute aqueous surfactant solutions, polar solutes tend to be solubilised in the outer regions of a surfactant micelle, whereas nonpolar solutes are solubilised in the micelle core [45].

1.4.2 Factors affecting solubilisation capacity

Structure of the surfactant

The solubilisation capacities of surfactants vary according to the surfactant type. For solubilisates which go into the micelle core or that penetrate deep into the palisade layer, it can be expected that there is a pronounced dependence of the solubilisation capacity on the surfactant alkyl chain length. An increase in the hydrocarbon chain length leads to increased solubilisation of hydrocarbon in the interior of the micelle, and the effect is more pronounced for surfactants with a charged head group [45, 50].

Arnarson and Elworthy [51], however, proposed that while the size of a nonionic surfactant micelle increases with increasing surfactant alkyl chain length, the increase in hydrophobe size does not lead to an increase in micellar solubilisation capacity. This effect was later explained as the result of a decreased solubilisation resulting from an intrusion of the polyoxyethylene head groups into the micelle core [34].

Kolthoff and Stricks [52] investigated the effect of chain length on the micellar solubilisation of solutes by ionic surfactants. These researchers showed a linear increase in the solubilisation capacity for the solute, dimethylaminobenzene, in the micelles formed by the ionic surfactants in the series, potassium dodecanoate to potassium octadecanoate. Vinarov et al. [53] also investigated the effect of the surfactant alkyl chain length (C_8 to C_{16}) on the solubilisation of drugs and these studies again showed that solubilisation capacity increases linearly with increasing surfactant alkyl chain length.

The solubilisation capacities of gliclazide in various micellar solutions were reported by Alkhamis et al. [54]. These authors showed that the solubility of gliclazide was dramatically increased in both cationic and anionic surfactants but that these two classes of surfactant showed opposite behaviour. When the carbon chain length was increased (from C_{10} to C_{16}) in cationic surfactants the solubilisation capacity for gliclazide increased, whereas an increase in chain length (from C_{10} to C_{14}) in anionic

surfactants led to a decrease in the solubilisation capacity. This difference in behaviour was explained as due to different sites of solubilisation of gliclazide within the cationic and anionic micelles: the drug being solubilised mainly in the inner core of the former and in the outer region of the latter.

It has also been found that solubilisation capacity is influenced by the head group structure of surfactants. The effect of a polar head group on the solubilisation capacity has been investigated by Jacobs and Anacker [55, 56]. In their study, using solutes solubilised within the hydrophilic head group region of micelles, the micelle aggregation number was shown to increase with the substitution of an ethanol group for an ethyl in decyltriethyl-, decyltripropyl- and decyltributylammonium bromide. For ionic surfactants with identical hydrophobes, the solubilisation capacity is seen to be proportional to the micelle aggregation number [57].

The effect of adding ethylene oxide units into dodecyl sulfate surfactants was shown by Vinarov et al. to cause a marked reduction in solubilisation capacity [50, 53]. This was taken to indicate that the ethoxylation disrupts the packing in the dodecyl sulfate micelles and so decreases the solubility of the drug molecules within the micelles.

In nonionic surfactants with polyoxyethylene head groups the effect of polyoxyethylene chain length on the solubilisation is dependent on the location of the solubilisate and Saito reports [58] that at a given temperature, an increase in polyoxyethylene chain length leads to a higher solubilisation capacity for aliphatic hydrocarbons, while Vinarov et al. [50] found that there is no significant effect on the extent of solubilisation of progesterone by increasing the ethoxy groups from 10 to 23.

Furthermore, for a given hydrocarbon chain length in a surfactant, branched chain surfactants appear to have lower solubilisation capacities than surfactants with an equivalent unbranched carbon chain [45].

Structure of the solubilisate

The most common classification for solubilisates is according to their polarity. For aliphatic and alkylaryl hydrocarbons, the extent of solubilisation in micelles appears to decrease with increasing chain length and increases with the addition of unsaturation and cyclization [45]. Alkyl hydrocarbons that have branched chains show no significant difference in solubilisation capacity to their normal chain isomers [45].

For solubilisates that contain aromatic rings, the solubilisation in micelles is dependent on their molecular size, with larger molecules exhibiting a lower solubility [59].

For polar compounds, it is presumed that the main locus of solubilisation is at the micelle-water interface, with interaction then between the solubilisate and both the surfactant hydrophilic head group and the surrounding water molecules. Generally, in surfactant solutions of low concentration the extent of solubilisation of polar compounds is higher than that of non-polar compounds. It is also found that polar compounds that are solubilised in the palisade layer of nonionic surfactant micelles exhibit a lower micelle loading than those that locate closer to the micelle surface [60-62].

The importance of solubilisate polarity has been further demonstrated by studies using substituted steroids. The solubility of testosterone in lysophosphatidylcholine is shown to be dramatically reduced by 17-α substitution of an ethinyl group. In contrast, the 17-α substitution of an ethinyl group in estradiol increases the solubility in lysophosphatidylcholine by more than 5-fold compared with that of estradiol. The difference here is attributed to a change in the net dipole moment of the steroids which results from introduction of the ethinyl group [63].

Effect of temperature

The effect of temperature on micellar solubilisation is dependent on the structures of both the surfactants and solubilisates.

Generally, an increase in temperature results in a higher solubilisation of both polar and non-polar solubilisates by ionic surfactants [52, 54]. Kolthoff and Stricks [52] also showed that the percentage increase seen in solubilisation capacity with change in temperature at high temperatures was opposite to that seen at lower temperatures, and similar findings were later reported by Bates et al. [64].

For nonionic polyoxyethylenated surfactants, the effect of temperature on solubilisation is dependent on the structure of solubilisate. For non-polar materials, which tend to be solubilised in the inner core of a nonionic surfactant micelle, an increase in temperature leads to a higher level of solubilisation, and the extent of this increase is greater when the temperature is close to the cloud point of the surfactant [58]. For polar solubilisates, the effect of temperature on solubilisation is more

complex, with the solubility of a solubilisate going through a maximum as the temperature approaches the surfactant cloud point [62]. The amount of the solubilised compounds first increased with increasing temperature due to the increase in thermal agitation of the surfactant molecules in aqueous solution. With further increase in temperature, the surfactant polyoxyethylene chains become progressively dehydrated and more tightly coiled, with the result that there is then less space to accommodate the solubilisates and the amount solubilised decreases. This effect is more pronounced for small polar compounds and for compounds that are solubilised close to the micelle surface [65].

1.5 Aim of the project

Over 70% of the new drug candidates discovered over recent years exhibit low aqueous solubility, and this presents as a major problem in drug development [66]. Much effort is expended in trying to improve the water solubility of these drug candidates and one of the strategies commonly explored in the pharmaceutical industries is to try and solubilise them inside colloidal aggregates – either polymeric or surfactant micelles.

Although micellar solubilisation is an extensively studied topic our understanding of such systems is not yet at a stage where we can predict the structure of the surfactant that is best to use to solubilise a given drug. The locus of solubilised drug within a micelle is thought to be important in determining the micelle's loading capacity, and it is this too that affects the drug's stability and its rate of release inside the body and so it also impacts the drug's therapeutic activity [67, 68]. We do not yet have sufficient understanding of the molecular mechanism that governs the solubilisation of drug in a micelle, however, and so we are unable, therefore, reliably to predict either the level of its solubilisation or its locus of solubilisation.

Accordingly, the aim of this project was to clarify the link between the structure of surfactant molecules and the micelles they form in aqueous solution, and then to determine how these influence the level and manner of solubilisation of poorly water soluble compounds. The resulting improved understanding of micellar solubilisation would hopefully then make it possible to optimize the design of drug delivery systems to improve drug loading.

A series of systematic studies have been performed to determine the extent and locus of solubilisation of two poorly water-soluble compounds in a range of surfactant micelles. Specifically, two steroidal molecules, 4-cholesten-3-one and adrenosterone have been solubilised in a range of C_{12}-chain surfactants with varying head group. The choice of these two steroids will be further discussed in Chapter 2. By altering the head groups of the surfactants, it was expected that the solubilisation capacities and micelle properties would vary. The physical chemical parameters of the surfactants were determined and these studies are described in Chapter 2. In order to estimate the preferred site(s) of solubilisation of the steroids within the surfactants/micelles, neutron techniques (neutron reflectivity and small-angle neutron scattering) were used and these are detailed in Chapter 3 and 4.

Chapter 2

Solubilisation, surface tensiometry, viscometry and densitometry studies

2.1 Solubilisation

2.1.1 Introduction

The solubilisation of drugs within surfactant micelles has long been considered as a means by which to facilitate the formulation and delivery of drugs that have poor aqueous solubility [66, 69, 70]. The factors governing the level of solubilisation which might be achieved for a given drug in a given surfactant system, however, are not yet fully understood.

Investigations into the factors influencing the micelle solubilisation of steroids were first reported in 1949, by Ekwall and Sjoblom [71]. These authors showed that water-insoluble steroid hormones could be solubilised using different types of surfactants, with the amount of solubilised hormone increasing with increased concentration of surfactant.

Guttman et al. later [72] investigated the solubilisation of the steroid drugs prednisolone, methylprednisolone, and fluorometholone in Triton X-100 solution, and found that the level of drug solubilised varied according to the drug's aqueous solubility. Thakkar and co-workers subsequently proved that was not the case for other steroid drugs [73], demonstrating that the level of solubilisation of testosterone in the micelles formed by non-ionic surfactants, polysorbate 20, 40 and 60, decreased in the order polysorbate 60 > 40 > 20 [74]. The same researchers also went on to determine the solubility of testosterone in ionic micellar solutions containing

dodecyltrimethylammonium bromide (DTAB), hexadecyltrimethylammonium bromide (HTAB) and potassium laurate (KL) [75]. They showed that the solubilisation capacity for testosterone in these ionic surfactant systems varied in the order KL > HTAB > DTAB and in all cases was higher than was achieved using the non-ionic surfactants. Since the solubilisation capacities of surfactants which have identical hydrophobic chain groups were different, the authors concluded that testosterone was not solubilised in the micelle interior.

Further studies, looking at the solubilisation of steroids in the micelles formed by non-ionic surfactants with polyoxyethylene (POE) head groups showed that the level of solubilisation could be increased by methylation or esterification of the terminal hydroxyl group of the POE head group. Ong and Manoukin [76] showed that for the corticosteroid timobesone acetate the solubilisation capacity of drug was increased by increasing the length of surfactant tail but unaffected by changes in the length of the POE head group. On the basis of their latter observation it was suggested that timobesone acetate was solubilised in the hydrophobic tail region of the micelle and not the palisade layer.

The solubilisation of the 17α-ethinylestradiol in non-ionic rhamnolipid micelles was reported by Guo et al. [77] and the micelle aggregation number and shape were shown to change as the concentration of the biosurfactant increased, with the suggestion made that the drug was solubilised at several loci within the micelle.

Barry and Eini also showed that the solubilisation capacity for some steroids increased with increasing ethylene oxide (EO) units in the head group [65]. In more recent times Vinarov et al. [78] studied the solubilisation of the hydrophobic steroid drug danazol both in ionic surfactants and non-ionic surfactants. It was shown that danazol has high solubility in ionic surfactants and this was attributed to ion-dipole interactions between the drug molecules and the charged head group of the surfactants, particularly those with head groups that contained sulfate or trimethyl ammonium bromide (TAB). It was further shown that the solubilisation capacities of all types of surfactants for danazol increased with the increased length of hydrocarbon chain, and that introducing an EO group into the dodecyl sulfate surfactants dramatically decreased the solubilisation of danazol (with the suggestion here that the incorporation of EO hindered the packing of dodecyl sulfate molecules in the micelles).

Vinarov et al.[50] have also recently reported an extensive and systematic study of the solubilisation of progesterone in 17 different types of surfactant systems using surfactants with different charges, lengths of hydrophobe and types of head group. From the results obtained in these studies the authors concluded that the best candidates to enhance the drug's solubility were surfactants with charged hydrophilic head groups and long hydrocarbon chains. For surfactants having a common C_{12} chain, the solubilisation capacity for the drug varied with the head group type, decreasing as SO_4^- > $(C_2H_4O)_1SO_4^-$ > $^+N(CH_3)_3$ > $(C_2H_4O)_3SO_4^-$. Surfactants with non-ionic head groups presented the lowest solubilisation capacity for progesterone. The general conclusion reached in these studies was that the progesterone was solubilised in the micelle palisade layer with its hydrophobic part inserted into the core of the micelles.

Another systemic study of micellar drug solubilisation has been performed [79] for a series of steroid drugs solubilised in the non-ionic surfactant, Polysorbate 80. In this study the aim was to find out the relationship between molar solubilisation capacity and the log octanol-water partition coefficient (log P) of testosterone and its derivatives. Alvarez-Núñez and Yalkowsky pointed out that although the solubilisation capacity was correlated to the log P for testosterone and its derivatives, such a relationship did not appear to hold for other steroids.

So far, many studies have proved that surfactants might have different solubilisation capacity depending on the types of drugs. Many reports have suggested that by increasing the alkyl chain length of the surfactant, the solubilisation capacity would also increase for most water insoluble drugs [80-82]. However, the influence of the surfactant head group on micellar drug solubilisation remains uncertain and there is no generally applicable theory to allow one to predict the amount of solubilised drug and its locus of solubilisation in a specific micelle system.

In the work reported here, the aim was to probe the effect of surfactant head group on the solubilisation of two steroidal molecules: 4-cholesten-3-one (4-CHOL) and adrenosterone (ADRENO), both of which have extremely poor water solubility (23 µg/L and 55 mg/L, respectively). 4-CHOL has a long hydrocarbon chain (2, 6 – dimethylheptyl chain) at C_{17} and a single carbonyl group at C_3; ADRENO contains three carbonyl groups, at C_{17}, C_3 and C_{11} and thus is more polar than 4-CHOL and exhibits a lower solubility in 1-octadecene than 4-CHOL (Table 2.1).

Systematic studies have been performed to determine the micellar solubilisation capacity of 4-CHOL and ADRENO in a range of surfactant systems, with surfactants chosen with the same C_{12} hydrocarbon chain but differing polar head groups (Figure 2.1).

Table 2. 1 Structures of the steroids 4-cholesten-3-one and adrenosterone

Steroid	Chemical structure	Log P*	Molecular weight g/mol
steroid skeleton	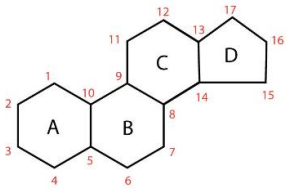	N/A	N/A
4-cholesten-3-one	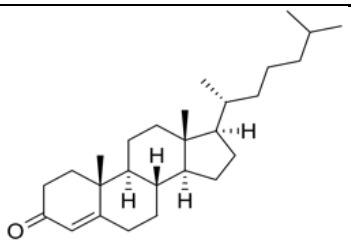	6.57	384.64
Adrenosterone	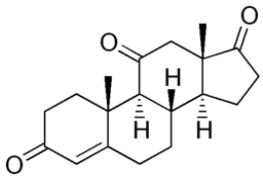	2.42	300.39
Testosterone	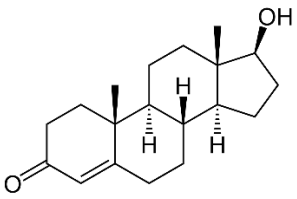	3.35	288.43
Testosterone enanthate	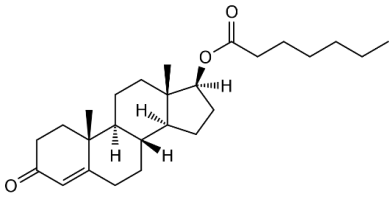	6.90	400.60
Testosterone propionate	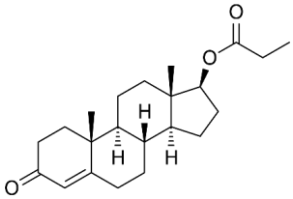	4.78	344.49

*Log P values were calculated by ALOGPS 2.1 program [83]

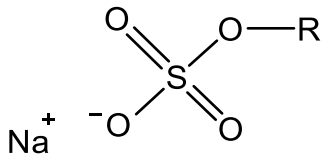

Sodium dodecyl sulfate (SDS)

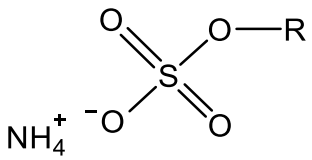

Ammonium dodecyl sulfate (ADS)

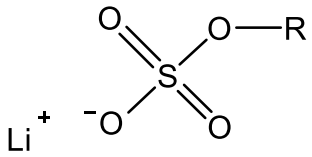

Lithium dodecyl sulfate (LDS)

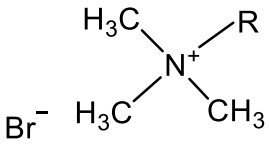

Dodecyl trimethylammonium bromide (DTAB)

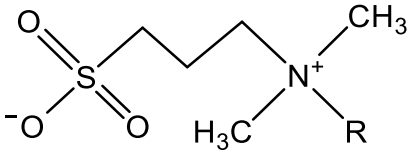

N-dodecyl-N, N-dimethyl-3-ammonio-1- propanesulfonate (DDAPS)

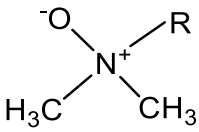

N, N-dimethyldecylamine N-oxide (DDAO)

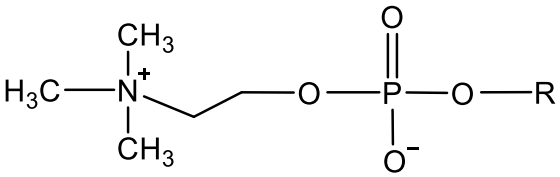

Dodecyl phosphocholine (DPC)

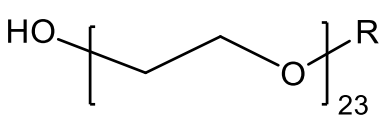

Polyoxyethylene (23) lauryl ether (Brij 35)

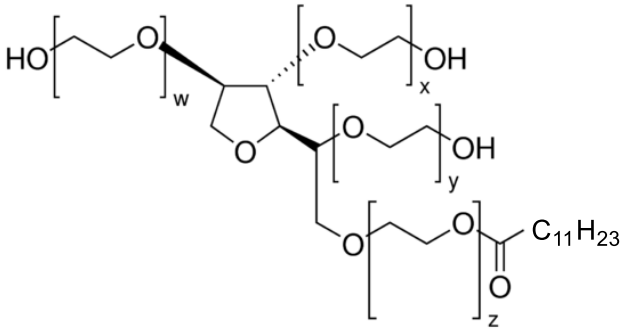

Polyoxyethylene sorbitan monolaurate (Tween 20)

Figure 2. 1 Chemical structures of the surfactants (R, in all cases = dodecyl, $C_{12}H_{25}$)

2.1.2 Materials

4-cholesten-3-one (98+ %) was purchased from Alfa Aesar (Heysham, UK) and adrenosterone (97+ %) from Santa Cruz Biotechnology (Heidelberg, Germany).

Sodium dodecyl sulfate (SDS), ammonium dodecyl sulfate (ADS), lithium dodecyl sulfate (LDS), dodecyl trimethylammonium bromide (DTAB) and N, N-dimethyldecylamine N-oxide (DDAO) were purchased from Sigma-Aldrich (Dorset, UK). N-dodecyl-N, N-dimethyl-3-ammonio-1-propanesulfonate (DDAPS) and polyoxyethylene (23) lauryl ether (Brij 35) were obtained from MP Biomedicals LLC (Ohio, USA). Dodecyl phosphocholine (DPC) was obtained from Avanti Polar Lipids (Alabama, USA) and ultra-pure polyoxyethylene sorbitan monolaurate (Tween 20) was supplied by National Diagnostics (Hull, UK).

Propan-2-ol was purchased from Fisher scientific (Loughborough, UK).

All chemicals were used as received.

2.1.3 Methods

The equilibrium solubilities of 4-cholesten-3-one and adrenosterone in the micellar solutions were measured by taking excess of the steroid into freshly prepared surfactant solution (1 mL), with the surfactant concentration varied between 2.5 wt% and 20 wt%. The steroid/surfactant systems were then subjected to continuous rotary mixing, with the sample vials placed on a rotary wheel (Stuart Tube Rotator SB2, Cole-Parmer Ltd, Staffordshire, UK) for 3-4 days at room temperature to achieve saturation. The rotary wheel was covered with aluminium foil to prevent possible photochemical degradation. After mixing, the samples were centrifuged at 13,000 rpm for 30 minutes (Biofuge pico, Kendro, U.S). The resulting supernatant was transferred to a new sample vial and the concentration of dissolved steroid measured by UV-Vis spectroscopy (LAMBDA 35 spectrophotometer, Perkin-Elmer). Surfactant solutions with no added steroid were also prepared using the same method.

UV calibration curves for the 4-cholesten-3-one and adrenosterone were obtained with steroid solutions prepared in propan-2-ol at concentrations from 4 μg/mL to 24 μg/mL. Absorbances were recorded at λ_{max} = 240nm. All measurements were recorded in triplicate.

The solubilisation capacity for steroid of a given surfactant micelle system was taken as the slope of the linear region from the solubilisation profile (wt% dissolved steroid vs. wt% surfactant). Solubilisation capacities were presented in g/g and also as molar solubilisation ratios (MSR), which define the number of moles of steroid solubilised in one mole of surfactant.

2.1.4 Results

Figures 2.2 to 2.6 show the amounts of 4-cholesten-3-one (4-CHOL) and adrenosterone (ADRENO) solubilised in 2.5 wt % to 15 wt % aqueous dispersions of C_{12}-chain surfactants with varying hydrophilic head groups (and these data are presented in tabular form in Appendix A, Tables A.1 and A.2). Beyond 15 wt% of surfactant (at 17.5 wt% and 20 wt%) the steroid/surfactant solutions were generally too viscous to allow accurate determination of solubility. For both steroids, irrespective of surfactant type, the amount of material solubilised increased linearly with increased surfactant concentration, demonstrating an association between the steroids and the micelles. The solubilisation capacities of each surfactant for 4-CHOL and ADRENO were calculated as the slope of the solubilisation profiles shown in Figures 2.2 to 2.6.

Solubilisation of 4-cholesten-3-one

From Figures 2.2 to 2.4, it is clear that 4-cholesten-3-one (4-CHOL) is solubilised much more efficiently by the anionic surfactants, the solubilisation capacity in sodium dodecyl sulfate (SDS) being more than five times that in any of the other surfactant systems (Table 2.2). It is interesting to note too, however, that if the counterion for the dodecyl sulfate is changed to NH_4^+ or Li^+, the level of 4-CHOL solubilisation capacity decreases, with the solubilisation capacities decreasing in the order SDS > ADS > LDS (0.432 ± 0.010 g/g vs 0.360 ± 0.014 g/g vs 0.328 ± 0.012 g/g, respectively).

When the C_{12} surfactant head group is replaced with the trimethyl ammonium bromide (TAB) group, the amount of 4-CHOL solubilised does not increase linearly with increasing concentration of surfactant solution. As shown in Figure 2.3, the amount of steroid solubilised rises rapidly for concentrations of DTAB above 10 wt%, the solubilisation profile then following a second order polynomial. The solubilisation capacity for 4-CHOL in DTAB was very much lower compared to that found for the anionic surfactants (as discussed above) and even at the highest concentration (15 wt%), the total amount of 4-CHOL solubilised into DTAB micelles (1.463 ± 0.070 wt%) was less than the amount solubilised into SDS micelles (1.616 ± 0.248 wt%) at a much lower surfactant concentration (5 wt%).

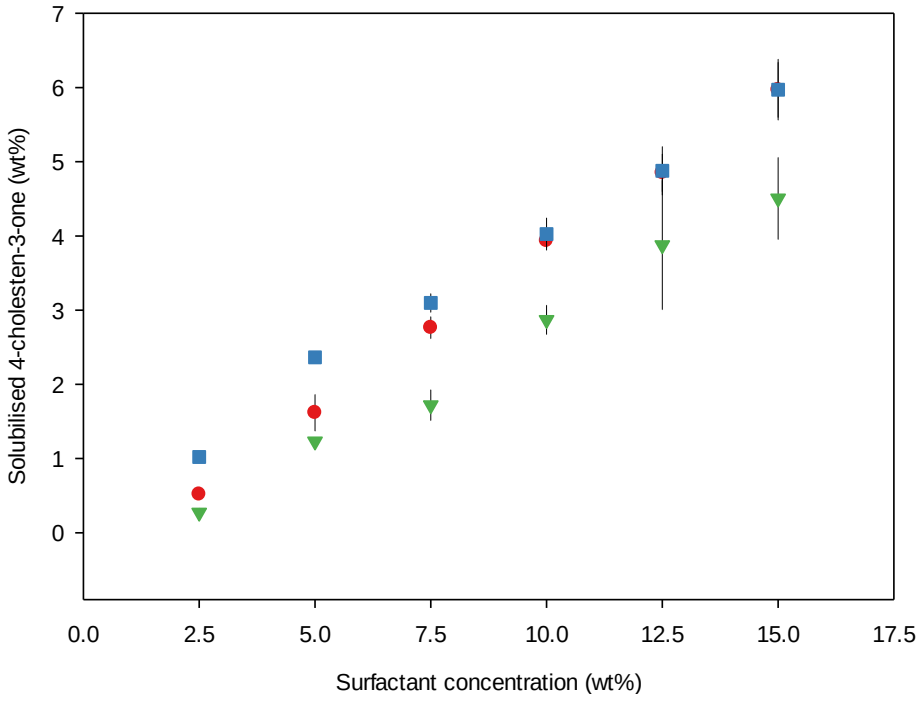

Figure 2. 2 Level of solubilisation of 4-cholesten-3-one in C_{12}-chain surfactant micelles ●: in SDS, ■: in ADS, ▼: in LDS (error bars shown indicate standard deviations, n=3). *Note that since the CMC's of these surfactants (which range from 10^{-3} to 10^{-1} wt%) are an order of magnitude smaller than the measured surfactant concentrations, the surfactant concentrations are not corrected for the surfactant CMC values.

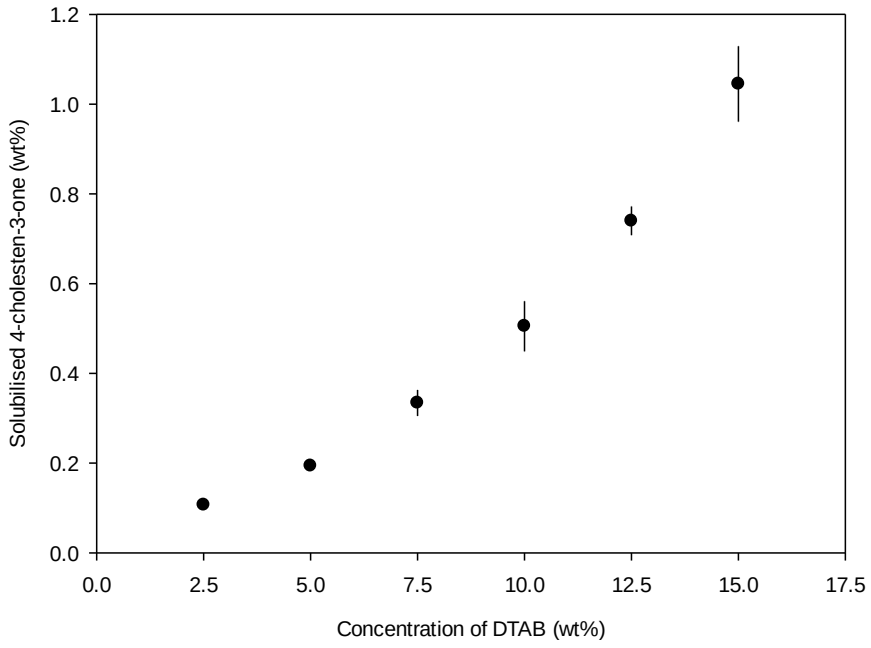

Figure 2. 3. Level of solubilisation of 4-cholesten-3-one in DTAB micelles (details as given in Figure 2.2).

The solubilisation capacity for 4-CHOL in zwitterionic surfactants decreased in the order DDAO > DDAPC > DPC (Figure 2.4). It is not surprising that DDAO shows the best solubilisation capacity among these surfactants as the superior solubilisation properties of surfactants with an N-oxide head group have been reported previously [84, 85]. The hydrophilic part of DDAPS has a strong interaction with water molecules [86] and might be detrimental to its solubilisation of 4-CHOL.

Among the investigated non-ionic surfactants Brij 35 and Tween 20, the latter showed a much higher solubilisation capacity for 4-CHOL. Given that the molecular weights for these surfactants are significantly higher than those of the other surfactants studied here (1200-1300 g/mol vs 250-350 g/mol), it is more instructive to compare their molar solubilisation ratios (MSR) and not their solubilisation capacities. When comparing the MSR of these surfactants for 4-CHOL, we see that 0.194 ± 0.007 mole of 4-CHOL molecules can be solubilised into 1 mole of Tween 20, which is slightly lower than achieved with LDS (0.232 ± 0.012) while only 0.020 ± 0.001 mole of 4-CHOL are solubilised into Brij 35 micelles. Tween 20 therefore presents a much better solubilisation for 4-CHOL than Brij 35 and this suggests that there are different solubilisation loci of 4-CHOL in the micelles of these two surfactants, or perhaps that

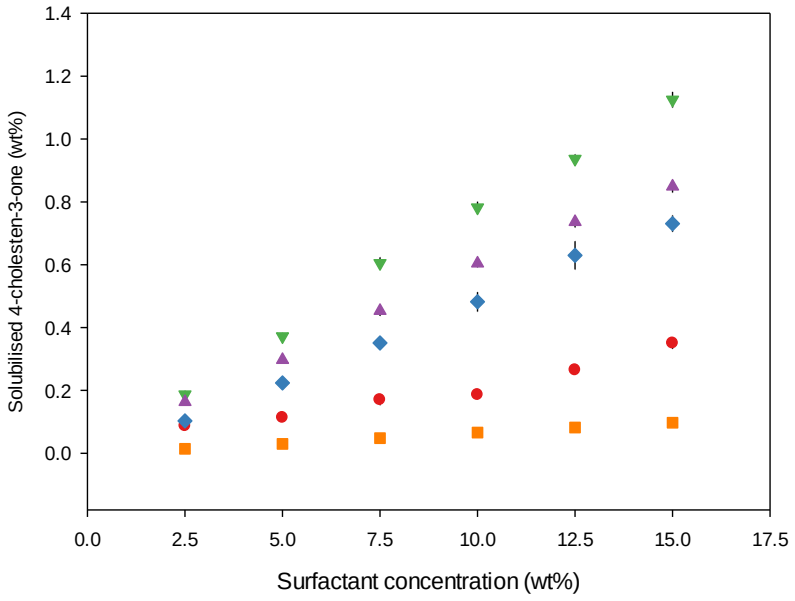

Figure 2. 4 Level of solubilisation of 4-cholesten-3-one in C_{12}-chain surfactant micelles. ●: in DPC, ♦: in DDAPS, ▼: in DDAO, ▲: in Tween 20, ■: in Brij 35 (details as given in Figure 2.2)

the level of solubilisation is influenced by the number of polyoxyethylene (POE) groups in the surfactant head group (Brij 35 having more POE units than Tween 20).

Table 2. 2 Solubilisation capacity (g/g) and molar solubilisation ratio (MSR) of C_{12} surfactant for 4-cholesten-3-one (n = 3)

SAA	Solubilisation capacity (g/g)	MSR
SDS	0.432 ± 0.010	0.324 ± 0.007
ADS	0.360 ± 0.014	0.265 ± 0.010
LDS	0.328 ± 0.012	0.232 ± 0.012
DTAB	0.086 ± 0.004	0.069 ± 0.003
DPC	0.023 ± 0.001	0.021 ± 0.001
DDAPS	0.051 ± 0.001	0.044 ± 0.001
DDAO	0.077 ± 0.004	0.046 ± 0.003
Tween 20	0.061 ± 0.002	0.194 ± 0.007
Brij 35	0.006 ± 0.000	0.020 ± 0.001

Solubilisation of adrenosterone

The solubilisation capacity for adrenosterone (ADRENO) is lower than found for 4-CHOL for all types of surfactant. The required time for ADRENO to achieve an equilibrium solubility, however, was in all cases much shorter than for 4-CHOL, with equilibrium achieved in a matter of hours, whereas 4-CHOL required several days.

As found for 4-CHOL, the anionic surfactants presented as the best solubilisers. For ADRENO, the rank order of the dodecyl sulfate solubilisation capacities decreased as $Na^+ > Li^+ > NH_4^+$. The amount of ADRENO solubilised in ADS micelles was only half that solubilised in SDS (0.048 ± 0.002 g/g for ADS and 0.090 ± 0.002 g/g for SDS).

Unlike 4-CHOL, the level of solubilisation of ADRENO in the cationic surfactant DTAB increased linearly as a function of surfactant concentration. The level of

solubilisation was only a third that achieved with SDS (0.031 ± 0.001 g/g) and a similar level of solubilisation was seen with the zwitterionic surfactant DDAPS, and lower levels of solubility in DDAO and DPC. The non-ionic surfactants exhibited the lowest solubilisation capacity for ADRENO with no benefit resulting from the increases in POE units provided by Tween 20 and Brij 35. When considering the MSR, the non-ionic surfactant Tween 20 gave a similar solubilisation capacity to the zwitterionic surfactants while Brij 35 only solubilised around half that amount of ADRENO.

Table 2. 3 Solubilisation capacity (g/g) and molar solubilisation ratio (MSR) of C_{12} surfactant for adrenosterone (n = 3)

SAA	Solubilisation capacity (g/g)	MSR
SDS	0.090 ± 0.002	0.087 ± 0.002
ADS	0.048 ± 0.002	0.045 ± 0.002
LDS	0.062 ± 0.006	0.056 ± 0.005
DTAB	0.031 ± 0.001	0.032 ± 0.001
DPC	0.020 ± 0.000	0.024 ± 0.000
DDAPS	0.033 ± 0.002	0.037 ± 0.002
DDAO	0.018 ± 0.001	0.015 ± 0.001
Tween 20	0.005 ± 0.000	0.020 ± 0.001
Brij 35	0.003 ± 0.001	0.011 ± 0.001

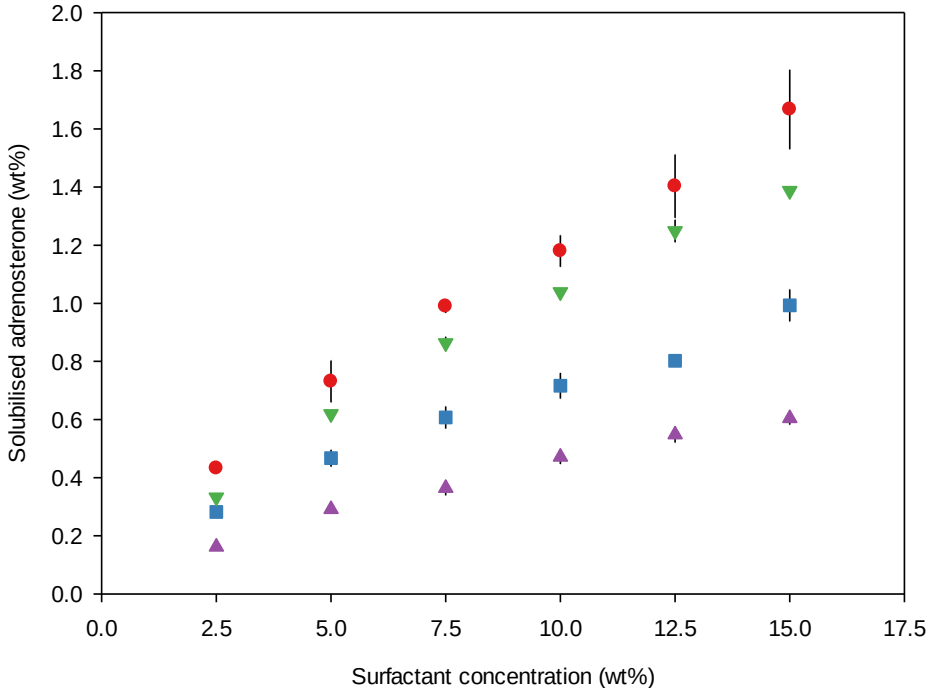

Figure 2. 5 Level of solubilisation of adrenosterone in C_{12}-chain surfactant (ionic) micelles. ●: in SDS, ■: in ADS, ▼: in LDS ▲: in DTAB (details as given in Figure 2.2).

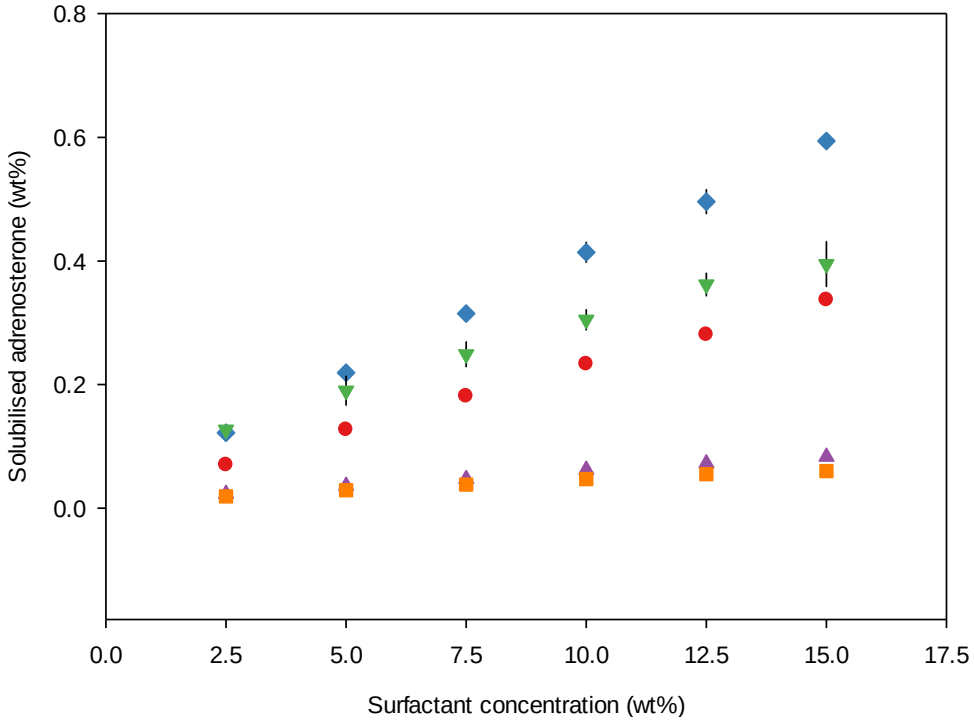

Figure 2. 6 Level of solubilisation of adrenosterone in C_{12}-chain surfactant (zwitterionic and nonionic) micelles. ●: in DPC, ♦: in DDAPS, ▼: in DDAO, ▲: in Tween 20, ■: in Brij 35 (details as given in Figure 2.2)

2.1.5 Conclusions

The effect of C_{12} chain surfactants with varying head group on solubilisation of two steroids 4-cholesten-3-one and adrenosterone was investigated. According to the results obtained, the solubilisation capacity was calculated (Table 2.4) and analysed, and the main conclusions drawn are as follows:

- The solubilisation capacity of C_{12} surfactants for 4-cholesten-3-one decreases in the order SDS > ADS > LDS > DTAB > DDAO > Tween 20 > DDAPS > DPC > Brij 35
- The solubilisation capacity of C_{12} surfactants for adrenosterone decreases in the order SDS > LDS > ADS > DTAB ≈ DDAPS > DPC ≥ DDAO > Tween 20 > Brij 35
- The ionic surfactants have the greatest capacity for solubilisation of both of the steroids studied but 4-cholesten-3-one is solubilised much better than adrenosterone. The non-ionic surfactant Brij 35 has the worst solubilisation capacity for both steroids while the zwitterionic surfactants afford an intermediate solubilisation capacity.
- Surfactants having a sulfate head group provide the best solubilisation for steroids, however, the level of solubilisation varies according to the type of counterion. This result is consistent with the observations reported by Vinarov et al. [78]. Saaka [87] also suggested that the head group of C_{12} surfactants might play an important role in solubilising the testosterone derivatives and the locus to solubilise the steroids might not be in the core of micelles.
- The high solubility of 4-cholesten-3-one in micelles formed by Tween 20 may be due to a different locus of solubilisation. Because of the large head group of this non-ionic surfactant, the penetration of drug molecules into the chain region of the surfactant micelle might be made more difficult.
- On the basis of the solubilisation measurements detailed above, the preferred site of solubilisation of the steroid molecules in the surfactant micelles still cannot be determined unequivocally, but the different polarities of the two

molecules might suggest that 4-cholesten-3-one and adrenosterone would be solubilised in different regions within the micelles.

Table 2.4 Solubilisation capacity (g/g) of C_{12} surfactant for 4-cholesten-3-one and adrenosterone (n = 3)

SAA	4-cholesten-3-one (g/g)	Adrenosterone (g/g)
SDS	0.432 ± 0.010	0.090 ± 0.002
ADS	0.360 ± 0.014	0.048 ± 0.002
LDS	0.328 ± 0.012	0.062 ± 0.006
DTAB	0.086 ± 0.004	0.031 ± 0.001
DPC	0.023 ± 0.001	0.020 ± 0.000
DDAPS	0.051 ± 0.001	0.033 ± 0.002
DDAO	0.077 ± 0.004	0.018 ± 0.001
Tween 20	0.061 ± 0.002	0.005 ± 0.000
Brij 35	0.006 ± 0.000	0.003 ± 0.001

2.2 Surface tensiometry

2.2.1 Introduction

When surfactants are added into an aqueous medium, their molecules – by virtue of their amphiphilic nature – tend to arrange at the air-water interface, as a layer with the hydrophilic/polar head groups immersed in the water and their hydrophobic/apolar parts directed away from the water toward the air. The surfactant molecules at the water surface disrupt the water structure, reducing the free energy of the system and thereby lowering the surface tension. As the concentration of the surfactant is increased, so the number of surfactant molecules at the water surface increases, and the surface tension progressively decreases. When the water surface is saturated, the surface tension remains constant and the additional molecules aggregate within the continuous phase to form micelles. The surfactant concentration at which micelles

begin to form is defined as the critical micelle concentration (CMC) of the surfactant, and this can be determined from surface tension measurements performed as a function of surfactant concentration.

The equilibrium surface tension of surfactant solution can be measured in several ways. The two most common methods used are the Du Noüy ring method and the Wilhelmy plate method, and the pendant drop and the bubble pressure methods [88] are usually used only in dynamic surface tension measurement.

The Wilhelmy plate method can be prone to errors arising through the adsorption of organic compounds from the environment, but compared to the Du Noüy ring method, this method is generally considered more accurate [89]. In the ring method, since the ring needs to be pulled through the liquid and results in a non-equilibrium state of the surface, the measured surface tension may vary with the pulling speed [88, 90]. With the Wilhelmy plate method, the surface tension is measured with the surface at equilibrium.

Given that the solubilisation of poorly water soluble solutes by surfactants is influenced by the structure and properties of the surfactant micelles, and because this in turn is influenced by their interfacial adsorption behaviour, an understanding of the latter can directly inform their use for solubilisation. Surfactants with lower CMCs potentially have higher solubilisation capacities due to their greater tendency for micelle formation.

The CMC of a given surfactant in aqueous solution is influenced by the structure of its hydrophobic and hydrophilic groups, by the presence of electrolyte or other organic compounds present in the solution, and by the solution temperature [45].

Table 2.5 shows the CMCs previously reported for some C_{12}-chained surfactants with varying head groups. It may be noted here that the zwitterionic surfactants have much lower CMCs than the anionic and cationic ones (~1 mM vs ~10 mM) and that the CMCs of the anionic surfactants vary according to the nature of the bound counterion. The CMC is higher when the centre of charge is close to the α-carbon of the C_{12} hydrocarbon chain. In some n-alkyl surfactants, the order of the effect of the head group on the CMC is aminium salts > carboxylates > sulfonates > sulfates [43]. Stigter explained that when an electric charge of surfactant is close to the hydrocarbon chain,

it requires more work to aggregate and form micelles due to an increase in electrostatic self-potential of the surfactant ion [42].

The binding of counterions to surfactant micelles is positively correlated with the polarizability and valence of the counterions and inversely correlated with their hydrated radius [45]. The increased binding of counterions to a given anionic surfactant causes a lowering of the surfactant's CMC and increases the micelle aggregation number [37].

In the studies reported here, surface tensiometric measurements were used to determine the CMCs for a range of C_{12}-chain surfactants in aqueous solution at 25 ± 0.1 ^{o}C. For the two surfactants studied which showed the highest levels of 4-CHOL solubilisation, *viz.*, SDS and DTAB, the surface tension measurements were also made in the presence of this steroid, and for the sake of completeness, the surface tension measurements for SDS and DTAB were also repeated in the presence of ADRENO. For DPC, DDAPS, DDAO, Tween 20 and Brij 35, however, the measurements of surface tension were not repeated in the presence of 4-CHOL or ADRENO because it was not considered likely that the steroids would cause significant changes in the surface tension curves for these surfactants given that their levels of solubilisation of the steroids were very low (generally, < 0.01 g/g).

Table 2. 5 The CMCs of C_{12}-chain surfactants

Surfactant	Name	Abbreviation	CMC (mM)	Reference
Anionic	Sodium dodecyl sulfate	SDS	8.0 – 8.4	[45, 91-94]
	Lithium dodecyl sulfate	LDS	8.5 – 10	[45, 95, 96]
	Ammonium dodecyl sulfate	ADS	6.2 – 7.1	[97-99]
Cationic	Dodecyl trimethylammonium bromide	DTAB	14.6 – 16	[45, 93, 100, 101]
Zwitterionic	N-dodecyl- N, N-dimethyl-3-ammonio-1-propanesulfonate	DDAPS	2 – 4	[90, 93, 102]
	Dodecyl phosphocholine	DPC	1 – 1.52	[103, 104]
	N, N-dimethyldodecylamine N-oxide	DDAO	1.6 – 2	[105, 106]

2.2.2 Materials

4-cholesten-3-one (98+ %) was purchased from Alfa Aesar (Heysham, UK) and adrenosterone (97+ %) from Santa Cruz Biotechnology (Heidelberg, Germany).

Sodium dodecyl sulfate (SDS), ammonium dodecyl sulfate (ADS), lithium dodecyl sulfate (LDS), dodecyl trimethylammonium bromide (DTAB) and N, N-dimethyldecylamine N-oxide (DDAO) were purchased from Sigma-Aldrich (Dorset, UK). N-dodecyl-N, N-dimethyl-3-ammonio-1-propanesulfonate (DDAPS) was obtained from MP Biomedicals LLC (Ohio, USA). Dodecyl phosphocholine (DPC) was obtained from Avanti Polar Lipids (Alabama, USA).

All chemicals were used as received.

2.2.3 Methods

Surface tension measurements were performed using a Tensionmeter K11 (Krüss, Germany). All glassware used was soaked in Decon® and then scrupulously rinsed with ultrapure water (resistivity of 18.2 MΩ.cm at 25 ± 0.1 ^{o}C). The external accuracy of measurements was checked by frequent measurement of the surface tension of ultrapure water, and comparing against the reference value, 71.99 mN/m at 25 ± 0.1 ^{o}C [107].

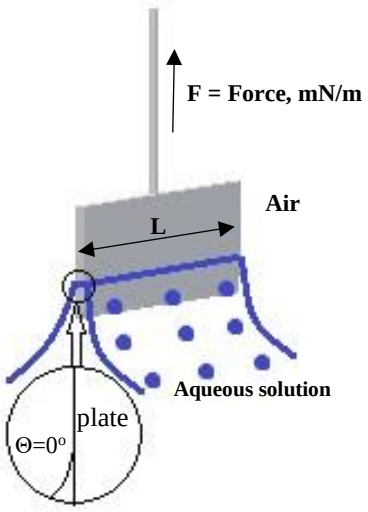

Figure 2. 7 A schematic of Wilhelmy plate method

Prior to measurement, the platinum plate of the tensiometer was soaked in Decon® and rinsed with ultrapure water, flamed until red-hot, and then allowed to cool to room temperature before use. The surface tension was measured by dipping a thin platinum

plate into the liquid and then raising the plate so that it was just within the surface of the liquid and the surface then allowed to relax and achieve equilibrium (Figure 2.7). From the measured force required to hold the plate in the surface, the surface tension of the liquid was calculated.

Dilutions were made in the vessel directly using the ultrapure water to minimize the effect of adsorption of surfactant onto the container thus ensuring the accuracy of the concentration. The measurement was made after 15 minutes after each dilution and the surface tension was checked at 5 minutes interval until no significant changes were observed. The platinum plate was cleaned and flamed after each reading to remove all adsorbed surface active material. Each measurement was made in triplicate to ensure the reproducibility of the results.

For a given surfactant solution, at a given concentration, the surface tension (γ, nM/m) is obtained from the measured force (F) as:

$$\gamma = -\frac{\mathrm{F}}{L \times cos\theta} \qquad [2.1]$$

where L (m) is the length of the Wilhemy plate and θ is the contact angle formed between the plate and the solution which here (because of the use a platinum plate) was taken as 0° [108]. With γ measured as a function of surfactant concentration, c, a plot of γ vs. log[c] is obtained and the slope, $d\gamma/d\log[c]$ is used to derive the surface excess Γ (mol cm^{-2}) via the Gibbs equation as:

$$\Gamma = -\frac{1}{nRT} \times \frac{\mathrm{d}\gamma}{d log[c]} \qquad [2.2]$$

where R is the gas constant (8.31 J K^{-1} mol^{-1}) , T is the absolute temperature (K), and n = 1 for non-ionic or ionic surfactants (DDAPS, DDAO and DPC) in the presence of excess electrolyte, or n = 2 in the case of 1:1 ionic surfactants (SDS, LDS, ADS and DTAB) [109].

The interfacial area per surfactant molecule, a_1^s, can be calculated as:

$$a_1^s = \frac{10^{16}}{N\Gamma} \qquad [2.3]$$

where N is Avogadro's number.

2.2.4 Results

Surface tensions for the seven C_{12}-chain surfactants measured as a function of concentration are shown in Figure 2.8.

In each case, as expected, the surface tension decreases with increasing surfactant concentration and then at a given concentration it ceases to change (significantly) as the water surface becomes saturated. For some systems (LDS, ADS and DTAB) there is a minimum seen in the surface tension plot and this can be attributed to impurities present in the commercially-obtained surfactant solutions [110]. According to ISO guidelines, the minima in the γ vs log[c] curve can still be used to determine the CMC of the surfactant [111].

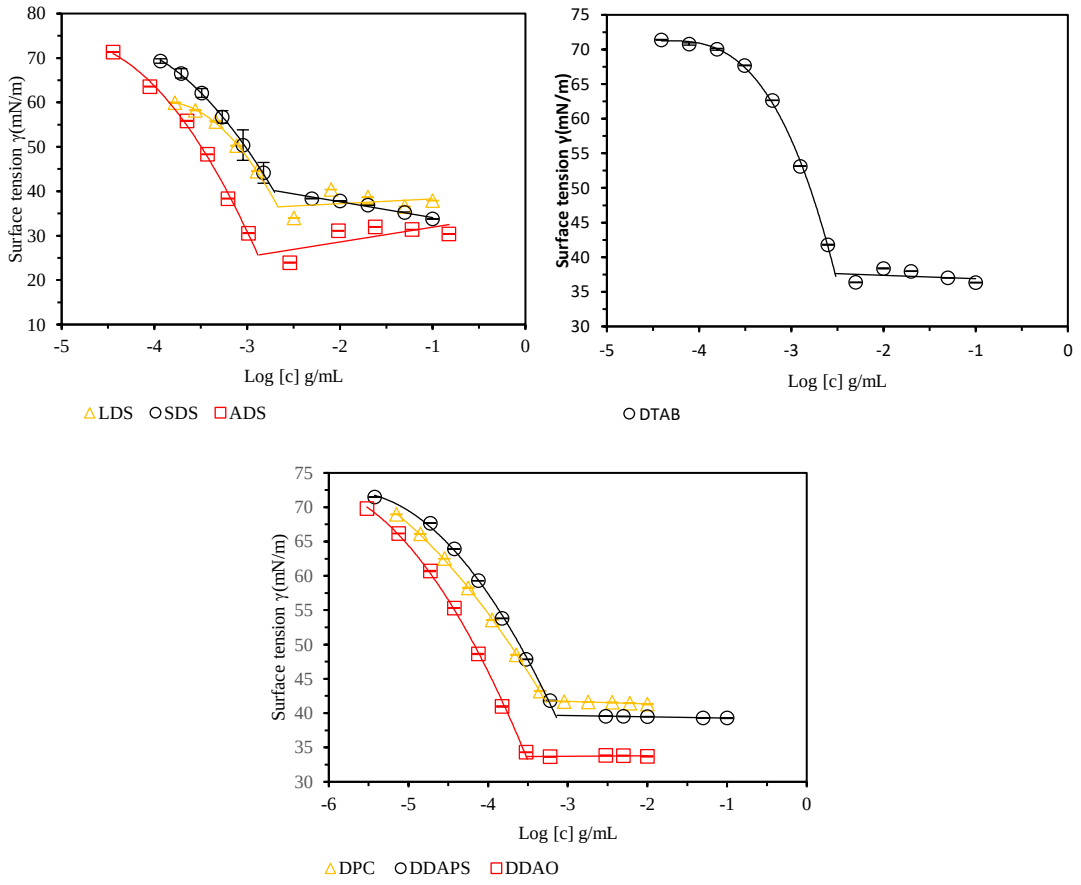

Figure 2. 8 Variation of surface tension (γ, nM/m) with the concentration (c, g/mL) for C_{12} surfactants dispersed in H_2O at 25 ± 0.1°C. Standard errors on the data are shown (n=3).

The CMCs calculated for each of the C_{12}-chain surfactants are given in Table 2.6, together with other interfacial properties: the effectiveness of the surfactant/the surface

tension at the CMC(γ_{CMC}), the surfactant surface excess (Γ) and its interfacial area per molecule (a_1^s).

It has been reported that the CMC of a surfactant is related to its degree of binding of counterions to its micelles [37]. The increased binding of counterions causes a decrease in the surfactant CMC, and the extent of binding of counterions increases with a decrease in the hydrated radius of the counterion [45]. The hydrated counterion radii for the anionic surfactants studied here decrease in the order $Li^+ > Na^+ > NH_4^+$, and the CMC of these dodecyl sulfate surfactants increase in the order ADS < SDS < LDS, as shown in Table 2.6.

Surface tension is related to the number of surfactant monomers per unit area adsorbed at the interface. Therefore, surface excess (Γ) and area per molecule (a_1^s) are calculated and used to give an indication of the packing of surfactant molecules at the air-water interface. In the case of LDS, due to its largest hydrated radius, the distance between its positive centre and negative centre is the largest, and this results in a higher Coulombic repulsion between the adjacent sulfate groups. Thus, the LDS molecules are more loosely packed at the interface. This is evidenced by the area per molecule (a_1^s) values shown in Table 2.6. The order of a_1^s for these anionic surfactants thus correlates with the variation in the hydrated counterion radii (Li^+, 0.382 nm, Na^+, 0.358 nm, and NH_4^+, 0.331 nm) and indicates that the packing of these surfactants in governed by their electrostatic interactions [112].

The cationic surfactant DTAB has the highest CMC of all the C_{12}-chain surfactants tested and its a_1^s is lower than those of the anionic surfactants which could suggest that the aggregation number for DTAB micelles is higher than that for the dodecyl sulfate surfactant micelles.

For the zwitterionic surfactants, the measured CMCs are around one order of magnitude lower than those of the ionic surfactants, and follow the order: DDAPS > DPC > DDAO. DDAO has the highest Γ and lowest a_1^s, so the DDAO monomers may be packed more closely at the interface than other surfactant monomers. The a_1^s of the zwitterionic surfactants are likewise lower than those of the ionic surfactants, indicating that the zwitterionic surfactant monomers are more closely packed at the interface and by extrapolation could be expected to pack more closely within micelles.

The differences seen in a_1^s between the surfactants probably result in the variation in the solubilisation capacity. If the locus of solubilisation is in the micelle core, the micelles having the more closely packed molecules may hinder the access of the steroids to the micelle core region and thus lead to a smaller number of solubilised steroids. However, if the hydrophilic head group of the surfactant is considered as the major locus of solubilisation, the higher a_1^s will result in a higher aggregation number for the micelles and will thus lead to a greater number of solubilised steroids per micelle. Such conclusions assume the same number of water molecules per surfactant head group but this, of course, may not be the case. The hydrodynamic properties of the surfactant dispersions will be further discussed in the next section.

The interfacial properties mentioned above were calculated from the Gibbs equation, whose application has been debated over the years. Menger et al. [113, 114] proposed that at the CMC, the adsorption of surfactant at the air-water interface is not yet at the saturation. Xu et al. [115] and Li et al. [116, 117] also found a disparity in the results of ionic surfactants from neutron reflectometry and surface tension while zwitterionic and non-ionic surfactants showed a good agreement from the results obtained using these two techniques. Neutron reflectivity is suggested as the better technique for determining Γ and a_1^s than surface tension measurement. However, the results obtained from these techniques are often reported to be comparable. It may be noted here, for example, that Lyttle et al. [118] have used neutron reflectivity measurements to study DTAB, and report an a_1^s of 48 Å^2 which is close to the value of 55 ± 3 Å^2 obtained via the surface tension measurements reported here.

The principle parameters of interest determined from the surface tension measurements reported here are the CMCs of the C_{12}-chain surfactants. The surface excess and area per molecule of the surfactants in the presence or absence of steroids were further measured using neutron reflectivity and these studies are described in Chapter 3.

The CMCs of surfactants in the presence of 4-cholesten-3-one and adrenosterone

Surface tension measurements were also performed to determine the CMCs of SDS and DTAB in the presence of saturated 4-cholesten-3-one and adrenosterone. As noted earlier (section 2.1), SDS and DTAB have the highest solubilisation capacities for 4-cholesten-3-one (4-CHOL) and adrenosterone (ADRENO), and the high levels of

these steroids solubilised in the surfactant monolayers could potentially lower the surface tension and lead to changes in the CMC. Meanwhile, as was found in solubilisation experiment, it took much longer for 4-CHOL (ca. 2 hours) than ADRENO (ca. 5 minutes) to reach the equilibrium in the SDS monolayer.

Figure 2.9 shows the surface tension curves for SDS and DTAB in the presence of 4-CHOL and ADRENO. It is clear that at the high SDS concentrations, the presence of 4-CHOL in the monolayer lowers the surface tension by ca. 10 mN/m while the presence of ADRENO causes no significant change in the surface tension. As with the pure surfactant systems, when the concentration of the surfactant is below the CMC, the surface tension increases with decreased surfactant concentration. For the DTAB/ADRENO and DTAB/4-CHOL system, the surface tension approaches the expected low concentration limit of 72 mN/m which is the surface tension of pure water. In the case of the SDS/ADRENO and SDS/4-CHOL systems, however, the low concentration limit is << 72mM/m and this would seem to suggest that there is significant steroid at the interface even when the SDS concentration is low.

Table 2.7 shows the interfacial properties of SDS and DTAB monolayers in the presence of 4-CHOL/ADRENO. The CMCs of the surfactants in the presence of these steroids were slightly lower than those determined for the pure surfactant systems. The increased area per molecule of the surfactants in the presence of ADRENO and 4-CHOL indicates simply that the surfactants monomers are less tightly packed at the interface, as the result of steroid molecules inserted in the interfacial layer. These effects are more pronounced for 4-CHOL than for ADRENO.

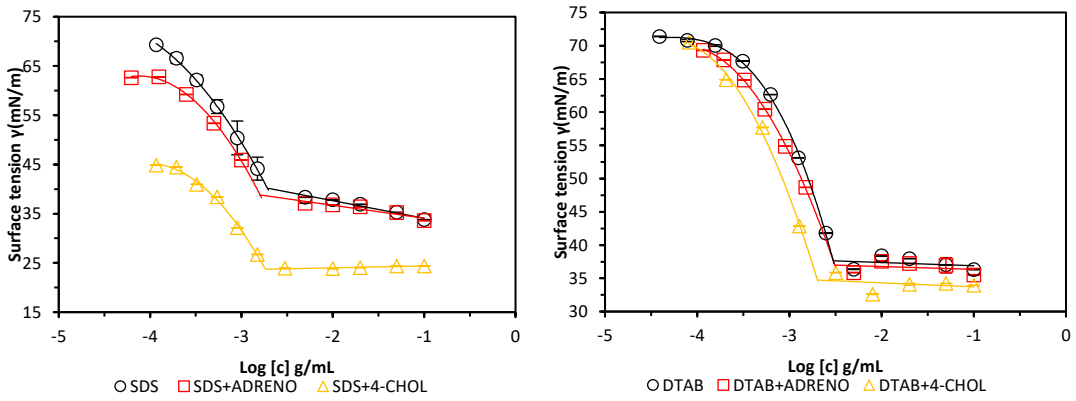

Figure 2. 9 Variation of surface tension (γ, nM/m) with the concentration (c, g/mL) for C_{12}-chain surfactants in the presence of 4-cholesten-3-one (4-CHOL) and adrenosterone (ADRENO) in H_2O at 25 ± 0.1ºC. Standard errors on the data are shown (n=3).

aTable 2. 6 Values of C_{12}-chain surfactants effectiveness (Υ_{CMC}), critical micelle concentration (CMC), surfactant surface excess (Γ) and area per molecule (a_1^s) (n = 3).

Surfactant	Υ_{CMC} (± 0.2 mN m^{-1})	CMC (± 0.02 wt%)	CMC (± 0.5 mM)	Γ (± 0.1 x 10^{-6} mol m^{-2})	a_1^s (± 3 Å^2)
SDS	36.4	0.23	8.0	2.4	70
LDS	38.4	0.26	9.7	2.2	75
ADS	31.2	0.18	6.2	2.7	60
DTAB	37.4	0.43	14.0	2.5	55
DDAPS	39.4	0.078	2.3	3.4	49
DDAO	33.9	0.032	1.4	4.1	40
DPC	41.5	0.056	1.6	3.0	55

Table 2. 7 Values of effectiveness (Υ_{CMC}), critical micelle concentration (CMC), surfactant surface excess (Γ) and area per molecule (a_1^s) of SDS and DTAB in the presence of steroids (n = 3).

Surfactant	Υ_{CMC} (± 0.2 mN m^{-1})	CMC (± 0.02 wt%)	CMC (± 0.5 mM)	Γ (± 0.1 x 10^{-6} mol m^{-2})	a_1^s (± 3 $Å^2$)
SDS	36.4	0.23	8.0	2.4	70
SDS + 4-cholesten-3-one	24.1	0.21	7.5	1.9	86
SDS + adrenosterone	35.8	0.22	7.8	1.9	86
DTAB	37.4	0.43	14.0	2.5	55
DTAB+ 4-cholesten-3-one	33.7	0.39	12.8	2.2	74
DTAB + adrenosterone	36.6	0.42	13.6	2.3	72

2.2.5 Conclusion

From the surface tensiometry results reported above, it can be concluded that:

- The measured CMCs of the C_{12} chain surfactants decreased in the order of DTAB > LDS > SDS > ADS > DDAPS > DPC > DDAO, and the CMCs are very close to or fall within the range of the CMC values determined by others (Table 2.8).

Table 2. 8 the comparison of CMC values of surfactants

Surfactant	CMC in this study (± 0.5 mM)	CMC from literature
SDS	8.0	8.0 – 8.4
LDS	9.7	8.5 – 10
ADS	6.2	6.2 – 7.1
DTAB	14.0	14.6 – 16
DDAPS	2.3	2 – 4
DDAO	1.4	1.6 – 2
DPC	1.6	1 – 1.52

- The CMCs of the ionic surfactants are seen to be influenced both by the nature of the surfactant head group and by the nature of the counterions.
- DDAO has the highest Γ and lowest a_1^s, thus the DDAO monomers are packed more closely at the interface than other surfactant monomers. In addition, ADS is more effective at lowering the surface tension.
- The CMCs of the C_{12}-chain surfactants in the presence of steroids were also determined, and although these were found to be a little lower than those for the corresponding pure surfactant systems, the differences are within the experimental error (and are ignored in the further studies).

- Observationally, the presence of steroid in the surfactant monolayers decreases the surface tension, and the effect is more pronounced for 4-CHOL than ADRENO.
- The difference in the a_1^s of the surfactant monomers in the presence of 4-CHOL or ADRENO is not significant.

2.3 Viscometry and densitometry

2.3.1 Theoretical background

Given that the solubilisation of solutes by surfactant micelles is likely to cause changes in the micelle size, shape and hydration, and because these micelle properties impact the viscosity of the systems, it is of interest to determine their viscosities experimentally.

The viscosity η is the resistance of a fluid to flow and the effect of surfactant molecules on a solution is given by the relative viscosity η_{rel}, which can be calculated from the time ratio:

$$\eta_{rel} = \frac{t}{t_0} \quad [2.4]$$

where t and t_0 are the flow times for a given volume of surfactant solution and solvent, respectively. The specific viscosity of a surfactant solution η_{sp} is obtained as:

$$\eta_{sp} = \eta_{rel} - 1 \quad [2.5]$$

and the reduced viscosity η_{red} (mL/g) as:

$$\eta_{red} = \frac{\eta_{sp}}{c} \quad [2.6]$$

where c is the surfactant concentration (g/mL). A related term, inherent viscosity (η_{inh}) is defined as the ratio of the natural logarithm of η_{rel} and c:

$$\eta_{inh} = \frac{\ln \eta_{rel}}{c} \quad [2.7]$$

As can be seen from equations 2.6 and 2.7, both η_{red} and η_{inh} are concentration dependent. In the limit as the surfactant concentration approaches zero ($c \rightarrow 0$), the limiting value of viscosity is defined and is referred to as the intrinsic viscosity $[\eta]$:

$$[\eta] = \lim_{c \rightarrow 0} \eta_{red} \quad [2.8]$$

$$[\eta] = \lim_{c \rightarrow 0} \eta_{inh} \quad [2.9]$$

$[\eta]$ reflects the capability of a surfactant to enhance the viscosity of the solution. To determine $[\eta]$, the viscosities of varying concentrations of surfactant solution are

measured and the dependence of the reduced viscosity on concentration is modelled according to the Huggins equation [119]:

$$\eta_{red} = \frac{\eta_{sp}}{c} = [\eta] + \mathrm{K}_H[\eta]^2 c \qquad [2.10]$$

where $\mathrm{K_H}$ is the Huggins constant and $[\eta]$ is taken as the intercept (see Figure 2.10).

Alternatively, $[\eta]$ can be determined through a linear extrapolation of the concentration dependent variation in the inherent viscosity η_{inh}, as modelled in the Kraemer equation [120]:

$$\eta_{inh} = \frac{\ln \eta_{rel}}{c} = [\eta] - \mathrm{K}_K[\eta]^2 c \qquad [2.11]$$

where $\mathrm{K_K}$ is the Kraemer constant, and $[\eta]$ is again taken as the intercept (see Figure 2.10).

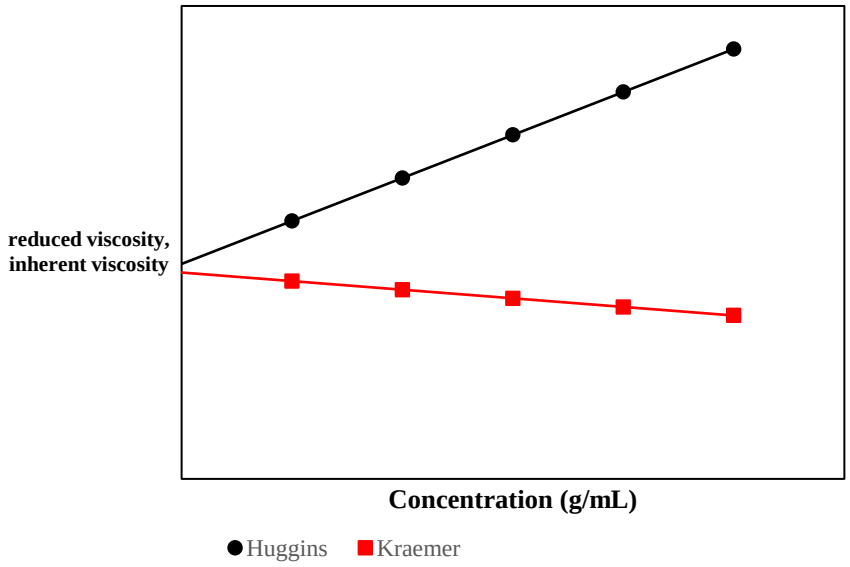

Figure 2. 10 Huggins and Kraemer extraction methods for intrinsic viscosity.

In practice, it is common to use [121-125] both Huggins and Kraemer formalisms in a dual Huggins-Kraemer plot, taking $[\eta]$ as the mean of the two intercepts on the ordinate (see Figure 2.10).

Measurement of the viscosities of surfactant solutions can be used to determine the hydration and asymmetry of the surfactant micelles. In the original treatment by Einstein, the viscosity is related to the volume fraction $\emptyset$, of dispersed spherical particles as:

$$\frac{\eta}{\eta_0} = 1 + F\emptyset \quad [2.12]$$

where η and η_0 are the viscosities of the solution and pure solvent. For a solution/dispersion of non-deformable, completely wetting non-interacting spherical particles (micelles), that are large in comparison with the molecule of the solvent, F takes the value 2.5 [126, 127].

As shown by Oncley [128], the volume fraction $\emptyset$ can be expressed in terms of the surfactant concentration c, the partial specific volume of the anhydrous surfactant $\bar{v}_1$, the hydration of the micelle (w gram of solvent bound by one gram of surfactant) and the density of solvent ρ_0:

$$\frac{\eta}{\eta_0} = 1 + 2.5\bar{v}_1 c(1 + \frac{w}{\bar{v}_1\rho_0}) \quad [2.13]$$

Polson later showed [129] that the specific viscosity $(\frac{\eta}{\eta_0} - 1)$ varied linearly with concentration only at very low surfactant concentration (<1% w/w) and so proposed that w could be more reliably determined by extrapolating a plot of $(\frac{\eta}{\eta_0} - 1)/c$ vs. concentration to infinite dilution. Simha [130, 131] also suggested that the parameter F could be expressed as a function of the axial ratio (v) when applied to ellipsoidal micelles. To conclude:

$$\lim_{c\to 0} = [\eta] = v\left(\bar{v}_1 + \frac{w}{\rho_0}\right) = v \cdot v_s \quad [2.14]$$

where v_s is the partial specific volume of the hydrated/swollen surfactant. The value of v can be used to predict the axial ratio via a polynomial function given by Simha [130, 131] if the shape of the micelle is known to be a prolate or oblate ellipsoid but generally, the Simha shape factor v is taken as 2.5 for most ellipsoidal micelles [132-134].

The partial specific volume of anhydrous surfactant $\bar{v}_1$ is usually determined by measuring the change in solution density as a function of concentration:

$$\rho = \rho_0 + c(1 - \bar{v}_1\rho_0) \quad [2.15]$$

with $\bar{v}_1$ obtained from the slope of the regression line:

$$\bar{v}_1 = \frac{1-slope}{\rho_0} \quad [2.16]$$

In cases where $\bar{v}_1$ is difficult to determine, Durchschlag and Zipper proposed an *ab – initio* method based on the additivity principle and the concept of atomic volume

increments [135]. By such means, the partial specific volume of the *i*th component is expressed as:

$$\bar{v}_i = \frac{\bar{V}_i}{M_i} \qquad [2.17]$$

where $\bar{V}_i$ is its partial molar volume and M_i is its molar mass. The partial molar volume is calculated from the volume increments with corrections applied for ionic and/or cyclic compounds as:

$$\bar{V} = \sum V_i + V_{CV} - \sum V_{RF} - \sum V_{ES} \qquad [2.18]$$

where $\sum V_i$ is the volume increment for a given atom or groups of atoms, V_{CV} is the covolume correction, and $\sum V_{RF}$ and $\sum V_{ES}$ are the volume decrements accounting for ring formation and ionization.

For ionic surfactant systems, where the solution viscosities measured in water are influenced by electro-viscous effects due to the charged head groups, the viscosity measurements can instead be performed in 0.2 M NaCl solution [136]. For nonionic surfactants, the intrinsic viscosities are much the same regardless of whether the measurements are made in water or in electrolyte solution [137].

2.3.2 Materials

4-cholesten-3-one (98+ %) was purchased from Alfa Aesar (Heysham, UK) and adrenosterone (97+ %) from Santa Cruz Biotechnology (Heidelberg, Germany).

Sodium dodecyl sulfate (SDS), dodecyl trimethylammonium bromide (DTAB) and N, N-dimethyldecylamine N-oxide (DDAO) were purchased from Sigma-Aldrich (Dorset, UK). N-dodecyl-N, N-dimethyl-3-ammonio-1-propanesulfonate (DDAPS) was obtained from MP Biomedicals LLC (Ohio, USA). Polyoxyethylene (23) lauryl ether (Brij 35) were obtained from MP Biomedicals LLC (Ohio, USA).

Ethanol was purchased from Sigma-Aldrich (Dorset, UK).

All chemicals were used as received.

2.3.3 Methods

Viscosity

The viscosities of the surfactant solutions were measured using a suspended-level (Ubbelohde, Schott-Geräte, Hofheim, Germany) viscometer immersed vertically in a thermostat controlled water bath (CT 1650, Schott-Geräte, Hofheim, Germany) maintained at 25 ± 0.1 ^{o}C. The flow times of solutions at a constant volume through a capillary tube were automatically recorded using an AVS 350 viscosity measurement unit (Schott-Geräte, Hofheim, Germany) with an accuracy of 0.01%.

Before the experiment, the viscometer was carefully rinsed with pure water and ethanol and dried by a stream of nitrogen gas. Approximately 15 mL of each test solution was transferred to the viscometer and the solution allowed to equilibrate for 5 minutes to the desired bath temperature. Flow times were measured at several concentrations (from high to low) and the dilutions of the surfactant solution within the Ubbelohde viscometer were performed using a programmable Visco Doser AVS 20 piston burette (Schott-Geräte, Hofheim, Germany).

Density

The densities of the surfactant solutions and solvent were measured with an Ostwald pycnometer (10 mL) maintained at 25 ± 0.1 ℃. The pycnometer was first filled with water and equilibrated in the water bath (RCT basic, IKA, Germany), and the filled mass corrected for the mass of the empty pycnometer, recorded as M_{H2O}.

The premade surfactant solution was then transferred into the same pycnometer (cleaned and dried), and after equilibrium the filled mass corrected for the mass of the empty pycnometer and recorded as M_s. The density (ρ_s) of the measured sample was then obtained as:

$$\rho_s = \frac{M_s}{M_{H2O}} \rho_{H2O} \qquad [2.19]$$

with ρ_{H2O} taken as 0.997 g/mL at 25 ^{o}C [138]. The measured sample was further diluted with solvent and the mass measured following the same procedures. Each measurement was repeated three times to ensure reproducibility.

2.3.4 Results

Surfactant solutions in the absence of steroids

In the present study, the intrinsic viscosity of the surfactant solutions [η] was taken as the average of the reduced viscosity (η_{sp}/c) and inherent viscosity ($\ln(\eta_{rel}/c)$) values extrapolated to zero concentration. The variations in the reduced and inherent viscosities of the surfactants as a function of concentration are presented in Tables A.3 to A.7 in Appendix A; the Huggins – Kraemer plots obtained from these data are shown in Figure 2.11, and the calculated intrinsic viscosities are summarized in Table 2.9. As discussed above, to correct for the electro-viscous effects of the ionic surfactants, the determination of viscosity was performed in 0.2 M NaCl solution. The [η] so obtained for the SDS and DTAB solutions were in good agreements with the value reported by others [87, 136].

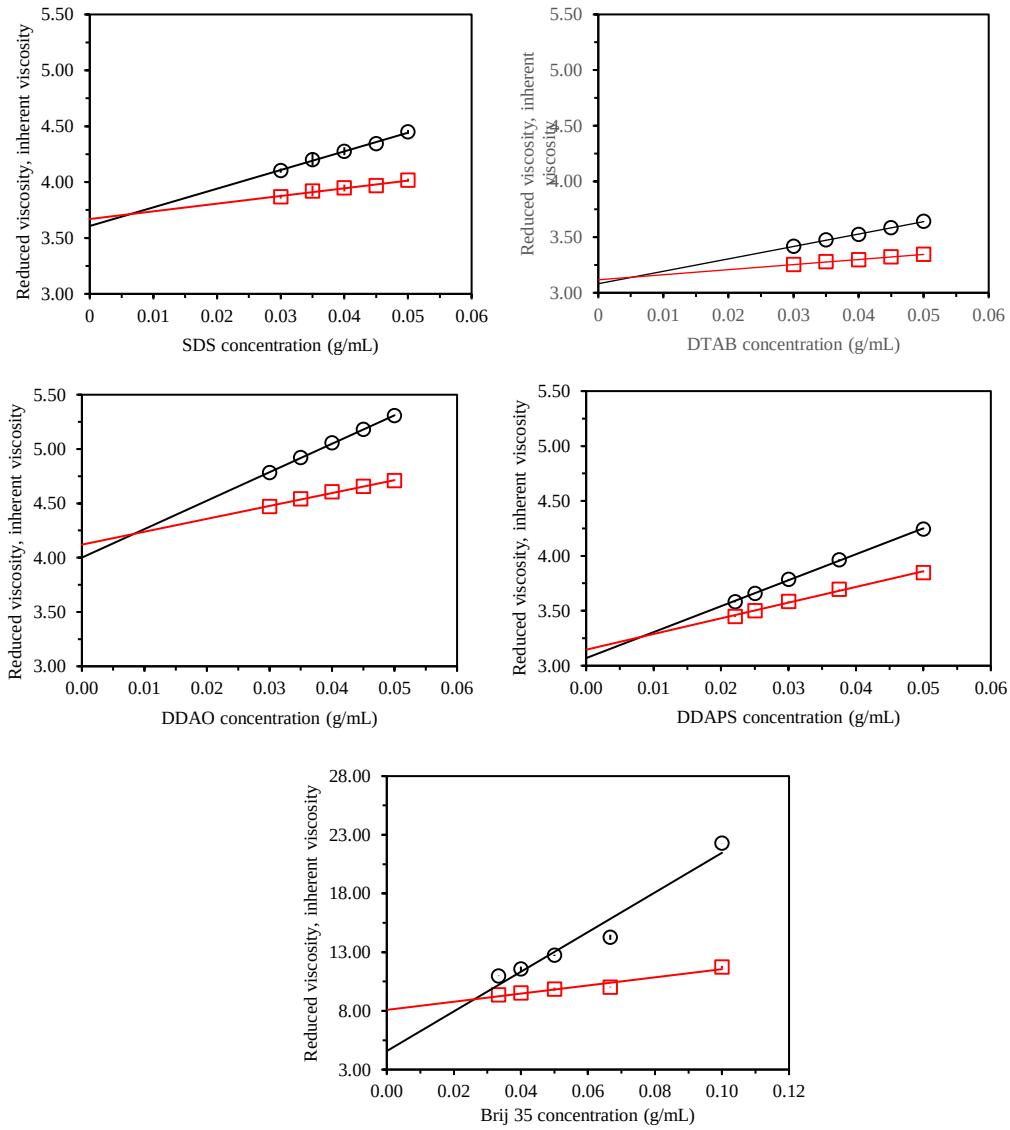

Figure 2. 11 Reduced and inherent viscosities of surfactant solutions as a function of surfactant concentration. Standard errors on the data are shown (n=3) but fall inside the plotted symbols.

The ionic surfactants (SDS and DTAB) and the zwitterionic surfactants (DDAO and DDAPS) show relatively similar [η] while the non-ionic surfactant Brij 35 has a much higher [η] (6.33 mL/g vs 3 – 4 mL/g). The increased [η] for Brij 35 is attributed to its much larger head groups and the fact that the ethylene oxide units in the head group provide more space for the mechanical trapping of water and hydrogen bonding. The change in nature of the head groups in the ionic surfactants is not expected to cause a significant change in size of their micelles and as expected causes little change in [η] [139].

To analyse the hydration of the surfactant micelles, the partial specific volume $\bar{v}_1$ of each surfactant was obtained using the *ab-initio* method [135]. The values of $\bar{v}_1$

obtained for SDS and DTAB were little different from those determined here through density measurements (SDS $\bar{v}_1$=0.867 vs 0.795 cm^3/g and DTAB $\bar{v}_1$ = 0.927 vs 0.933 cm^3/g respectively), and for all of the surfactants studied, the results generally accord with those reported in the literature [87, 135, 140, 141].

Table 2. 9 The intrinsic viscosity [η] of surfactant solution and the surfactant partial specific volume $\bar{v}_1$, molar volume V, hydration properties.

Surfactant	[η] (mL/g)	$\bar{v}_1$(cm^3/g)[a]	V ($Å^3$)[a]	H_2O/single SAA molecule	Hydration %
SDS	3.62 ± 0.07	0.795	380.8	9.2 ± 0.1	82.0
DTAB	3.13 ± 0.02	0.933	477.7	5.4 ± 0.1	54.1
DDAO	4.06 ± 0.07	1.110	422.6	6.6 ± 0.1	74.1
DDAPS	3.11 ± 0.04	0.960	534.7	5.3 ± 0.0	47.2
Brij 35	6.33 ± 1.77	0.892	1774.2	109.2 ± 1.8	69.7

a: values calculated *ab-initio* [135]

Many early studies of aqueous surfactant studies concluded that surfactant micelles are heavily hydrated, with 4 – 10 water molecules bound per surfactant molecules, and with the total number of the bound waters accounting for almost half the total volume of a micelle [142-144]. In the micelles formed by ionic surfactants, water molecules can readily insert between their relatively small head groups and are tightly bound through charge-dipole interactions. The hydration number obtained here for SDS falls within the range 7 – 12 reported by Tokiwa et al. [132] and also agrees with the result presented by Lindman et al. [145].

Likewise, for the cationic surfactant DTAB, the hydration number determined here (5.4 ± 0.1 H_2O/molecule) agrees with the result presented by Griffiths et al. [146], who reported a hydration of 54% determined through electron paramagnetic resonance experiments. Griffiths et al suggested [146] that water molecules were displaced from the polar shell due to the larger size of the Br^- / DTA^+ head group by comparison with the sulfate headgroup of SDS and that this lead to the lower hydration of DTAB compared with SDS.

The calculated hydration of 6.6 ± 0.1 H_2O per DDAO molecules in much lower than the 10 H_2O/molecules reported by Courchene [140], but does accord with the values later reported by Barlow et al. (4 – 8 H_2O/molecules; [141]) and Lorenz et al. (~8 H_2O/molecules; [147]).

The hydration of 5.3 H_2O/molecule here for DDAPS is a little lower than the 6 – 7 H_2O/molecule reported by La Mesa et al. [148] on the basis of their nuclear magnetic resonance (NMR) measurement, and the hydration of 4.8 H_2O/EO unit determined here for Brij 35 is rather higher than was reported by Tanford et al. [149] (2.5 – 3.3 H_2O/EO) but close to the value (of ~4 H_2O/EO) reported by Shikata et al. [150].

Surfactant solutions in the presence of steroids

The intrinsic viscosities of SDS, DTAB and DDAPS micelle solutions in the presence of 4-cholesten-3-one (4-CHOL) and adrenosterone (ADRENO) were determined and the Huggins-Kraemer plots are shown in Figure 2.12. (The concentration-dependent variations in the reduced and inherent viscosities of these systems are presented in Tables A.8 – A.13 in Appendix A). As can be seen, the presence of steroids in the surfactant micelles causes an increase in the intrinsic viscosities. The densities of the solutions, however, did not change significantly (see Table A.14, in Appendix A).

The extent of the increase in [η] in the presence of steroids seems dependent on the level of steroid solubilisation within the micelle. The solubilisation capacity of SDS for 4-CHOL was much higher than was found for ADRENO (Chapter 2.1) and so 4-CHOL causes a greater increase in [η] relative to that for SDS alone (vis, 30% vs 5%). Likewise, because the solubilisation capacities of DTAB micelles for 4-CHOL and ADRENO were far less than were found for SDS, the resulting changes in [η] caused by steroids were much smaller.

Interestingly, although the solubilisation capacity of DTAB for 4-CHOL was found to be 3-fold higher than for ADRENO, the [η] of DTAB micelles saturated with 4-CHOL was slightly lower than with ADRENO (3.30 ± 0.05 mL/g and 3.44 ± 0.10 mL/g for ADRENO/DTAB micelles and 4-CHOL/DTAB micelles, respectively). The likely reason for the reverse trend can be explained by the low solubility of 4-CHOL in DTAB micelles at low concentration (see section 2.1).

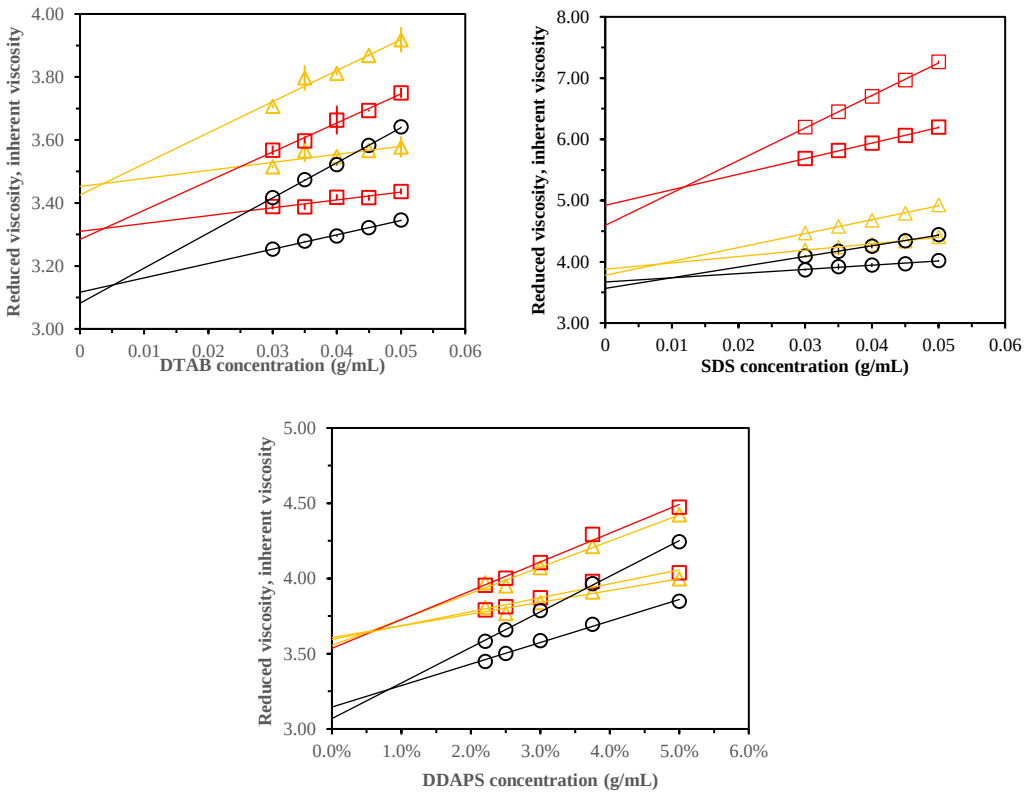

Figure 2. 12 Reduced and inherent viscosity of surfactant/steroid solutions as a function of surfactant concentration (○: pure surfactant system, □: surfactant system saturated with 4-cholesten-3-one, △: surfactant system saturated with adrenosterone). Standard errors are shown (n = 3) but fall inside the plotted symbols.

The intrinsic viscosities of DDAPS micelles in the presence of 4-CHOL and ADRENO did not show noticeable differences. The solubilities of 4-CHOL and ADRENO in DDAPS micelles at concentrations below 5 wt% were found to be very similar (see section 2.1), and the intrinsic viscosities of DDAPS micelles in the presence of these two steroids show little difference (both ~3.6 mL/g).

Saturation of the surfactant micelles with the steroids, however, leads to a higher level of hydration (Table 2.10). This might be because the shape factor ν used in equation 2.14 was assumed to be 2.5, with the assumption that the micelles were spherical. If the micelles are not spherical, however, the value of 2.5 used for ν might not be appropriate. With steroids solubilised in the surfactant micelles, the increased intrinsic viscosities would suggest larger micelles which in turn might suggest that the aggregates could become more rod-like, and so the shape factor ν would then be higher than 2.5. The value of the shape factor to be used in calculating the micelle hydration cannot be determined from the experiments detailed here, but the calculated values of

micelle hydration are nevertheless of use in guiding the model-fitting of small angle neutron scattering data (as presented in Chapter 4).

Table 2. 10 The intrinsic viscosity [η] and hydration properties for surfactant micelles in the presence and absence of 4-cholesten-3-one and adrenosterone. (n=3)

Surfactant	[η] (mL/g)	H_2O/single SAA molecule	Hydration %[b]
SDS	3.62 ± 0.07	9.2	82.0
SDS + 4-cholesten-3-one	4.76 ± 0.17	16.7	89.2
SDS + adrenosterone	3.83 ± 0.05	10.6	84.0
DTAB	3.13 ± 0.02	5.4	54.1
DTAB + 4-cholesten-3-one	3.30 ± 0.05	6.8	59.9
DTAB + adrenosterone	3.44 ± 0.10	7.7	62.8
DDAPS	3.11 ± 0.04	5.3	47.2
DDAPS+ 4-cholesten-3-one	3.57 ± 0.06	8.7	59.5
DDAPS+ adrenosterone	3.58 ± 0.13	8.8	59.8

b: calculated assuming a Simha shape factor, ν = 2.5

2.3.5 Conclusions

The measurement of the surfactant intrinsic viscosities and densities have been used to determine the hydration of the C_{12}-chain surfactant micelles. The hydration number of the non-ionic surfactant, Brij 35 was the largest due to its large, EO-containing, head group.

The anionic surfactant SDS has a relatively higher hydration compared with the other surfactants studied (Table 2.11). The hydration of ionic surfactant head groups also has been determined by Allen et al. [151]. They investigated surfactants with a C_{12} hydrocarbon chain and DS^- head group but bound with different counterions and found that although the micelle size did not change with a change in counterion, the hydration of the head group did change. With counterions that more strongly bound to the head group, the head group became less heavily hydrated.

The presence of steroids in the micelles did not change the density to a large extent, however, the intrinsic viscosity changed significantly and was shown to be dependent on the solubility of steroids in the micelles.

From the solubilisation measurements performed here, the poorly water-soluble steroids 4-cholesten-3-one (4-CHOL) and adrenosterone (ADRENO) both have the lowest solubilities in dispersions of the non-ionic surfactant, Brij 35, and this may be because of the large number of waters bound to the surfactant head groups, which could perhaps hinder entry of the steroids into the micelle interior.

Given that the Simha shape factor for ellipsoidal micelles, ν, is a function of their semi-axis dimensions, it can be used – if determined independently – to predict the axial ratios of micelles. It is generally taken to be 2.5 for surfactant micelles [140, 152, 153], and increased values of ν indicate higher axial ratios. It is not possible, however, to use ν to distinguish whether a surfactant's micelles are prolate or oblate.

On the basis of the solubilisation and surface tension studies it can be concluded, therefore, that the ideal surfactant for solubilising 4-CHOL and ADRENO should either be an ionic surfactant and/or have a relatively small number of water molecules hydrating the polar head group. More detailed insights into the influence of the structural features of surfactants on the structures and properties of their micelles (in

the presence and absence of steroids) are afforded through small angle neutron scattering studies, and these are reported in Chapter 4.

Table 2. 11 Summary of the results obtained from solubilisation (solubilisation capacity, S_{cap}), surface tensiometry (the critical micelle concentration, CMC and area per surfactant molecule, α_1^s), number of water molecules per surfactant head group (H_2O / SAA), hydration value (% H_2O) and solubilisation capacity (S_{cap}^*)

	CMC ± 0.02 wt%	α_1^s ± 3 Å^2	H_2O / SAA (± 3.3)	% H_2O	S_{cap}^* 4-CHOL	S_{cap}^* ADRENO
SDS	0.23	70	9.3	82	1	1
ADS	0.18	60	6.6 [a]	70 [a]	2	3
LDS	0.26	75	7.3 [a]	53 [a]	3	2
DTAB	0.43	55	5.6	55	4	5
DDAPS	0.078	49	5.3	47	7	4
DPC	0.056	55	7.6 [b]	55 [b]	8	6
DDAO	0.032	40	6.6	74	5	7
Tween 20	0.0078 [b]	110 [b]	61.8 [b]	56 [b]	6	8
Brij 35	0.0057 [b]	70 [b]	109.1	70	9	9

S_{cap}^* Solubilisation capacity (g/g) expressed as a rank order, where 1 presents the best solubilizer and 9 presents the worst.

[a] determined by Allen et al. [151]

[b] determined by Saaka [87]

Chapter 3

Neutron reflectivity

3.1 Introduction

Neutron reflectometry allows the study of thin film structure on the sub-nanometre length scale and is a non-destructive and non-invasive technique that has been extensively used in the study of the structure and behaviour of surfaces and interfaces in soft matter systems since the mid-1980s.

Lu et al. [154] have reviewed the used of the technique in investigations of surfactant/mixed surfactant adsorption at the air-water interface showing how it can be used to reveal the surface excess, and the organisation thickness and composition of the adsorbed layers.

The applications of neutron reflectivity in studies of the adsorption of surfactant and mixed surfactant systems at the liquid-solid interface have been widely reported [155-158]. A more general review of the applications of the technique and a perspective on recent progress has been provided by Penfold and Thomas [155, 159].

3.1.1 The specular neutron reflection technique

Neutrons are reflected from the interface between media of differing refractive index in the same way as light, and the intensity of the specular reflected beam is measured as a function of wave vector transfer in the perpendicular direction (Q_z). Q_z varies according to the glancing angle (θ) and the radiation wavelength (λ) as:

$$Q_z = \frac{4\pi sin\theta}{\lambda} \qquad [3.\ 1]$$

The neutron reflectivity measurement can either be made keeping the wavelength of the neutron beam, λ, constant and then varying the angle of incidence, θ, or else by selecting a constant θ while varying λ.

The neutron refractive index is the ratio of the wave vectors inside and outside at the interface (Figure 3.1). The refractive index of a material against vacuum can be expressed as:

$$n = 1 - \lambda^2 \frac{Nb}{2\pi} \qquad [3.\ 2]$$

where N is atomic number density, and b is bound scattering length of the material.

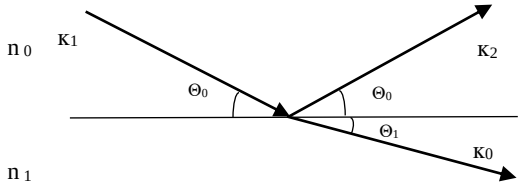

Figure 3. 1 Interface between two bulk media of refractive index n_0 and n_1 showing the incident (k_1) and reflected waves (k_2) at angel θ_0 and the transmitted wave of angel θ_0 (k_o).

For most materials, n is less than 1, and so total external reflection can be observed, with Snell's law giving the critical glancing angle (θ_c) under which the total reflection would occur. At the air-water interface, given that the refractive index of air is very close to 1, θ_c is obtained as:

$$\theta_c = \lambda \sqrt{\frac{\rho}{\pi}} \qquad [3.\ 3]$$

where ρ refers to the scattering length density of the material at the interface.

When $\theta \leq \theta_c$, R = 1 and for $\theta \geq \theta_c$, the reflectivity (R) is given by Fresnel's law as:

$$R = \left| \frac{n_0 sin\theta_0 - n_1 sin\theta_1}{n_0 sin\theta_0 + n_1 sin\theta_1} \right|^2 \qquad [3.\ 4]$$

For a uniform thin film with a thickness d (Figure 3.2), the incident neutron beam will be partially transmitted and partially reflected, and analysis of the specular reflectivity can either be performed using an exact optical matrix method, or the kinematic (Born) approximation method. In the neutron reflectivity studies reported here, the data were modelled using the optical matrix methodology, as explained below. For details of the kinematic analysis methodology, the reader is referred to Lu et al. [160].

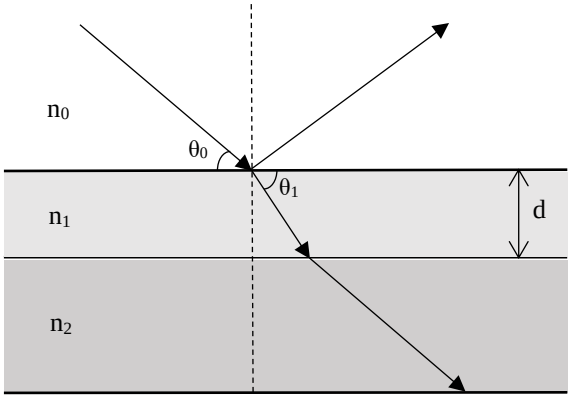

Figure 3. 2 Interfacial film of thickness, d, and refractive index n_1 separating bulk media of refractive index, n_0 and n_2 showing the angle of incident (θ_0) and refraction (θ_1) for neutrons incident on the film

For a uniform layer of material of thickness d at the interface between two bulk media with refractive index n_0 and n_2, the reflectivity can be expressed using the standard optical method as:

$$R = \left|\frac{r_{01}+r_{12}e^{2i\beta}}{1+r_{01}r_{12}2i\beta}\right|^2 \quad [3.\ 5]$$

where r_{ij} is the Fresnel coefficient at the interface ij:

$$r_{ij} = \frac{p_i - p_j}{p_i + p_j}, \quad [3.\ 6]$$

and $p_i = n_i sin\theta_i$, and the optical path length in the film $\beta = (2\pi/\lambda)n_1 d sin\theta_1$.

The reflectivity for a system including several interfacial layers is generally calculated using the optical matrix method [161]. For each layer j in such a film, this standard method gives a characteristic matrix by applying the condition that the wave functions and their gradients are continuous across the layer boundaries:

$$M_j = \begin{bmatrix} cos\beta_j & -\left(\frac{i}{p_j}\right)sin\beta_j \\ -ip_j sin\beta_j & cos\beta_j \end{bmatrix} \quad [3.\ 7]$$

The resulting reflectivity for a system comprising n layers is then obtained from the characteristic matrices $M_R = [M_1]\,[M_2]\,\ldots\,[M_n]$ for n layers, as:

$$R = \left|\frac{(M_{11}+M_{12}p_s)p_a-(M_{21}+M_{22})p_s}{(M_{11}+M_{12}p_s)p_a+(M_{21}+M_{22})p_s}\right|^2 \quad [3.\ 8]$$

In this study, the NR profiles were analysed by the optical matrix method using MOTOFIT software [162]. The main features of interest for surfactant monolayers adsorbed at the air-water interface include the thickness of the film, surface coverage,

relative position of the surfactant head and chain groups, and the level of solvent penetration. For the surfactant systems in the absence of steroid, the thickness of the monolayer (d), the surface excess concentration (Γ_{SAA}) and the limiting area per molecule (a_1^s) were determined. For the systems with steroid incorporated in the monolayer (4-cholesten-3-one or adrenosterone), the volume fraction (V_f) of steroid was also determined.

3.2 Experimental details

3.2.1 Materials

Sodium dodecyl sulfate (SDS), ammonium dodecyl sulfate (ADS), lithium dodecyl sulfate (LDS), dodecyl trimethylammonium bromide (DTAB) and N, N-dimethyldecylamine N-oxide (DDAO), N-dodecyl-N, N-dimethyl-3-ammonio-1-propanesulfonate (DDAPS) were purchased from Sigma (Dorset, UK) and dodecyl phosphocholine (DPC) was obtained from Avanti Polar Lipids (Alabama, USA)

Alkyl chain deuterated d_{25}SDS, d_{25}ADS, d_{25}LDS, d_{25}DTAB, d_{25}DDAO and d_{25}DDAPS were kindly provided by the Oxford Deuteration Facility (Didcot, UK). d_{38}DPC was obtained from CDN Isotopes (New Jersey, USA)

4-cholesten-3-one (98+%) was purchased from Alfa aesar (Thermo fisher Scientific, UK) and adrenosterone (97+%) from Santa cruz (Germany).

n-Hexane was from Fisher Scientific (Loughborough, UK) and D_2O (99.9 atom % D) was supplied by Oxford Deuteration Facility (Didcot, UK).

3.2.2 Sample preparation

Each surfactant and surfactant/steroid system was studied using four isotopic contrasts: h_{25}SAA (protiated surface-active agent) in D_2O; h_{25}SAA in air contrast matched water (8.1 % D_2O/91.9 % H_2O by volume; ACMW); d_{25}SAA (alkyl chain deuterated surfactant) in D_2O; d_{25}SAA in ACMW. All solutions for the study were prepared at the concentrations required for the reflectivity measurement.

For surfactant/steroid systems, excess steroid was added into the surfactant micellar solution and left on a rotary wheel for 7 days until equilibrium was achieved. Excess steroid was then removed by filtration through a 0.2 μm filter. For surfactant/steroid samples prepared at surfactant concentrations below the surfactant CMC, the solutions were prepared using the solvent pre-saturated with steroid.

3.2.3 Neutron reflectometry

Neutron reflectivity measurements on the monolayers adsorbed at the surface of surfactant micellar solutions in the presence and absence of saturating levels of 4-cholesten-3-one (4-CHOL) or adrenosterone (ADRENO) were made in time-of-flight mode using the FIGARO reflectometer at ILL (Grenoble, France) and INTER at ISIS (Didcot, UK). At FIGARO, neutrons of wavelength (λ) 2-25 Å were selected and data collected at fixed incident angles $\theta = 0.62^{\circ}$ and 3.8° with a Q_z resolution of 7%. At INTER, the θ were at 0.8° and 2.3° with a resolution Q_z of 5.5% and neutrons were selected with wavelengths (λ) from 2 to 30 Å. The background scattering was subtracted from the data obtained at FIGARO but not for the data obtained at INTER.

The procedure for each measurement was the same. The prepared sample was poured into a 5 cm x 22 cm Teflon trough. The height of trough with the sample was aligned automatically using a laser, and the trough was then covered with a lid before measuring. To ensure the surface was equilibrated, a kinetic run was first determined until the structure of the air-water interface became stable. Most of the samples reached equilibrium within 30 minutes. In some cases, the surface equilibrium was achieved after a much longer time. After each measurement, the height of each sample was aligned again to make sure the evaporation effect was not significant.

Hexane containing steroid was spread onto the interface after the measurement for each sample and left for at least 20 minutes to make sure the hexane had fully evaporated before measuring again.

3.2.4 NR data fitting

The fitting of neutron reflectivity data is most commonly carried out using the optical matrix method, but there have been no systematic studies conducted to aid, for example in selecting an appropriate choice of surface roughness or number of layers to include, with most workers adopting an *ad hoc* strategy that they consider appropriate to the system studied. Recently, however, Campbell et al. [163] have proposed a robust model for the fitting of neutron reflectivity data, suggesting to split the adsorbed layer into separate layers, but with the layer roughness treated as conformal, and constraints applied to ensure that the volume fractions of the surfactant chains and head groups within the separate layers sum to unity. With such constraints,

the number of free-fitted parameters is minimized. In this study, the fitting of the reflectivity data was performed according to this approach.

To fit the obtained profiles, the surfactant monolayer was divided into two layers. Layer 1 consists of the hydrophobic chain groups and layer 2 contains the hydrophilic head groups. When the monolayer was saturated with 4-CHOL or ADRENO, the steroid molecules were assumed to insert with layer 1 (Model 1), or layer 2 (Model 2), or to insert beneath layer 2 in the subphase (Model 3)

Table 3. 1. The assumptions made in models 1-3 regarding the locations of the steroids in relation to the surfactant monolayer formed at the air-water interface

	Model 1	Model 2	Model 3
Layer 1	SAA_{tail} + steroid	SAA_{tail}	SAA_{tail}
Layer 2	SAA_{head}	SAA_{head} + steroid	SAA_{head}
Layer 3	/	/	steroid

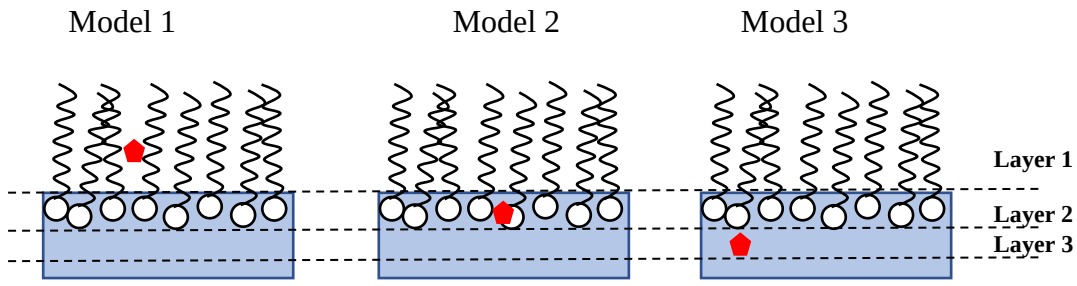

Figure 3. 3 Schematics showing the different interfacial layer structures assumed in modelling the NR data for surfactant monolayers in the presence of steroid (⬟)

Due to the similar neutron scattering length density between the protiated surfactant and steroids, neutrons could not distinguish between the steroids and surfactant molecules. Thus the neutron reflectivity profile for contrasts with h_{25}SAA show little change in the presence of steroids and yield little information. The difference in the neutron reflectivity profiles of the monolayers of deuterated surfactants in the presence and absence of steroids is more pronounced, and the d_{25}SAA/ACMW contrast gives more information about the thickness of the monolayer while the d_{25}SAA/D_2O contrast is more sensitive to solvent penetration. For all of the systems studied all four contrasts (involving protiated and deuterated surfactant on ACMW and D_2O) were

used to fit the reflectivity data, but only the two contrasts involving deuterated surfactant are presented here.

Likewise, instead of fitting the full Q-range of the neutron profiles, different regions were fitted according to their sensitivity to changes in specific fitted parameters. For the d_{25} SAA/ACMW neutron profile, the experimental data within the Q-range 0.05-0.10 $Å^{-1}$ were fitted, while for d_{25} SAA/D_2O data, a high Q-range between 0.10-0.15 $Å^{-1}$ was refined.

The variable parameters in the global fit of each layer included the layer thickness (d), roughness (σ) and neutron scattering length density (ρ). The scattering length density was calculated from the scattering lengths and molecular volumes as given in Table 3.2. As reported by Fullagar et al. [164], the interfacial roughness of both layer 1 and layer 2 was fixed at 4 Å.

A quantitative assessment of the fit between the calculated and observed NR profile was obtained as [163]:

$$\boldsymbol{\chi^2} = \frac{1}{N-N_p}\sum_{i=1}^{N}\frac{\left(R_{exp}(Q_{Z,i})-R_{theo}(Q_{Z,i})\right)^2}{\varepsilon_i^2} \qquad [3.\ 9]$$

where N is the number of experimental points and N_p is the number of free parameters, R_{exp} and R_{theo} are the experimental and theoretical reflectivity values. Note that χ^2 is a measure of the difference between the calculated curve and the error bars, and not the difference between the observed and calculated data points.

Table 3. 2 The chemical formulae, scattering length densities (ρ), scattering lengths (b) and molecular volume (V_m) for each surfactant and steroid.

Chemical	Molecular formula	ρ (x 10^{-6} Å^{-2})		b_c (x 10^{-5} Å)		V_m (Å^3)
		h_{25}	d_{25}	h_{25}	d_{25}	
4-cholesten-3-one	$C_{27}H_{44}O$	0.34	N/A	20.80	N/A	/
Adrenosterone	$C_{19}H_{24}O_3$	1.27	N/A	54.01	N/A	/
DTAB	$C_{15}H_{34}BrN$	-0.23	5.08	-11.24	249.05	489.9
TAB	C_3H_9BrN	0.18	N/A	2.46	NA	136.2
DPC	$C_{17}H_{38}NO_4P$	0.16	7.53	8.64	404.28	536.7
PC	$C_5H_{13}NO_4P$	1.22	8.62	22.34	148.32	183.0
DDAO	$C_{14}H_{31}NO$	-0.18	6.04	-7.67	252.62	422.4
DAO	C_2H_6NO	0.88	N/A	6.03	N/A	68.7
DDAPS	$C_{17}H_{37}O_3SN$	0.08	4.98	4.25	264.54	531.4
DAPS	$C_5H_{12}O_3SN$	1.01	N/A	17.95	N/A	177.7
SDS	$NaC_{12}H_{25}SO_4$	0.39	6.66	15.94	276.22	414.4
SS	$NaSO_4$	4.89	N/A	29.65	N/A	60.7
ADS	$NH_4C_{12}H_{25}SO_4$	0.13	6.42	6.72	267.01	414.8
AS	NH_4SO_4	3.35	N/A	20.42	N/A	61.1
LDS	$LiC_{12}H_{25}SO_4$	0.26	6.64	14.31	274.60	417.7
LS	$LiSO_4$	4.40	N/A	28.02	N/A	64.0
Dodecyl	$C_{12}H_{25}$	-0.39	6.95	-13.70	246.59	353.7

3.2.5 Modelling parameters

If an adsorbed surfactant monolayer is treated as a single uniform layer, the surface excess of the adsorbed species (i), Γ is obtained as:

$$\Gamma_i = \frac{1}{N_A a i} = \frac{\rho_i \times d_i}{\sum b_i \times N_A} \quad [3.\ 10]$$

where $a_i, \sum b_i$ and ρ_i are the area per molecule, scattering length and scattering length density of species, d is the layer thickness, and N_A is Avogadro's number. If the adsorbed layers include more than one species, Γ_i is given by:

$$\Gamma_i = \frac{\rho_i \times d_i \times V_{f,i}}{\sum b_i \times N_A} \quad [3.\ 11]$$

$V_{f,i}$ is the volume fraction of species *i* in the layer and the volume fraction of solvent in the layer, V_s is obtained as:

$$V_s = (1 - V_{f,i} - V_{f,j}) \times 100 \quad [3.\ 12]$$

And if there is no solvent in the layer:

$$V_{f,i} + V_{f,j} = 1 \quad [3.\ 13]$$

Model 1

For Model 1 the adsorbed monolayer was taken to comprise two layers. Layer 1, the upper layer (on the air side of the interface) was taken to involve surfactant hydrocarbon chains and any added steroid, with no solvent. Layer 2, the lower layer (on the aqueous subphase side of the interface) was taken to involve surfactant hydrophilic head groups and solvent.

For layer 1, given that $v_s = 0$, the scattering length density ρ_1 thus taken as:

$$\rho_1 = \rho_{SAA\_tail} \times V_{f,\ SAA\_tail} + \rho_{steroid} \times V_{f,\ steroid} \quad [3.\ 14]$$

and

$$V_{f,\ SAA\_tail} + V_{f,\ steroid} = 1 \quad [3.\ 15]$$

Combining equations 3.14 and 3.15, the volume fraction for each species is:

$$V_{f,\ SAA\text{-}tail} = \frac{\rho_1 - \rho_{steroid}}{\rho_{SDS\_tail} - \rho_{steroid}} \quad [3.\ 16]$$

$$V_{f,\ steroid} = \frac{\rho_{SDS\_tail} - \rho_1}{\rho_{SDS\_tail} - \rho_{steroid}} \quad [3.\ 17]$$

and the surface excess for the surfactant tail region and steroid in layer 1 are obtained as:

Surface excess of tail (Γ_{SAA_tail}) = $\frac{\rho_{SAA\_tail} \times d_1 \times V_{f,tail}}{\Sigma b_{SAA\_tail} \times N_A}$

$$= \frac{\boldsymbol{\rho_{SAA\_tail} \times d_1 \times (\rho_1 - \rho_{steroid})}}{\boldsymbol{\rho_{SAA\_tail} \times N_A \times (\rho_{SDS_{tail}} - \rho_{steroid})}} \quad [3.\ 18]$$

Surface excess of steroid ($\Gamma_{steroid}$) = $\frac{\rho_{steroid} \times d_1 \times V_{f,steroid}}{\Sigma b_{steroid} \times N_A}$

$$= \frac{\boldsymbol{\rho_{steroid} \times d_1 \times (\rho_{SDS\_tail} - \rho_1)}}{\boldsymbol{\Sigma b_{steroid} \times N_A \times (\rho_{SDS\_tail} - \rho_{steroid})}} \quad [3.\ 19]$$

For layer 2, d_2 was fixed and $\rho_2 = \rho_{SAA\_head}$. Since $\Gamma_{SAA\_tail} = \Gamma_{SAA\_head} = \Gamma_{SAA}$,

$$V_{f,\ SAA\_head} = \frac{\boldsymbol{\Gamma_{SAA\_tail} \times \Sigma b_{SAA\_head} \times N_A}}{\boldsymbol{\rho_{SAA\_head} \times d_2}} \quad [3.\ 20]$$

and $V_{s,2} = (1 - V_{f,\ SAA\_head}) \times 100$ [3. 21]

In model fitting the NR data assuming model 1, the only parameters fitted were thus d_1 and ρ_1, and $V_{s,2}$ was constrained to satisfy equation 3.12.

Model 2

For model 2, the added steroid molecules were assumed to reside in layer 2, the surfactant head group layer. Layer 1 was taken to involve surfactant, with $\rho_1 = \rho_{SAA\_tail}$, $V_{s,1}=0$. The surface excess of surfactant was obtained as:

$$\Gamma_{SAA\_tail} = \Gamma_{SAA} = \frac{\boldsymbol{\rho_{SAA\_tail} \times d_1}}{\boldsymbol{\Sigma b_{SAA\_tail} \times N_A}} \quad [3.\ 22]$$

Layer 2 was taken to include the surfactant head groups, the added steroid and solvent, with:

$$V_{f,\ SAA\_head} = \frac{\boldsymbol{100 - V_{s,2}}}{\boldsymbol{100}} \times \frac{\boldsymbol{\rho_2 - \rho_{steroid}}}{\boldsymbol{\rho_{SAA\_head} - \rho_{steroid}}} \quad [3.\ 23]$$

$$V_{f,\ steroid} = \frac{\boldsymbol{100 - V_{s,2}}}{\boldsymbol{100}} \times \frac{\boldsymbol{\rho_{SAA\_head} - \rho_1}}{\boldsymbol{\rho_{SAA\_head} - \rho_{steroid}}} \quad [3.\ 24]$$

and the surface excess for the surfactant head groups obtained as:

$$\Gamma_{SAA\_head} = \frac{\rho_{SAA\_head} \times d_2 \times V_{f,\ SAA\_head}}{\Sigma b_{SAA\_head} \times N_A} = \frac{\rho_{SAA\_head} \times (\rho_2 - \rho_{steroid}) \times d_2 \times (100 - V_{s,2})}{\Sigma b_{SAA\_head} \times (\rho_{SAA\_head} - \rho_{steroid}) \times N_A \times 100} \quad [3.\ 25]$$

Given the constraint then that $\Gamma_{SAA} = \Gamma_{SAA\_head}$, the volume fraction of solvent in layer 2, $V_{s,2}$ is obtained as:

$$V_{s,2} = 100 - \frac{\rho_{SAA\_tail} \times d_1 \times \Sigma b_{SAA\_head} \times (\rho_{SAA\_head} - \rho_{steroid})}{\rho_{SAA\_head} \times d_2 \times \Sigma b_{SAA\_tail} \times (\rho_2 - \rho_{steroid})} \times 100 \quad [3.\ 26]$$

In model fitting assuming model 2, d_1 and ρ_2 were fitted, with $V_{s,2}$ constrained as above. The fitting process was repeated until the minimum χ^2 was obtained with input value $V_{s,2}$. The surface excess of steroid was obtained as:

$$\Gamma_{steroid} = \frac{\rho_{steroid} \times d_1 \times (\rho_{SAA\_head} - \rho_1) \times (100 - V_{s,2})}{\Sigma b_{steroid} \times N_A \times (\rho_{SAA\_head} - \rho_{steroid}) \times 100} \quad [3.\ 27]$$

Model 3

For model 3, the adsorbed layer was taken to consist of three layers. Layer 1 was taken to involve the surfactant hydrocarbon chains as in model 2. Layer 2 was taken to include the surfactant head groups and solvent. Layer 3 – a layer assumed to lie underneath Layer 2 – was taken to contain the added steroid and solvent.

The surface excess of surfactant was obtained as in model 2:

$$\Gamma_{SAA\_tail} = \Gamma_{SAA} = \frac{\rho_{SAA\_tail} \times d_1}{\Sigma b_{SAA\_tail} \times N_A} \quad [3.\ 28]$$

In layer 2 there is only one specie present, the surfactant head groups, and so $\rho_2 = \rho_{SAA\_head}$, and $V_{s,2}$ is obtained as:

$$V_{s,2} = 100 - 100 \times \frac{\rho_{SAA\_tail} \times d_1 \times \Sigma b_{SAA\_head}}{\rho_{SAA\_head} \times d_2 \times \Sigma b_{SAA\_tail}} \quad [3.\ 29]$$

For model 3 the model fitting was performed taking the fitted parameters as d_1 and $V_{s,3}$, with $V_{s,2}$ constrained to satisfy equation 3.29. The thickness of layer 3 (d_3) was taken as fixed at 4 Å. For the surface excess of steroid:

$$\Gamma_{steroid} = \frac{\rho_{steroid} \times d_3 \times (100 - V_{s,3})}{\Sigma b_{steroid} \times N_A \times 100} \quad [3.\ 30]$$

3.3 Results

3.3.1 Characteristics of the C_{12} surfactant monolayers in the absence of steroid

Neutron reflectivity (NR) studies were performed for the various C_{12} surfactant monolayers adsorbed at the air-water interface. The studies were carried out using surfactant concentrations both below and above the CMC. The NR profiles obtained were analysed using a simple 2-layer model in which the adsorbed surfactant monolayer was partitioned with the C_{12}-chains in one layer and the hydrated surfactant head groups in a second layer.

Figure 3.4 shows the NR profiles obtained for SDS monolayers, with concentrations of SDS at 0.5, 1.5 and 2 times the CMC (with the CMC for SDS taken as 0.23 wt%). It can be seen here that while the scattering curves obtained for d_{25}SDS adsorbed on a sub-phase of D_2O show no significant change with changing surfactant concentration, this is not true for the profiles obtained for d_{25}SDS on ACMW. For the d_{25}SDS/ACMW monolayers there is a significant difference between the NR profiles obtained for surfactant concentrations above and below the CMC, but no significant change in the profiles obtained for concentrations above the CMC.

Modelling of these data gave the best-fitted structural parameters summarized in Table 3.3. As would be expected (and wholly consistent with the surface tension measurements presented earlier, see section 2.2), these results show that the adsorbed SDS monolayer is not fully saturated when the surfactant concentration is below its CMC. At this concentration the SDS molecules are less tightly packed, and so they occupy a larger interfacial area (48 ± 2 $Å^2$ vs. 40 ± 2 $Å^2$) and give rise to a slightly thinner alkyl chains layer (7.5 ± 0.3 Å vs. 9.0 ± 0.3 Å). The results are broadly consistent with those presented by Lu et al. [160] who reported an interfacial area for SDS (at a concentration of 3 x CMC) of 44 ± 4 $Å^2$ and noted changes in monolayer thickness of the order of 1 Å with SDS concentrations varied between 0.13 and 1.3 x CMC. The results obtained here are also in agreement with those presented more recently by Yanez Arteta et al. [165] who reported a C_{12} layer thickness of 11 ± 3 Å with an SDS concentration of 1.2 x CMC.

Table 3. 3 Model-fitted structural parameters for SDS monolayers

SDS (x CMC)	d_{tail} (± 0.3 Å)	$V_{f\ H2O}$ (± 1%)	Γ_{SAA} (± 0.1 x10^{-10} mol. cm^{-2})	α (± 2 $Å^2$)
0.5	7.5	68	3.5	48
1.5	9.0	62	4.2	40
2.0	9.0	62	4.2	40

NR measurements performed to determine the structures of the monolayers formed at the air-water interface by the related anionic surfactants ADS and LDS showed the same concentration-dependent changes as seen with SDS (see Figure 3.5), with the interfacial area per molecule decreasing and the alkyl chains layer thickness increasing as the surfactant concentration is increased up to the CMC (see Table 3.4).

Comparison of the three anionic surfactant monolayers shows that the interfacial molecular areas and C_{12} layer thicknesses are closely similar for the monolayers formed in the presence of the alkali metal counterions, lithium and sodium – a result that accords with the observations reported by Allen et al. [151] – but they are somewhat different for the monolayer formed in the presence of ammonium counterions. With a surfactant concentration of 2 x CMC, the ADS area per molecule is around 5 $Å^2$ smaller and the alkyl chains layer thickness around 1 Å thinner. This difference in packing of the ADS monolayer by comparison with the LDS and SDS monolayers might lead to differences in regard to its solute encapsulation properties.

Table 3. 4 Model-fitted structural parameters for ADS and LDS monolayers

ADS (x CMC)	d_{tail} (± 0.3 Å)	$V_{f\ H2O}$ (± 1%)	Γ_{SAA} (± 0.1 x10^{-10} mol cm^{-2})	α (± 2 $Å^2$)
0.2	6.4	72	3.0	55
0.5	7.8	66	3.7	45
1.5	10.6	55	4.9	34
2.0	10.0	57	4.7	35
LDS (x CMC)	d_{tail} (± 0.3 Å)	$V_{f\ H2O}$ (± 1%)	Γ_{SAA} (± 0.1 x10^{-10} mol cm^{-2})	α (± 2 $Å^2$)
0.2	6.9	69	3.2	52
0.5	8.1	63	3.8	44
1.5	9.0	60	4.2	39
2.0	9.2	59	4.3	39

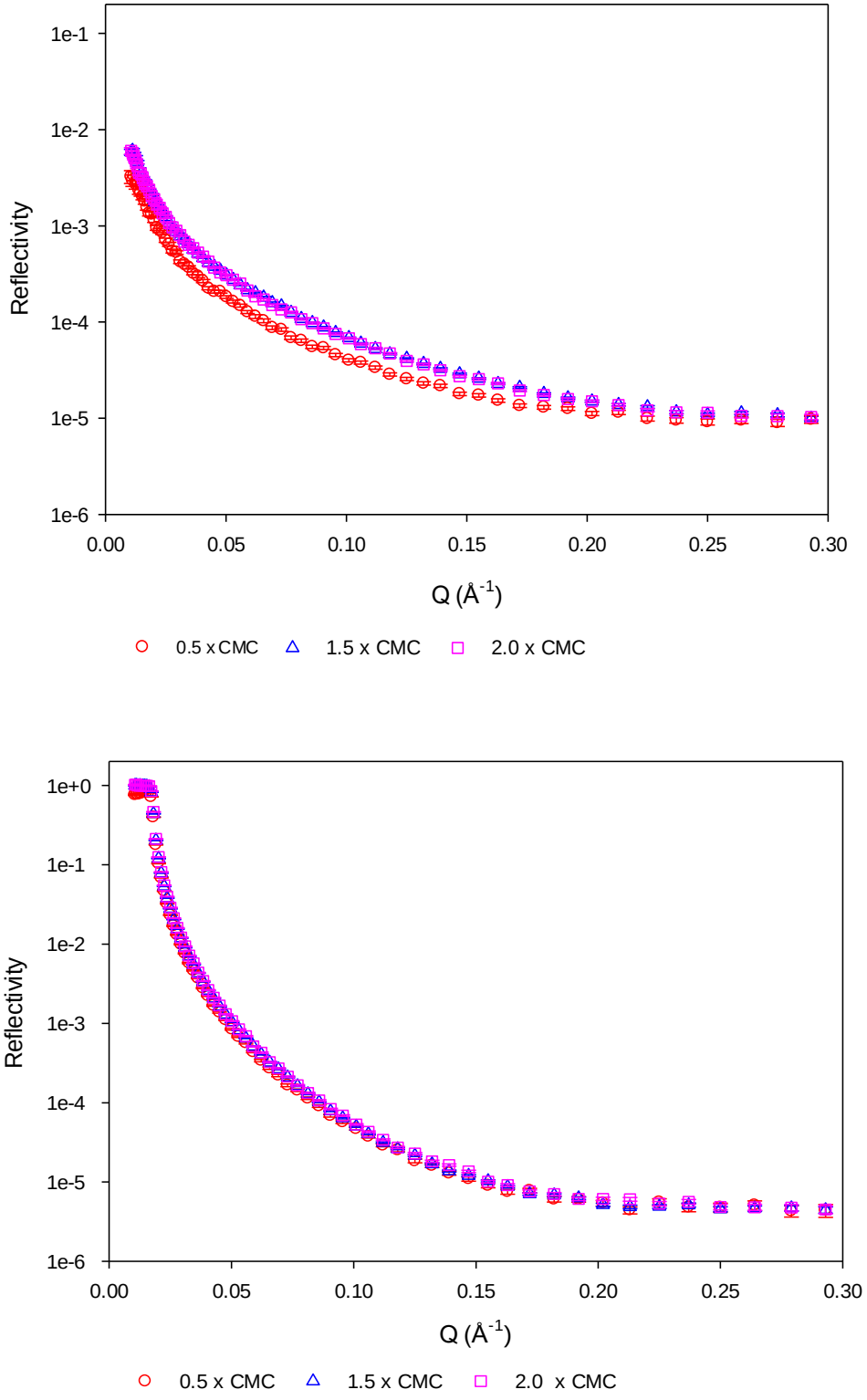

Figure 3. 4 NR profiles for d_{25}-SDS monolayers adsorbed at the air-water interface, on sub-phases of ACMW and D_2O, with concentrations above and below the CMC (ACMW, upper panel, D_2O, lower panel).

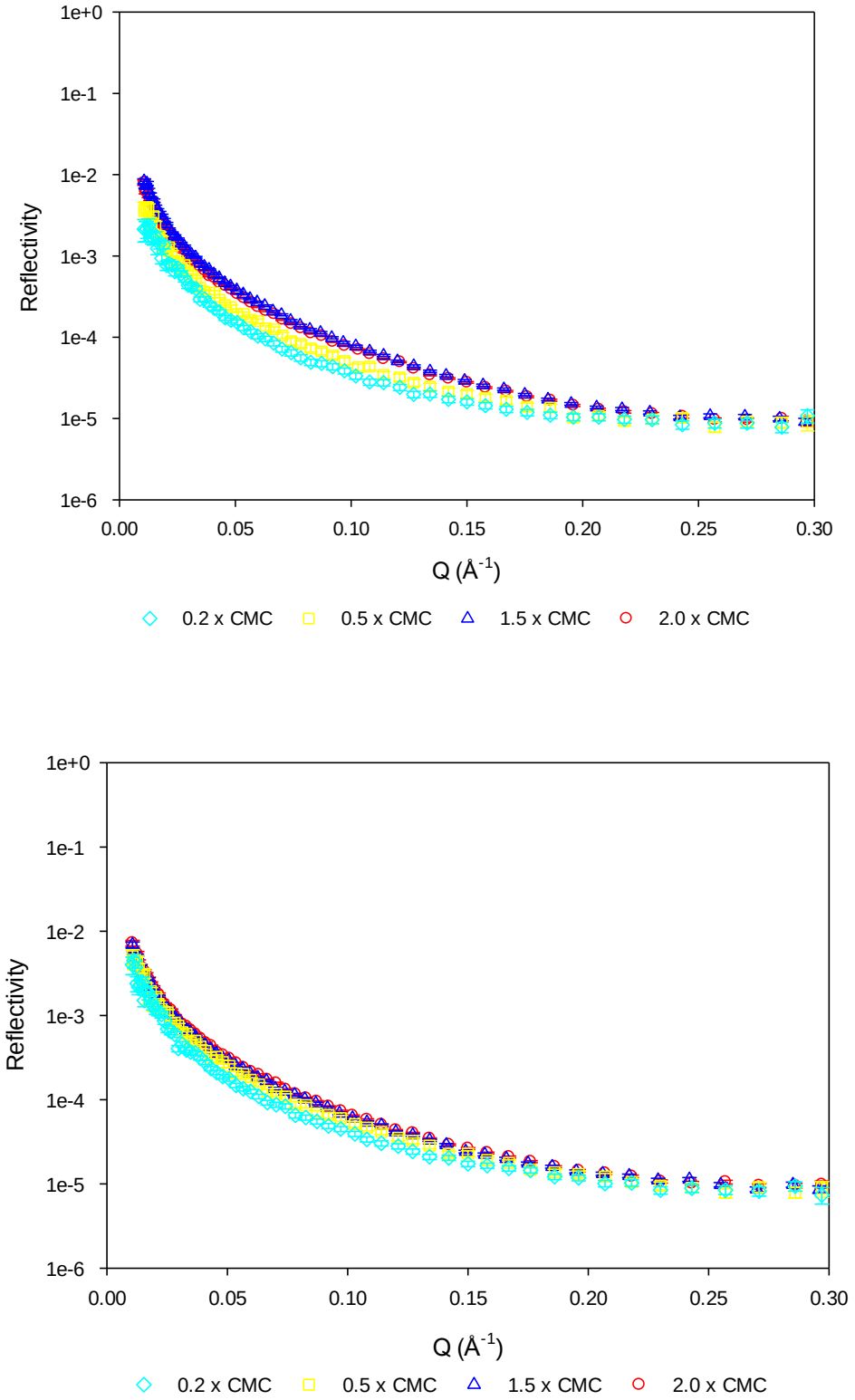

Figure 3. 5 NR profiles for d_{25}-ADS and d_{25}-LDS monolayers adsorbed at the air-water interface, on sub-phases of ACMW and D_2O, with concentrations above and below the CMC (ACMW, upper panel, D_2O, lower panel).

Given that there were no significant changes seen in the structures of the SDS, ADS and LDS monolayers when the surfactant concentration was increased beyond the CMC, the NR measurements for the other C_{12} surfactants studied were only performed using a surfactant concentration of 2 x CMC. The structural parameters obtained in model-fitting these data are summarized in Table 3.5.

The results obtained for DPC agree with those reported by Lu et al. [166], and those for DTAB and DDAPS are likewise consistent with the findings reported by Lyttle et al. [118] and Qu et al. [167].

It is significant to note here that although these surfactants all share the same C_{12} alkyl chain, they form monolayers with quite different alkyl chain layer thicknesses (ranging from 7.1 Å for DPC to 11.0 Å for DDAO) and as a consequence of their differing polar head groups they show differences in their surface excess and area per molecule. While six of the seven surfactants studied here have interfacial molecular areas of 45-50 $Å^2$, the interfacial area of DDAO is much smaller – only ca. 50% greater than the cross-sectional area of the C_{12} chain (32 $Å^2$ *vs.* 21 $Å^2$) – and the surface excess for DDAO is thus ca. 50% greater than that of the other surfactants (*viz.*, 5.1 x 10^{10} $mol.cm^{-2}$ *vs.* ~3.5 x 10^{10} $mol.cm^{-2}$).

Table 3. 5 Model-fitted structural parameters for DTAB, DDAO, DDAPS and DPC monolayers (with surfactant concentration, 2 x CMC).

	d_{tail} (± 0.3 Å)	$V_{f\ H2O}$ (± 1%)	Γ_{SAA} (± 0.1 x10^{-10} mol cm^{-2})	α (± 2 $Å^2$)
DTAB	7.8	55	3.6	46
DDAO	11.0	62	5.1	32
DDAPS	8.1	55	3.8	44
DPC	7.1	57	3.3	50

3.3.2 Characteristics of the C_{12} surfactant monolayers in the presence of 4-cholesten-3-one and adrenosterone

NR studies were performed to determine the structure of the C_{12} surfactant monolayers in the presence of 4-cholesten-3-one and adrenosterone, in all cases using a surfactant concentration of 2 x CMC. Model fits to the NR profiles were explored using models with the steroid incorporated within the C_{12} alkyl chains layer (model 1), within the polar head group layer (model 2), or otherwise present in the aqueous sub-phase forming a separate layer immediately beneath the polar head group layer (model 3). Table 3.6 shows the best-fitted structural parameters obtained in modelling the NR data for the surfactant monolayers saturated with 4-cholesten-3-one (4-CHOL) and Table 3.7 shows the corresponding parameters obtained in modelling the monolayers formed in the presence of adrenosterone (ADRENO).

For the SDS monolayers formed in the presence of 4-CHOL, model fits performed assuming models 2 and 3 gave significantly poorer fits than that obtained using model 1 (with χ^2 values of 91 and 40 *vs*. 6; see Appendix B, Figure B.1 and Table B.1). The use of models 2 and 3 also resulted in a counterintuitive *decrease* in the monolayer thickness (of 1.2 Å), while the use of model 1 gave a more physically reasonable *increase* in the monolayer thickness of 2.9 Å, and with the introduction of additional 4-CHOL onto the surface of the monolayer leading to a further small increase in the thickness, taking it to 12 Å. It is concluded, therefore, that the 4-CHOL sits within the alkyl chains layer of the SDS monolayer. The surface excess is consequently seen to decrease from 4.2 x 10^{10} mol.cm^{-2} to 3.7 x 10^{10} mol.cm^{-2}, thereby leading to an increase in the interfacial molecular area of the SDS, from 40 Å^2 to 45 Å^2. From the ratio of the surface excesses calculated for the SDS and 4-CHOL, it is found that the monolayer contains one steroid molecule for every 3.5 molecules of SDS.

When the SDS monolayer is saturated with ADRENO, the use of model 1 again provides the best fit to the NR data (giving the lowest χ^2), and so this steroid too is concluded to lie within the alkyl chains layer of the monolayer. In this case, however, the thickness of the C12 layer remains unchanged at approximately 8 Å. There is a slight difference in the surface excess for SDS between the 4-CHOL- and ADRENO-containing monolayers, and there is a difference too in the surface excesses of the two steroids in these layers, and these differences lead to compositional differences, with

the steroid:surfactant ratio being much lower for ADRENO compared with 4-CHOL (*viz*., 1:7.3 *vs*. 1:3.5). This difference in stoichiometry is consistent with the results obtained in the solubilisation experiments reported earlier (section 2.1).

For the cationic surfactant DTAB, the use of model 1 once again provides the best fit to the NR data for the monolayers containing 4-CHOL. The model fits achieved using model 2 give a higher χ^2 and show that there are no 4-CHOL molecules in the polar head groups layer, which seems unreasonable given the findings from the solubilisation studies (section 2.1). Although there is very little difference in χ^2 between the fits achieved using models 1 and 3, the use of model 3 is not considered satisfactory. The use of model 3 shows that if 4-CHOL forms a separate layer underneath the surfactant molecules at the air-water interface, the length of the alkyl chains layer and the surface excess of surfactant decrease, and such changes seem physically unreasonable. In addition, the fit achieved using model 3 shows that the number of solubilised 4-CHOL molecules is much lower than is found if model 1 is used, and the surfactant:steroid stoichiometry is not then consistent with the results obtained in the solubilisation studies.

Much the same observations are made for the DTAB/ADRENO monolayers as for the DTAB/4-CHOL monolayers, with models 1 and 3 giving comparable fits to the NR data in terms of χ^2 but the use of model 1 leading to a DTAB:4-CHOL stoichiometry that better agrees with the findings from solubilisation studies.

For both the DTAB/ADRENO and DTAB/4-CHOL monolayers the NR data show that there is no change in the thickness of the alkyl chains layer caused by the addition of steroid, and the surface excesses calculated in the two cases show that there are 2-3 times more 4-CHOL molecules inserted into the surfactant layer compared with ADRENO. The addition of extra steroid onto the surface of these monolayers caused changes in the NR profiles which indicated slight increases in the C_{12} layer thickness and small increases too in the numbers of steroid molecules inserted into the layers.

In the case of the zwitterionic DDAPS monolayer, regardless of which of the three models was used to fit the NR data, the calculated stoichiometries of the 4-CHOL and ADRENO were always close to zero, and it had to be concluded that the NR experiments could not provide the sensitivity necessary to discriminate between the

different models. The locus of solubilisation of the 4-CHOL and ADRENO in the DDAPS monolayer could not therefore be determined.

Modelling of the NR data for the steroid-containing monolayers of the zwitterionic surfactants, DDAO and DPC, showed once again that the steroid molecules insert into the surfactant chains layer of the monolayers, but in these systems there were some differences seen for the 4-CHOL and ADRENO. In the case of the DDAO monolayers, the insertion of 4-CHOL led to a slight decrease in the alkyl chains layer thickness (from 11 Å to 10 Å), and the addition of extra 4-CHOL onto the surface of the monolayer resulted in an increase in surface excess of the steroid (from 0.4×10^{10} $mol.cm^{-2}$ to 0.7×10^{10} $mol.cm^{-2}$). With the insertion of ADRENO, however, there was no change in the alkyl chains layer thickness of the DDAO monolayer and no change in the surface excess of the steroid after the addition of extra material onto the surface of the monolayer.

In the case of the DPC monolayers, the fits to the NR data showed that the addition of the steroids caused small increases in the alkyl chains layer thickness (to 9.4 Å and 8.4 Å, for 4-CHOL and ADRENO, respectively), and no significant changes were seen in either monolayer when extra steroid was added on the surface.

At the culmination of these studies, it was thus concluded that the locus of solubilisation of 4-CHOL and ADRENO in all the (anionic, cationic, and zwitterionic) C_{12} surfactant monolayers was in the alkyl chains layer – albeit that the NR data for the DDAPS systems did not afford the sensitivity necessary to provide conclusive proof of this.

Table 3. 6 Model-fitted structural parameters for C_{12} surfactant monolayers in the presence of 4-cholesten-3-one (with surfactant concentration, 2 x CMC).

	d_{tail} (± 0.3 Å)	$V_{f\ H2O}$ (± 2%)	Γ_{SAA} (± 0.1 x 10^{-10} mol cm^{-})	$\Gamma_{4\text{-CHOL}}$ (± 0.1 x 10^{-10} mol cm^{-2})	α (± 2 $Å^2$)	Composition (SAA : 4-cholesten-3-one)
SDS	11.9	66	3.7	1.1	45	3.5 ± 0.1
DTAB	7.9	55	3.2	0.3	51	12.7 ± 0.4
DDAO	10.3	66	4.2	0.4	40	11.1 ± 0.3
DDAPS	7.4	54	3.5	0.0	48	/
DPC	9.4	66	2.6	1.0	63	2.6 ± 0.1

Table 3. 7 Model-fitted structural parameters for C_{12} surfactant monolayers in the presence of adrenosterone (with surfactant concentration, 2 x CMC).

	d_{tail} (± 0.3 Å)	$V_{f\ H2O}$ (± 2%)	Γ_{SAA} (± 0.1 x 10^{-10} mol cm^{-})	Γ_{ADRENO} (± 0.0 x 10^{-10} mol cm^{-2})	α (± 2 $Å^2$)	Composition (SAA : adrenosterone)
SDS	8.9	67	3.6	0.5	46	7.3 ± 0.2
DTAB	7.7	52	3.5	0.1	48	31.0 ± 0.9
DDAO	11.3	66	4.1	1.0	40	4.0 ± 0.1
DDAPS	7.7	52	3.6	0.0	46	/
DPC	8.4	64	2.7	1.0	61	2.7 ± 0.1

3.3.3 Characteristics of the SDS monolayer as a function of SDS concentration in the presence of 4-cholesten-3-one and adrenosterone

NR studies of the structure of the SDS monolayer in the presence of 4-CHOL and ADRENO were carried out using concentrations of SDS of 0.2, 0.5, 1.0, 1.5 and 2.0 times the surfactant CMC (0.23 wt%). Given the observations which were noted above, all these data were modelled using model 1 – wherein the steroid molecules were assumed to reside within the alkyl chains layer of the SDS monolayer. Since the scattering length densities of the 4-CHOL and ADRENO are close to zero (0.34 x 10^{-6} $Å^{-2}$ and 1.27 x 10^{-6} $Å^{2}$) – and so would not cause a significant/detectable change in the NR profile obtained using the chain protiated surfactant contrasts – these systems were modelled using only the contrasts of d_{25}SDS on ACMW and d_{25}SDS on D_2O.

The NR profiles obtained for d_{25}SDS on ACMW in the presence of 4-CHOL show, as was found for the corresponding system studied in the absence of steroid, that the NR signal increases as the concentration of SDS is increased (Figure 3.6). The NR profiles obtained for the d_{25}SDS/4-CHOL system in D_2O, however, show no noticeable change in the reflected signal (Figure 3.7). This lack of a change in the NR signal for the d_{25}SDS/D_2O contrast, however, is just as would be expected given that this contrast is sensitive to changes in the structure and composition of the polar head group layer of the monolayer but much less sensitive to changes in the alkyl chains layer – which is where the 4-CHOL and ADRENO appear to insert.

The model-fitted structural parameters for the SDS/4-CHOL monolayers are summarized in Table 3.8. These data show that the thickness of the alkyl chains layer of the monolayer generally increases as the concentration of SDS is increased, and that there is a concomitant decrease in the surfactant area per molecule, and a decrease in the level of head group hydration. It is interesting to note too that when the concentration of SDS was 0.5 x CMC, the surfactant surface excess was much the same as that calculated for the SDS monolayer formed in the absence of 4-CHOL (3.9 vs. 3.5 x 10^{10} $mol.cm^{-2}$), whereas when the SDS concentration is at 1.5 x and 2 x CMC, the surface excess of the surfactant is seen to be decreased. This decrease in the surfactant excess at the higher SDS concentrations might be explained by the replacement of SDS by 4-CHOL in the monolayer when the SDS molecules are more

closely packed at the interface. Such an exchange of 4-CHOL for SDS would lead to a lowering of the CMC for SDS in the presence of 4-CHOL, and this is just as was observed in the surface tension studies (see section 2.2).

The NR profiles obtained for SDS monolayers in the presence of ADRENO are shown in Figure 3.7, and the associated model fitted values of the various structural parameters are summarized in Table 3.9. As expected, the thickness of the alkyl chains layer of the monolayer increases until the CMC is achieved, but thereafter (at 1.5 x and 2 x CMC) the thickness of the layer is seen to decrease to ca. 9 Å, which is the thickness of the layer found for the SDS monolayer in the absence of steroid. Given that the surface excess of ADRENO is also seen to drop from 0.7 $x10^{-10}$ mol cm^{-2} to 0.6 $x10^{-10}$ mol cm^{-2} when the concentration of SDS is increased from 0.5 x to 1.5 x CMC, it may be the case that when SDS micelles are formed in the bulk, some of the ADRENO partitions out of the monolayer and into the micelles. In contrast to what was seen with 4-CHOL, the presence of ADRENO in the SDS monolayer does not appear to change the thickness of the alkyl chains layer when the concentration of SDS is above the CMC, and the ratio of SDS to ADRENO at these higher concentrations is much higher than the ratios determined for SDS in the presence of 4-CHOL, which is entirely consistent with the findings from the solubilisation experiments (see section 2.1)

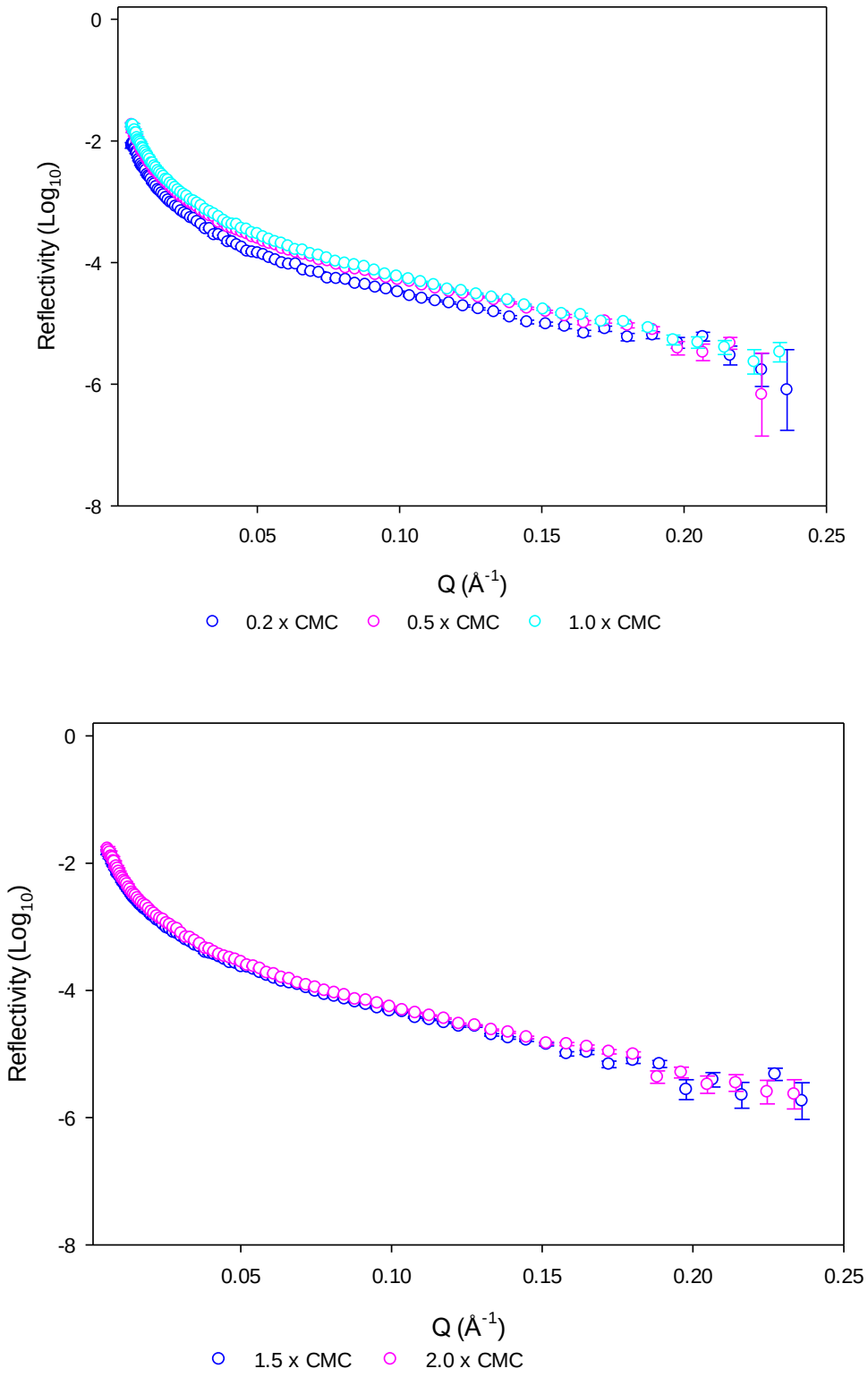

Figure 3. 6 NR profiles for monolayers of d_{25}-SDS on a sub-phase of ACMW, in the presence of 4-CHOL, with the SDS concentration below the CMC (upper panel) and above the CMC (lower panel).

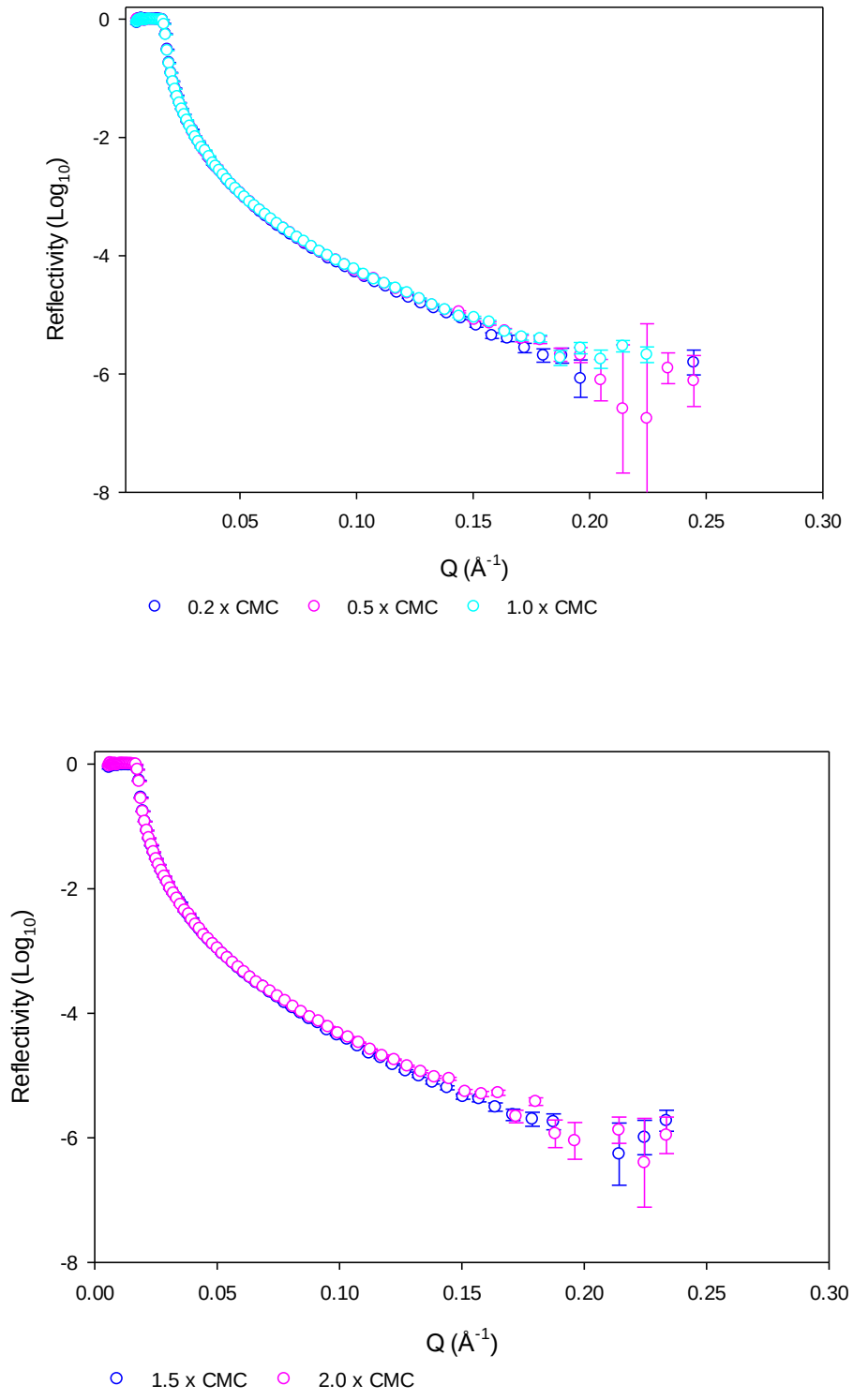

Figure 3. 7 NR profiles for monolayers of d_{25}-SDS on a sub-phase of D_2O, in the presence of ADRENO, with the SDS concentration below the CMC (upper panel) and above the CMC (lower panel).

Table 3. 8 Model-fitted structural parameters for SDS monolayers in the presence of 4-CHOL

Concentration of SDS (x CMC)	0.2	0.5	1.0	1.5	2.0
d_{tail} (± 0.3 Å)	7.0	8.6	9.7	11.6	11.9
Vf_{H2O} (± 1%)	73	65	62	66	66
Γ_{SDS} (± 0.1 x 10^{-10} mol cm^{-2})	3.0	3.9	4.2	3.8	3.7
$\Gamma_{4\text{-CHOL}}$ (± 0.1 x10^{-10} mol cm^{-2})	0.2	0.1	0.2	1.0	1.1
Stoichiometry (SDS:4-cholesten-3-one)	15.6 ± 0.5	51.7 ± 1.4	20.1 ± 0.5	3.9 ± 0.1	3.5 ± 0.1
α (± 2 $Å^2$)	56	43	40	44	45

Table 3. 9 Model-fitted structural parameters for SDS monolayers in the presence of ADRENO

Concentration of SDS (x CMC)	0.1	0.2	0.5	1.5	2.0
d_{tail} (± 0.3 Å)	9.7	12.1	13.7	9.2	9.0
Vf_{H2O} (± 1%)	64	53	49	68	67
Γ_{SDS} (± 0.1 x 10^{-10} mol cm^{-2})	4.0	5.1	5.53	3.5	3.6
Γ_{ADRENO} (± 0.1 x 10^{-10} mol cm^{-2})	0.5	0.5	0.7	0.6	0.5
Stoichiometry (SDS : adrenosterone)	8.4 ± 0.2	11.3 ± 0.2	7.4 ± 0.1	5.7 ± 0.2	6.7 ± 0.2
α (± 2 $Å^2$)	42	32	30	47	46

3.3.4 Monitoring changes in the C_{12} surfactant/steroid monolayers following addition of extra steroid

The NR studies of the C_{12} surfactant monolayers formed at the air-water interface in the presence of 4-CHOL and ADRENO clearly show that the steroid molecules are incorporated into the surfactant monolayers both above and below the CMC in each surfactant system. The effect of steroids on the monolayer and their location were probed when the monolayer was fully saturated with steroids. For monolayers where the surfactant concentrations were below the CMC, and where the level of steroid in the monolayer was below saturation, additional steroid was added externally onto the surface of the sub-phase. The theoretical amounts of steroids required to saturate the surface were calculated based on the solubilisation results given in Chapter 2.1.4.

These additional NR measurements which were performed to determine the effects of additional steroid added to the surfactant monolayers were in some cases carried out using the FIGARO reflectometer at the ILL and in other cases were carried out using Inter at the ISIS facility.

The NR profiles obtained after the external addition of 4-CHOL onto the surface of equilibrated SDS monolayers are shown in Figure 3.8. It is clearly seen here that the reflected signal decreases after spreading extra 4-CHOL on the surface when the concentration of SDS is below the CMC, indicating that the additional (protiated) 4-CHOL has inserted into the (chain-deuterated) SDS monolayer. From the model-fitted values of the structural parameters for the monolayers (summarized in Table 3.10) it is apparent that the level of solvent in the monolayer decreases following the external addition of 4-CHOL, and that there is a concomitant decrease in the surface excess of surfactant (from 3.0 to 2.2 $x10^{10}$ $mol.cm^{-2}$) and a dramatic increase in the surface excess of 4-CHOL. Given that the SDS molecules in the monolayer will not be close packed at the water surface due to the low concentration in this system (0.2 x CMC), it is concluded that the externally introduced 4-CHOL has inserted into the monolayer occupying the space between the surfactant molecules, altering the packing within the monolayer and causing an extension of the SDS alkyl chains (and thus increasing the alkyl chain layer thickness, d_{tail}). For the SDS monolayer formed with the SDS concentration at 2 x CMC, there is little difference between the NR profiles obtained before and after the external application of additional 4-CHOL. Model-fitting of these

data show that there is a slight increase in the surface excess of steroid in the monolayer (from 1.1 to 1.7 $x10^{10}$ $mol.cm^{-2}$) after the additional 4-CHOL was introduced at the surface, but the surface excess is still lower than that found for the monolayer formed with the SDS concentration at 0.2 x CMC. For the monolayer formed with the SDS concentration at 2 x CMC, it is concluded that the surfactant molecules are sufficiently tightly packed at the surface that the excess 4-CHOL cannot intrude (deeply) into the layer, although some of the steroid molecules might perhaps sit within the extremities of the SDS dodecyl chains and this would then explain the small increase seen in d_{tail}, and would also account for the change in 4-CHOL stoichiometry from 3 to 2.

The corresponding results obtained for the SDS monolayers formed in the presence of ADRENO (Figure 3.9), show much the same effect of externally applied steroid. With the SDS concentration below the CMC, there is an increase in surface excess of the steroid, and this seems to cause in reduction in the alkyl chains layer thickness (Table 3.11). When the SDS concentration is above the CMC, the externally applied ADRENO causes no change in the monolayer structure and no change in its composition (Table 3.11).

The NR profiles obtained after the external addition of 4-CHOl and ADRENO onto the surfaces of the equilibrated monolayers formed with the other C_{12} chain surfactants studied show the same sorts of change as seen with the SDS monolayers. In these studies, the concentration of each surfactant was fixed just at 2 x CMC. Tables 3.12 and 3.13 show the model fitted values of the various structural parameters for these systems.

For the DTAB and DPC surfactant monolayers formed in the presence of 4-CHOL and ADRENO, the external application of additional steroid resulted in no significant change in the structures of the monolayers, with the small differences seen in the model-fitted parameter values falling within experimental error. The DDAO monolayer, however, showed what appeared to be an increase in the amount of 4-CHOL within the monolayer when further steroid was applied externally, but there was no such increase seen for the DDAO monolayers in the presence of ADRENO. The levels of the two steroids that inserted into the DDAPS monolayers were so low

that no definitive conclusion can be drawn regarding the effect of externally applied material.

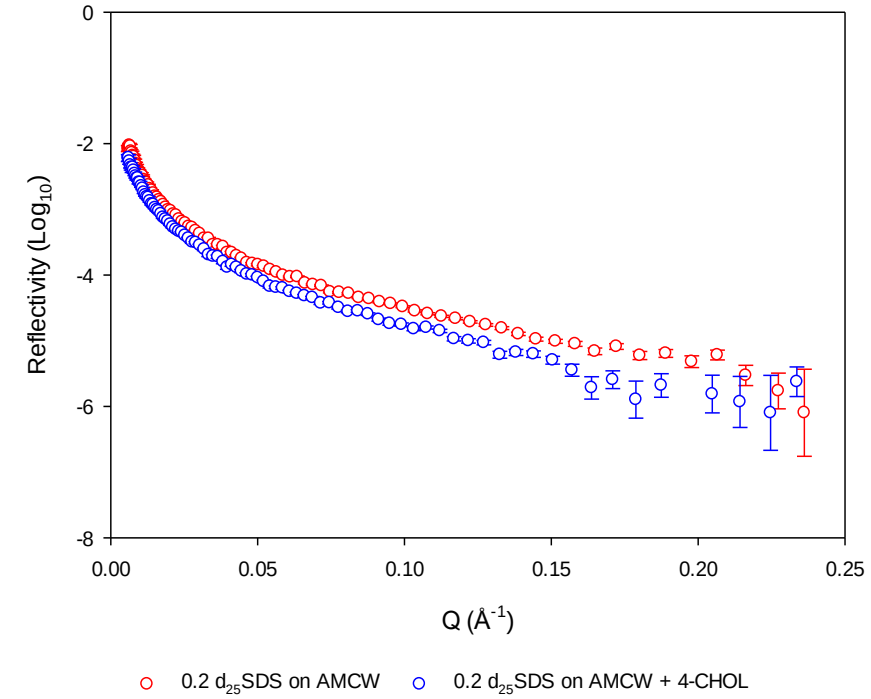

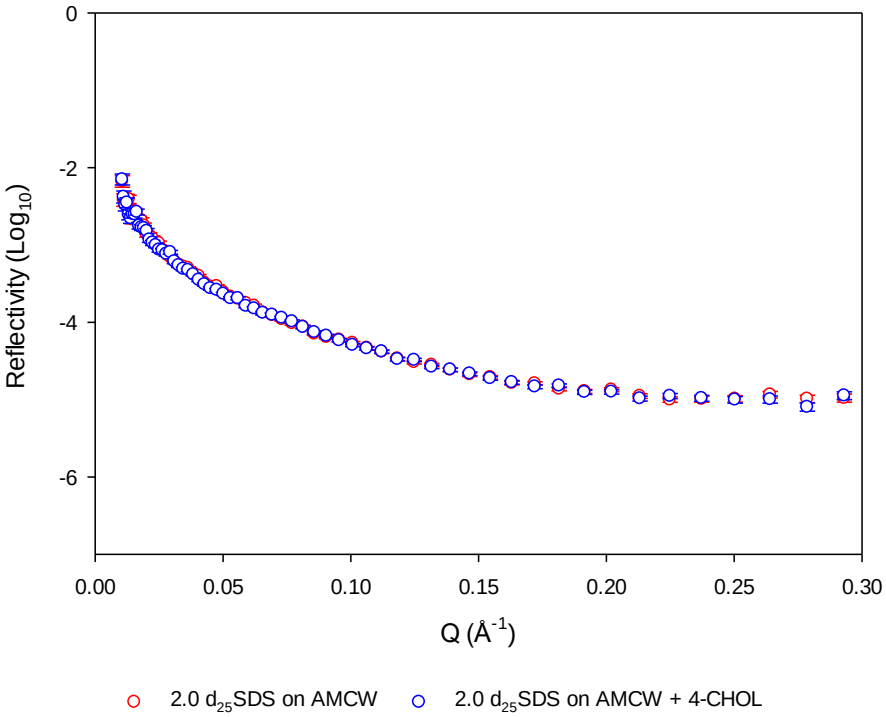

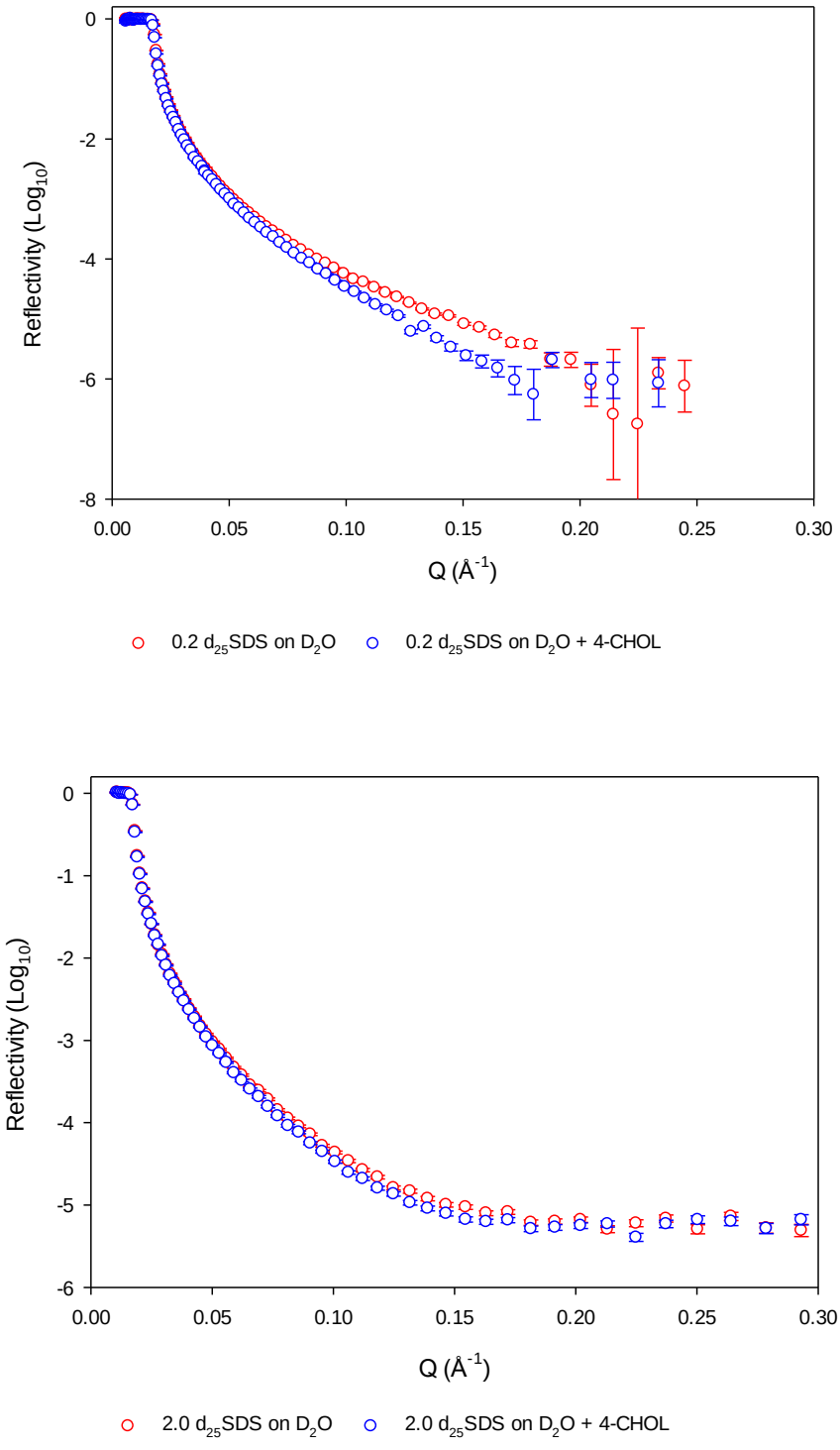

Figure 3. 8 NR profiles for d_{25}SDS monolayers formed in the presence of 4-cholesten-3-one on sub-phases of ACMW (previous page) and D_2O (this page), with SDS concentrations below the CMC (upper panels) and above the CMC (lower panels).

Table 3. 10 Model-fitted structural parameters for SDS monolayers in the presence of 4-CHOL and with additional 4-CHOL added to the monolayer.

	d_{tail} (± 0.3Å)	$V_{f\ H2O}$ (± 1%)	Γ_{SAA} (± 0.1 x10^{-10} mol cm^{-2})	$\Gamma_{4\text{-}CHOL}$ (± 0.1 x10^{-10} mol cm^{-2})	α (± 2 $Å^2$)	Stoichiometry (SDS: 4-CHOL)
0.2 x CMC	7.0	0.90	3.0	0.2	56	15.6 ± 0.5
0.2 x CMC + 4-CHOL	13.0	0.36	2.2	2.3	77	1.0 ± 0.1
2.0 x CMC	11.9	0.67	3.7	1.1	45	3.5 ± 0.3
2.0 x CMC + 4-CHOL	14.3	0.56	3.8	1.7	44	2.2 ± 0.1

Table 3. 11 Model-fitted structural parameters for SDS monolayers in the presence of ADRENO and with additional ADRENO added to the monolayer.

	d_{tail} (± 0.3Å)	$V_{f\ H2O}$ (± 1%)	Γ_{SAA} (± 0.1 x10^{-10} mol cm^{-2})	Γ_{ADRENO} (± 0.1 x10^{-10} mol cm^{-2})	α (± 2 $Å^2$)	Stoichiometry (SDS:ADRENO)
0.2 x CMC	12.1	0.53	5.1	0.5	32	11.4 ± 0.2
0.2 x CMC + ADRENO	10.2	0.63	4.1	0.6	41	6.9 ± 0.2
2.0 x CMC	9.0	0.67	3.6	0.5	46	6.8 ± 0.2
2.0 x CMC + ADRENO	9.0	0.67	3.6	0.5	46	6.8 ± 0.2

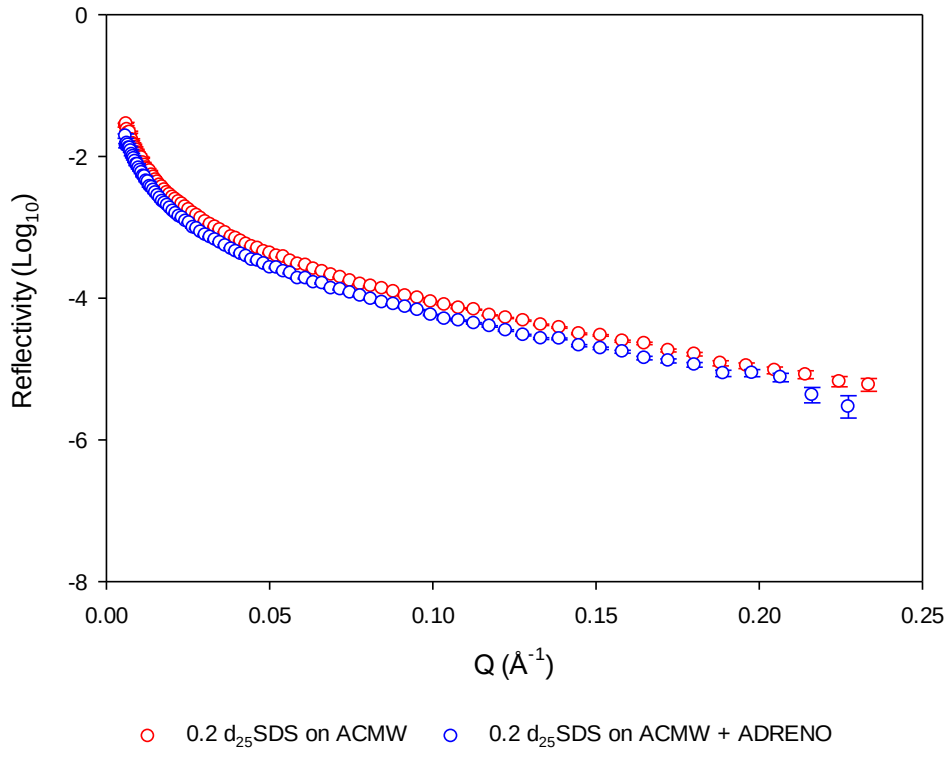
0
-2
-4
-6
-8
Reflectivity (Log10)
0.00
0.05
0.10
0.15
0.20
0.25
Q (Å-1)
0.2 d25SDS on ACMW
0.2 d25SDS on ACMW + ADRENO

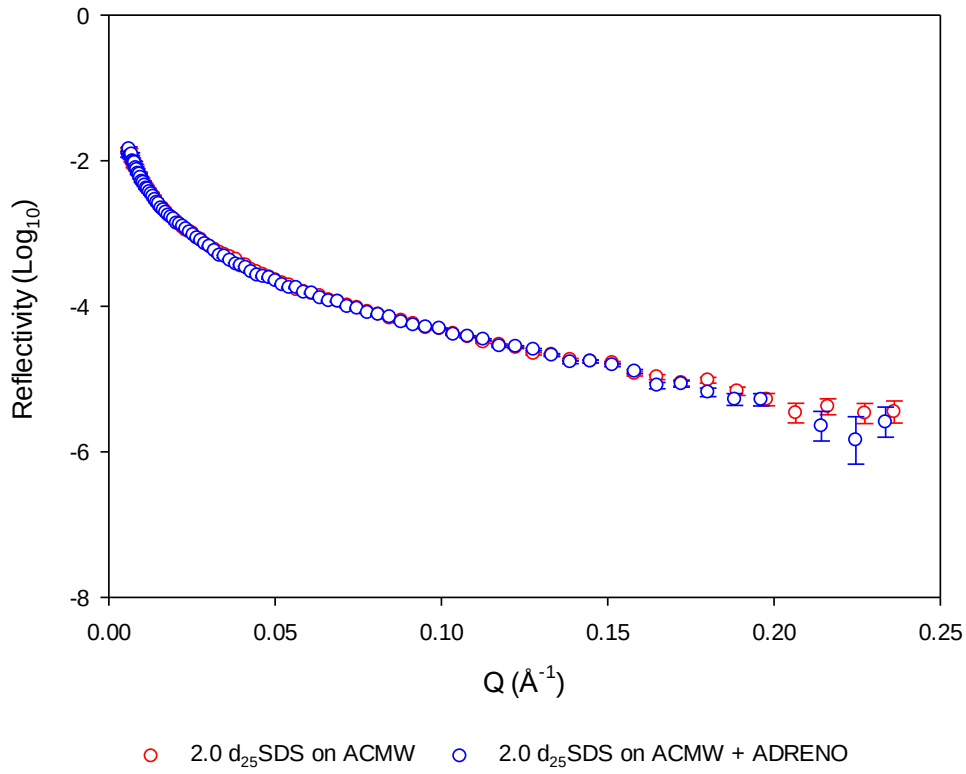
0
-2
-4
-6
-8
Reflectivity (Log10)
0.00
0.05
0.10
0.15
0.20
0.25
Q (Å-1)
2.0 d25SDS on ACMW
2.0 d25SDS on ACMW + ADRENO

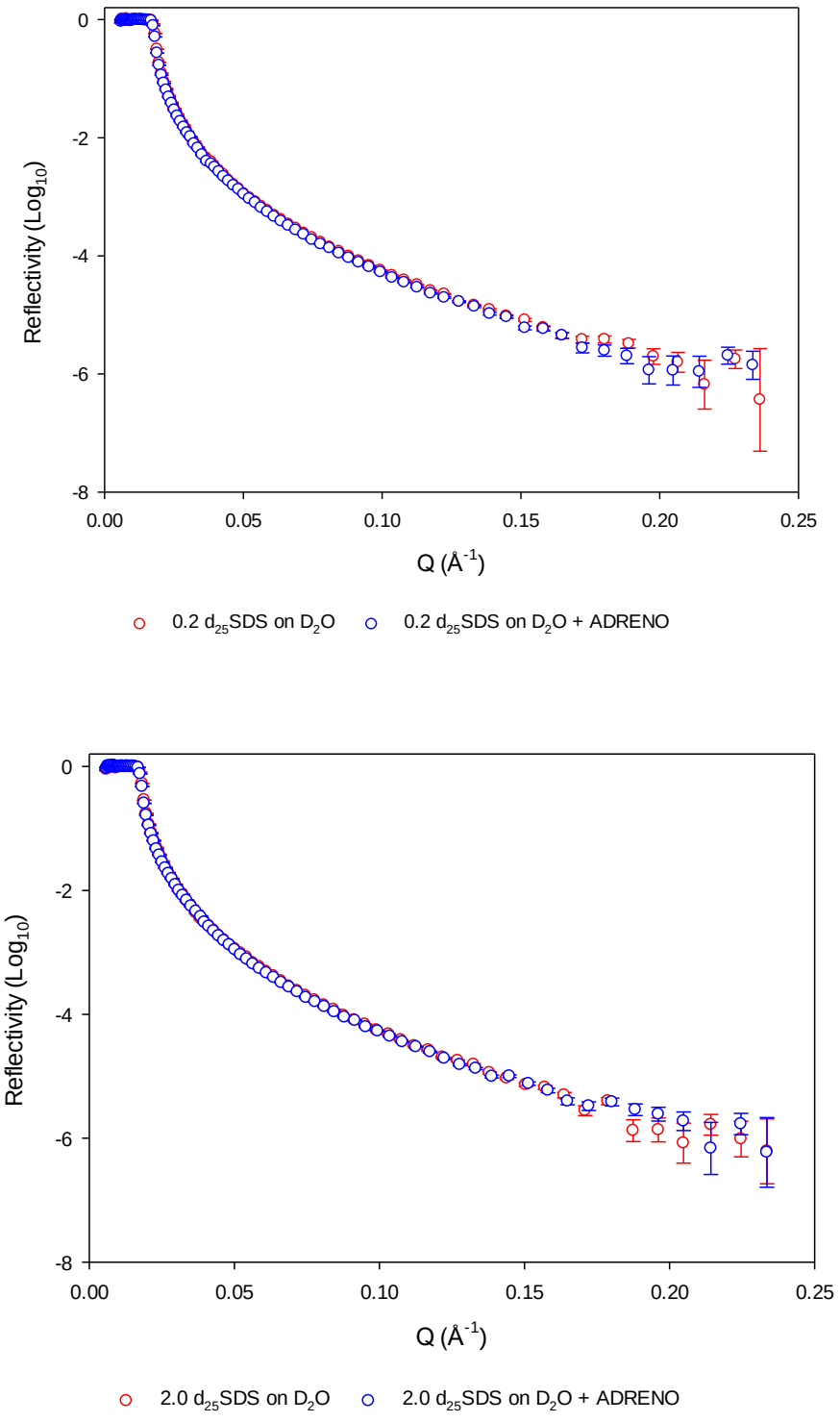

Figure 3. 9 NR profiles for d_{25}SDS monolayers formed in the presence of adrenosterone on sub-phases of ACMW (previous page) and D_2O (this page), with SDS concentrations below the CMC (upper panels) and above the CMC (lower panels).

Table 3. 12 Model-fitted structural parameters for C_{12} surfactant monolayers in the presence of 4-CHOL and with additional 4-CHOL added to the monolayer.

		d_{tail} (± 0.3 Å)	$V_{f\ H2O}$ (± 1%)	Γ_{SAA} (± 0.1 x 10^{-10} mol cm^{-2})	$\Gamma_{4\text{-CHOL}}$ (± 0.1x 10^{-10} mol cm^{-2})	α (± 2 $Å^2$)	Stoichiometry (SAA:4-cholesten-3-one)
DTAB	**2.0 x CMC**	7.9	0.55	3.3	0.3	51	12.7 ± 0.4
	2.0 x CMC + 4-CHOL	8.5	0.53	3.4	0.3	48	10.5 ± 0.3
DDAO	**2.0 x CMC**	10.3	0.66	4.2	0.4	40	11.0 ± 0.3
	2.0 x CMC + 4-CHOL	10.6	0.69	3.7	0.7	45	5.0 ± 0.1
DDAPS	**2.0 x CMC**	7.4	0.54	3.5	0.0	48	NA
	2.0 x CMC + 4-CHOL	7.3	0.43	3.4	0.2	49	15.6 ± 0.5
DPC	**2.0 x CMC**	9.4	0.66	2.6	1.0	63	2.6 ± 0.1
	2.0 x CMC + 4-CHOL	9.8	0.67	2.6	1.2	65	2.2 ± 0.1

Table 3. 13 Model-fitted structural parameters for C_{12} surfactant monolayers in the presence of ADRENO and with additional ADRENO added to the monolayer.

		d_{tail} (± 0.3 Å)	$V_{f\ H2O}$ (± 1%)	Γ_{SAA} (± 0.10 x 10^{-10} mol cm^{-2})	Γ_{ADRENO} (± 0.10 x 10^{-10} mol cm^{-2})	α (± 2 $Å^2$)	Stoichiometry (SAA:ADRENO)
DTAB	**2.0 x CMC**	7.7	0.52	3.5	0.1	48	31.5 ± 0.9
	2.0 x CMC + ADRENO	7.7	0.52	3.5	0.1	48	31.5 ± 0.9
DDAO	**2.0 x CMC**	11.3	0.66	4.1	1.0	40	4.1 ± 0.1
	2.0 x CMC + ADRENO	11.3	0.66	4.1	1.0	41	4.1 ± 0.1
DDAPS	**2.0 x CMC**	7.7	0.52	3.6	0	46	NA
	2.0 x CMC + ADRENO	7.7	0.52	3.6	0	46	NA
DPC	**2.0 x CMC**	8.4	0.64	2.7	1.0	61	2.7 ± 0.1
	2.0 x CMC + ADRENO	8.4	0.64	2.7	1.0	61	2.7 ± 0.1

3.3.5 SDS/steroid monolayer structure as a function of time

The surface tension studies described earlier (section 2.2) showed that the time taken for a surfactant monolayer to reach equilibrium in the presence of added steroid could vary significantly depending upon the particular surfactant and steroid involved. For SDS, for example, it was found that the monolayer took much longer to reach equilibrium in the presence of 4-CHOL compared with ADRENO (ca 2 hours *vs*. 5 minutes). In the NR experiments reported above, therefore, it would be expected that when the sample solutions were poured into the Teflon trough, the surfactant (and steroid) molecules would take time to diffuse from the bulk to the surface, and they would then take time to orient and adsorb at the interface. For different samples and sample concentrations, the time taken for this diffusion and adsorption might vary from milliseconds to days [168]. It was thus considered worthwhile to determine the kinetics of the surfactant and steroid adsorption using neutron reflectivity, modelling the changes in monolayer structure as a function of time. Note that all the NR data obtained in this section were measured on INTER.

NR measurements performed for SDS monolayers in the absence of steroids showed no noticeable change between the profile recorded over the first hour and the profile recorded several hours later, and this was the case regardless of whether the SDS concentration was below or above the CMC (see Figure 3.10). The same observation was made for the SDS monolayers formed in the presence of ADRENO (see Figure 3.11).

In order to monitor the kinetics of formation of the SDS monolayers formed in the presence of 4-CHOL, the NR measurements were recorded at 15 min intervals over a 1 h period following sample preparation and instrument set-up, with the SDS concentration at 0.5 x CMC. As shown in Figure 3.12, the NR profiles collected over the initial one-hour period showed no noticeable difference, and no differences were apparent several hours later. It was therefore concluded that the SDS/4-CHOL monolayer attained equilibrium within the first hour.

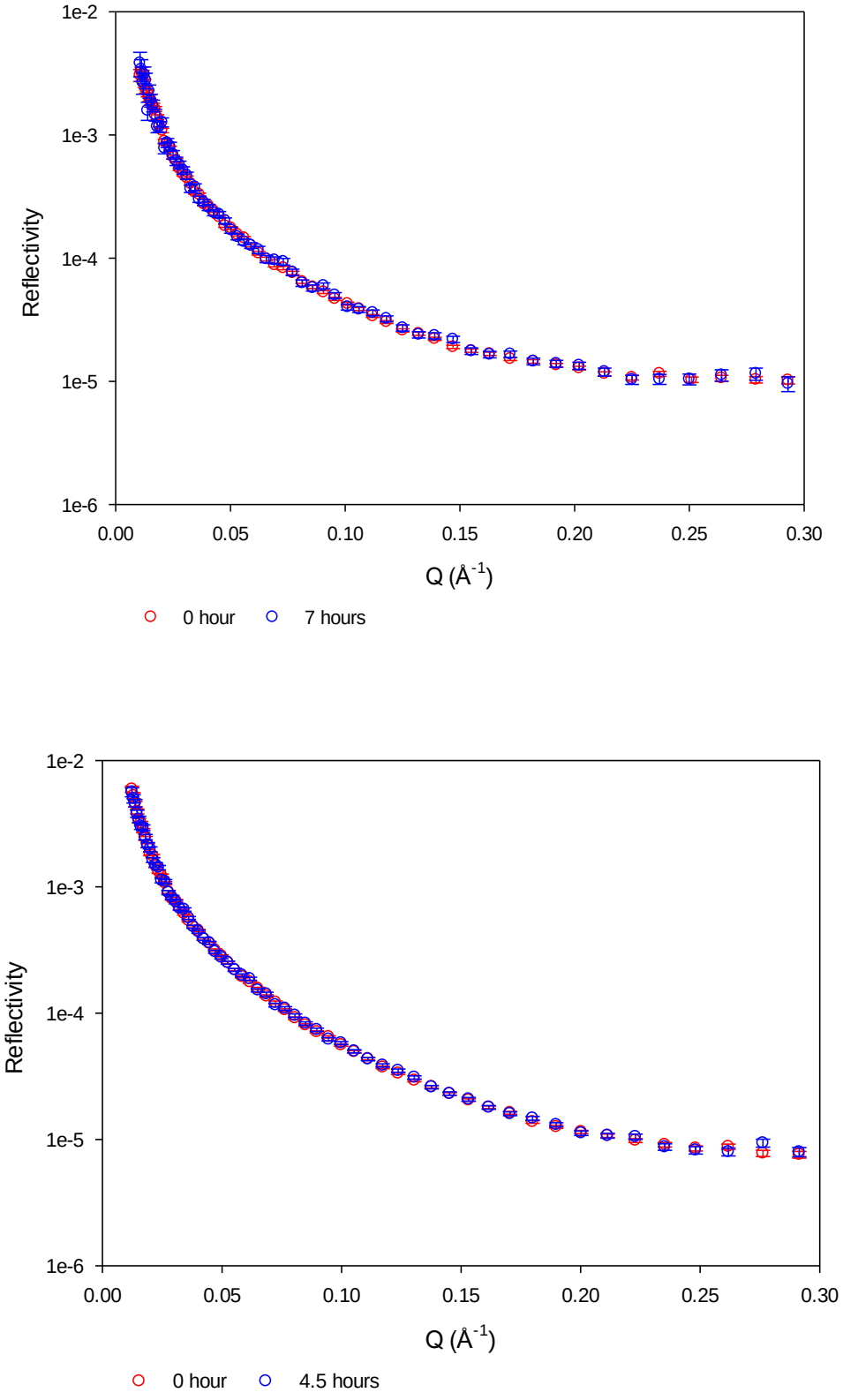

Figure 3. 10 NR profiles of d_{25}SDS monolayer on ACMW at 0.5 x CMC (upper panel) and 1.5 x CMC (lower panel)

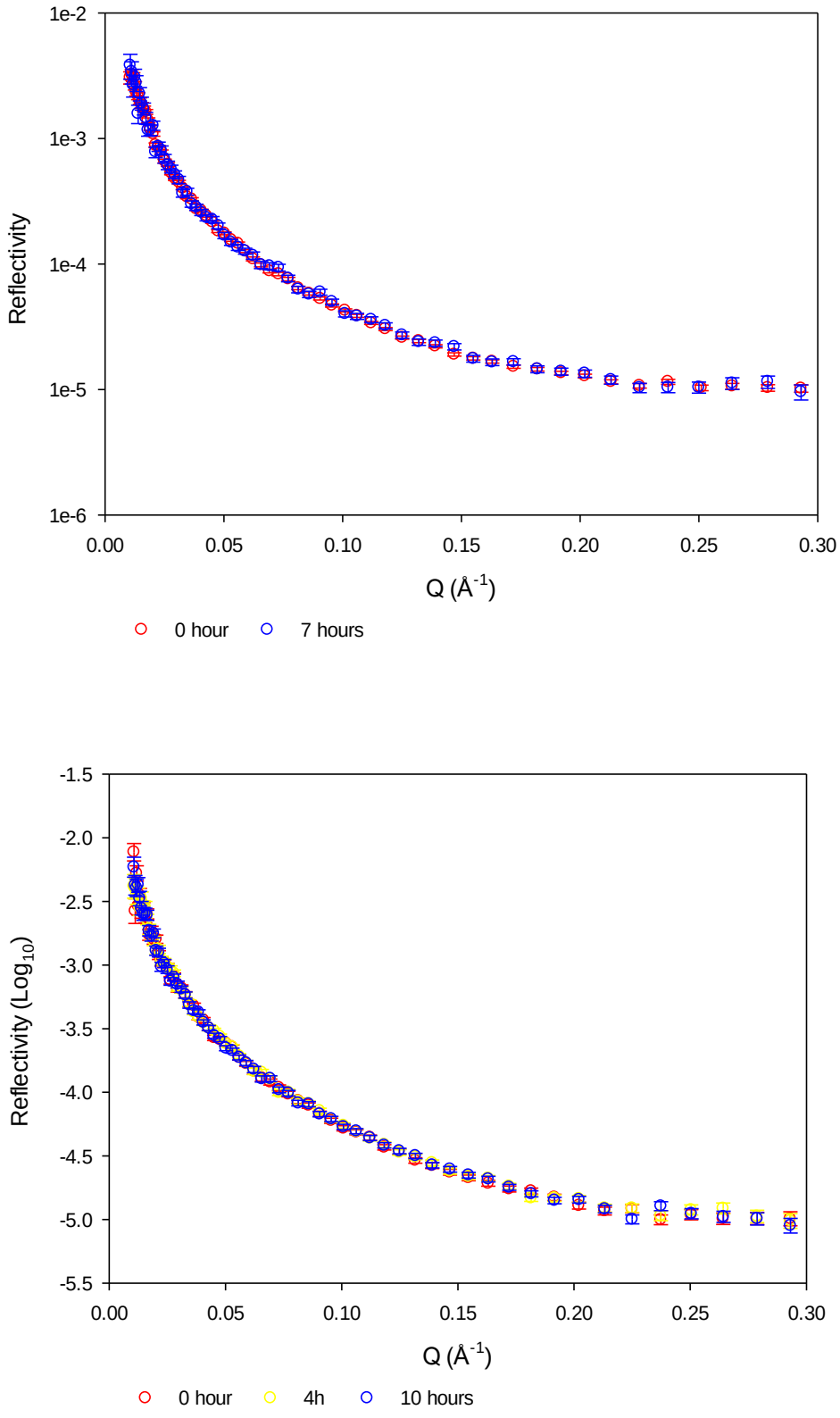

Figure 3. 11 NR profiles of d_{25}SDS monolayer on ACMW in the presence of adrenosterone at 0.5 x CMC (upper panel) and 1.5 x CMC (lower panel)

With the same experiments repeated for the SDS monolayer formed in the presence of 4-CHOL and with an SDS concentration of 1.5 x CMC, the NR profiles showed that the measured reflectivity was slightly lower at 1 h than was measured at 0.25 h, but the difference was quite small (Figure 3.13). However, after 6 hours the reflected signal was seen to decrease further. The NR profile recorded at 9 h overlaid perfectly with the profiles recorded > 9 hours (Appendix B), and it was thus concluded that this system attained equilibrium somewhere between 6 and 9 hours according to the NR profiles.

To further study the kinetics on the SDS monolayer in the presence of 4-CHOL, samples with an SDS concentration at 2 x CMC were also studied and the NR profiles recorded are shown in Figure 3.14. Comparisons of the various profiles recorded show that at this higher SDS concentration the monolayer attained equilibrium only after ca. 12 hours. Moreover, a comparison made between the initial NR profile recorded for the SDS/4-CHOL system and the one recorded initially for SDS at 2 x CMC showed no difference between the two, which would suggest that there were few if any 4-CHOL molecules present in the SDS monolayer when the monolayer was newly-formed. The slow progressive change in reflectivity for these systems seen over time, therefore, would seem to be explained by a slow diffusion and penetration of the steroid molecules into the SDS monolayer.

Table 3.14 shows the model fitted values of the structural parameters for the SDS monolayers formed at an SDS concentration of 1.5 x CMC and in the presence of 4-CHOL. Over the first hour it can be seen that the composition and structure of the monolayer remain more-or-less unchanged but then at 1-3 hours the surface excess of SDS begins to decrease, while d_{tail} and the surface excess of 4-CHOL begin to increase. After 20 hours, $\Gamma_{4\text{-CHOL}}$ has increased almost three-fold to 1.5 $x10^{-10}$ $mol.cm^{-2}$, and the replacing of SDS by the steroid has increased the thickness of the alkyl chains layer by ca. 4 Å taking it to 13 Å. It is clear, therefore, that the 4-CHOL penetrates the SDS monolayer only quite slowly and that the time taken for it to attain equilibrium is much longer than found for any of the other systems studied. Much the same behaviour is seen when the monolayer of SDS/4-CHOL is prepared with an SDS concentration of 2 x CMC (Table 3.15).

When the same kinetics experiments were performed using monolayers prepared with the other C_{12} surfactants in the presence of 4-CHOL, only the anionic surfactants, ADS and LDS showed time effects like those seen with SDS (Figure 3.15; Tables 3.16 and 3.17). The time taken for these systems to attain equilibrium at the air-water interface was much quicker than was seen in the SDS system. Equilibrium was achieved after 3.5 hours for the ADS/4-CHOL monolayer and after 5 hours for the LDS/4-CHOL monolayer.

The anomalously slow adsorption of 4-CHOL into the C_{12} surfactant monolayers thus seems to be associated with the sulfate head group, with the rate also depending on the nature of the cationic counter-ion. The same behaviour is not seen in the adsorption of ADRENO into the anionic surfactant monolayers, nor was it reported by Saaka et al. for the adsorption of the steroidal drug testosterone enanthate [169].

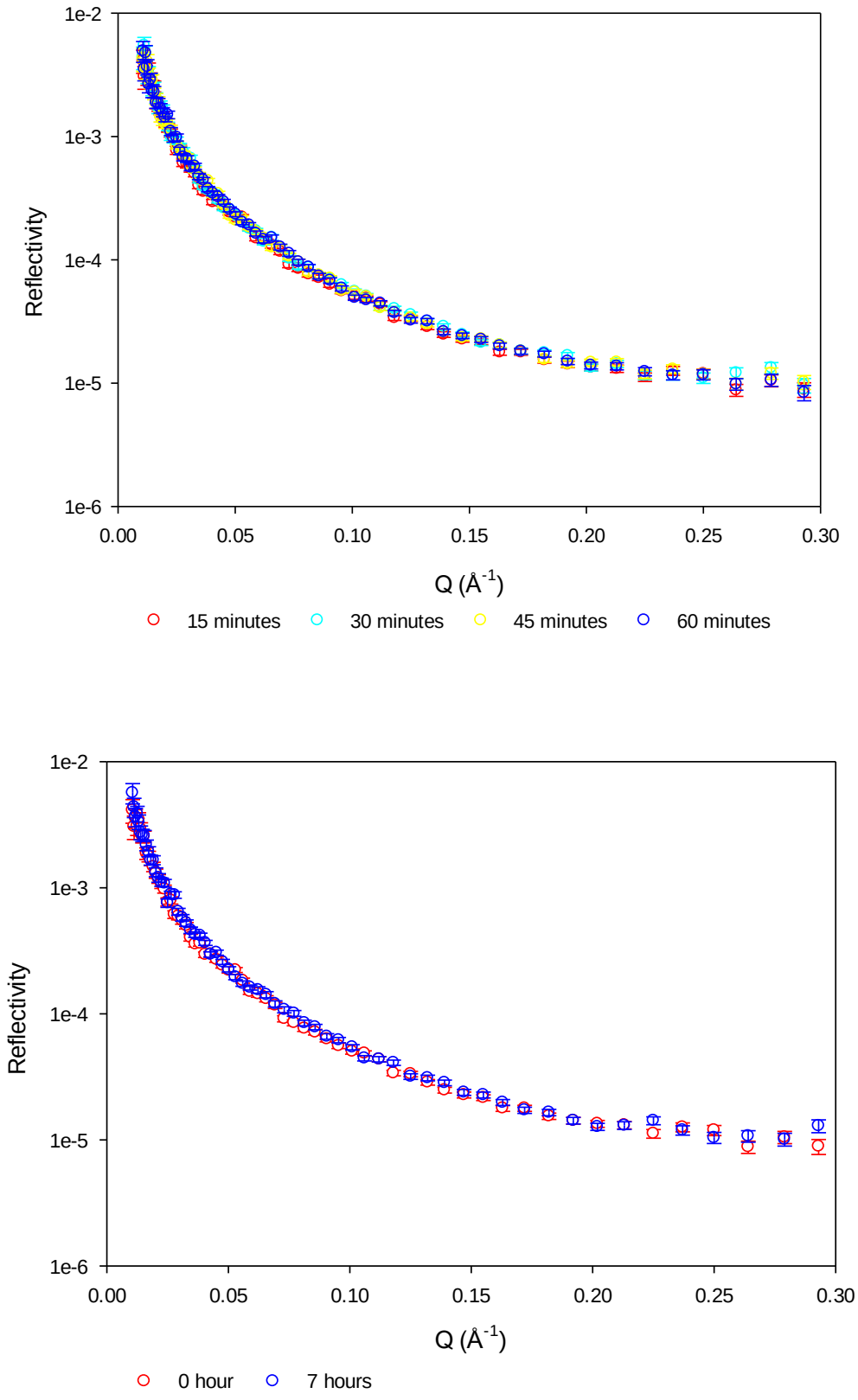

Figure 3. 12 NR profiles of d_{25}SDS in ACMW monolayer in the presence of 4-cholesten-3-one at 0.5 x CMC

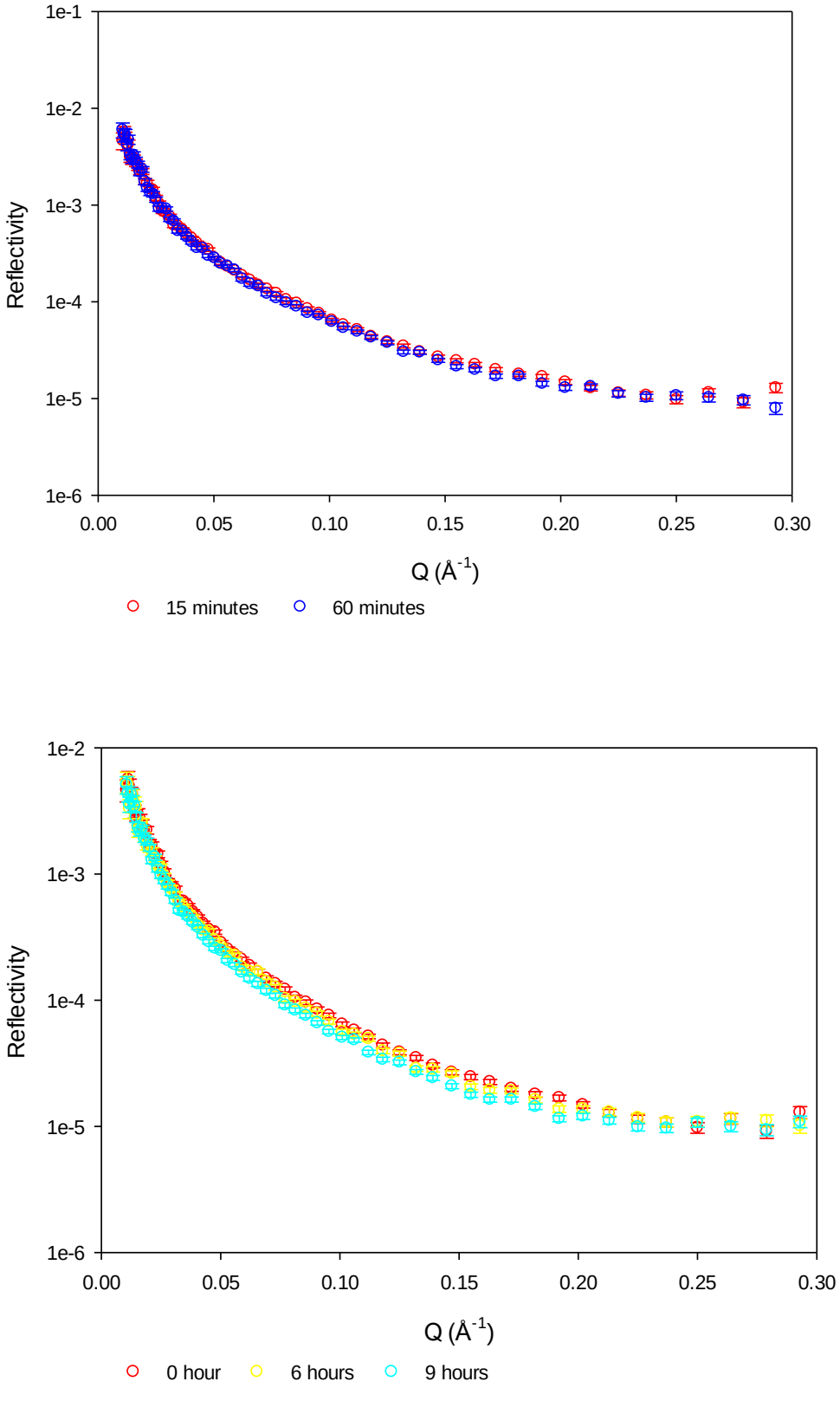

Figure 3. 13 NR profile of SDS monolayer in the presence of 4-cholesten-3-one at 1.5 x CMC

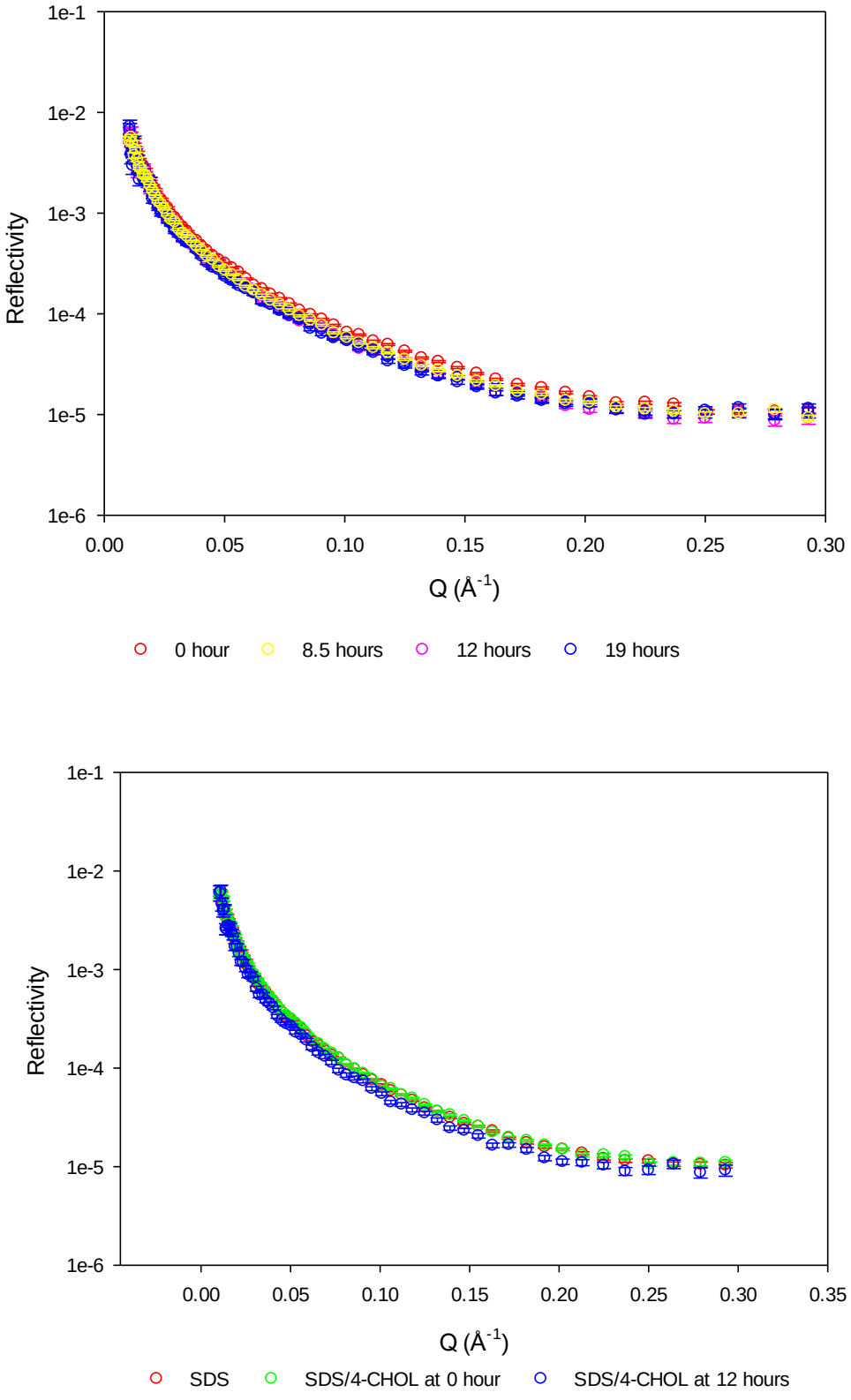

Figure 3. 14 NR profiles of d_{25}SDS monolayer in ACMW in the presence of 4-cholesten-3-one at 2.0 x CMC

Table 3. 14 Model-fitted structural parameters SDS monolayers in the presence of 4-CHOL and with additional 4-CHOL added to the monolayer at 1.5 x CMC

Time (hours)	0.25	0.5	0.75	1	3	6	9	16	20
d_{tail} (± 0.3 Å)	10.5	10.4	10.8	10.7	11.1	11.7	11.9	12.3	13.2
$V_{f\ H2O}$ (± 1 %)	0.63	0.63	0.61	0.63	0.64	0.65	0.67	0.69	0.68
Γ_{SDS} (± 0.1 x 10^{-10} mol cm^{-2})	4.1	4.0	4.2	4.0	4.0	3.8	3.6	3.4	3.5
$\Gamma_{4\text{-CHOL}}$ (± 0.1 x 10^{-10} mol cm^{-2})	0.5	0.5	0.5	0.6	0.7	1.0	1.1	1.4	1.5
Stoichiometry (SDS:4-CHOL)	8.2 ± 0.2	8.6 ± 0.2	8.5 ± 0.2	7.0 ± 0.2	5.7 ± 0.2	4.0 ± 0.1	3.2 ± 0.1	2.5 ± 0.1	2.3 ± 0.1
α (± 2 $Å^2$)	41	41	39	42	42	43	46	48	47

Table 3. 15 Model-fitted structural parameters for SDS monolayers in the presence of 4-CHOL and with additional 4-CHOL added to the monolayer at 2.0 x CMC

Time (hours)	0	8.5	12	19
d_{tail} (± 0.3Å)	10.3	11.4	11.6	11.9
$V_{f\ H2O}$ (± 1%)	0.61	0.62	0.65	0.66
Γ_{SDS} (± 0.1 x 10^{-10} mol cm^{-2})	4.2	4.1	3.8	3.7
$\Gamma_{4\text{-}CHOL}$ (± 0.1 x 10^{-10} mol cm^{-2})	0.3	0.7	1.2	1.1
Stoichiometry (SDS:4-CHOL)	12.6 ± 0.3	5.8 ± 0.1	3.2 ± 0.1	3.5 ± 0.1
α (± 2$Å^2$)	39	40	44	45

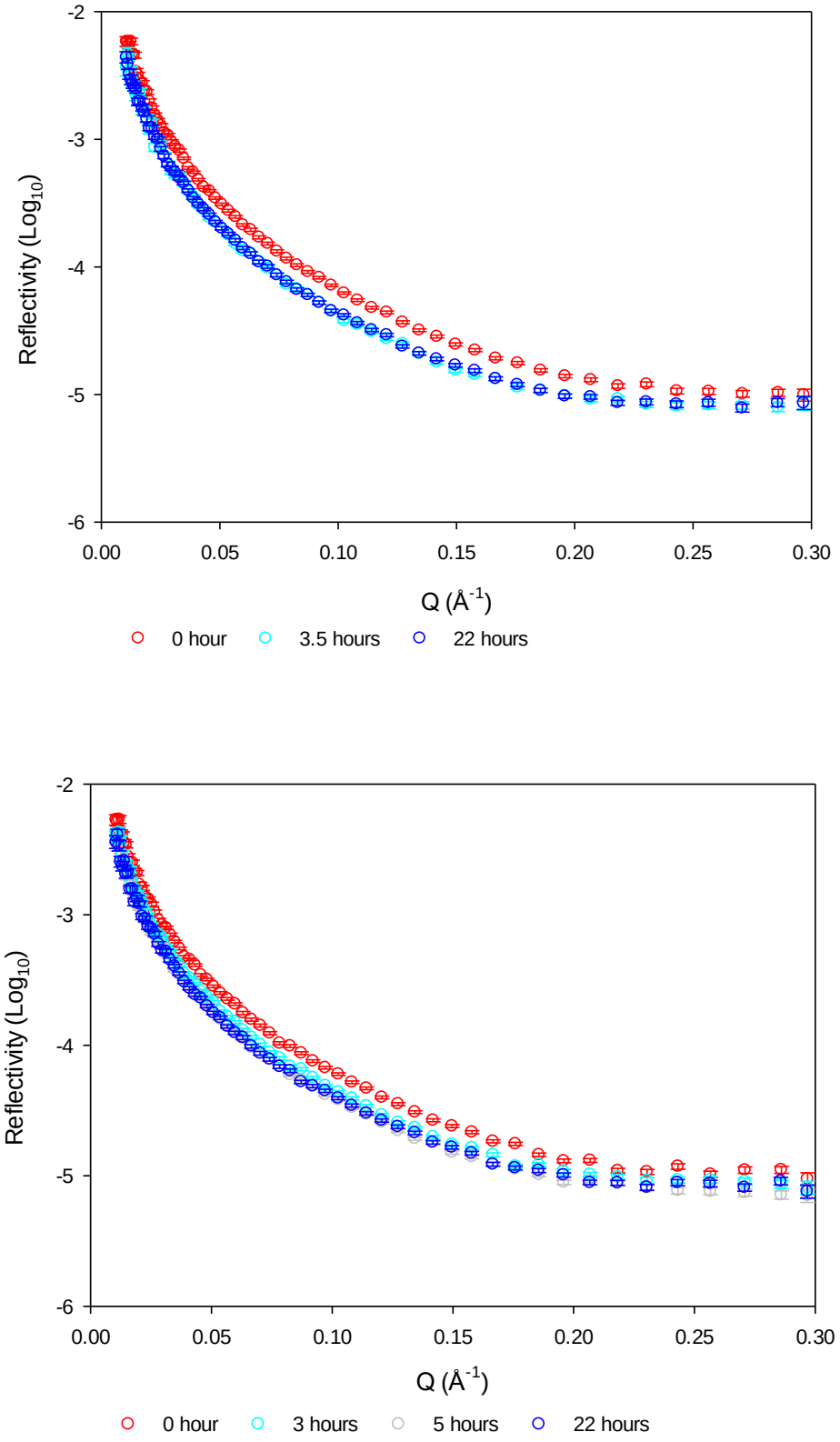

Figure 3. 15 NR profiles of ADS (upper panel) and LDS (lower panel) monolayer in the presence of 4-cholesten-3-one at 2.0 x CMC

Table 3. 16 Fitting parameters (chain thickness, volume fraction of solvent, surface excess, area per molecule and stoichiometry) for ADS monolayer in the presence of 4-CHOL at 2.0 x CMC

Time (hours)	0	3.5	8	12	18	22
d_{tail} (± 0.3Å)	9.7	13.0	13.1	13.5	13.7	13.4
$V_{f\ H2O}$ (± 1%)	0.60	0.69	0.70	0.69	0.69	0.68
Γ_{SDS} (± 0.1 x 10^{-10} mol cm^{-2})	4.3	3.4	3.3	3.4	3.4	3.5
$\Gamma_{4\text{-CHOL}}$ (± 0.1 x 10^{-10} mol cm^{-2})	0.1	1.6	1.7	1.7	1.8	1.6
Stoichiometry (ADS:4-CHOL)	33.5 ± 0.8	2.2 ± 0.1	2.0 ± 0.1	2.0 ± 0.1	1.9 ± 0.1	2.2 ± 0.1
α (± 2$Å^2$)	38	49	51	49	49	48

Table 3. 17 Fitting parameters (chain thickness, volume fraction of solvent, surface excess, area per molecule and stoichiometry) for LDS monolayer in the presence of 4-CHOL at 2.0 x CMC

Time (hours)	0	3	5	13	18	22
d_{tail} (± 0.3 Å)	10.4	12.5	13.3	13.6	14.4	14.3
$V_{f\ H2O}$ (± 1 %)	0.61	0.66	0.70	0.71	0.69	0.69
Γ_{SDS} (± 0.1 x 10^{-10} mol cm^{-2})	4.0	3.5	3.1	3.1	3.2	3.2
$\Gamma_{4\text{-}CHOL}$ (± 0.1x 10^{-10} mol cm^{-2})	0.5	1.3	1.8	1.9	2.0	2.0
Stoichiometry (LDS:4-CHOL)	8.4 ± 0.2	2.6 ± 0.1	1.7 ± 0.1	1.6 ± 0.1	1.6 ± 0.1	1.6 ± 0.1
α (± 2 $Å^2$)	41	47	53	54	51	51

3.4 Conclusions

The neutron reflectometry revealed the structure and composition of the C_{12}-chain surfactant monolayers in the presence/absence of steroids 4-cholesten-3-one (4-CHOL) and adrenosterone (ADRENO). In this study, the interfacial properties were investigated and linked to the bulk properties for a better understanding of the surfactants' solubilisation of the steroids 4-CHOL and ADRENO. To conclude:

- The 4-CHOL and ADRENO appear to insert into the surfactant monolayers between the C_{12} chains.
- No significant change was found at the air-water interface after introducing extra steroid into the monolayers at surfactant concentrations above the CMC. However, at surfactant concentrations below the CMC, externally applied steroid gave rise to an increase in the amount steroid in the monolayer, and this was more pronounced for the surfactant monolayers in the presence of 4-CHOL.
- For a freshly formed surfactant monolayer, the time taken for the surfactants adsorbed at the surface to reach equilibrium might range from milliseconds to days [168]. In the NR studies reported here, the steroid-free monolayers of surfactant and those saturated with ADRENO reached equilibrium within one hour. For the air-water interface of dodecyl sulfate surfactants in the presence of 4-CHOL, the time taken to reach equilibrium was much longer than for any of the other systems studied and this is consistent with the time effects seen for these systems in the surface tension studies (Chapter 2.2).
- Significant time effects were only found in the dodecyl sulfate surfactant/4-CHOL system, and the equilibration times varied depending on the nature of the associated counterions. The dodecyl sulfate monolayers with Na^+ counterions were found to have the longest equilibration time while the equilibration time for the ammonium dodecyl sulfate monolayer was the shortest.

Chapter 4

Small angle neutron scattering

4.1 Introduction

Scattering techniques are widely used to study the relationship between the physical properties and molecular structure in micellar systems [170-173]. For micelles of the order of 10^2 Å in size that are formed from hydrogen-rich organic or biological materials, there are particular advantages provided by small angle neutron scattering (SANS). With this technique, the use of neutrons as probe allows that samples can be studied in a non-invasive and non-destructive manner, yielding quantitative information on the size, shape and internal structures of micelles. In addition, by exploiting the neutron's isotopic sensitivity, contrast variation can be used, exchanging hydrogen (^{1}H) for deuterium (^{2}D), for example, so that different molecules or parts of molecules within a system can be selectively highlighted. Some recent reports in which SANS has been used to determine the structures of surfactant micelles are given in [174-177].

4.1.1 Scattering basics

Neutron beams are either produced continuously by nuclear fission in reactor-based neutron sources or in pulses by spallation in accelerator-based neutron sources. Immediately after production, the neutrons are slowed by passage through moderating materials such as liquid hydrogen so that they have the right energy to be used in the application of interest. The incident neutron beam will be collimated to an appropriate size and shape before it encounters the sample. The neutron instruments count the number of scattered neutrons as a function of scattering vector, Q. The scattering vector, Q, describes the relationship between the incident and scattered wave vectors (k_i and k_s respectively) and depends on the scattering angle θ and wavelength, λ:

$$Q = |Q| = |k_s - k_i| = \frac{4\pi}{\lambda}\sin\frac{\theta}{2} \quad [4.1]$$

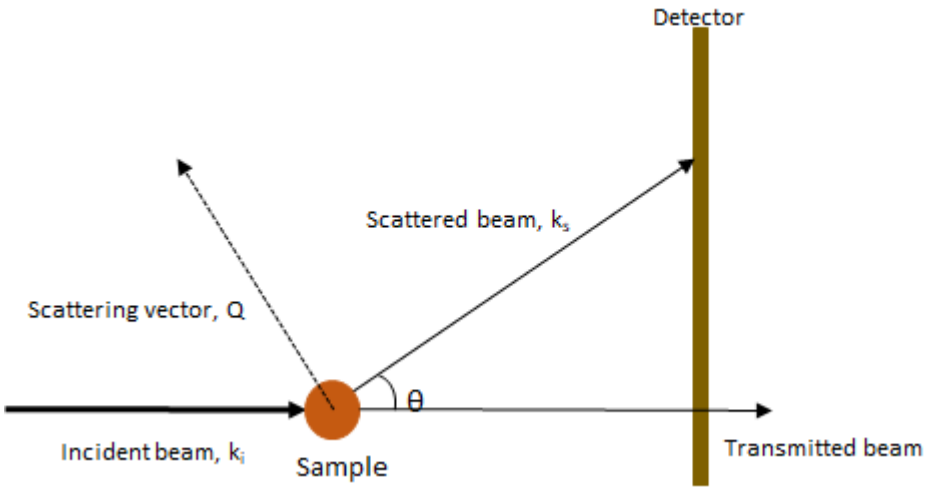

Figure 4. 1 The geometry of a SANS experiment

Q has dimensions of reciprocal length and units are normally $Å^{-1}$. Large structures scatter to low Q and small structures at high Q values.

According to Bragg's low of diffraction:

$$\lambda = 2d\sin\theta/2 \quad [4.2]$$

and by substituting in equation 2 we thus have that:

$$d = \frac{2\pi}{Q} \quad [4.3]$$

where d is a molecular-level length scale by virtue of the Q-range accessible from SANS [178].

4.1.2 Differential scattering cross-section

The differential scattering cross-section, $(d\Sigma/d\Omega)(Q)$, is generally referred to as the intensity of scattering, I(Q). When neutrons of a given wavelength are scattered through a particular angle and are incident on a small area of the detector, the neutron flux – the number of neutrons arriving in unit time – can be measured, and I(Q. $(d\Sigma/d\Omega)(Q)$ contains information on the size, shape and interaction between particles within a scattering sample, and can be defined as:

$$\left(\frac{d\Sigma}{d\Omega}\right)(Q) = NV^2(\Delta\rho)^2P(Q)S(Q) + B \quad [4.4]$$

where N is the number concentration of scattering centres, V is the volume of a scattering centre, $(\Delta\rho)^2$ is the neutron contrast, $P(Q)$ and $S(Q)$ are the form factor and structure factor (discussed below), and B is the sample background.

4.1.3 Form factor

The form factor, P(Q), can provide the intra-particle information and is dependent on the size and shape of the scattering centre. In general, the form factor is a dimensionless function that describes how $(d\Sigma/d\Omega)(Q)$ is modulated by interference effects between neutrons scattered by different parts of the same scattering centre [178]. The function P(Q) is defined as 1.0 at Q=0. For a sphere of radius R:

$$P(Q) = \left[\frac{3(\sin(QR) - QR\cos(QR))}{(QR)^3}\right]^2 \qquad [4.5]$$

4.1.4 Structure factor

The inter-particle structure factor, S(Q), is another dimensionless function but describes how $(d\Sigma/d\Omega)(Q)$ is modulated by interference effects between neutrons scattered by different scattering centres. Consequently, it depends on the type of interactions between scattering centres (i.e., whether the interactions are repulsive or attractive) and is given by:

$$\mathrm{S(Q)} = 1 + \frac{4\pi N}{QV_S}\int_0^{\infty}[g(r) - 1]\, r\sin(Qr)dr \qquad [4.6]$$

where g(r) is the pair correlation function for the scattering objects and is related to the radial distribution function.

P(Q) is independent of the concentration of a scattering sample while S(Q) can be obtained from the measured $(d\Sigma/d\Omega)(Q)$ at two different concentrations. Alternatively, the data of $(d\Sigma/d\Omega)(Q)$ can be model-fitted by approximating S(Q) using some analytical expression developed for a particular type of system. Attractive interactions between the scattering centre leads to an increase in $[(d\Sigma/d\Omega)(Q)]_{Q\to 0}$ with increasing concentration and vice versa.

4.1.5 Neutron contrast variation

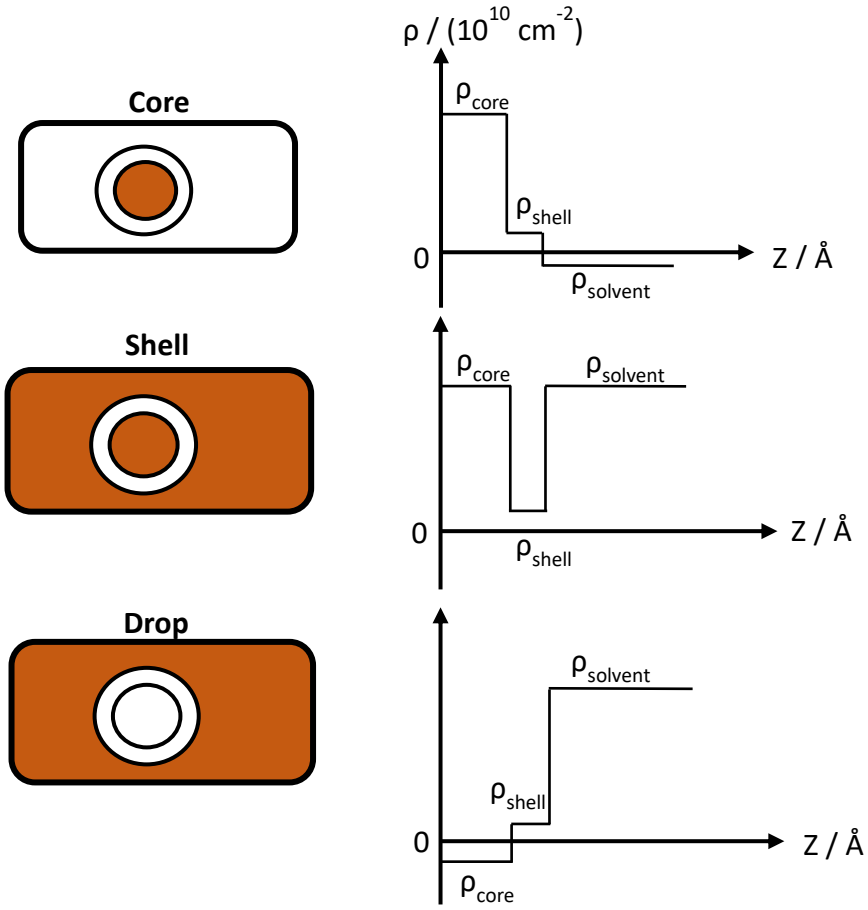

Figure 4. 2 Elucidation of the structure of micellar solution by contrast variation. The scattering length density ρ, depends on Z, the distance from the centre of a droplet.

As mentioned earlier, the significant difference in neutron scattering lengths (b) between hydrogen and deuterium can be exploited in small-angle neutron scattering to provide information on selected components within a scattering sample. In practice, the scattering length density, ρ, is more frequently used to quantify the difference in scattering efficiency. ρ can be calculated from the composition and density of the *i*th set of atoms in the system:

$$\rho = N_A \sum_i b_i = \frac{\delta N_A}{M} \sum_i b_i \qquad [4.7]$$

where b is the coherent neutron scattering length (Å), N_A is Avogadro's number, δ is the bulk density of the molecule (g/cm^{-3}) and M is the molar mass (g/mol). It should be noted that ρ has dimensions of (length)$^{-2}$ with units of 10^{-6} Å^{-2} or 10^{10} cm^{-2}.

The very different neutron scattering properties of hydrogen and deuterium can be applied to great advantage in the study of micellar systems, with different regions "highlighted" by selectively varying the ρ of the surfactant and solvent.

There are three solvent contrasts that are commonly used in such studies, generally referred to as the core, shell and drop contrasts, and these are illustrated schematically in Figure 4.2. By using these three contrasts in the SANS study of a micellar system the micelle can be considered as comprising a poorly solvated core and a well-solvated corona, and equation 4 can be rewritten as

$$\left(\frac{d\Sigma}{d\Omega}\right)(Q) = \frac{16\pi^2}{9} NP(Q)S(Q) + B \qquad [4.8]$$

where

$$\begin{aligned} \mathrm{P(Q)} = {} & [(\rho_{shell} - \rho_{core})^2 R_{outer}^6 P(Q, R_{outer})] \\ & + \left[2(\rho_{shell} - \rho_{medium})(\rho_{core} - \rho_{shell}) R_{inner}^3 R_{outer}^3 \right. \\ & \left. \times P(Q, R_{inner})^{1/2} P(Q, R_{outer})^{1/2}\right] \\ & + [(\rho_{core} - \rho_{shell})^2 R_{inner}^6 P(Q, R_{inner})] \end{aligned} \qquad [4.9]$$

$P(Q, R_{outer})$ and $P(Q, R_{inner})$ are the form factors for spheres of drop radius R_{outer} and core radius R_{inner}, respectively. Clearly, for the core contrast, only the scattering from the core can be observed since the shell of the micelle is contrast matched to the continuous phase/solvent medium, so $\rho_{shell} = \rho_{medium}$, and for the shell contrast $\rho_{core} = \rho_{medium}$. Therefore

$$\begin{aligned} \mathrm{P(Q)} = {} & \left[(\rho_{shell} - \rho_{medium}) R_{outer}^3 P(Q, R_{outer})^{\frac{1}{2}} \right. \\ & \left. - (\rho_{shell} - \rho_{medium}) R_{inner}^3 P(Q, R_{inner})^{\frac{1}{2}}\right]^2 \\ = {} & \left[(\rho_{shell} - \rho_{medium}) R_{outer}^3 P(Q, R_{outer})^{\frac{1}{2}} \right. \\ & \left. + (\rho_{core} - \rho_{shell}) R_{inner}^3 P(Q, R_{inner})^{\frac{1}{2}}\right]^2 \end{aligned} \qquad [4.10]$$

By fitting these equations to the measured scattering, it is possible to obtain the thickness of the micelle core, and shell and their respective scattering length densities. In addition, the hydration of the surfactant micelles can be obtained.

4.2 Small angle neutron scattering measurement and data treatment

The SANS measurements performed in the studies reported here were performed on the LOQ and SANS 2D instruments at the ISIS Facility (Rutherford Appleton Laboratory, UK). Both instruments use time-of-flight (TOF) while SANS2D uses neutrons within an incident wavelength (λ) between 2.2 to 14 Å and for LOQ the incident wavelength range is 2.2 Å < λ < 10 Å, giving a scattering vector Q = $(4\pi/\lambda)/\sin(\theta/2)$ ranges of 0.006 $Å^{-1}$ < Q < 0.7 $Å^{-1}$ and 0.008 $Å^{-1}$ < Q < 0.24 $Å^{-1}$ respectively. The measured samples were placed in 1 mm or 2 mm Banjo cells (Hellma, UK) and the SANS measurements recorded with the samples maintained at 25 ± 0.1 ^{o}C, using an incident beam diameter of 12 mm. The scattering patterns of neutrons passing through the samples were recorded on a detector with a sample-to-detector distance of 4 m. (NB, For all the measurements reported here – other than those presented in section 4.4.4, the samples were at equilibrium.)

The scattering of the empty cell and solvent background were firstly measured as transmission measurements. The raw SANS data were corrected by subtracting the data from transmission and converted to scattered intensity data as a function of wave vector transfer (I(Q) vs Q) and placed on an absolute scale ($Å^{-1}$) using standard procedures [179, 180]. Background was subtracted manually.

SANS profiles were analysed using Heenan's FISH software [179]. The structure of micelles was established by fitting the SANS data using standard models for the structure factor S(Q). The scattering data were fitted with different models in order to obtain the best fit.

Consequently, the core-shell form factor was used to describe the micelle geometry. The form factor can be modelled assuming either spherical or elliptical micelles. For a sphere with a radius of R, the micelle volume, $V_{micelle} = \frac{4}{3}\pi R^3$, whereas for an

ellipsoid, $V_{micelle} = \frac{4}{3}\pi R_{major} {R_{minor}}^2$ (R_{major} and R_{minor} are the semi major axis and semi minor axis, respectively). The aggregation number, N_{agg}, was then obtained by dividing $V_{micelle}$ by the calculated swollen molecular volume of its corresponding surfactant (V_s). For surfactant micelles in the presence of steroids, the surfactant volume was recalculated according to the molar solubilisation ratio determined in the earlier studies (see section 2.1).

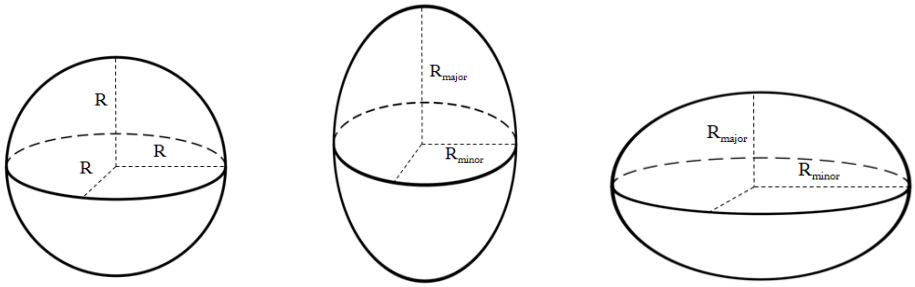

Sphere **Prolate** **Oblate**

Figure 4. 3 Schematic representation of micelle shape

The surface area of a spherical micelle is obtained as $4\pi R^2$. For a prolate ellipsoid (where $R_{major} > R_{minor}$), the surface area, S_{pro}, can be expressed as:

$$S_{pro} = 2\pi R_{minor}^2 \left(1 + \frac{R_{major}}{eR_{minor}} \cdot arc\sin(e)\right), \text{ where } e^2 = 1 - \frac{R_{minor}^2}{R_{major}^2} \quad [4.11]$$

and for oblate ellipsoids (where $R_{minor} > R_{major}$), the surface area, S_{obl} , takes the form:

$$S_{obl} = 2\pi R_{minor}^2 \left(1 + \frac{R_{major}^2}{eR_{minor}^2} \cdot arc\tanh(e)\right), \text{ where } e^2 = 1 - \frac{R_{major}^2}{R_{minor}^2} \quad [4.12]$$

4.2.1 SANS studies and model-fitting of the surfactant/steroid systems

In the SANS studies for the surfactant micelles formed in the presence of the steroids 4-cholesten-3-one (4-CHOL) and adrenosterone (ADRENO), the steroids were used at concentrations that ensured the solute saturation in each system (as determined earlier; see 2.1)

Given the conclusion reached in the monolayer neutron reflectivity studies of these systems that the 4-CHOL and ADRENO inserted into the hydrocarbon chain layers of the monolayers, the initial working hypothesis that was assumed when model-fitting

the SANS profiles for the corresponding surfactant/steroid micellar systems was that the steroids would be solubilised within the hydrophobic cores of the micelles.

4.3 Materials

Sodium dodecyl sulfate (SDS), ammonium dodecyl sulfate (ADS), lithium dodecyl sulfate (LDS), dodecyl trimethylammonium bromide (DTAB) and N, N-dimethyldecylamine N-oxide (DDAO), N-dodecyl-N, N-dimethyl-3-ammonio-1-propanesulfonate (DDAPS) were purchased from Sigma (Dorset, UK) and dodecyl phosphocholine (DPC) was obtained from Avanti Polar Lipids (Alabama, USA). Ultra-pure polyoxyethylene sorbitan monolaurate (Tween 20) was supplied by National Diagnostics (Hull, UK) and polyoxyethylene (23) lauryl ether (Brij 35) was purchased from MP Biomedicals LLC (Ohio, USA)

Alkyl chain deuterated d_{25}SDS, d_{25}ADS, d_{25}LDS, d_{25}DTAB, d_{25}DDAO and d_{25}DDAPS were kindly provided by the Oxford Deuteration Facility (Didcot, UK). The ethylene oxide deuterated Tween 20 was also supplied by the Oxford Deuteration Facility (Didcot, UK). d_{25}DPC was obtained from CDN Isotopes (New Jersey, USA).

4-cholesten-3-one (98+%) was purchased from Alfa aesar (Thermo fisher Scientific, UK) and adrenosterone (97+%) from Santa cruz (Germany).

D_2O (99.9 atom % D) was supplied by the Oxford Deuteration Facility (Didcot, UK).

4.4 Results

4.4.1 SANS studies for ionic surfactants

Fitting parameters for ionic surfactant micelles

For ionic surfactants, the two-shell ellipsoid model incorporating the Hayter-Penfold structure factor was used to fit the data [181]. The parameters fitted in this model included the micelle's core radius (R_1), core axial ratio (x), and charge (Z) and the inverse Debye length (AKK). For spheres, the axial ratio x has a value of 1, and for ellipsoidal micelles it is < 1 if they are oblate and > 1 if they are prolate. The inner core radius R_1 was constrained to a value close to the maximum C_{12} alkyl chain length

(l_{ext}, 16.7 Å), acceptable values taken to lie in the range 95% to 105% of l_{ext} (*viz.*, ca. 16 – 17 Å). The micelle shell thickness (δ) was constrained by R_1 and the molecular volume and hydration of the surfactant head group. In some studies, model fits were also explored wherein part of the surfactant alkyl tail intruded into the micelle shell. As was previously reported by Saaka [87], however, there was no significant effect on the outcome fits choosing either of these criteria.

Other parameters which were used to fit the SANS data are shown in Table 4.1. The molecular volume and hydration were obtained from viscosity and density measurements (section 2.3) or else were calculated *ab-initio*. The scattering length densities of each component were calculated from equation 4.7.

Table 4. 1 Molecular formulas, molecular volume (V_m), molecular weight (M_w) and scattering length density (ρ) of the constituents of the ionic surfactants and steroids studied.

Chemical	Molecular formula		V_m (Å^3)	M_w (g mol^{-1})		ρ (x 10^{-6} Å^{-2})	
	Protiated	Deuterated		Protiated	Deuterated	Protiated	Deuterated
4-CHOL	$C_{27}H_{44}O$	N/A	652.5	384.6	N/A	0.34	N/A
ADRENO	$C_{19}H_{24}O_3$	N/A	422.6	300.4	N/A	1.27	N/A
DTAB	$C_{15}H_{34}BrN$	$C_{15}D_{25}H_9BrN$	477.7	308.4	333.5	-0.23	5.08
TAB	C_3H_9BrN	N/A	124.0	139.0	N/A	0.18	N/A
SDS	$NaC_{12}H_{25}SO_4$	$NaC_{12}D_{25}SO4$	414.0	288.4	313.0	0.39	6.66
SS	$NaSO_4$	N/A	60.3	119.0	N/A	4.89	N/A
ADS	$NH_4C_{12}H_{25}SO_4$	$NH_4C_{12}D_{25}SO4$	414.8	288.4	313.4	0.16	6.45
AS	NH_4SO_4	N/A	61.1	119.1	N/A	3.35	N/A
LDS	$LiC_{12}H_{25}SO_4$	$LiC_{12}D_{25}SO4$	410	272.3	297.3	0.25	6.60
LS	$LiSO_4$	N/A	56.3	103.0	N/A	4.4	N/A
Alkyl chain	$C_{12}H_{25}$	$C_{12}D_{25}$	353.7	169.3	194.5	-0.39	6.95

Aggregation behaviour of DTAB micelles

SANS measurements for DTAB micelles were made at concentrations of 3 wt% and 5 wt% in three contrasts as shown in Figure 4.4. From the SANS profiles, the scattering intensities increased with increasing surfactant concentration. For ionic surfactant micelles generally the electrostatic repulsion between the charged head groups could result in the existence of a peak in the SANS profile, located at $Q = 2\pi/d$, where d here is the mean distance between micelles. The peaks for DTAB micelles were observed at 0.06 – 0.07 Å in each contrast, and they shift to the right (higher Q value) at higher concentration indicating (as would be expected) that the inter-micelle distance decreases as the concentration of particles increases.

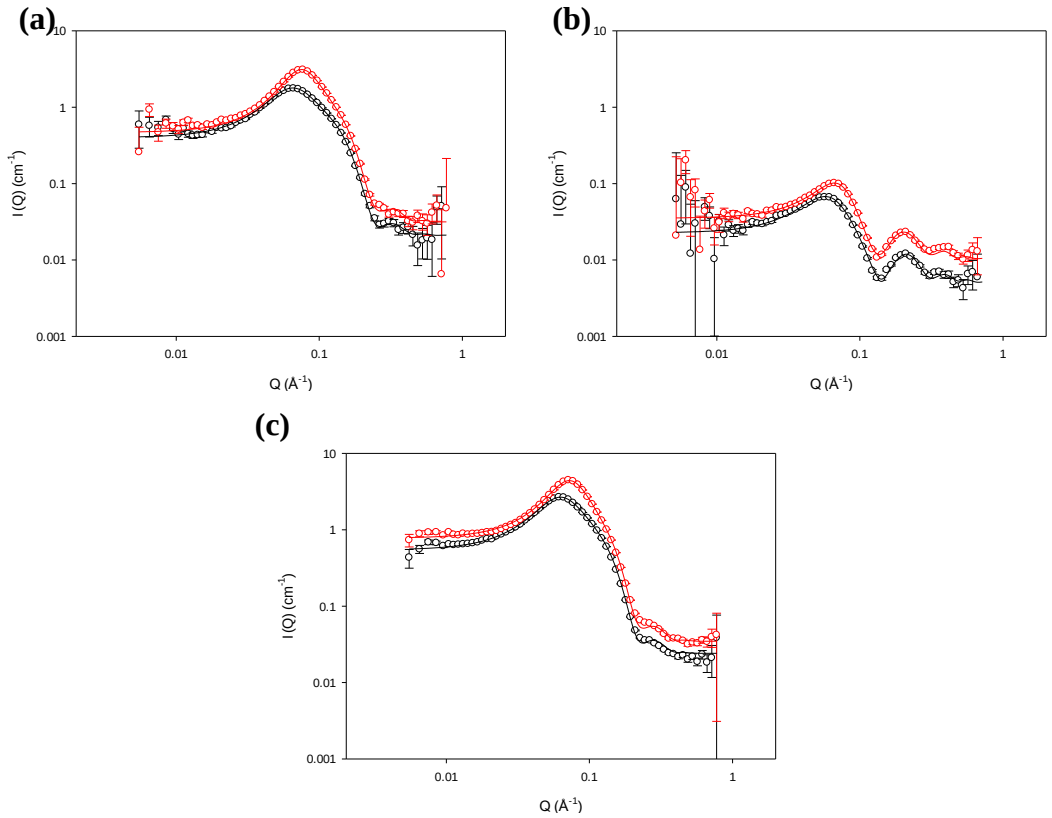

Figure 4. 4 SANS profiles and model fits (solid line) for 3 wt % (black) and 5 wt % (red) d_{25}DTAB in H_2O (a), d_{25}DTAB in D_2O (b) and h_{25}DTAB in D_2O (c).

The SANS data for DTAB micelles were modelled assuming that the micelle shell was composed of the trimethylammonium headgroups (TAB^+) together with their associated counterions and solvent of hydration, while the core was taken to comprise just the C_{12} hydrocarbon chains. The SANS model fits consistently showed that the DTAB micelles were prolate ellipsoids as the core axial ratios (x) were greater 1 (Table 4.2). The DTAB micelles grew with surfactant concentration as the micelle

volume increased from ~51k to ~55k $Å^3$ while the thickness of the surfactant head group layer (the micelle shell thickness) remained unchanged (~5 Å). This results in more elongated ellipsoidal aggregates as x was seen to increase as the concentration was increased from 3 wt% to 5 wt%. The larger micelles caused higher values for the aggregation number and micelle charge, while the area per molecule decreased slightly.

Griffiths et al. [146] previously determined the structure of DTAB micelles using SANS. They also chose an elliptical core-shell model to fit the obtained SANS data using FISH [179]. In their model, the aggregation number was calculated from the volume of the hydrophobic core and the composition weight volume per tail, and the shell of the micelle was taken to consist of the surfactant head groups and water with the thickness of the shell taken as the size of the head group. Thus, it is valuable comparing the results from Griffiths et al. with the data obtained in this study because of the similar fitting procedure used.

At a surfactant concentration of 1.5 wt%, Griffiths et al. found the core radius (R_1) of DTAB micelles to be 16.7 ± 0.1 Å with the micelle axial ratio (x) of 1.1 ± 0.1, and the shell thickness was determined as 5.3 ± 0.2 Å, with the micelle charge, 11.7 e. It is encouraging that these results are in good agreement with the results presented here.

Rodenas et al. [182, 183] also studied the geometry of DTAB micelles and reported an aggregation number at ~3 wt% in the range 66 to 73, which again is comparable with the results obtained here. In these studies, only one contrast was determined, as opposed to the three contrasts used in the present study and so small differences in the values of the fitted micelle parameters are not, therefore, unacceptable.

Table 4. 2 Values of model fitted parameters for 3 wt% and 5 wt% DTAB micelles.

Contrast	R_1 (Å)	x	R_3 (Å)	δ (Å)	V_m ($Å^3$)	Z e	SAA N_{agg}	S_{core} ($Å^2$)	A_{core} ($Å^2$)	S_m ($Å^2$)	A_m ($Å^2$)
3% Drop	15.8	1.52	24.5	4.9	49731	14	73	4339	60	6678	92
3% Shell	15.8	1.52	24.1	4.9	52013	14	71	4277	60	6867	96
3% Core	15.8	1.49	23.6	4.9	51325	14	70	4210	60	6794	97

Contrast	R_1 (Å)	x	R_3 (Å)	δ (Å)	V_m ($Å^3$)	Z e	SAA N_{agg}	S_{core} ($Å^2$)	A_{core} ($Å^2$)	S_m ($Å^2$)	A_m ($Å^2$)
5% Drop	15.9	1.62	25.7	4.8	52464	15	77	4528	59	6954	91
5% Shell	16.1	1.58	25.4	4.8	57226	15	78	4554	59	7341	95
5% Core	15.9	1.60	25.4	5.0	55787	15	76	4493	59	7225	95

Fitting parameters include the core equatorial radius (R_1), core axial radius (R_3), core axial ratio (x), shell thickness (δ), micelle volume (V_m), micelle charge (Z), micelle aggregation number (SAA N_{agg}), surface area for hydrocarbon chain (S_{core}) and whole micelle (S_m) and the corresponding areas per molecule (A_{core} and A_m). Uncertainty for R_1, x, δ, N_{agg}, S and A = ± 0.3, ± 0.03, ± 0.3, ± 7, ± 250, and ± 1 respectively

DTAB micelles in the presence of steroids

Saturation of the DTAB micelles with either 4-CHOL or ADRENO did not alter the scattering intensities significantly in the 'core' and 'drop' contrasts (Figure 4.5/4.6, (a) and (c)). The greatest changes in I(Q) for DTAB micelles in the presence of the steroids presented in the 'shell' contrast (Figure 4.5/4.6, (b)). A slight shift in the peak to lower Q was observed in the 4-CHOL-saturated micelles, suggesting that the distance between the micelles became larger upon the addition of 4-CHOL. A much smaller shift of the interaction peak was found upon saturation of the DTAB micelles with ADRENO, indicating there was only a very slight change in the inter-micelle distance in this system. A comparable study was performed by Saaka [87] and showed that the presence of testosterone enanthate in the DTAB micelles exhibited significant changes in micelle scattering curves with the interaction peak shifted to lower Q.

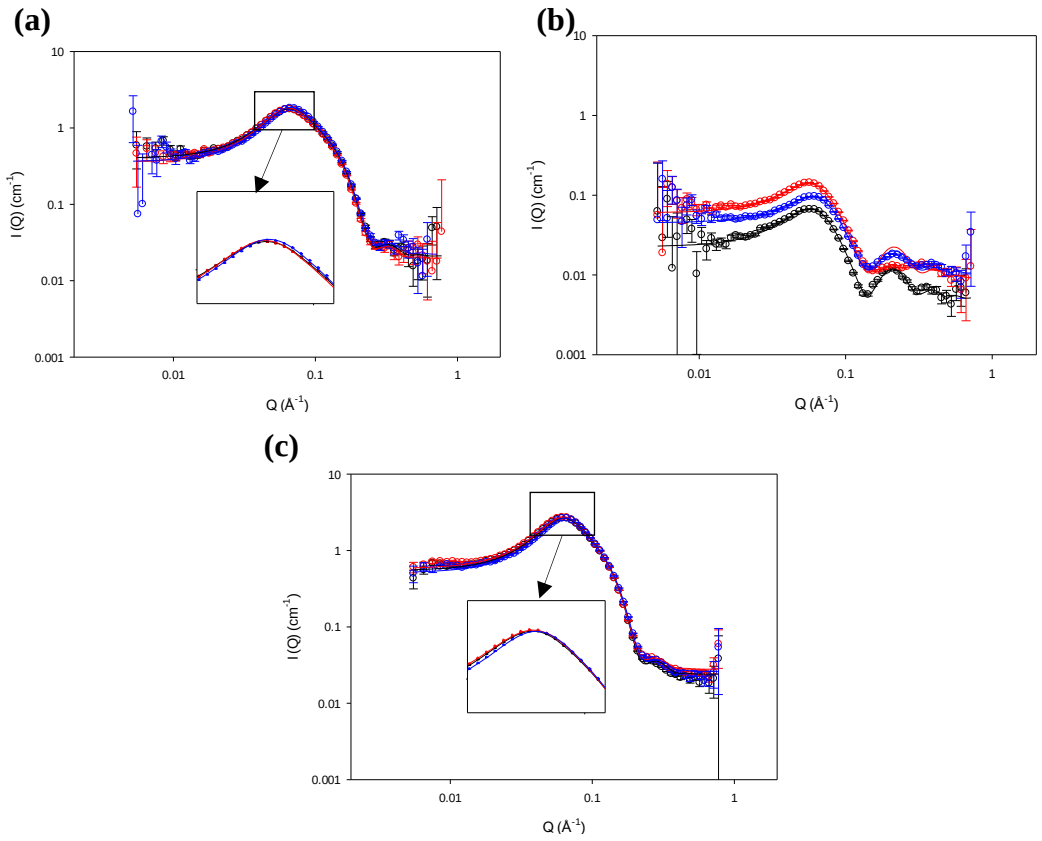

Figure 4. 5 SANS profiles and model fits (solid line) for d_{25}DTAB in H_2O (a), d_{25}DTAB in D_2O (b) and h_{25}DTAB (c) in D_2O micelles alone (black), micelles in the presence of saturation amounts of 4-CHOL (red) and ADRENO (blue) at 3 wt %

The model-fitted parameters for DTAB micelles in the presence of 4-CHOL and ADRENO are presented in Table 4.3. The model used for fitting was the same as that used for these micelles in the absence of the steroids.

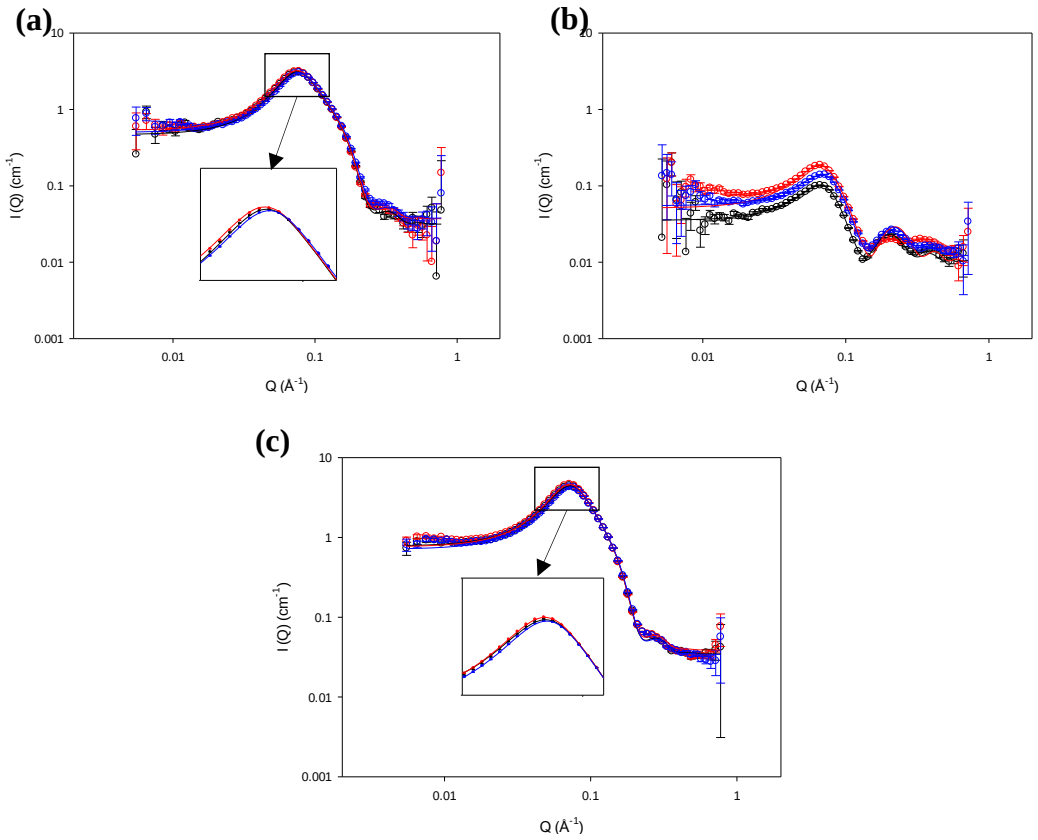

Figure 4. 6 SANS profiles for d_{25}DTAB in H_2O (a), d_{25}DTAB in D_2O (b) and h_{25}DTAB (c) in D_2O micelles alone (black), micelles in the presence of saturation amounts of 4-CHOL (red) and ADRENO (blue) at 5 wt %.

As no significant changes were found in the shapes of the scattering curves, it is concluded that the 4-CHOL and ADRENO cause very little perturbation of the DTAB micelle structure. The core axial ratio of the micelles upon addition of 4-CHOL was increased by ~5% while the saturation amount of ADRENO in the micelle caused no significant change in x.

There were also no significant changes seen in the aggregation numbers of the DTAB micelles formed in the presence of saturating levels of 4-CHOL and ADRENO. The same observation was also noted by Saaka who found that there was no change in the aggregation number of DTAB micelles in the presence of testosterone and testosterone propionate (both of these steroids having low solubilities in DTAB micelles) [87].

Assuming the micelle core as the locus of steroid solubilisation and exploiting the large difference in scattering length density between the steroids and the deuterated C_{12} chain (~ 0 x 10^{-6} Å^{-2} vs 6.95 x 10^{-6} Å^{-2}), the scattering length density of the micelle core determined through model-fitting the SANS profiles for the shell and core contrasts can, in principle, be used to establish the presence and level of 4-CHOL and

ADRENO incorporated within the micelles. In practice, however, the experimental uncertainty in the fitted scattering length densities, of ± 0.5 x 10^{-6} $Å^{-2}$, means that it is not possible unequivocally to demonstrate the presence of 4-CHOL and ADRENO within the micelle core. The apparent molar ratios of 4-CHOL:DTAB and ADRENO:DTAB are determined as 1:15 and 1:30, respectively (see section 2.1) and so the expected scattering length density for the deuterated micelle core is greater than 6.5 x 10^{-6} $Å^{-2}$, and so is very close to the dC_{12} scattering length density of 6.95 x 10^{-6} $Å^{-2}$. It is not surprising here, therefore, to find that the fitted micelle core scattering length density remained unchanged from that for the steroid-free DTAB micelles.

Moreover, since the scattering length density of the protiated DTAB head groups (and indeed those of the protiated head groups of any of the surfactants studied here) are very similar to the scattering length densities of 4-CHOL and ADRENO, it is also difficult to use the fitted scattering length density of the micelle shell to provide a clear and reliable demonstration of the presence of the steroids in this region of the aggregates.

Table 4. 3 Individual SANS fitting results for 3 wt% and 5 wt% DTAB micelles in the presence of steroids.

Steroids	Contrast	R_1 (Å)	x	R_3 (Å)	δ (Å)	V_m (Å^3)	Z e	SAA N_{agg}	Steroids N_{agg}	S_{core} (Å^2)	A_{core} (Å^2)	S_m (Å^2)	A_m (Å^2)
4-CHOL	3% Drop	15.8	1.61	25.4	4.5	51400	14	70	5	4462	63	6854	97
	3% Shell	15.3	1.61	23.7	4.8	48256	14	66	5	4065	62	6542	99
	3% Core	15.8	1.61	25.3	5.0	54875	14	75	5	4448	59	7148	95
ADRENO	3% Drop	15.5	1.55	24.0	4.4	46843	14	67	2	4156	62	6419	96
	3% Shell	15.2	1.55	23.6	4.8	47932	14	68	2	4028	59	6512	95
	3% Core	15.5	1.55	24.0	4.9	50509	14	72	2	4172	58	6743	94

Steroids	Contrast	R_1 (Å)	x	R_3 (Å)	δ (Å)	V_m ($Å^3$)	Z e	SAA N_{agg}	Steroids N_{agg}	S_{core} ($Å^2$)	A_{core} ($Å^2$)	S_m ($Å^2$)	A_m ($Å^2$)
4-CHOL	5% Drop	16.0	1.61	25.5	4.5	53843	16	74	5	4552	62	7071	96
	5% Shell	15.8	1.61	25.5	4.8	53834	16	74	5	4477	61	7066	96
	5% Core	16.0	1.61	25.8	5.1	57420	16	78	5	4591	59	7374	94
ADRENO	5% Drop	15.7	1.60	25.1	4.5	50824	16	73	2	4433	61	6807	94
	5% Shell	15.2	1.60	24.3	4.8	48565	16	69	2	4100	59	6589	95
	5% Core	15.5	1.60	24.8	4.9	51862	16	74	2	4281	58	6884	93

Fitting parameters include the core equatorial radius (R_1), core axial radius (R_3), core axial ratio (x), shell thickness (δ), micelle volume (V_m), micelle charge (Z), aggregation number of micelle and steroids(SAA N_{agg} and steroids N_{agg}), surface area for hydrocarbon chain (S_{core}) and whole micelle (S_m) and its corresponding the area per molecule (A_{core} and A_m). Uncertainty for R_1, x, δ, N_{agg}, S and A = ± 0.3, ± 0.03, ± 0.3, ± 7, ± 250, and ± 1 respectively

Aggregation behaviour of SDS micelles

The SANS profiles for all three contrasts of SANS data obtained for SDS micelles in the absence of steroids at 3 wt% and 5 wt% are presented in Figure 4.7. The data were modelled using the same model as used in analysis of the SANS data for DTAB micelles. As was seen for the DTAB micelles, there is an interaction peak in the SDS SANS profiles in the Q range 0.06 to 0.07 $Å^{-1}$ which arises due to the electrostatic repulsion between the micelles, and the peak shifts to higher Q with increased SDS concentration. The increase in concentration of SDS, is also seen to cause an increase in I(Q), indicating the presence of larger micelles and/or an increased aggregation number.

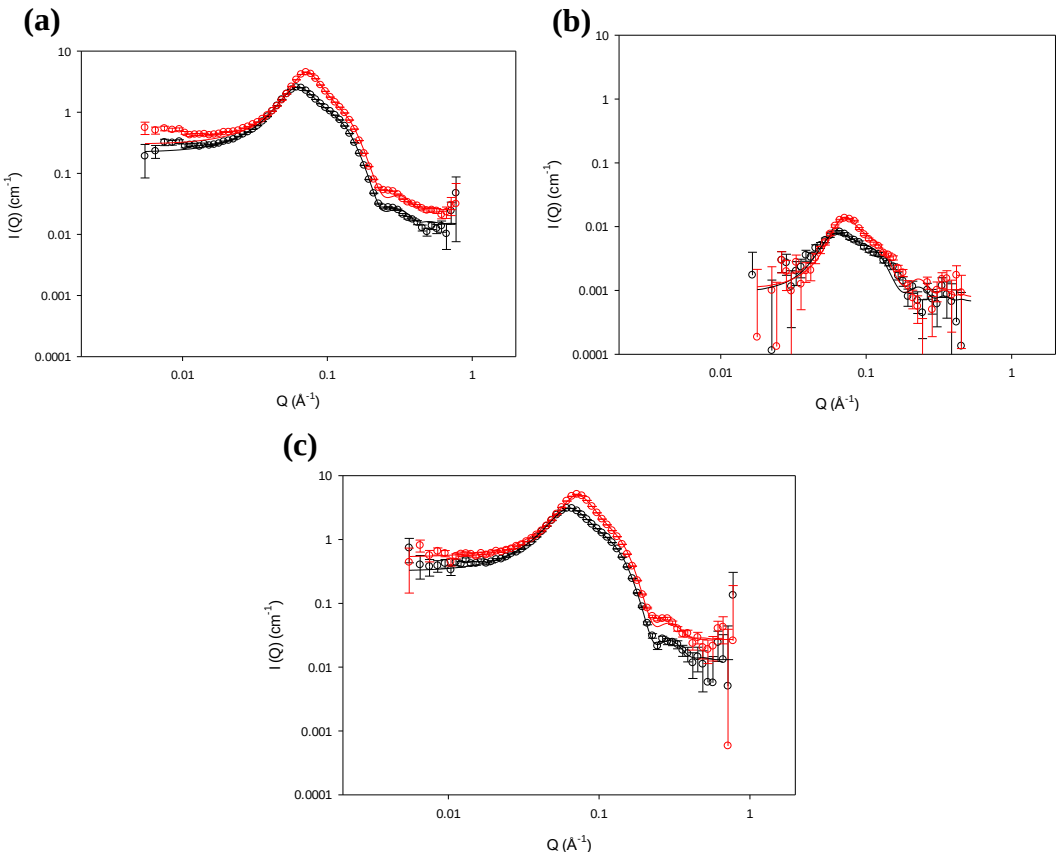

Figure 4. 7 SANS profiles and model fits (solid line) for 3 wt % (black) and 5 wt % (red) d_{25}SDS in H_2O (a), d_{25}SDS in D_2O (b) and h_{25}SDS in D_2O (c).

The scattering in the SDS 'shell' contrast was much lower than that seen with DTAB micelles, and the scattering at high Q is much noisier with higher error bars.

The SANS profile for the shell contrast for SDS micelles (Figure4.7 (b)) shows only very low scattering because the scattering length densities for the deuterated C_{12} chains and D_2O are virtually the same (6.95 and 6.38 x 10^{-6} $Å^{-2}$ respectively), and the

scattering length density for the SDS head group (DS^-, 4.89 x 10^{-6} $Å^{-2}$) is so close (and the surfactant head group layer of the micelle so thin) that there is very little contrast in this system.

The model-fitted parameters of the SDS micelles are shown in Table 4.4. Consistent results are obtained for all three SANS contrasts. The micelles here are again prolate ellipsoids, with an axial ratio above 1. The micelles become more elongated as the surfactant concentration is increased, as evidenced by the increased core axial ratio and larger core radius. The shell thickness and micelle charge, however, do not show noticeable differences when the surfactant concentration is increased. The aggregation number for SDS micelles at 3 wt% and 5 wt% were 83 and 93 respectively, and the corresponding areas per molecule at these concentrations are much the same.

The results presented here are reassuringly consistent with those presented by other workers and give confidence that the fitted models provide a reliable description of the SDS micelles. In the SANS studies reported by Caponetti et al. [184] and Hassan et al. [185] the SDS micelles were also found to be prolate ellipsoids, and the aggregation numbers and micelle charges found were close to the values obtained here (90 ± 5 and 79 ± 1, respectively, and 17 ± 5 and 33 ± 10, respectively). In the more comprehensive (three contrast) SANS study on 3 wt% and 5 wt% of SDS micelles conducted by Saaka [87], the micelle core axial ratios were determined as 1.5 at 3 wt%, increasing by 12% at 5 wt%, with the core radius remaining unchanged.

Table 4. 4 Individual SANS fitting results for 3 wt% and 5 wt% SDS micelles.

Contrast	R_1 (Å)	x	R_3 (Å)	δ (Å)	V_m (Å^3)	Z e	SAA N_{agg}	S_{core} (Å^2)	A_{core} (Å^2)	S_m (Å^2)	A_m (Å^2)
3% Drop	16.7	1.51	25.2	3.0	46122	21	83	4743	57	6354	76
3% Shell	16.7	1.51	25.2	3.1	46185	21	83	4743	57	6360	76
3% Core	16.7	1.51	25.2	3.1	46185	21	83	4743	57	6360	76

Contrast	R_1 (Å)	x	R_3 (Å)	δ (Å)	V_m (Å^3)	Z e	SAA N_{agg}	S_{core} (Å^2)	A_{core} (Å^2)	S_m (Å^2)	A_m (Å^2)
5% Drop	16.7	1.68	16.7	3.1	51368	21	93	5171	56	6909	75
5% Shell	16.7	1.68	16.7	3.1	51368	21	93	5171	56	6909	75
5% Core	16.7	1.68	16.7	3.1	51368	21	93	5171	56	6909	75

Fitting parameters include the core equatorial radius (R_1), core axial radius (R_3), core axial ratio (x), shell thickness (δ), micelle volume (V_m), micelle charge (Z), micelle aggregation number (SAA N_{agg}), surface area for hydrocarbon chain (S_{core}) and whole micelle (S_m) and its corresponding the area per molecule (A_{core} and A_m). Uncertainty for R_1, x, δ, N_{agg}, S and A = ± 0.3, ± 0.03, ± 0.3, ± 7, ± 250, and ± 1 respectively

SDS micelles in the presence of steroids

The SANS profiles for SDS micelles formed in the presence of saturating amounts of 4-cholesten-3-one (4-CHOL) were measured on LOQ and these data are shown in Figure 4.8. It may be noted here that the errors on the data at high Q are much higher than those of the data obtained on SANS 2D (see Figure 4.7) and also that the Q range is different for the different instruments. The model-fits to the SANS profiles measured on LOQ and SANS 2D were wholly consistent, however.

The SANS profiles obtained for the SDS/4-CHOL micellar system show a shift of the interaction peaks to lower Q, indicating that the inter-micelle distance is increased. There is also an increase in the scattering intensities of the SDS micelles in the presence of 4-CHOL (Figure 4.8) and the shapes of the scattering curves also change, these observations clearly indicating that there are changes in both the size and shape of the micelles when the 4-CHOL is present – a finding that seems perfectly reasonable given that the solubilisation capacity of SDS for 4-CHOL is dramatically higher than that for any of the other C_{12} surfactants.

Whereas the scattering intensity seen in the shell contrast for SDS micelles is very low, the intensity seen following the addition of 4-CHOL is very much higher, and it might thus be possible to make a reliable determination of the locus of solubilisation of 4-CHOL within the SDS micelles.

The model-fitted parameters for the SDS/4-CHOL micelles are presented in Table 4.5. Surprisingly, the volume of the 4-CHOL-saturated SDS micelles is found to increase dramatically, with R_1 increasing by more than 100%. The aggregation number of the SDS/4-CHOL micelles is found to be about twice that of the SDS micelles, and the volume of the micelles increases 3-fold. It should also be noted that the shape of the micelles changed from prolate ellipsoid to oblate ellipsoid in the presence of 4-CHOL. There are also increases seen in the shell thickness of the micelles upon the addition of 4-CHOL – 50% in the case of the 3 wt% system and 35 % in the case of the 5 wt% system.

Despite the significant change in geometry of the SDS micelles in the presence of 4-CHOL, however, there was no significant change seen in the surfactant area per molecule, and it is thus concluded that the 4-CHOL is solubilised in the core of the micelles. Moreover, for the core and shell SANS contrasts measured for the SDS/4-

CHOL systems, the scattering length densities of the deuterated core were fitted as 4 ± 0.5 $Å^{-2}$ and 3.5 ± 0.5 x 10^{-6} $Å^{-2}$ for the 3 wt% and 5 wt% respectively, which would suggest the presence of 4-CHOL in the C_{12} hydrophobic core of the SDS micelles.

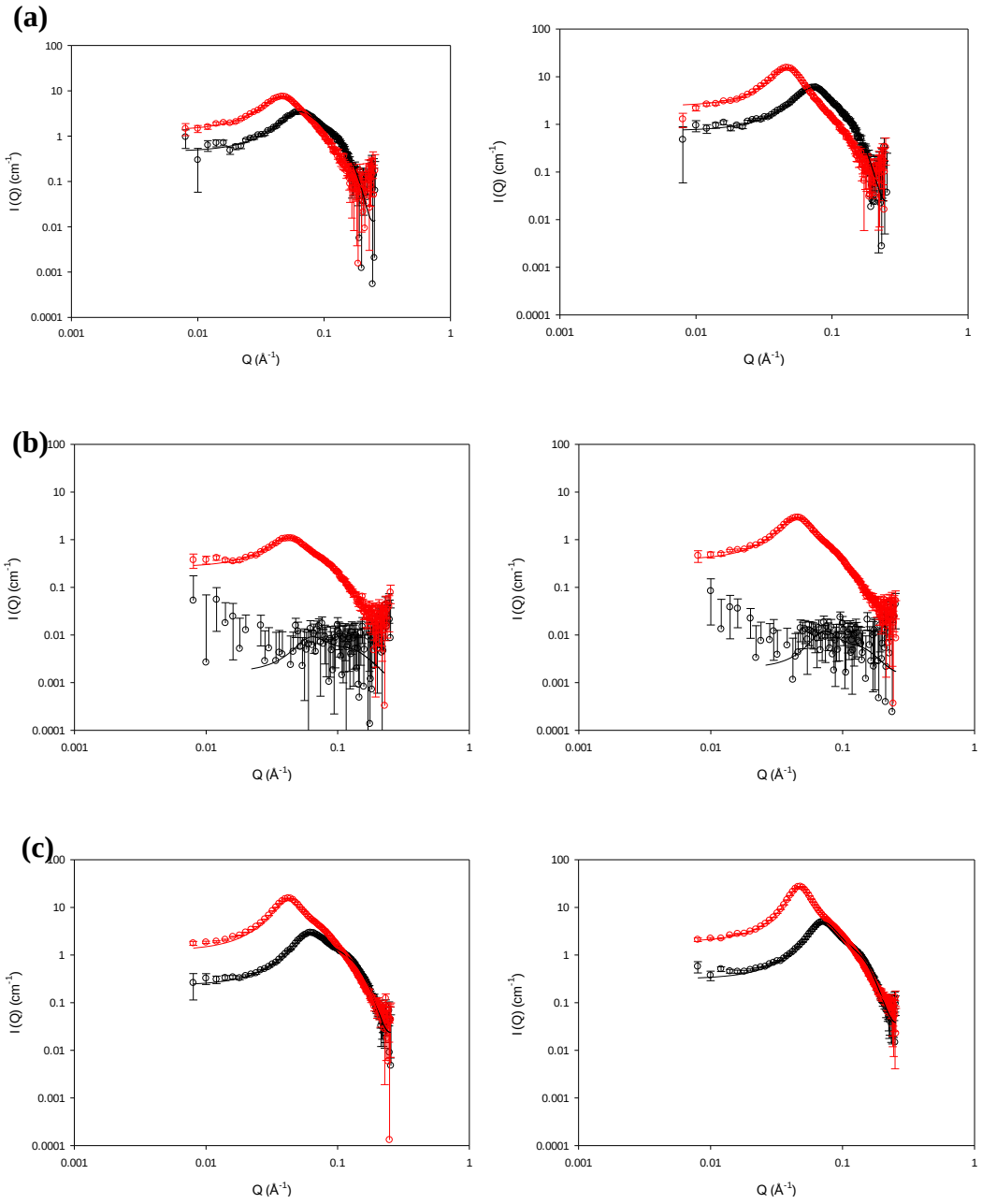

Figure 4. 8 SANS profiles and model fits (solid line) for 3 wt % (left column) and 5 wt % (right column) d_{25}SDS in H_2O (a), d_{25}SDS in D_2O (b) and h_{25}SDS (c) in D_2O in the presence (red) or absence (black) of 4-CHOL (SANS data obtained from LOQ).

The SANS profiles obtained for SDS micelles in the presence of ADRENO are shown in Figure 4.9. Unlike the 4-CHOL-saturated SDS micelles, the SANS profiles obtained for the SDS/ADRENO micelles showed no noticeable change in shape and no change in position of the interaction peak. As the solubilisation capacity of SDS

for ADRENO is much lower than for 4-CHOL, it is unsurprising, therefore, that the SANS profiles obtained for the SDS micelles and the ADRENO-saturated SDS micelles are virtually superimposable.

The model-fitted parameters for the SDS/ADRENO micelles are given in Table 4.5. The ADRENO-saturated SDS micelles are nearly spherical. The R_1 of the micelle was increased by 13% in the presence of ADRENO, while the shell thickness remained unchanged. Best fits obtained for the core and shell SANS contrasts were obtained when the scattering length density of the micelle core was changed, indicating that the ADRENO is solubilised in the hydrophobic chain region of the micelle.

The aggregation numbers of the SDS and steroids were calculated according to the molar ratio of surfactant to solubilised steroid (as reported in section 2.1). For SDS/ADRENO micelles, the aggregation number was slightly smaller than that of the SDS micelles. For 4-CHOL-saturated SDS micelles, because of the much increased volume of the micelles, the aggregation number was higher than that of the pure SDS micelles, and increased with increased SDS concentration.

The properties of SDS micelles in the presence of testosterone enanthate (TE), another steroid with high logP value, were determined by Saaka [87]. He determined the steroid-saturated SDS micelle aggregation numbers to be 147 at 3 wt% and 165 at 5 wt %, and he found that the TE/SDS micelle remained as a prolate ellipsoid with a core axial ratio of 1.9 ± 0.1. Moreover, he also observed the aggregation numbers for SDS micelles in the presence of testosterone and testosterone propionate at 3 wt% were 80 and 76, respectively. However, in Saaka's studies, the SDS micelles with saturation amounts of steroids were all prolate ellipsoidal. It should be noted here, however, that it is difficult to distinguish between oblate and prolate shapes by comparing the model fits to SANS profiles measured for low surfactant concentrations [186]. In the present study, the qualities of fits to the scattering curves for most of the pure surfactant micelles assuming prolate or oblate ellipsoid models were quite similar, but the fits to the SANS profiles for the 4-CHOL-saturated SDS micelles were appreciably better assuming oblate micelles. Moreover, it should be noted that for most prolate ellipsoid micelles observed in this study, model fits showed that increasing surfactant concentration resulted in a moderate increase in the core radius R_1 and a lesser increase in the core axial ratio, x. The R_1 of the oblate ellipsoidal

micelles, as seen here in the case of the 4-CHOL/SDS micelles in this study, increases significantly in length as the surfactant concentration is increased.

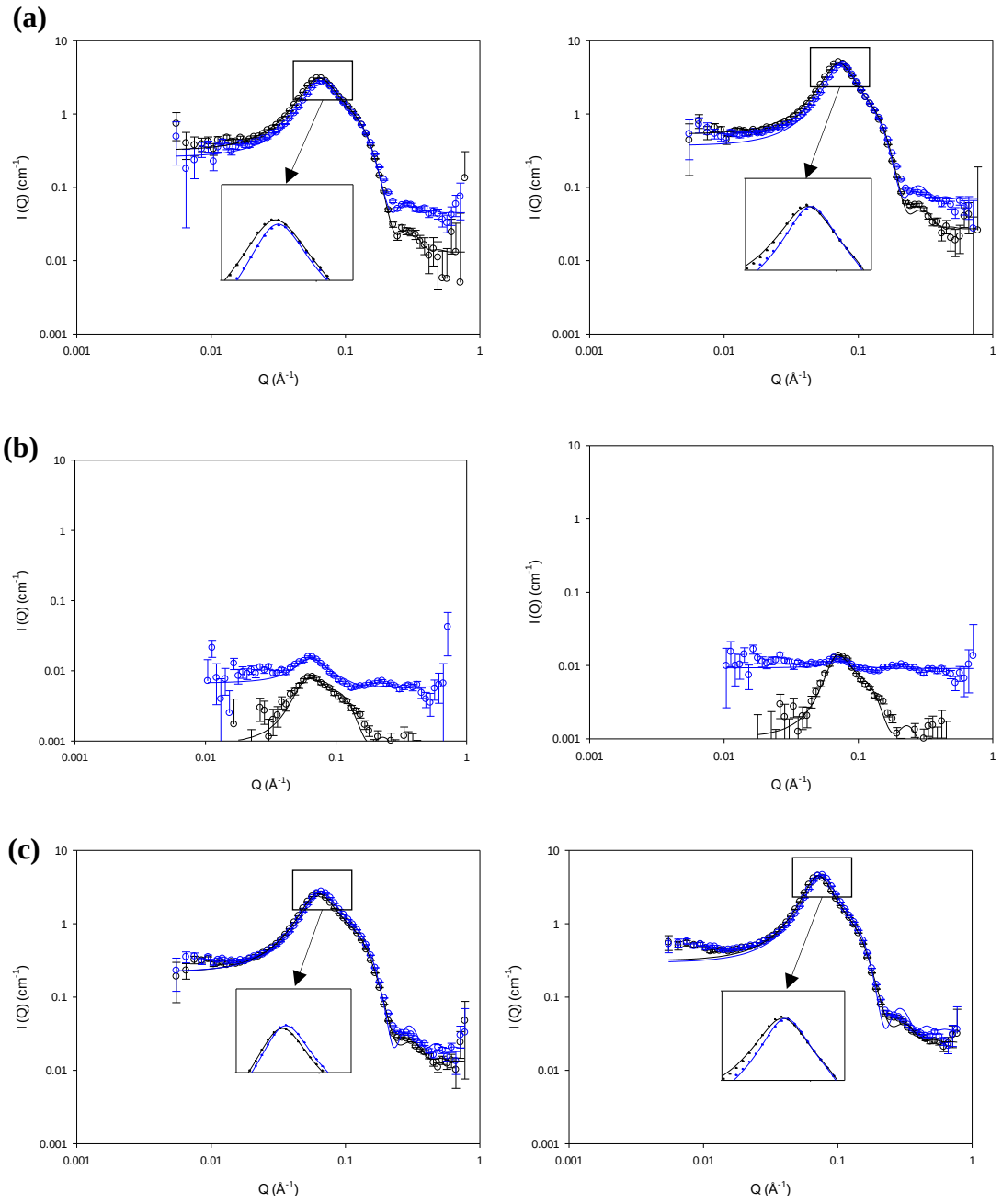

Figure 4. 9 SANS profiles model fits (solid line) for 3 wt % (left column) and 5 wt % (right column) d_{25}SDS in H_2O (a), d_{25}SDS in D_2O (b) and h_{25}SDS (c) in D_2O in the presence (blue) or absence (black) of ADRENO.

Table 4. 5 Values of model fitted parameters for 3 wt% and 5 wt% SDS micelles in the presence of steroids.

Steroids	Contrast	R_1 (Å)	x	R_3 (Å)	δ (Å)	V_m ($Å^3$)	Z e	SAA N_{agg}	Steroids N_{agg}	S_{core} ($Å^2$)	A_{core} ($Å^2$)	S_m ($Å^2$)	A_m ($Å^2$)
4-CHOL	3% Drop	38.0	0.40	15.2	4.2	144001	34	188	61	11555	61	15185	81
	3% Shell	38.0	0.40	15.2	4.2	144001	34	188	61	11555	61	15185	81
	3% Core	38.0	0.40	15.2	4.2	144001	34	188	61	11555	61	15185	81
ADRENO	3% Drop	18.9	1.05	19.8	3.1	46403	22	78	7	4489	57	6082	78
	3% Shell	18.9	1.05	19.8	3.1	46403	22	78	7	4489	57	6082	78
	3% Core	18.9	1.05	19.8	3.1	46403	22	78	7	4489	57	6082	78

Steroids	Contrast	R_1 (Å)	x	R_3 (Å)	δ (Å)	V_m ($Å^3$)	Z e	SAA N_{agg}	Steroids N_{agg}	S_{core} ($Å^2$)	A_{core} ($Å^2$)	S_m ($Å^2$)	A_m ($Å^2$)
4-CHOL	5% Drop	44.6	0.36	16.0	4.6	208770	35	273	88	15389	56	19997	73
	5% Shell	44.6	0.36	16.0	4.6	208770	35	273	88	15389	56	19997	73
	5% Core	44.6	0.36	16.0	4.6	208770	35	273	88	15389	56	19997	73
ADRENO	5% Drop	18.9	1.11	21.0	3.2	49232	22	83	7	4821	58	6505	78
	5% Shell	18.9	1.11	21.0	3.2	49232	22	83	7	4821	58	6505	78
	5% Core	18.9	1.11	21.0	3.2	49232	22	83	7	4821	58	6505	78

Fitting parameters include the core equatorial radius (R_1), core axial radius (R_3), core axial ratio (x), shell thickness (δ), micelle volume (V_m), micelle charge (Z), micelle and steroids aggregation number (SAA N_{agg} and steroids N_{agg}), surface area for hydrocarbon chain (S_{core}) and whole micelle (S_m) and the corresponding the area per molecule (A_{core} and A_m). Uncertainty for R_1, x, δ, N_{agg}, S and A = ± 0.3, ± 0.03, ± 0.3, ± 7, ± 250, and ± 1 respectively.

Aggregation behaviour of LDS micelles

The SANS profiles measured for the core, shell and drop contrasts for LDS micelles at concentrations of 3 wt% and 5 wt% are presented in Figure 4.10. Given that LDS and SDS share the same dodecyl sulfate moiety but different counterions, we can predict that the aggregation behaviour of LDS and SDS micelles should be very similar. The interaction peak caused by electrostatic repulsion between the LDS micelles was observed (as for SDS micelles) in the Q range of 0.06 to 0.07 $Å^{-1}$, and this agrees with the observations made by Liu et al [187]. At the higher LDS concentration there was a higher scattering intensity in the interaction peak observed for all three contrasts, indicating a greater repulsion between the aggregates at the higher concentration. The increased scattering seen at low Q with increased LDS concentration was assumed to arise because of large particles involving impurities in the samples and the fit to the data in this part of the SANS profiles was accordingly given lower weight in the model-fitting. This issue taken together with the generally low scattering intensity seen in the shell contrast (caused by the high scattering length density of the lithium sulfate head group, 4.4 x 10^{-6} $Å^{-2}$) results in a less than satisfactory fitting of the SANS profiles for the shell contrast data but the values of the model-fitted parameters for the micelles are nevertheless considered reliable.

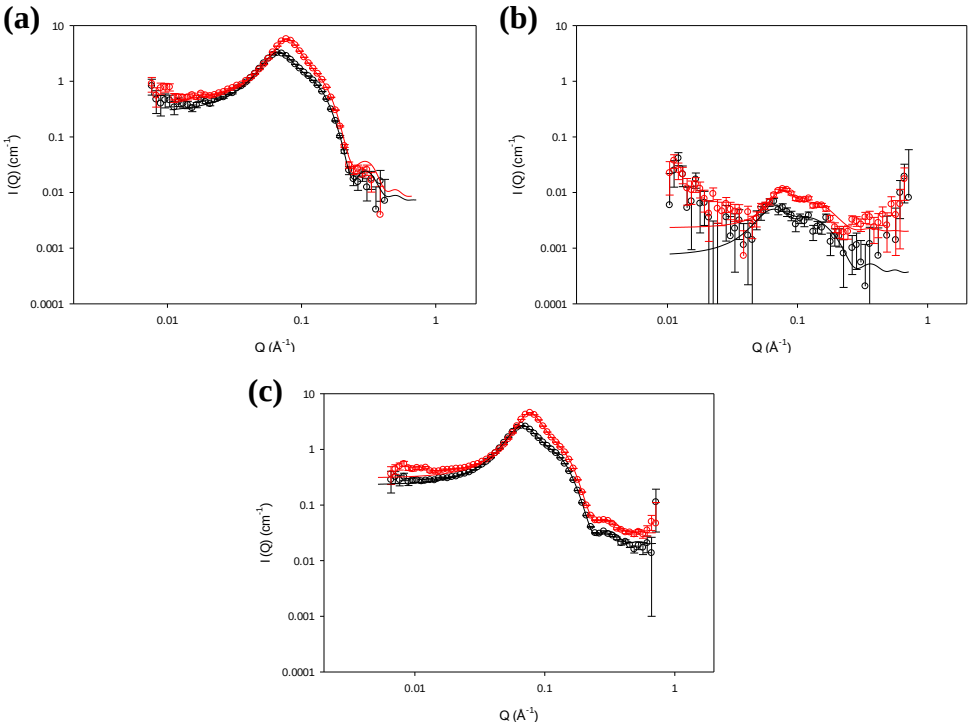

Figure 4. 10 SANS profiles and model fits (solid line) for 3 wt % (black) and 5 wt % (red) d_{25}LDS in H_2O (a), d_{25}LDS in D_2O (b) and h_{25}LDS in D_2O (c).

The values of the model-fitted parameters for the LDS micelles are tabulated in Table 4.6. The core radius of the micelles was determined as 16.6 ± 0.3 Å, and the axial ratio, x, was seen to increase from 1.4 to 1.6 when the concentration of LDS was increased from 3 wt% to 5 wt%. In the SANS studies of LDS micelles reported by Bendedouch and Chen, the micelles were also fitted as prolate ellipsoids, with an axial ratio of about 1.3 at 1 wt% [188], and the micelle aggregation number was determined to be 60 when the core of the micelle was constrained as 17 Å. The results obtained here are also consistent with those reported previously by Liu et al [187].

The shell thickness of LDS micelles is found to be a little higher than that of the SDS micelles (4 ± 0.3 Å vs 3.1 ± 0.3 Å), as too are the volume and charge of the LDS micelles (48k $Å^3$ vs 46k $Å^3$ and 24 vs 21, respectively). As noted here earlier (section 2.3) and also reported by Li et al. [189] these differences between the SDS and LDS micelles can be attributed to the larger size of the hydrated $Li^+ SO_4^-$ head group by comparison with that of the $Na^+ SO_4^-$ head group.

Table 4. 6 Values of model fitted parameters for 3 wt% and 5 wt% LDS micelles.

Contrast	R_1 (Å)	x	R_3 (Å)	δ (Å)	V_m (Å^3)	Z e	SAA N_{agg}	S_{core} (Å^2)	A_{core} (Å^2)	S_m (Å^2)	A_m (Å^2)
3% Drop	16.6	1.42	23.6	4.0	48815	24	77	4465	58	6553	85
3% Shell	16.6	1.42	23.6	4.0	48815	24	77	4465	58	6553	85
3% Core	16.6	1.43	23.7	4.0	49109	24	77	4490	58	6583	85

Contrast	R_1 (Å)	x	R_3 (Å)	δ (Å)	V_m (Å^3)	Z	SAA N_{agg}	S_{core} (Å^2)	A_{core} (Å^2)	S_m (Å^2)	A_m (Å^2)
5% Drop	16.6	1.55	25.7	4.1	53332	24	84	4786	57	7006	83
5% Shell	16.6	1.55	25.7	4.1	53332	24	84	4786	57	7006	83
5% Core	16.6	1.55	25.7	4.1	53332	24	84	4786	57	7006	83

Fitting parameters include the core equatorial radius (R_1), core axial radius (R_3), core axial ratio (x), shell thickness (δ), micelle volume (V_m), micelle charge (Z), micelle aggregation number (SAA N_{agg}), surface area for hydrocarbon chain (S_{core}) and whole micelle (S_m) and the corresponding areas per molecule (A_{core} and A_m). Uncertainty for R_1, x, δ, N_{agg}, S and A = ± 0.3, ± 0.03, ± 0.3, ± 7, ± 250, and ± 1 respectively.

LDS micelles in the presence of steroids

The model-fits to the SANS profiles measured for the LDS micelles in the presence and absence of steroids are shown in Figure 4.11. The scattering intensity of the micelles in the presence of both 4-CHOL and ADRENO is found to be higher than that for the LDS micelles alone, while the changes in the scattering for the 4-CHOL-saturated LDS micelles in the shell and drop contrasts are much more pronounced than those seen in the same contrasts for the ADRENO-saturated micelles. It is thus concluded that the steroids might be solubilised within the micelle core region. The interaction peak for the 4-CHOL/LDS micelles is shifted to lower Q, suggesting an increased inter-micelle distance. Again, in the shell contrast SANS profile there is a high scattering intensity in the low Q range which is attributed to large particles of impurities and this was treated with less weight in the fitting process.

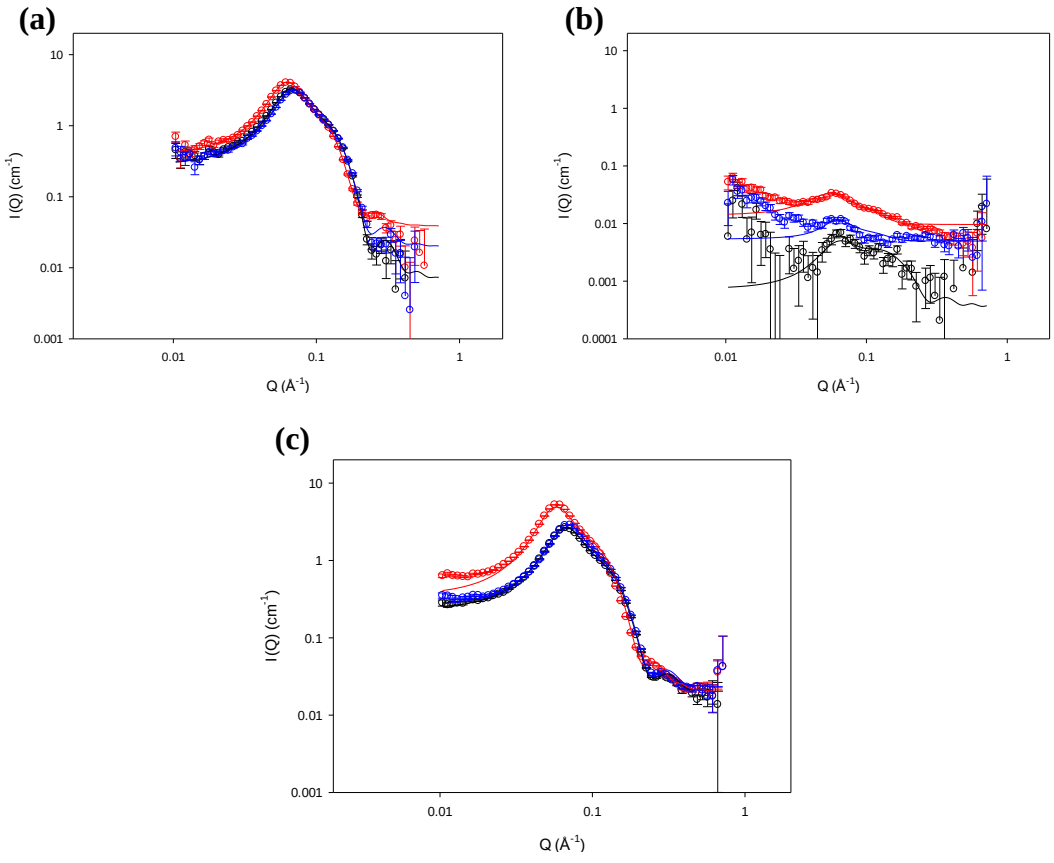

Figure 4. 11 SANS profiles and model fit (solid line) for d_{25}LDS in H_2O (a), d_{25} LDS in D_2O (b) and h_{25} LDS (c) in D_2O micelles alone (black), micelles in the presence of saturation amounts of 4-CHOL (red) and ADRENO (blue) at 3 wt %

The values of the model-fitted parameters for the LDS micelles in the presence of steroids are shown in Table 4.7. For these micelles, the fitting did not allow to a

decision to be made as to whether the micelles were prolate or oblate (the quality of fit being similar for the two cases), but since the SDS micelles were determined to be oblate ellipsoid when saturated with 4-CHOL, it was assumed that the same shape would hold true for the 4-CHOL/LDS micelles.

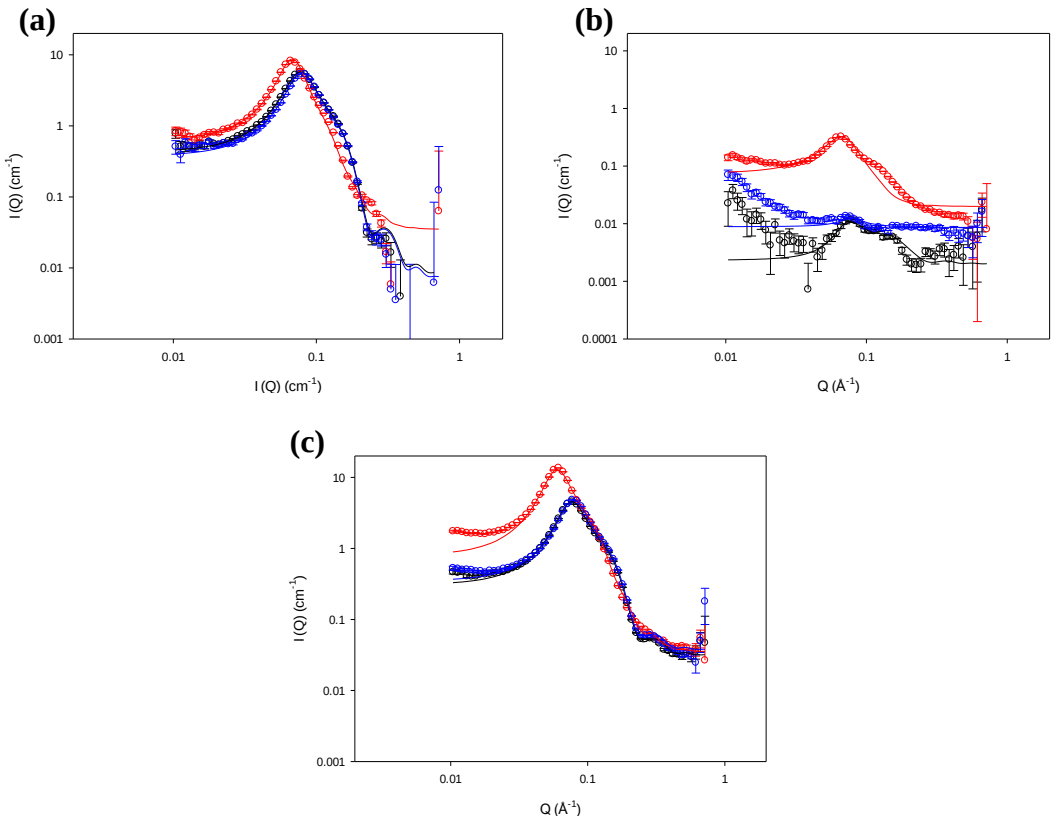

Figure 4. 12 SANS profiles and model fits (solid line) for d_{25}LDS in H_2O (a), d_{25} LDS in D_2O (b) and h_{25} LDS (c) in D_2O micelles alone (black), micelles in the presence of saturation amounts of 4-CHOL (red) and ADRENO (blue) at 5 wt %

The modelled parameters show that the 4-CHOL-saturated micelles grow with an increasing LDS concentration while R_3 remained the same (at ca. 16 Å). The micelle shell thickness was found to increase slightly in the presence of steroid, whereas the charge on the micelles seemed unaffected by addition of the steroids.

By comparison with the changes in the SANS profiles seen for SDS micelles in the presence of 4-CHOL and ADRENO, the corresponding changes seen for the LDS micelles were much smaller. These observations are consistent with the findings from the solubilisation experiments (presented in section 2.1) which showed that the molar ratios of surfactant:steroid for the LDS:steroid micelles were higher than those of the SDS:steroid micelles (viz., 4:1 vs. 3:1 for the 4-CHOL-containing LDS and SDS micelles, and 18:1 vs. 11:1, for the corresponding ADRENO-containing micelles).

In the modelling of the SANS profiles for the shell and core contrasts for the LDS-steroid systems, the fitted values of the micelle core scattering length densities were lower than those for pure SDS micelle cores, indicating the presence of the steroids in the hydrophobic core of the micelles. The area per molecule of the LDS micelles in the presence of steroids, however, only increased by 10% or less. It is concluded, therefore, that the major solubilisation locus for 4-CHOL and ADRENO lies within the hydrophobic core of the LDS micelles.

Table 4. 7 Values of model fitted parameters for 3 wt% and 5 wt% LDS micelles in the presence of steroids.

Steroids	Contrast	R_1 (Å)	x	R_3 (Å)	δ (Å)	V_m (Å^3)	Z e	SAA N_{agg}	Steroids N_{agg}	S_{core} (Å^2)	A_{core} (Å^2)	S_m (Å^2)	A_m (Å^2)
4-CHOL	3% Drop	24.1	0.68	16.4	4.5	71568	24.7	91	21	5803	64	8638	95
	3% Shell	24.1	0.68	16.4	4.5	71568	24.7	91	21	5803	64	8638	95
	3% Core	24.1	0.68	16.4	4.5	71568	24.7	91	21	5803	64	8638	95
ADRENO	3% Drop	16.7	1.42	23.7	4.0	49677	24.7	75	4	3505	46	6630	88
	3% Shell	16.7	1.42	23.7	4.0	49677	24.7	75	4	3505	46	6630	88
	3% Core	16.7	1.42	23.7	4.0	49677	24.7	75	4	3505	46	6630	88

Steroids	Contrast	R_1 (Å)	x	R_3 (Å)	δ (Å)	V_m (Å^3)	Z e	SAA N_{agg}	Steroids N_{agg}	S_{core} (Å^2)	A_{core} (Å^2)	S_m (Å^2)	A_m (Å^2)
4-CHOL	5% Drop	33.9	0.46	15.6	5.3	134488	25.1	171	40	9650	56	14017	82
	5% Shell	33.9	0.46	15.6	5.3	134488	25.0	171	40	9650	56	14017	82
	5% Core	33.9	0.46	15.6	5.3	134488	25.0	171	40	9650	56	14017	82
ADRENO	5% Drop	16.7	1.52	25.4	4.1	53224	24.7	81	5	4768	59	6983	86
	5% Shell	16.7	1.52	25.4	4.1	53224	24.7	81	5	4768	59	6983	86
	5% Core	16.7	1.52	25.4	4.1	53224	24.7	81	5	4768	59	6983	86

Fitting parameters include the core equatorial radius (R_1), core axial radius (R_3), core axial ratio (x), shell thickness (δ), micelle volume (V_m), micelle charge (Z), micelle and steroids aggregation number (SAA N_{agg} and steroids N_{agg}), surface area for hydrocarbon chain (S_{core}) and whole micelle (S_m) and the corresponding the area per molecule (A_{core} and A_m). Uncertainty for R_1, x, δ, N_{agg}, S and A = ± 0.3, ± 0.03, ± 0.3, ± 7, ± 250, and ± 1 respectively.

Aggregation behaviour of ADS micelles

The SANS profiles measured for the core, shell and drop contrasts for ADS micelles at concentrations of 3 wt% and 5 wt% are presented in Figure 4.13. As was noted for the SDS and LDS micellar systems, the scattered intensities increase with increasing surfactant concentration, and the interaction peaks shift to higher Q at higher concentration indicating smaller mean inter-micelle distances, resulting from decreased repulsive interactions.

As expected, given the low scattering length density of the hydrophilic head group of ADS (3.35 x 10^{-6} $Å^{-2}$) the scattering intensity for the shell contrast is found to be low, and since the NH_4^+ ion associated with the sulfate head group is expected to be less heavily hydrated by comparison with Na^+ and Li^+, the surfactant molecular surface area is also expected to be lower.

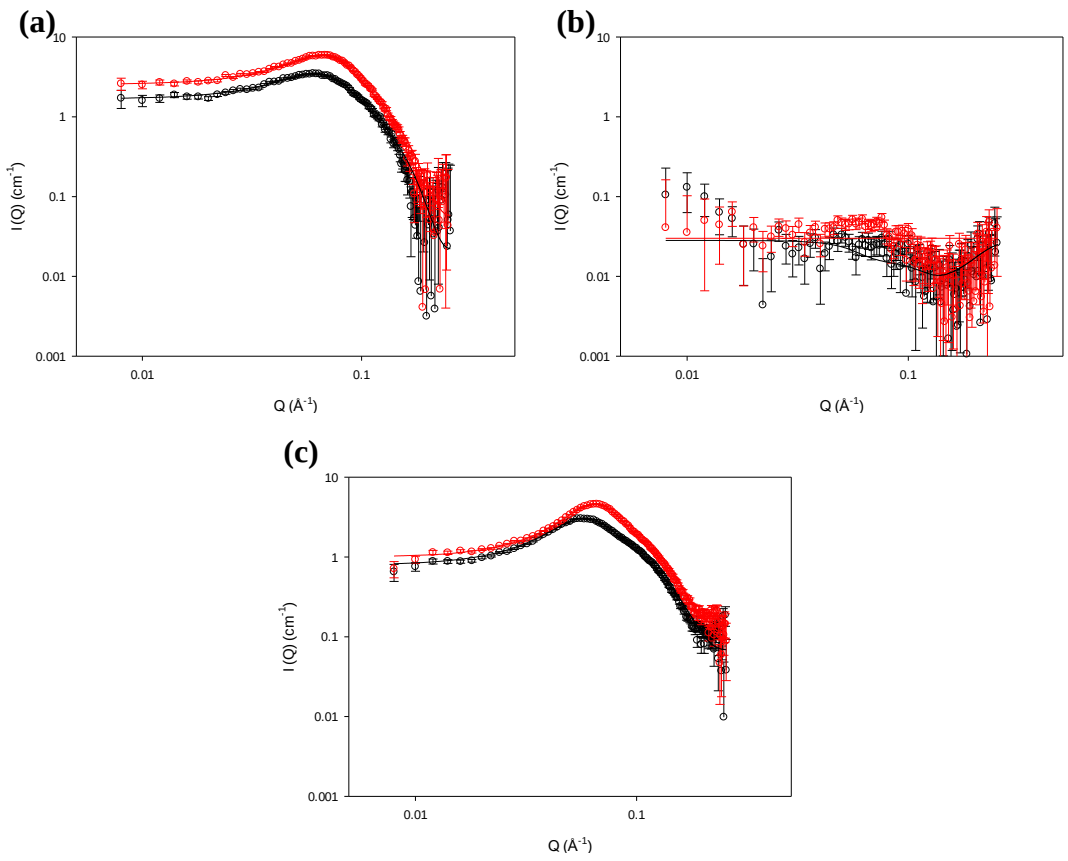

Figure 4. 13 SANS profiles and model fits (solid line) for 3 wt % (black) and 5 wt % (red) d_{25}ADS in H_2O (a), d_{25}ADS in D_2O (b) and h_{25}ADS in D_2O (c). SANS data obtained from LOQ

The values of the model-fitted parameters for the ADS micelles in the absence of steroids are shown in Table 4.8. Like the SDS and LDS micelles these micelles are

best modelled as prolate ellipsoids, but they are much more elongated than the SDS and LDS micelles, with core axial ratios ranging from 2.5 at 3 wt% to 2.7 at 5 wt%.

Kang and Lim investigated the size and structure of ADS micelles at various concentrations [190] and reported that the micelles were spherical at low surfactant concentrations and became progressively more ellipsoidal as the surfactant concentration was increased. While Kang and Lim modelled the ADS micelles formed at the higher concentrations as oblate ellipsoids, Vass et al. showed that the SANS data do not allow an unequivocal choice between oblate and prolate ellipsoids [191]. Vass et al., were clear, however, that the ADS aggregates become more elongated at higher surfactant concentration, with the micelle cross-section limited by the extended length of the surfactant hydrocarbon chain.

In the present study, the best fits to the ADS micelle SANS data were likewise obtained with the thickness of the core constrained as the maximum extended length of the C_{12} hydrocarbon chains (16.7 Å). The shell thickness of the ADS micelles was determined as 2.8 Å, which, as expected, was smaller than the shell thickness of the micelles formed with lithium and sodium counterions.

Using time-resolved fluorescence methods, Tcacenco et al. found an aggregation number of 103 ± 5 for ~4.6 wt % ADS micelles at 25 ^{o}C [192], and this is 30% less than the value obtained on the basis of the SANS studies here. Saaka [87] reported the aggregation number of ADS micelle of 132 at 5 wt%, which is much closer to the value obtained in this study.

With increasing concentration of ADS, the micelles are seen to grow, their aggregation number thus increasing, and the surface area per ADS molecule decreasing. In addition it is found that by comparison with the interaction peaks see in the SANS profiles for SDS and LDS micelles, the peak for ADS micelles becomes sharper and is moved to higher Q, indicating that the ADS micelles show a narrower distribution of inter-micellar distances due to a stronger repulsive interaction between the aggregates [190]. The charge on the dodecyl sulfate micelles is found to increase as expected with ADS < SDS < LDS.

Table 4. 8 Values of model fitted parameters for 3 wt% and 5 wt% ADS micelles.

Contrast	R_1 (Å)	x	R_3 (Å)	δ (Å)	V_m (Å^3)	Z e	SAA N_{agg}	S_{core} (Å^2)	A_{core} (Å^2)	S_m (Å^2)	A_m (Å^2)
3% Drop	16.7	2.49	41.6	2.9	71313	20	137	7267	53	9194	67
3% Shell	16.7	2.49	41.6	2.9	71313	20	137	7267	53	9194	67
3% Core	16.7	2.49	41.6	2.9	71313	20	137	7267	53	9194	67

Contrast	R_1 (Å)	x	R_3 (Å)	δ (Å)	V_m (Å^3)	Z e	SAA N_{agg}	S_{core} (Å^2)	A_{core} (Å^2)	S_m (Å^2)	A_m (Å^2)
5% Drop	16.7	2.73	45.6	2.9	78126	20	151	7900	52	9960	66
5% Shell	16.7	2.73	45.6	2.9	78126	20	151	7900	52	9960	66
5% Core	16.7	2.73	45.6	2.9	78126	20	151	7900	52	9960	66

Fitting parameters include the core equatorial radius (R_1), core axial radius (R_3), core axial ratio (x), shell thickness (δ), micelle volume (V_m), micelle charge (Z), micelle aggregation number (SAA N_{agg}), surface area for hydrocarbon chain (S_{core}) and whole micelle (S_m) and the corresponding areas per molecule (A_{core} and A_m). Uncertainty for R_1, x, δ, N_{agg}, S and A = ± 0.3, ± 0.03, ± 0.3, ± 7, ± 250, and ± 1 respectively.

ADS micelles in the presence of steroids

The SANS profiles and model-fits for ADS micelles in the absence and presence of 4-CHOL are shown in Figure 4.14. The data shown here were obtained from LOQ, and so the backgrounds and Q range are different from those of the SANS profiles measured on SANS 2D. Moreover, the scattering intensity in the low Q range appears anomalously high in the shell contrast for these systems and this is attributed to the presence of large particles of unknown composition. In model-fitting these SANS data, therefore, the quality of the fits to the data at low Q were regarded with caution.

The addition of 4-CHOL to the ADS micelles caused a dramatic increase in the scattered intensities and the shape of the SANS profiles also changed significantly. The interaction peak for the 4-CHOL-saturated micelles was shifted to lower Q, indicating a significant effect of the 4-CHOL on the inter-micellar separation. It is interesting to note that in Figure 4.14 (b), there is a peak at Q ~ 0.12 $Å^{-1}$ which could perhaps be attributed to formation of a lamellar phase. This peak, however, is not seen in Figures 4.14 (a) and (c), and so no attempts were made to fit the SANS data using a lamellar model.

As noted earlier, when the SANS measurements are made for dilute solutions of ionic surfactants without added salt, it is generally not easy when modelling the data to distinguish between prolate and oblate ellipsoidal micelles. In the case of the 4-CHOL/ADS micelles, however, the large amount of 4-CHOL solubilised allowed for an unequivocal assignment of oblate ellipsoid geometry and the fitted parameters values are shown in Table 4.9.

By comparison with the ADS micelles, the 4-CHOL/ADS micelles are much more elongated and the micelle volume is found to increase by more than 400% in the presence of the steroid, which is consistent with the low mole ratio of 3.8:1 ADS:4-CHOL.

The shell thickness and charge on the ADS micelles were seen to increase slightly in the presence of 4-CHOL, and the change in the fitted values of the scattering length densities for the micelle cores in the shell and core contrasts were found to be similar to the scattering length densities model-fitted for the cores of 4-CHOL-saturated SDS micelles.

The core axial ratio of the 4-CHOL-saturated ADS micelles is seen to decrease with increasing ADS concentration, with R_1 increasing by 11% and R_3 decreasing by 7% when the surfactant concentration is raised from 3 wt% to 5 wt%. The increase in ADS concentration also results in an increase in volume of the 4-CHOL/ADS micelles (from 37,000 to 42,000 $Å^3$) and an increase too in the number of 4-CHOL molecules solubilised within the aggregates. The best model fits to the SANS data for these systems were obtained assuming that 4-CHOL was solubilised within the micelle core region.

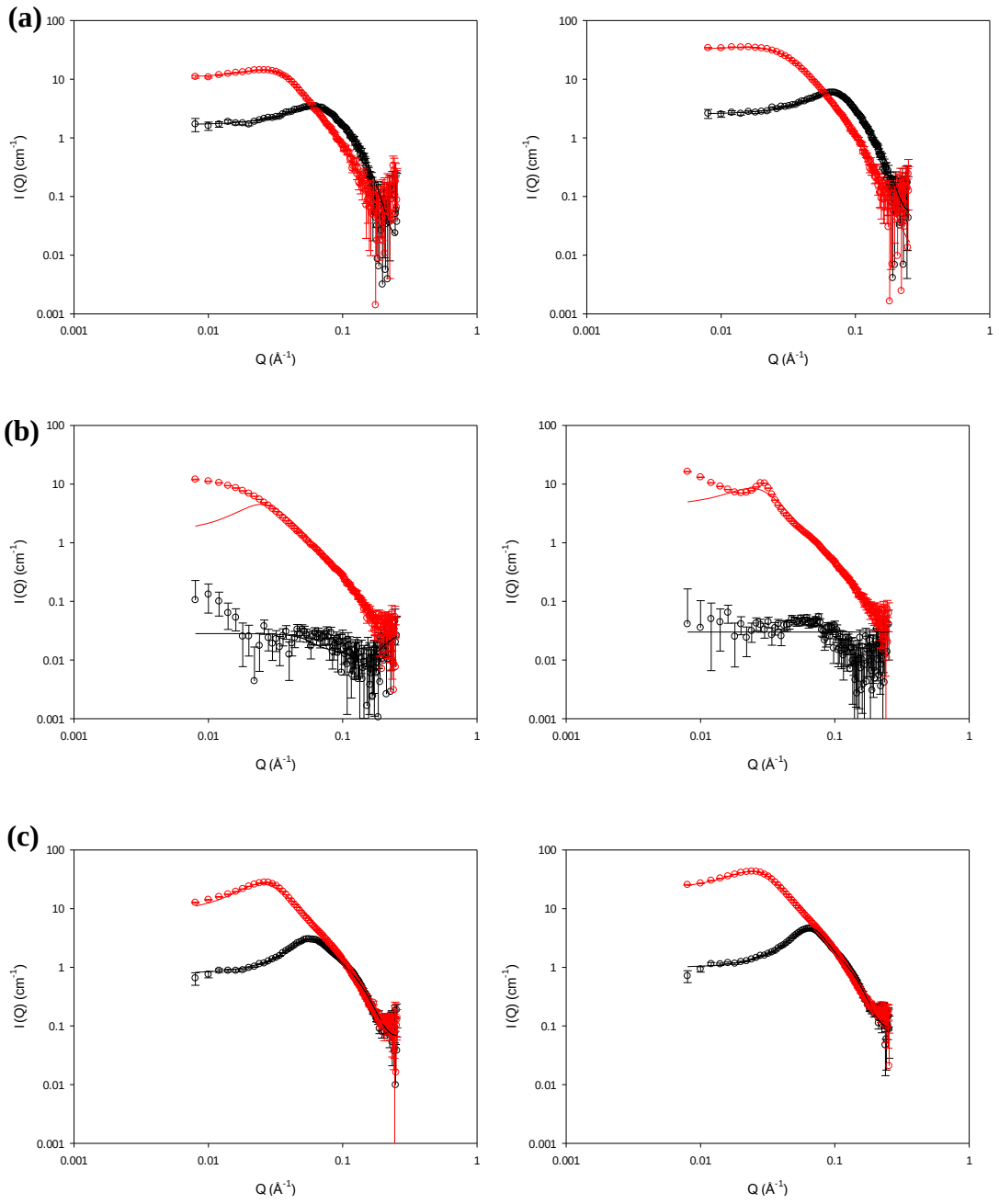

Figure 4. 14 SANS profiles and model fits (solid line) for 3 wt % (left column) and 5 wt % (right column) d_{25}ADS in H_2O (a), d_{25}ADS in D_2O (b) and h_{25}ADS in D_2O (c) in the presence (red) or absence (black) of 4-CHOL (SANS data obtained from LOQ).

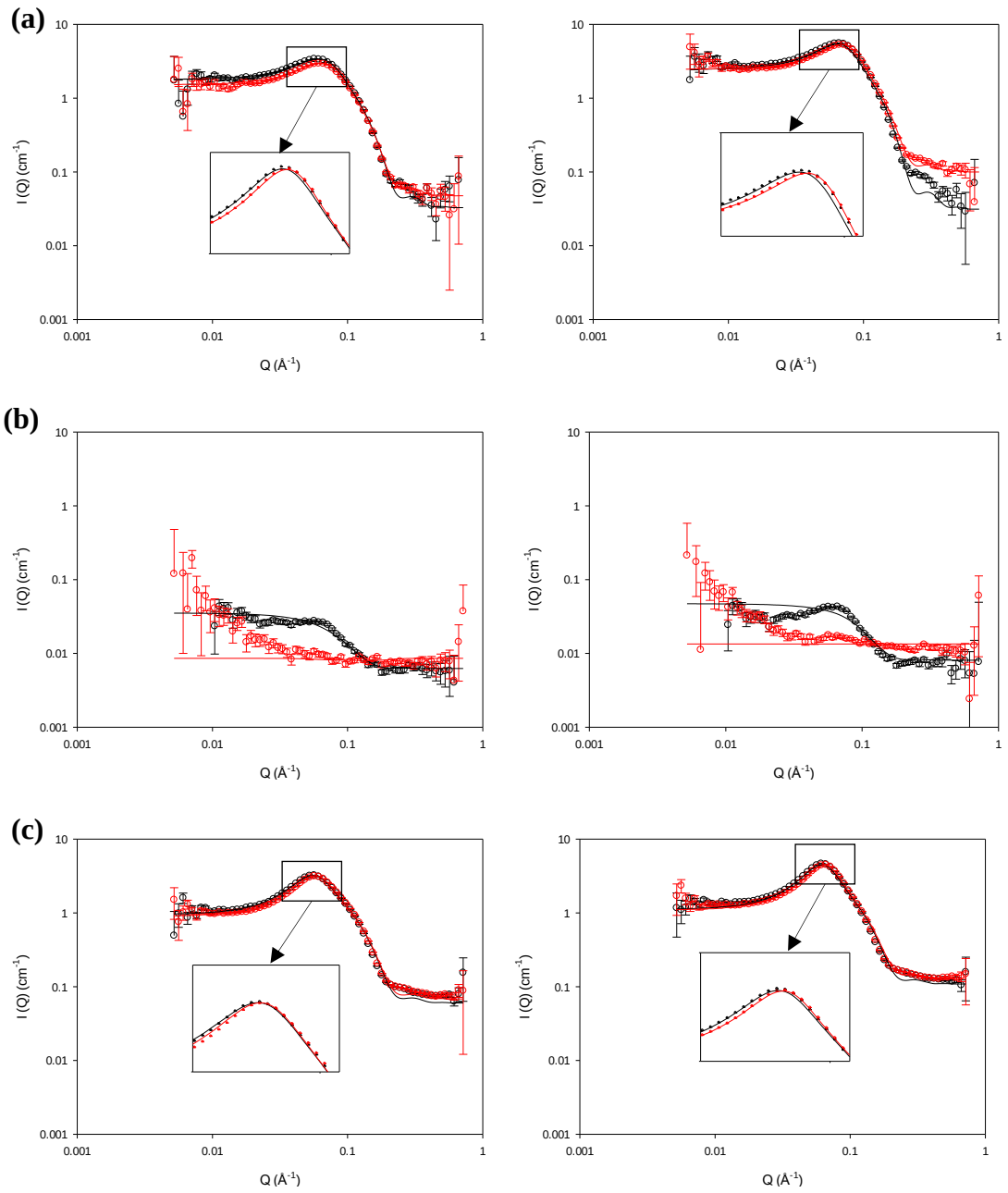

Figure 4. 15 SANS profiles and model fits (solid line) for 3 wt % (left column) and 5 wt % (right column) d_{25}ADS in H_2O (a), d_{25}ADS in D_2O (b) and h_{25}ADS in D_2O (c) in the presence (red) or absence (black) of ADRENO.

Figure 4.15 shows the model-fitted SANS profiles for ADS micelles in the presence of ADRENO. In contrast to the case for the 4-CHOL/ADS system, the addition of ADRENO to the ADS micelles caused no change in the shape of the scattering curve and the SANS profiles for the ADRENO/ADS micelle core and drop contrasts (Figure 4.15 (a) and (c)) are superimposable on the corresponding profiles recorded for ADS micelles in the absence of steroids. It is concluded, therefore, that there is no change in geometry of the ADS micelles upon the addition of saturating amounts of

ADRENO. Model-fitting of the core and shell contrast data for the ADRENO/ADS system does show, however, that the presence of the steroid reduces the scattering length density of the alkyl chain region in the micelle, indicating that the ADRENO is solubilised within the micelle core.

Table 4. 9 Values of model fitted parameters for 3 wt% and 5 wt% ADS micelles in the presence of steroids.

Steroids	Contrast	R_1 (Å)	x	R_3 (Å)	δ (Å)	V_m (Å^3)	Z e	SAA N_{agg}	Steroids N_{agg}	S_{core} (Å^2)	A_{core} (Å^2)	S_m (Å^2)	A_m (Å^2)
4-CHOL	3% Drop	62.0	0.25	15.5	4.4	366337	20.5	529	140	27370	52	32950	62
	3% Shell	62.0	0.25	15.5	4.4	366337	20.5	529	140	27370	52	32950	62
	3% Core	62.0	0.25	15.5	4.4	366337	20.5	529	140	27370	52	32950	62
ADRENO	3% Drop	16.7	2.49	41.6	2.9	71313	19.9	132	6	7267	55	9194	69
	3% Shell	16.7	2.49	41.6	2.9	71313	19.9	132	6	7267	55	9194	69
	3% Core	16.7	2.49	41.6	2.9	71313	19.9	132	6	7267	55	9194	69

Steroids	Contrast	R_1 (Å)	x	R_3 (Å)	δ (Å)	V_m ($Å^3$)	Z e	SAA N_{agg}	Steroids N_{agg}	S_{core} ($Å^2$)	A_{core} ($Å^2$)	S_m ($Å^2$)	A_m ($Å^2$)
4-CHOL	5% Drop	69.0	0.21	14.3	4.3	417888	22.5	604	160	32872	54	38750	64
	5% Shell	69.0	0.21	14.3	4.3	417888	22.5	604	160	32872	54	38750	64
	5% Core	69.0	0.21	14.3	4.3	417888	22.5	604	160	32872	54	38750	64
ADRENO	5% Drop	16.7	2.76	46.1	2.9	79029	20.5	147	7	7979	54	10060	69
	5% Shell	16.7	2.76	46.1	2.9	79029	20.5	147	7	7979	54	10060	69
	5% Core	16.7	2.76	46.1	2.9	79029	20.5	147	7	7979	54	10060	69

Fitting parameters include the core equatorial radius (R_1), core axial radius (R_3), core axial ratio (x), shell thickness (δ), micelle volume (V_m), micelle charge (Z), micelle and steroids aggregation number (SAA N_{agg} and steroids N_{agg}), surface area for hydrocarbon chain (S_{core}) and whole micelle (S_m) and the corresponding the area per molecule (A_{core} and A_m). Uncertainty for R_1, x, δ, N_{agg}, S and A = ± 0.3, ± 0.03, ± 0.3, ± 7, ± 250, and ± 1 respectively.

4.4.2 SANS studies for zwitterionic surfactants

Fitting parameters

The SANS profiles for the zwitterionic surfactant micelles were model-fitted using a monodisperse two-shell ellipsoid model. With this model the micelles were considered to have an outer shell containing the surfactant head groups and associated water and an inner core containing only the C_{12} alkyl chains. The micelles were treated as electrically neutral and the model therefore differs from that used in modelling the SANS profiles for the ionic surfactants in that there is no account taken of electrostatic repulsion between the micelles. All fitted parameters other than micelle charge were thus the same as were considered for the ionic surfactant micelles, i.e., the micelle equatorial core radius (R_1), axial core radius (R_3), core axial ratio (x), and the micelle shell thickness (δ). The molecular volumes and scattering length densities used in the model-fitting are shown in Table 4.10.

Note here that since the CMCs of zwitterionic surfactants are much lower than those of ionic surfactants, the micellar solutions of the DDAPS, DPC and DDAO were prepared at lower concentrations (*viz*., 2 wt% and 3.5 wt% *vs* 3 wt and 5 wt%).

Table 4. 10 Molecular formulas, molecular volume (V_m), molecular weight (M_w) and scattering length density (ρ) of the constituents of the zwitterionic surfactants and steroids studied.

Chemical	Molecular formula		V_m (Å^3)	M_w (g mol^{-1})		ρ (x 10^{-6} Å^{-2})	
	Protiated	Deuterated		Protiated	Deuterated	Protiated	Deuterated
4-CHOL	$C_{27}H_{44}O$	N/A	652.5	384.6	N/A	0.34	N/A
ADRENO	$C_{19}H_{24}O_3$	N/A	422.6	300.4	N/A	1.27	N/A
DDAPS	$C_{17}H_{37}O_3SN$	$C_{17}D_{25}H_{12}O_3SN$	534.7	335.5	360.5	0.08	4.98
DAPS	$C_5H_{12}O_3SN$	N/A	181.0	166.2	N/A	1.01	N/A
DDAO	$C_{14}H_{31}NO$	$C_{14}D_{25}H_6NO$	422.6	229.4	254.4	-0.18	6.04
DAO	C_2H_6NO	N/A	68.9	60.1	N/A	0.88	N/A
DPC	$C_{17}H_{38}NO_4P$	$C_{17}D_{25}H_{13}NO_4P$	536.7	351.5	389.7	0.16	5.20
PC	$C_5H_{13}NO_4P$	$C_5D_{13}NO_4P$	183.0	182.1	N/A	1.22	8.62
Alkyl chain	$C_{12}H_{25}$	$C_{12}D_{25}$	353.7	169.3	194.5	-0.39	6.95

Aggregation behaviour of DDAPS micelles

The SANS profiles and model-fitted curves obtained for the 2 wt% and 3.5 wt% DDAPS micelles are shown in Figure 4.16. Given that these micelles are electrically neutral, there is no interaction peak seen in the SANS profiles. The increase in DDAPS concentration gives rise to an increase in scattering intensity but there is no change in the shape of the SANS profile.

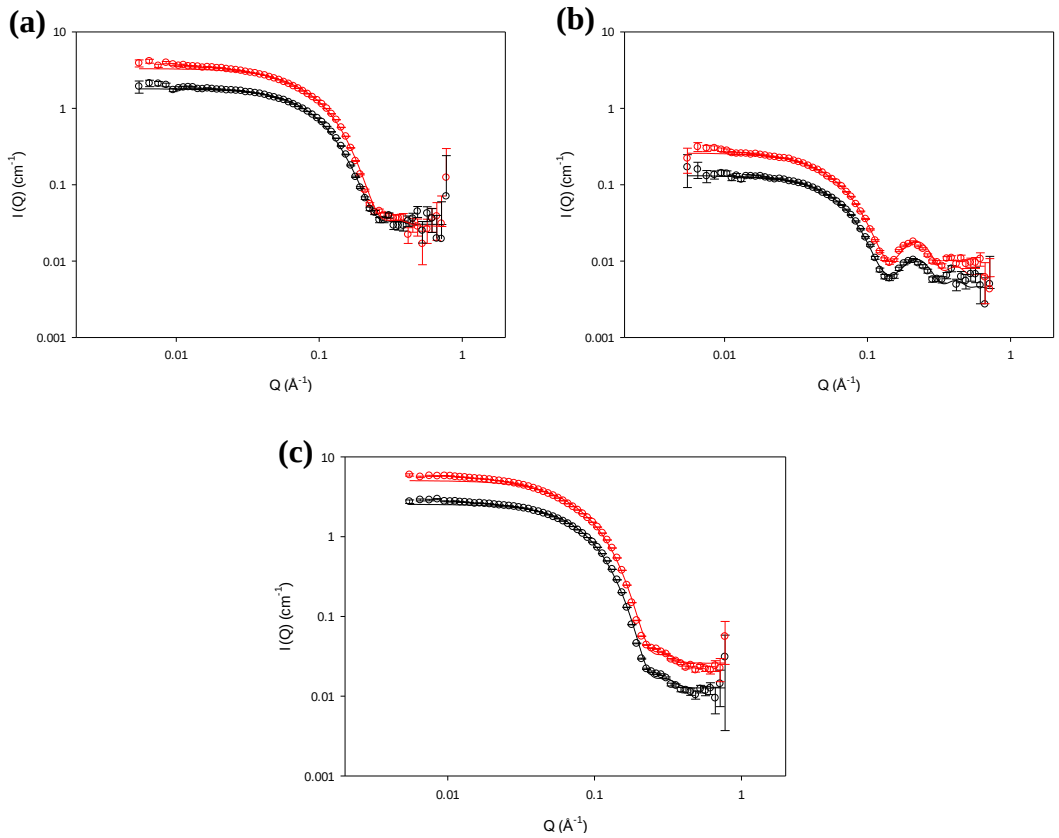

Figure 4. 16 SANS profiles and model fits (solid line) for 2 wt % (black) and 3.5 wt % (red) d_{25}DDAPS in H_2O (a), d_{25}DDAPS in D_2O (b) and h_{25}DDAPS in D_2O (c).

Table 4.11 shows the values of the model-fitted parameters for the DDAPS micelles. As evidenced by the increase in core axial ratio and radius, the micelles are seen to be become more elongated at the higher surfactant concentration. The aggregates are best modelled as prolate ellipsoids with axial ratios of 2.5 and 3.3 at 2 wt% and 3.5 wt%, respectively, and the concomitant increase in the micelle volume results in a higher aggregation number.

Ullah et al. [193] have also studied DDAPS micelles, but using light scattering techniques, and these workers report an aggregation number of 90 ± 5 for DDAPS

concentrations of 2-3 wt%, and this is consistent with the values found in the studies reported here.

The shell thickness of the DDAPS micelles was found to be around 50% larger than that of the ionic surfactant micelles and this is as expected given that the sulfopropyl group of DDAPS is significantly larger than the head groups of the dodecyl sulfate surfactants and DTAB. The best-fitted value of R_1 (core equatorial radius) obtained in the studies here was 14 Å, which is ~85% of the fully extended C_{12} alkyl chain length. Any attempt to fit with an increased R_1 resulted in a much poorer fit to the data. The fact that the DDAPS alkyl chains in the micelles are shorter than those in the SDS and DTAB micelles is in keeping with the larger area per molecule of DDAPS (62 ± 1 $Å^2$ *vs.* ca. 46 $Å^2$) and indicates that the C12 chains in the DDAPS micelle have a different conformation to those in the ionic micelles.

Masudo and Okada [194] used light scattering too to study DDAPS micelles and reported that the micelles were spherical with an aggregation number of 67 and a core radius of 17 Å. The concentration of DDAPS used in these studies was not given, however, and so no comparison can be made with the results presented here.

Encouragingly, Hsieh also performed SANS studies for DDAPS micelles at 2 wt% and 3.5 wt% and determined R_1 as 14.1 Å and 13.5 Å, respectively, with the corresponding core axial ratios, 2.5 and 3.6 [49].

Qu et al. [86] studied the structure of DDAPS micelles using molecular dynamics and they too found that R_1 was less than the C12 extended length, on average around 14.9 Å.

In the SANS studies performed by Saaka, the DDAPS micelles were modelled as prolate ellipsoids with the core axial ratios increasing from 2.8 to 3.4 when the surfactant concentration was increased from 2 wt% to 3.5 wt% [87].

Table 4. 11 Values of model fitted parameters for 2 wt% and 3.5 wt% DDAPS micelles.

Contrast	R_1 (Å)	x	R_3 (Å)	δ (Å)	V_m (Å^3)	SAA N_{agg}	S_{core} (Å^2)	A_{core} (Å^2)	S_m (Å^2)	A_m (Å^2)
2% Drop	14.3	2.54	36.3	5.4	67824	88	5425	62	8760	100
2% Shell	14.3	2.54	36.3	5.4	67824	88	5425	62	8760	100
2% Core	14.3	2.54	36.4	5.4	68155	89	5448	62	8789	99

Contrast	R_1 (Å)	x	R_3 (Å)	δ (Å)	V_m (Å^3)	SAA N_{agg}	S_{core} (Å^2)	A_{core} (Å^2)	S_m (Å^2)	A_m (Å^2)
3.5% Drop	14.1	3.30	46.6	5.6	84890	110	6742	61	10698	97
3.5% Shell	14.2	3.27	46.3	5.6	84514	110	6707	61	10649	97
3.5% Core	14.2	3.29	46.5	5.6	84968	110	6740	61	10698	97

Fitting parameters include the core equatorial radius (R_1), core axial radius (R_3), core axial ratio (x), shell thickness (δ), micelle volume (V_m), micelle aggregation number (SAA N_{agg}), surface area for hydrocarbon chain (S_{core}) and whole micelle (S_m) and the corresponding areas per molecule (A_{core} and A_m). Uncertainty for R_1, x, δ, N_{agg}, S and A = ± 0.3, ± 0.03, ± 0.3, ± 7, ± 250, and ± 1 respectively.

DDAPS micelles in the presence of steroids

The scattering curves for DDAPS in the presence and absence of steroids in all three contrasts at surfactant concentration of 2 and 3.5 wt% are shown in Figures 4.17 and 4.18. It can be seen here that the scattering intensities increase when saturating amounts of the steroids are added to the DDAPS micelles, with the increase for 4-CHOL clearly larger than that for ADRENO, particularly in the case of the shell contrast (Figure 4.17/4.18, (b)). The addition of the steroids, however, does not cause any noticeable change in the shapes of the SANS profiles.

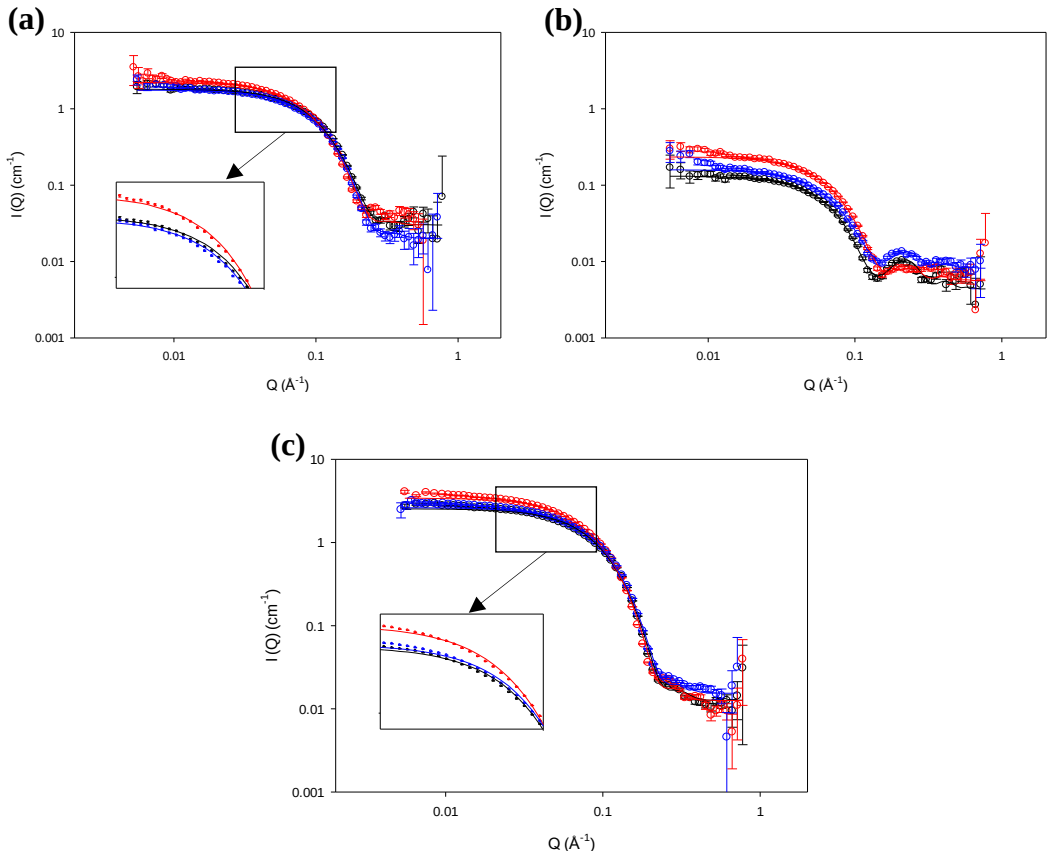

Figure 4. 17 SANS profiles and model fits (solid line) for d_{25}DDAPS in H_2O (a), d_{25} DDAPS in D_2O (b) and h_{25} DDAPS (c) in D_2O micelles alone (black), micelles in the presence of saturation amounts of 4-CHOL (red) and ADRENO (blue) at 2 wt %.

The values of the model-fitted parameters for the DDAPS micelles in the presence of steroids are shown in Table 4.12. While the addition of ADRENO causes very little change in the structure of the DDAPS micelles, the addition of 4-CHOL leads to increases of about 6% in R_1 and δ and an increase in the micelle volume of around 25%. In order to improve the quality of the fitting, the scattering length density of the deuterated core region had been adjusted.

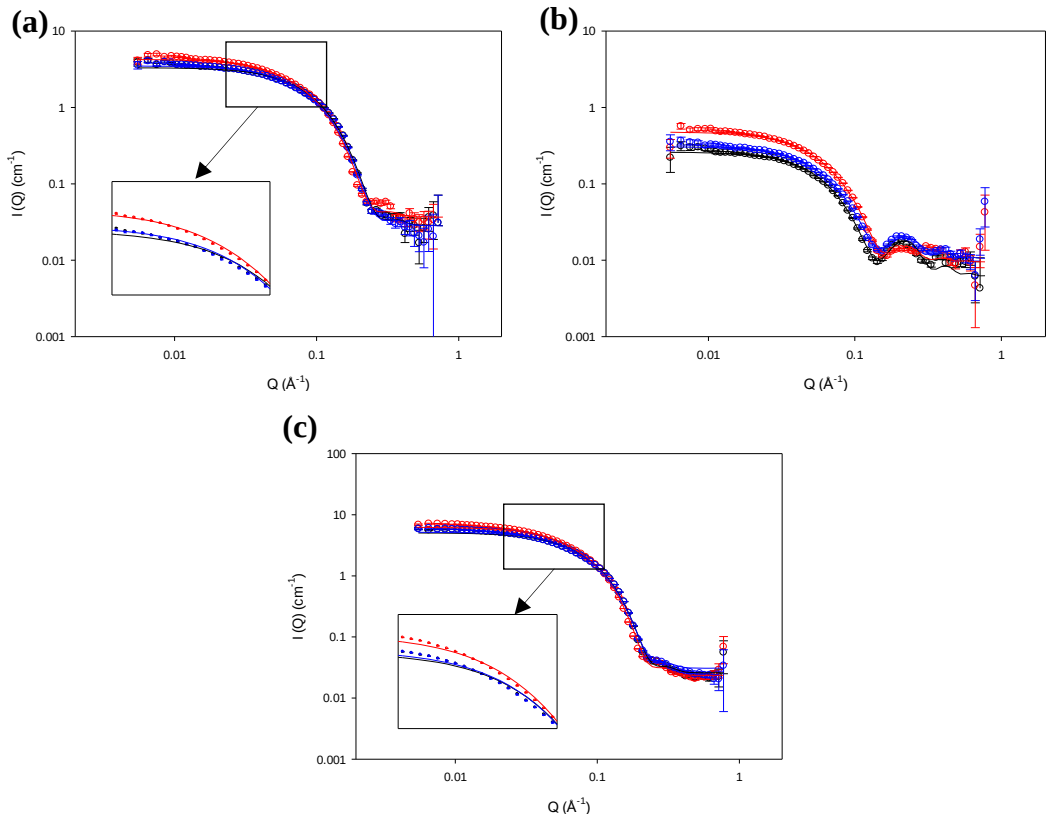

Figure 4. 18 SANS profiles for d_{25}DDAPS in H_2O (a), d_{25} DDAPS in D_2O (b) and h_{25} DDAPS (c) in D_2O micelles alone (black), micelles in the presence of saturation amounts of 4-CHOL (red) and ADRENO (blue) at 3.5 wt %.

For the micelle containing 4-CHOL, the scattering length density of the deuterated surfactant core changed from 6.95 x 10^{-6} Å^{-2} to 6.0 ± 0.5 x 10^{-6} Å^{-2}, giving clear evidence of the solubilisation of the steroid in the micelle core. There was no change in the deuterated core scattering length density, however, on addition of ADRENO to the DDAPS micelles. The model-fitting of the DDAPS/ADRENO data also showed no evidence of ADRENO within the hydrophilic shell of the micelles. The solubilisation locus of ADRENO thus remains undetermined but it would seem likely, however, that the ADRENO is solubilised in the micelle core but that there is so little solubilised that the change in core scattering length density cannot be detected.

It is pertinent here to note that in the SANS studies performed by Saaka [87] it was the micelle core that was identified as the major locus of solubilisation of testosterone derivatives in DDAPS micelles.

Although the volume of the DDAPS micelles is seen to be larger than those of the other ionic surfactant micelles investigated, this does not lead to a higher solubilisation

capacity for the steroids because their aggregation numbers in the DDAPS micelles are found to be much lower than those for ionic surfactant micelles.

Table 4. 12 Values of model fitted parameters for 2 wt% and 3.5 wt% DDAPS micelles in the presence of steroids.

Steroids	Contrast	R_1 (Å)	x	R_3 (Å)	δ (Å)	V_m (Å^3)	SAA N_{agg}	Steroids N_{agg}	S_{core} (Å^2)	A_{core} (Å^2)	S_m (Å^2)	A_m (Å^2)
4-CHOL	2% Drop	15.1	2.73	41.2	5.7	85036	106	5	6459	61	10323	97
	2% Shell	15.1	2.73	41.2	5.7	85436	107	5	6459	60	10353	97
	2% Core	15.1	2.72	41.1	6.0	87581	110	5	6437	59	10503	96
ADRENO	2% Drop	14.2	2.65	37.6	5.4	69242	88	3	5559	63	8949	102
	2% Shell	14.2	2.65	37.6	5.4	69156	88	3	5559	63	8942	102
	2% Core	14.2	2.65	37.6	5.4	69242	88	3	5559	63	8949	102

Steroids	Contrast	R_1 (Å)	x	R_3 (Å)	δ (Å)	V_m (Å^3)	SAA N_{agg}	Steroids N_{agg}	S_{core} (Å^2)	A_{core} (Å^2)	S_m (Å^2)	A_m (Å^2)
4-CHOL	3.5% Drop	14.9	3.56	53.0	6.0	107426	134	6	8049	60	12724	95
	3.5% Shell	14.9	3.56	53.0	6.0	107426	134	6	8049	60	12724	95
	3.5% Core	15.1	3.56	53.8	6.0	111438	139	6	8267	59	13042	94
ADRENO	3.5% Drop	14.2	3.35	47.6	5.6	87314	111	4	6904	62	10939	99
	3.5% Shell	14.2	3.35	47.6	5.6	87314	111	4	6904	62	10939	99
	3.5% Core	14.2	3.35	47.6	5.6	87314	111	4	6904	62	10939	99

Fitting parameters include the core equatorial radius (R_1), core axial radius (R_3), core axial ratio (x), shell thickness (δ), micelle volume (V_m), micelle and steroids aggregation number (SAA N_{agg} and steroids N_{agg}), surface area for hydrocarbon chain (S_{core}) and whole micelle (S_m) and the corresponding the area per molecule (A_{core} and A_m). Uncertainty for R_1, x, δ, N_{agg}, S and A = ± 0.3, ± 0.03, ± 0.3, ± 7, ± 250, and ± 1 respectively.

Aggregation behaviour of DDAO micelles

The aggregation behaviour of the zwitterionic surfactant DDAO in the presence and absence of steroids was determined through SANS measurements made on SANS 2D. The SANS profiles and model-fitted curves are shown in Figure 4.19. In the profile for the core contrast it will be noted that there is a peak at Q = 0.06 $Å^{-1}$, indicating that the DDAO micelles carry a small net charge. Barlow et al. [141] also reported a peak in the SANS data for DDAO micelles (at high concentration) and suggested that the hard sphere S(Q) model was not adequate to treat the repulsive forces between the micelles, and that a stronger and more repulsive potential should be included in the model. The data for the DDAO micelles were, therefore, re-fitted using the core-shell model with the Hayter-Penfold structure factor (H-P S(Q)) applied.

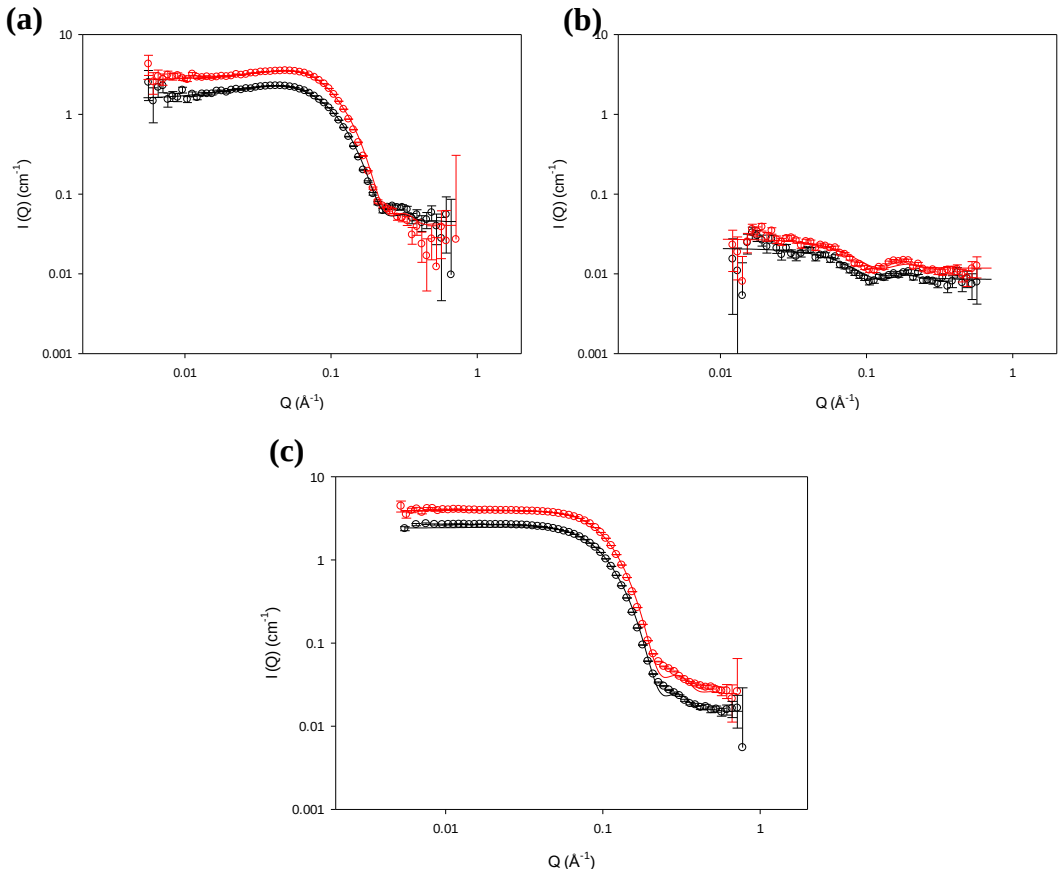

Figure 4. 19 SANS profiles and model fits (solid line) for 2 wt % (black) and 3.5 wt % (red) d_{25}DDAO in H_2O (a), d_{25}DDAO in D_2O (b) and h_{25}DDAO in D_2O (c).

The values of the model-fitted parameters for the DDAO micelles in the absence of steroids are presented in Table 4.13. These micelles are found to be prolate ellipsoids with a core radius, R_1 of 16.6 ± 0.3 Å. In contrast to the situation seen with the other surfactant micelles determined in this study, which typically become more elongated

with increased surfactant concentration, the results obtained for the DDAO micelles show that the aggregates have the same size and shape at both 2 wt% and 3.5 wt%. This was also found by Barlow et al. who determined the structure of DDAO micelles at various concentrations [141]. These workers showed too that with 8 H_2O per head group and an area per molecule of 82 Å, the micelle aggregation number remained the same (97 ± 2), regardless of concentration [141]. Saaka [87] also reported the DDAO micelles as prolate ellipsoidal, and quoted a similar aggregation number of ~ 90. He suggested too, however, that while R_1 remained constant at 16.6 Å, there was a slight decrease in size of the micelles when the concentration was increased from 2 wt% to 5 wt%, with a concomitant decrease in the core axial ratio from 1.7 to 1.6. A similar small decrease in x is also found in the present study, but this is not regarded as significant since the difference falls within the experimental uncertainty (± 0.03). The shell thickness of the DDAO micelles in this study was determined as 4.1 Å, regardless of concentration, which again agrees with the results found by Saaka (~ 4 Å) [87].

Table 4. 13 Values of model fitted parameters for 2 wt% and 3.5 wt% DDAO micelles.

Contrast	R_1 (Å)	x	R_3 (Å)	δ (Å)	V_m (Å^3)	Z e	SAA N_{agg}	S_{core} (Å^2)	A_{core} (Å^2)	S_m (Å^2)	A_m (Å^2)
2% Drop	16.6	1.71	28.4	4.1	58308	4	93	5185	56	7516	81
2% Shell	16.6	1.71	28.4	4.1	58308	4	93	5185	56	7516	81
2% Core	16.6	1.71	28.4	4.1	58308	4	93	5185	56	7516	81

Contrast	R_1 (Å)	x	R_3 (Å)	δ (Å)	V_m (Å^3)	Z e	SAA N_{agg}	S_{core} (Å^2)	A_{core} (Å^2)	S_m (Å^2)	A_m (Å^2)
3.5% Drop	16.6	1.67	27.7	4.1	56897	3	90	5085	56	7374	82
3.5% Shell	16.6	1.67	27.7	4.1	56897	3	90	5085	56	7374	82
3.5% Core	16.6	1.68	27.9	4.1	57194	3	91	5110	56	7405	81

Fitting parameters include the core equatorial radius (R_1), core axial radius (R_3), core axial ratio (x), shell thickness (δ), micelle volume (V_m), micelle charge (Z), micelle aggregation number (SAA N_{agg}), surface area for hydrocarbon chain (S_{core}) and whole micelle (S_m) and the corresponding areas per molecule (A_{core} and A_m). Uncertainty for R_1, x, δ, N_{agg}, S and A = ± 0.3, ± 0.03, ± 0.3, ± 7, ± 250, and ± 1 respectively.

DDAO micelles in the presence of steroids

The SANS profiles and model-fitted curves for DDAO micelles in the presence of 4-CHOL and ADRENO in all three contrasts at 2 wt% and 3.5 wt% are presented in Figures 4.21 and 4.22. For the contrast provided by d_{25}DDAO in D_2O, the addition of the steroids is seen to cause an increase in the scattering intensity, with 4-CHOL giving rise to greater increase than ADRENO. For the other two contrasts, there is no observable increase in I(Q) for the DDAO micelles upon addition of ADRENO, while the presence of 4-CHOL in the micelles gives rise to a slight increase in I(Q).

The values of the model-fitted parameters for the DDAO micelles in the presence of steroids are shown in Table 4.14.

Model-fitting of the SANS data for the ADRENO/DDAO micelles shows that this steroid causes no change in the micelle structure, suggesting that there is very little ADRENO solubilised within the aggregates, and this is wholly consistent with the findings from the solubilisation experiments (section 2.1).

The model-fitting of the SANS data does show, however, that there are changes in the DDAO micelle structure caused by addition of 4-CHOL. For the micelles containing 4-CHOL, the scattering length density of the deuterated surfactant core is seen to change from 6.95×10^{-6} Å^{-2} to $6.0 \pm 0.5 \times 10^{-6}$ Å^{-2}, giving clear evidence of the solubilisation of 4-CHOL in the DDAO micelle core. In addition it is found that R_1 increases by ~15% in the presence of 4-CHOL, with the core axial ratio also decreasing slightly. It is interesting to note too, however, that the thickness of the shell of the DDAO micelles is also found to increase upon the addition of 4-CHOL, with increases of 15% and 10% at the surfactant concentrations of 2 wt% and 3.5 wt%, respectively. Notwithstanding this change in shell thickness, it is concluded that the main locus of solubilisation of 4-CHOL is in the core of the DDAO micelles.

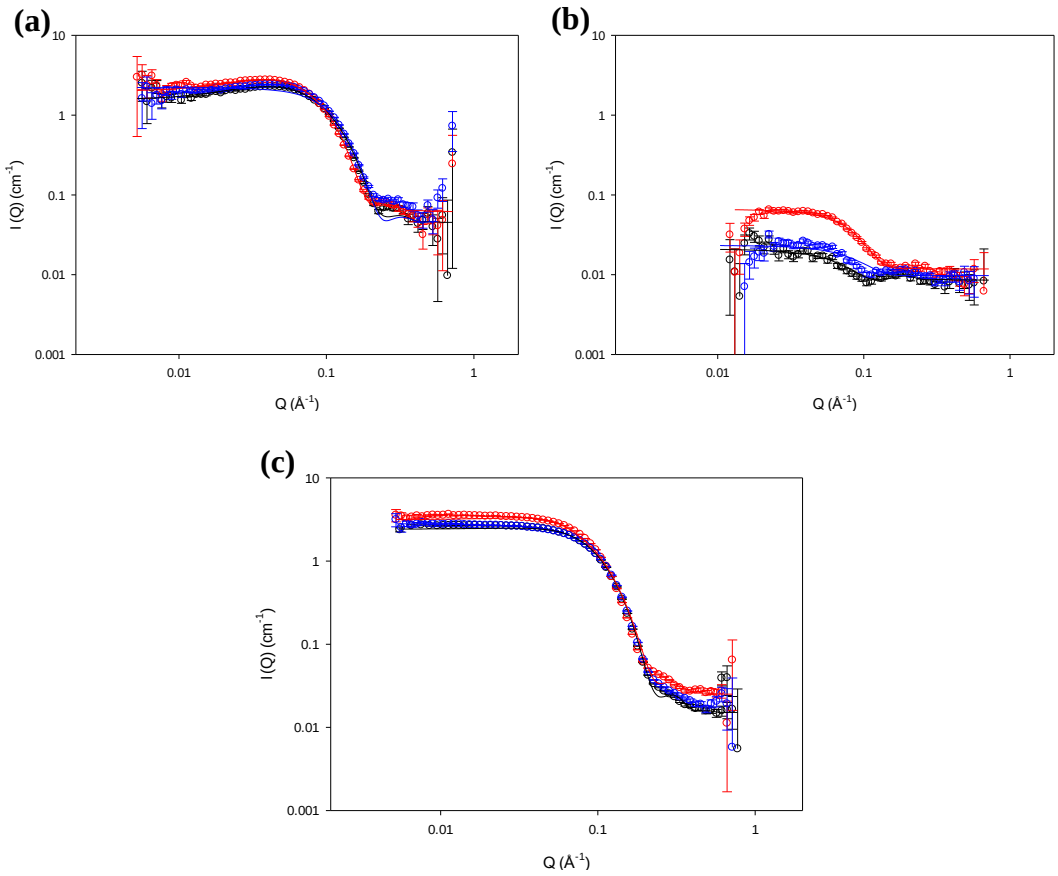

Figure 4. 20 SANS profiles and model fits (solid line) for d_{25}DDAO in H_2O (a), d_{25} DDAO in D_2O (b) and h_{25} DDAO in D_2O(c) micelles alone (black), micelles in the presence of saturation amounts of 4-CHOL (red) and ADRENO (blue) at 2 wt %.

As noted earlier, the model-fitting of the SANS data for the DDAO micelles showed that they tended to become more spherical with increasing concentration, and the same trend is also observed here for DDAO micelles in the presence of 4-CHOL or ADRENO. This trend was reported too by Saaka for the case of DDAO micelles in the presence of testosterone derivatives [87].

Although the model-fitted values of the parameters R_1, x, δ and N_{agg} for the DDAO micelles were very similar to those of the parameters for the ionic surfactant micelles, there are large differences between the DDAO and ionic surfactant micelle solubilisation capacities and this would suggest that the level of steroid solubilisation is influenced by the differing nature of the hydrophilic head groups of the surfactants and the resulting differences in micelle charge.

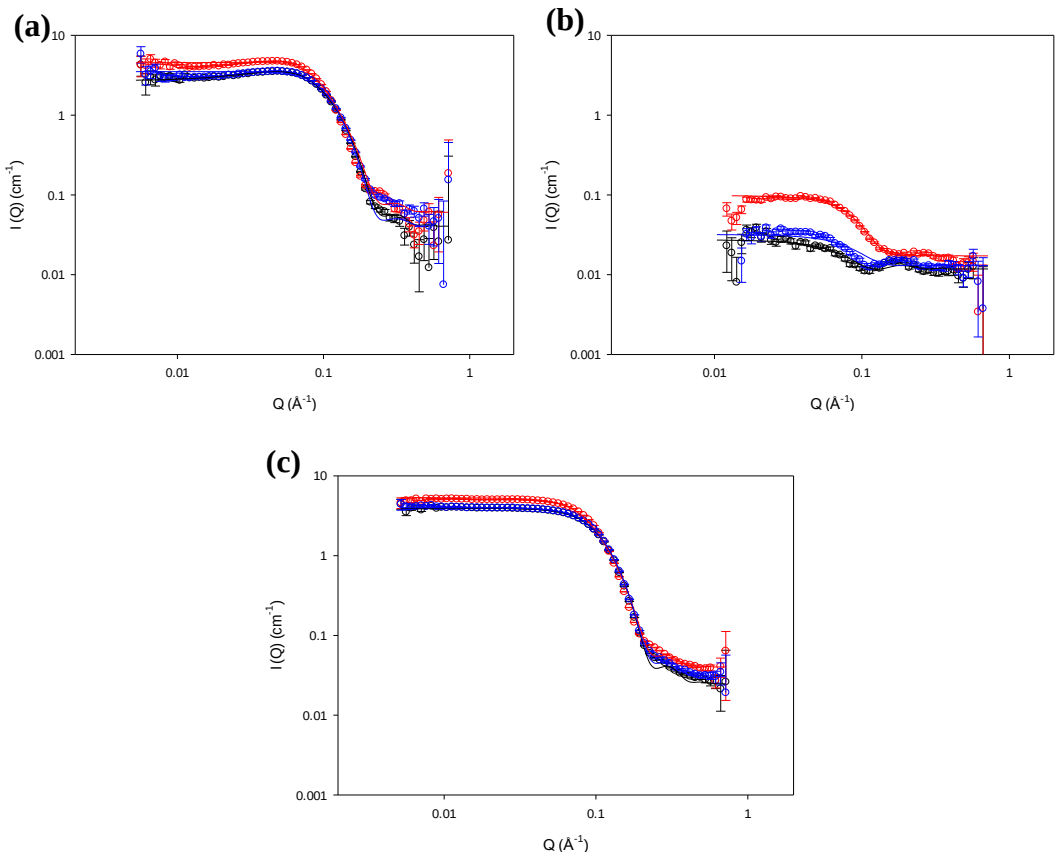

Figure 4. 21 SANS profiles and model fits (solid line) for d_{25}DDAO in H_2O (a), d_{25} DDAO in D_2O (b) and h_{25} DDAO in D_2O (c) micelles alone (black), micelles in the presence of saturation amounts of 4-CHOL (red) and ADRENO (blue) at 3.5 wt %.

Table 4. 14 Values of model fitted parameters for 2 wt% and 3.5 wt% DDAO micelles in the presence of steroids.

Steroids	Contrast	R_1 (Å)	x	R_3 (Å)	δ (Å)	V_m (Å^3)	Z e	SAA N_{agg}	Steroids N_{agg}	S_{core} (Å^2)	A_{core} (Å^2)	S_m (Å^2)	A_m (Å^2)
4-CHOL	2% Drop	19.6	1.57	30.7	4.7	87807	5	130	9	6727	52	9782	75
	2% Shell	19.6	1.57	30.8	4.7	88029	5	131	9	6741	52	9799	75
	2% Core	19.6	1.57	30.78	4.7	88029	5	131	9	6741	52	9799	75
ADRENO	2% Drop	16.6	1.76	29.2	4.1	59994	4	94	2	5310	56	7688	82
	2% Shell	16.6	1.76	29.2	4.1	59994	4	94	2	5310	56	7688	82
	2% Core	16.6	1.76	29.2	4.1	59994	4	94	2	5310	56	7688	82

Steroids	Contrast	R_1 (Å)	x	R_3 (Å)	δ (Å)	V_m (Å^3)	Z e	SAA N_{agg}	Steroids N_{agg}	S_{core} (Å^2)	A_{core} (Å^2)	S_m (Å^2)	A_m (Å^2)
4-CHOL	3.5% Drop	18.6	1.54	28.6	4.5	73910	4	110	7	5977	54	8704	79
	3.5% Shell	18.6	1.54	28.6	4.5	73910	4	110	7	5977	54	8704	79
	3.5% Core	18.6	1.54	28.6	4.5	73910	4	110	7	5977	54	8704	79
ADRENO	3.5% Drop	16.6	1.66	27.6	4.1	56818	3	89	2	5060	57	7362	83
	3.5% Shell	16.6	1.66	27.6	4.1	56818	3	89	2	5060	57	7362	83
	3.5% Core	16.6	1.66	27.6	4.1	56818	3	89	2	5060	57	7362	83

Fitting parameters include the core equatorial radius (R_1), core axial radius (R_3), core axial ratio (x), shell thickness (δ), micelle volume (V_m), micelle charge (Z), micelle and steroids aggregation number (SAA N_{agg} and steroids N_{agg}), surface area for hydrocarbon chain (S_{core}) and whole micelle (S_m) and the corresponding the area per molecule (A_{core} and A_m). Uncertainty for R_1, x, δ, N_{agg}, S and A = ± 0.3, ± 0.03, ± 0.3, ± 7, ± 250, and ± 1 respectively.

Aggregation behaviour of DPC micelles

For DPC micelles, the SANS profiles and model-fitted curves for all three contrasts at 2 wt% and 3.5 wt% are shown in Figure 4.22. It can be seen that the scattering intensities increase with increasing surfactant concentration while there is no significant change in the shape of the curves. As expected, there is no evidence of any interaction peak in the scattering curves, suggesting no significant electrostatic repulsion between the micelles.

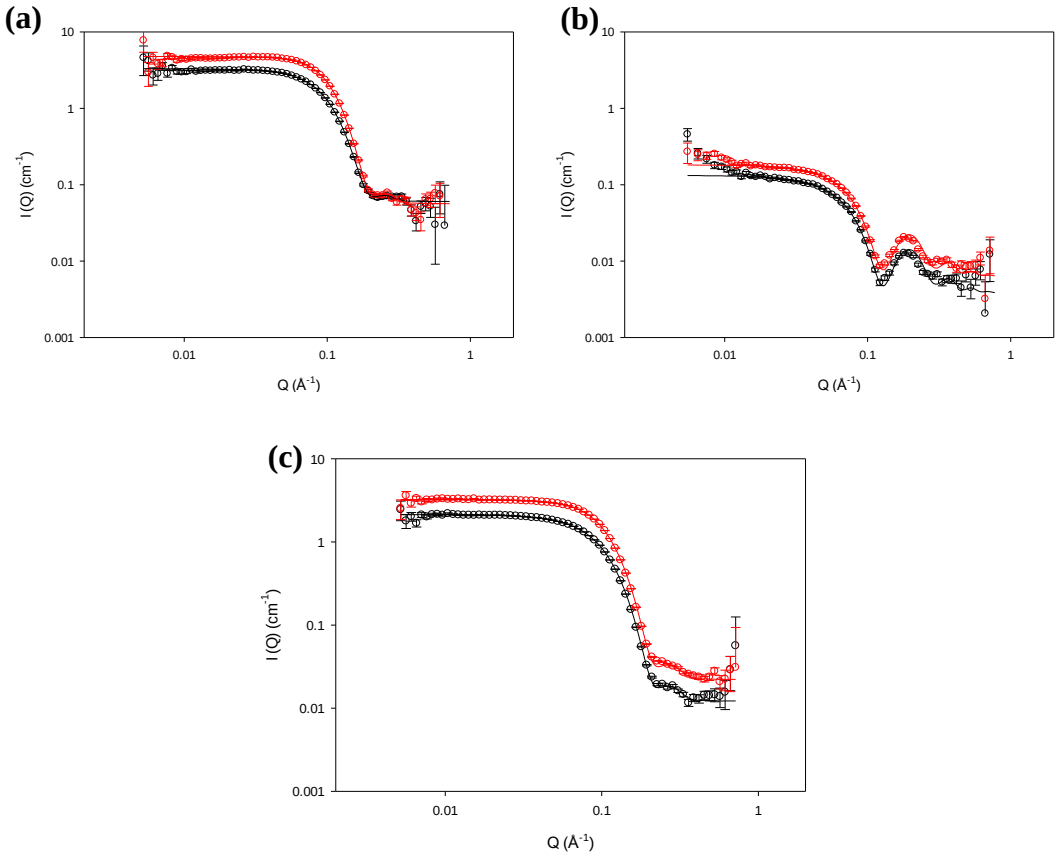

Figure 4. 22 SANS profiles and model fits (solid line) for 2 wt % (black) and 3.5 wt % (red) d_{25}DPC in H_2O (a), d_{25}DPC in D_2O (b) and h_{25}DPC in D_2O (c).

The values of the model-fitted parameters found for the DPC micelles in the absence of steroids at surfactant concentrations of 2 wt% and 3.5 wt% are given in Table 4.15. At both concentrations, the micelles are found to be best modelled as prolate ellipsoids with a core axial ratio of 1.5, and a core radius consistent with the fully extended C_{12} chain length. Just as with DDAO micelles, there is no evidence that the DPC micelles become more asymmetric with increasing surfactant concentration, the change in x (of ca. 1%) falling within experimental error.

The thickness of the shell of the DPC micelles was determined as 5.6 ± 0.3 Å, which is higher than that of the DDAO micelles, and is just as expected given the difference in size of the surfactants' head groups.

In the scattering studies conducted by Pambou et al. the shapes and structures of DPC micelles were determined for four different concentrations of surfactant using a spherical core-shell model [195]. These researchers report a decrease in the micelle shell thickness from 10 ± 2 Å to 5.5 ± 2 Å when the DPC concentration is increased from 0.35 wt% to 7 wt%. This thinning of the shell they suggested was due to a dehydration of the DPC head groups at the higher concentrations due to a closer packing of the surfactant molecules.

Molecular dynamics simulations of DPC micelles in water have been reported by Wymore et al. [196] and Tieleman et al. [197] and these workers report that the micelles are slightly asymmetric at low concentration, and that they become more spherical as the surfactant concentration is increased. More recently, Oliver et al. used small-angle X-ray scattering to study DPC micelles and determined the core equatorial radius (R_1) to be 16.1 - 16.4 Å with the micelle aggregation number estimated as ~80 at 2.7 wt% [35]. In addition, they suggested that the micelles form prolate ellipsoids with an axial ratio of ~1.5, which is in good agreement with the results presented here.

Table 4. 15 Values of model fitted parameters for 2 wt% and 3.5 wt% DPC micelles.

Contrast	R_1 (Å)	x	R_3 (Å)	δ (Å)	V_m (Å^3)	SAA N_{agg}	S_{core} (Å^2)	A_{core} (Å^2)	S_m (Å^2)	A_m (Å^2)
2% Drop	16.6	1.55	25.7	5.6	64836	84	4786	57	7961	95
2% Shell	16.6	1.55	25.7	5.6	64836	84	4786	57	7961	95
2% Core	16.6	1.55	25.7	5.6	64836	84	4786	57	7961	95

Contrast	R_1 (Å)	x	R_3 (Å)	δ (Å)	V_m (Å^3)	SAA N_{agg}	S_{core} (Å^2)	A_{core} (Å^2)	S_m (Å^2)	A_m (Å^2)
3.5% Drop	16.6	1.53	25.4	5.6	63992	83	4736	57	7882	95
3.5% Shell	16.6	1.53	25.4	5.7	63992	83	4736	57	7882	95
3.5% Core	16.6	1.53	25.4	5.7	63992	83	4736	57	7882	95

Fitting parameters include the core equatorial radius (R_1), core axial radius (R_3), core axial ratio (x), shell thickness (δ), micelle volume (V_m), micelle aggregation number (SAA N_{agg}), surface area for hydrocarbon chain (S_{core}) and whole micelle (S_m) and the corresponding areas per molecule (A_{core} and A_m). Uncertainty for R_1, x, δ, N_{agg}, S and A = ± 0.3, ± 0.03, ± 0.3, ± 7, ± 250, and ± 1 respectively.

DPC micelles in the presence of steroids

Figures 4.23 and 4.24 show the SANS profiles and model-fitted curves for DPC micelles in the presence and absence of 4-CHOL and ADRENO. The addition of the steroids to the DPC micelles leads to an increase in scattering intensity for the shell SANS contrast. The increase seen for ADRENO at 2 wt% surfactant is higher than that for 4-CHOL but the increases for the two steroids are much the same at a surfactant concentration of 3.5 wt%.

The model-fitted parameters for these systems (Table 4.16), show that the micelle volume increases by 10% upon the addition of ADRENO, and the best fit to the SANS profile is found when the scattering length density of the micelle core is lowered to 6.4 ± 0.5 x 10^{-6} $Å^{-2}$. According to the solubilisation experiment (section 2.1), the solubilisation capacity of DPC for ADRENO is slightly higher than for 4-CHOL, so it is reasonable to find that the scattering length density of the deuterated core of DPC in the presence of ADRENO is lowered, but remains unchanged in 4-CHOL/DPC micelles.

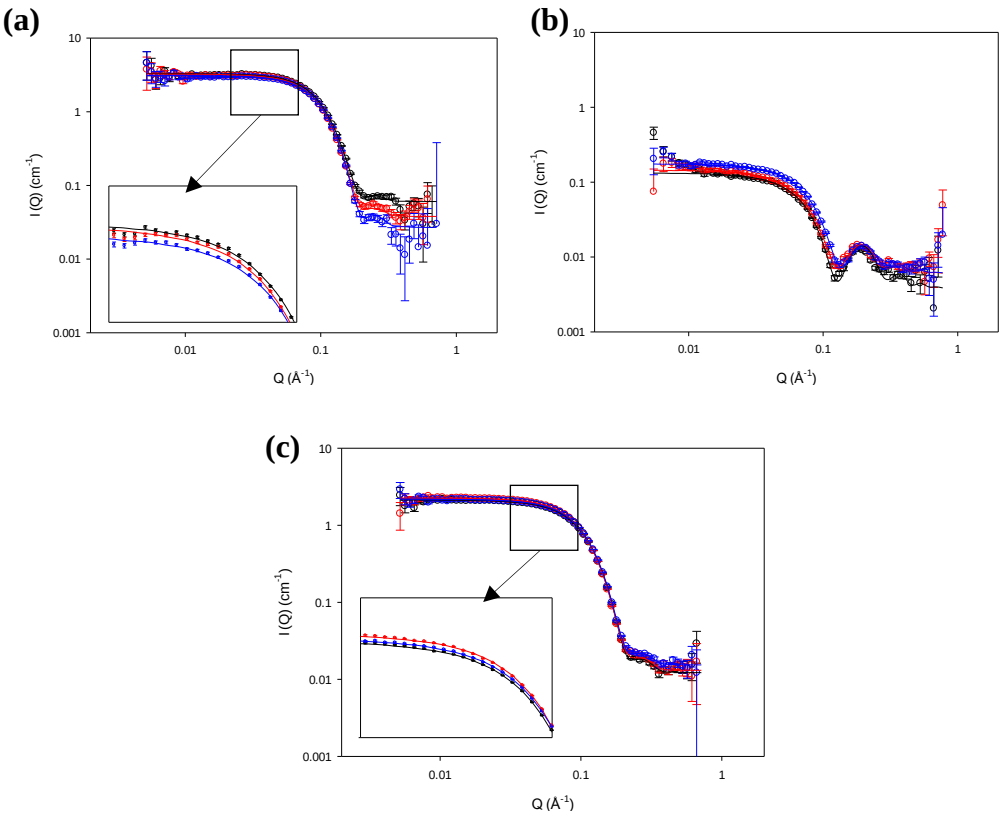

Figure 4. 23 SANS profiles and model fits (solid line) for d_{25}DPC in H_2O (a), d_{25} DPC in D_2O (b) and h_{25} DPC in D_2O (c) micelles alone (black), micelles in the presence of saturation amounts of 4-CHOL (red) and ADRENO (blue) at 2 wt %.

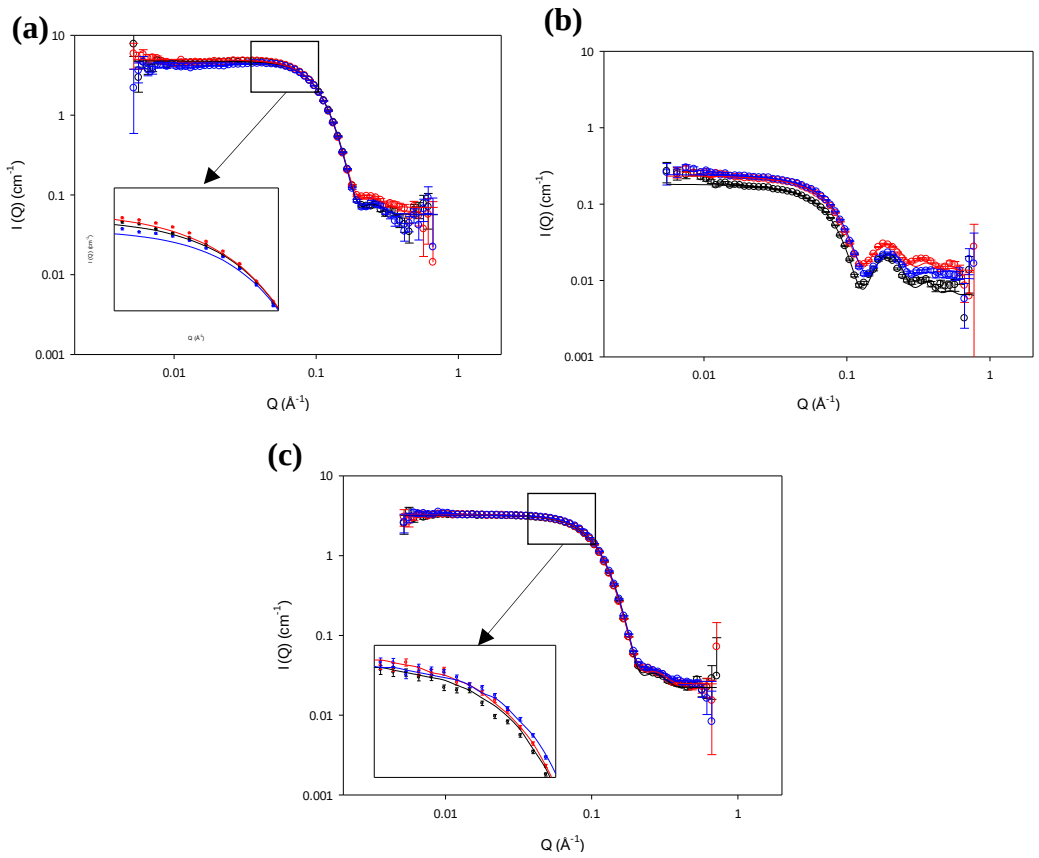

Figure 4. 24 SANS profiles and model fits (solid line) for d_{25}DPC in H_2O (a), d_{25} DPC in D_2O (b) and h_{25} DPC in D_2O (c) micelles alone (black), micelles in the presence of saturation amounts of 4-CHOL (red) and ADRENO (blue) at 3.5 wt %.

In contrast to what was seen for the other surfactant micelle systems investigated in this study, the addition of 4-CHOL in the DPC micelles did not lead to any noticeable change in scattering intensity. The micelle volume increased by only 3% in the presence of 4-CHOL and no changes were seen in the scattering length density of either the core region or the shell of the micelle.

Given the relatively large head group of DPC, one might expect an interaction between the steroids and its hydrophilic head group. Wymore et al. studied the interaction between the DPC head group and water via molecular dynamics simulation [196]. They suggested that the water molecules formed strong hydrogen bonds with the phosphate oxygen atoms, while the charged choline group interacted with the water oxygen. It is not unreasonable to assume, therefore, that the ADRENO molecules are solubilised within the shell of the DPC micelles because the head group has three carbonyl groups.

Saaka [87] determined the structure of DPC micelles in the presence of testosterone derivatives and suggested a significant involvement of the C_{12} chain in the

solubilisation of testosterone enanthate, with testosterone and testosterone propionate being solubilised instead within the hydrophilic head group region of the DPC micelle.

Table 4. 16 Values of model fitted parameters for 2 wt% and 3.5 wt% DPC micelles in the presence of steroids.

Steroids	Contrast	R_1 (Å)	x	R_3 (Å)	δ (Å)	V_m (Å^3)	SAA N_{agg}	Steroids N_{agg}	S_{core} (Å^2)	A_{core} (Å^2)	S_m (Å^2)	A_m (Å^2)
4-CHOL	2% Drop	16.6	1.59	26.4	5.7	66450	85	2	4885	58	8111	96
	2% Shell	16.6	1.59	26.4	5.7	66450	85	2	4885	58	8111	96
	2% Core	16.6	1.59	26.4	5.7	66450	85	2	4885	58	8111	96
ADRENO	2% Drop	16.6	1.70	28.2	5.8	71079	91	2	5160	57	8540	94
	2% Shell	16.6	1.70	28.2	5.8	71079	91	2	5160	57	8540	94
	2% Core	16.6	1.70	28.2	5.8	71079	91	2	5160	57	8540	94

Steroids	Contrast	R_1 (Å)	x	R_3 (Å)	δ (Å)	V_m (Å^3)	SAA N_{agg}	Steroids N_{agg}	S_{core} (Å^2)	A_{core} (Å^2)	S_m (Å^2)	A_m (Å^2)
4-CHOL	3.5% Drop	16.6	1.55	25.7	5.6	64757	82	2	4786	58	7954	97
	3.5% Shell	16.6	1.55	25.7	5.6	64678	82	2	4786	58	7948	97
	3.5% Core	16.6	1.55	25.7	5.6	64757	82	2	4786	58	7954	97
ADRENO	3.5% Drop	16.6	1.65	27.4	5.7	68928	88	2	5035	57	8341	95
	3.5% Shell	16.6	1.65	27.4	5.7	68928	88	2	5035	57	8341	95
	3.5% Core	16.6	1.65	27.4	5.7	68928	88	2	5035	57	8341	95

Fitting parameters include the core equatorial radius (R_1), core axial radius (R_3), core axial ratio (x), shell thickness (δ), micelle volume (V_m), micelle and steroids aggregation number (SAA N_{agg} and steroids N_{agg}), surface area for hydrocarbon chain (S_{core}) and whole micelle (S_m) and the corresponding the area per molecule (A_{core} and A_m). Uncertainty for R_1, x, δ, N_{agg}, S and A = ± 0.3, ± 0.03, ± 0.3, ± 7, ± 250, and ± 1 respectively.

4.4.3 SANS studies for non-ionic surfactants

Fitting models and parameters

The SANS profiles for the non-ionic surfactant micelles were model-fitted using the same monodisperse two-shell ellipsoid model incorporating a hard sphere structure factor that was used in modelling the data for the zwitterionic surfactant micelles. The details of the model were described earlier (section 4.4.2) and the fitted parameters are summarised in Table 4.17. Given that the CMCs of the non-ionic surfactants are much lower than those of ionic surfactants, the micellar solutions of Brij 35 and Tween 20 were prepared at lower concentrations (*viz*., 2 wt% and 3.5 wt% *vs* 3 wt% and 5 wt%).

Table 4. 17 Molecular formulas, molecular volume (V_m), molecular weight (M_w) and scattering length density (ρ) of the constituents of the zwitterionic surfactants and steroids studied.

Chemical	Molecular formula		V_m (Å^3)	M_w (g mol^{-1})		ρ (x 10^{-6} Å^{-2})	
	Protiated	Deuterated		Protiated	Deuterated	Protiated	Deuterated
4-CHOL	$C_{27}H_{44}O$	N/A	652.5	384.6	N/A	0.34	N/A
ADRENO	$C_{19}H_{24}O_3$	N/A	422.6	300.4	N/A	1.27	N/A
Tween 20	$C_{58}H_{114}O_{26}$	$C_{12}H_{25}D_{89}O_{26}$	1782.3	1227.5	1316.5	0.62	4.10
Tween20 [20]	$C_{46}H_{89}O_{26}$	$C_{46}D_{89}O_{26}$	1438.6	1058.2	1147.2	0.87	7.35
Brij35	$C_{58}H_{118}O_{24}$	$C_{58}D_{25}H_{93}O_{24}$	1778.6	1428.6	N/A	1.12	N/A
Brij35 [23]	$C_{46}H_{93}O_{24}$	N/A	1424.9	1030.2	N/A	1.20	N/A
Alkyl chain	$C_{12}H_{25}$	$C_{12}D_{25}$	353.7	169.3	194.5	-0.39	6.95

Tween20 [20] and Brij35 [23] represent head groups of Tween 20 and Brij 35, respectively

Aggregation behaviour of Tween 20 micelles

Tween 20 is a non-ionic surfactant with 20 ethylene oxide groups in its head group. SANS measurements were made for Tween 20 with both protiated and deuterated ethylene oxide groups either in D_2O or H_2O, at surfactant concentrations of 2 wt% and 3.5 wt%. For this surfactant, the shell SANS contrast sample involved d-Tween 20 dispersed in H_2O (d-/h- here used to refer to the presence of deuterated/protiated ethylene oxide groups), and the sample having d-Tween 20 dispersed in D_2O is referred to as the core contrast. The drop SANS contrast for this system remains the same as described previously (viz., h-Tween 20 dispersed in D_2O).

As expected, the SANS profiles for the Tween 20 micelles show an increase in scattering intensity with increasing concentration, while the shape of the profiles remains unchanged.

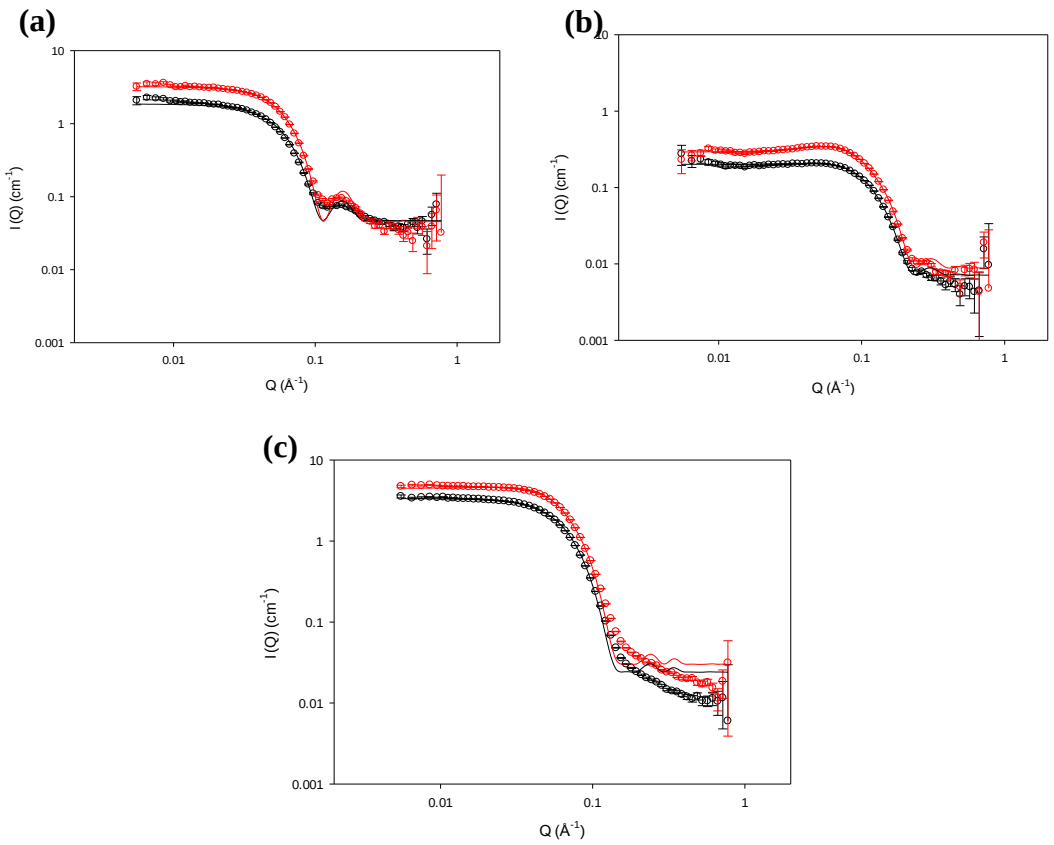

Figure 4. 25 SANS profiles and model fits (solid line) for 2 wt % (black) and 3.5 wt % (red) d-Tween 20 in H_2O (a), d-Tween 20 in D_2O (b) and h-Tween 20 (c) in D_2O.

The values of the model-fitted parameters for the Tween 20 micelles are summarized in Table 4.18. The micelles are found to be prolate ellipsoidal with a core axial ratio of ~1.1 and a core radius of ~16 Å. With increasing surfactant concentration, the shape

and structure of the prolate micelles is not seen to change significantly, and the shell thickness too remains the same (19.6 Å).

The aggregation number of 55 determined here for the Tween 20 micelles is in good agreement with the value obtained by Ullah et al. [198] who used dynamic light scattering (N_{agg} = 52) in their study. However, in the SANS studies performed by Penfold et al. [199], an aggregation number of 90 ± 10 was reported for Tween 20 concentrations in the range 0.5 wt% to 2 wt% and these workers also reported prolate ellipsoids with a larger core axial ratio of 1.6.

The results from Saaka's studies of Tween 20 micelles are reassuringly closer to those reported here, with an aggregation number of ~50 quoted for surfactant concentrations in the range 2 wt% to 5 wt%. While the model-fitting conducted in the present studies showed the micelles as prolate ellipsoids, however, Saaka proposed that they were oblate ellipsoidal and tended to become more oblate with increasing concentration [87]. As noted earlier, however, there is generally very little difference between the quality of the fits obtained assuming prolate and oblate ellipsoids and so it is often not possible to make an unequivocal choice between the two geometries.

Table 4. 18 Values of model fitted parameters for 2 wt% and 3.5 wt% Tween 20 micelles.

Contrast	R_1 (Å)	x	R_3 (Å)	δ (Å)	V_m (Å^3)	SAA N_{agg}	S_{core} (Å^2)	A_{core} (Å^2)	S_m (Å^2)	A_m (Å^2)
2% Drop	16.0	1.14	18.2	19.6	200881	55	3521	64	16598	300
2% Shell	16.0	1.14	18.2	19.6	201213	55	3521	64	16616	300
2% Core	16.0	1.14	18.2	19.6	201213	55	3521	64	16616	300

Contrast	R_1 (Å)	x	R_3 (Å)	δ (Å)	V_m (Å^3)	SAA N_{agg}	S_{core} (Å^2)	A_{core} (Å^2)	S_m (Å^2)	A_m (Å^2)
3.5% Drop	16.0	1.11	17.8	19.4	195061	54	3455	64	16272	302
3.5% Shell	16.0	1.11	17.8	19.4	195061	54	3455	64	16272	302
3.5% Core	16.0	1.11	17.8	19.5	195061	54	3455	64	16272	302

Fitting parameters include the core equatorial radius (R_1), core axial radius (R_3), core axial ratio (x), shell thickness (δ), micelle volume (V_m), micelle aggregation number (SAA N_{agg}), surface area for hydrocarbon chain (S_{core}) and whole micelle (S_m) and the corresponding areas per molecule (A_{core} and A_m). Uncertainty for R_1, x, δ, N_{agg}, S and A = ± 0.3, ± 0.03, ± 0.3, ± 7, ± 250, and ± 1 respectively.

Tween 20 micelles in the presence of steroids

The SANS profiles and the model-fitted curves for the Tween 20 micelles in the presence and absence of steroids are displayed in Figure 4.26. The addition of the steroids to the micelles causes an increase in the scattering intensity as expected. In this case, these changes are much more noticeable for the d-Tween 20/H_2O (shell) contrast because of the deuterated head group of the Tween 20.

Since the head group of Tween 20 is very much larger than the head groups of all the other surfactants studied here, it might be expected that the solubilisation of the steroid molecules will cause very little change to the geometry of the micelles.

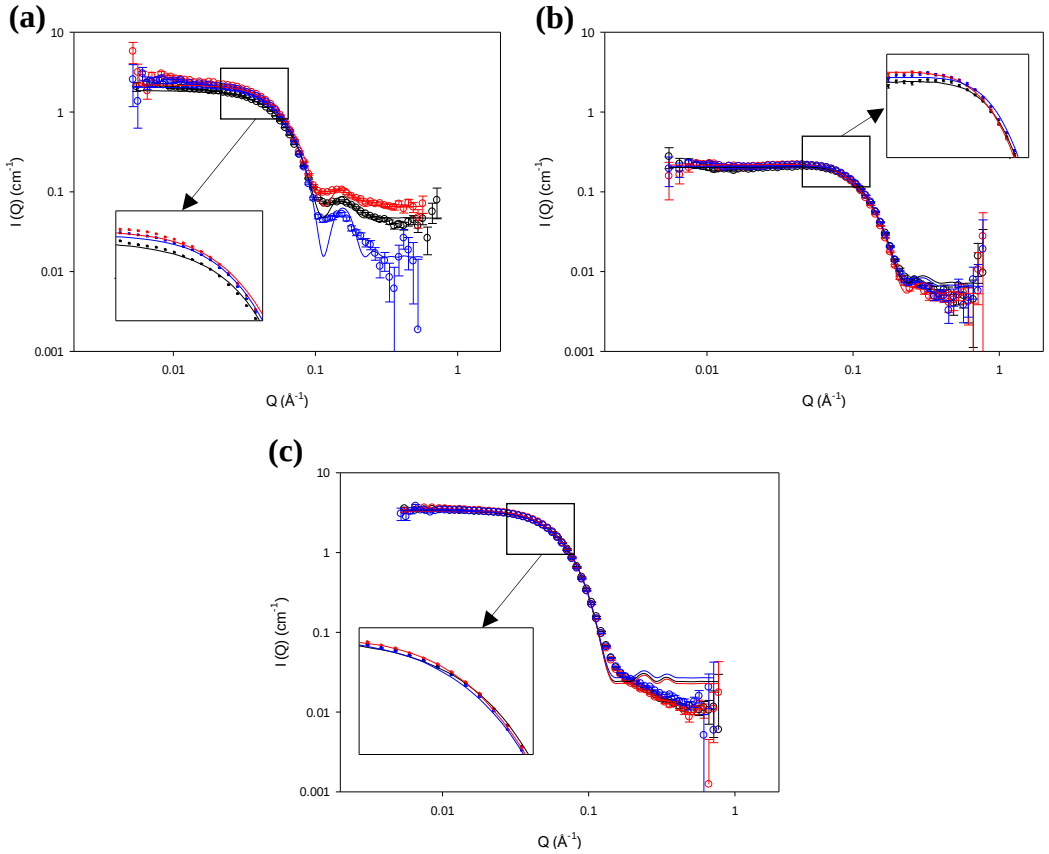

Figure 4. 26 SANS profiles and model fits (solid line) for d-Tween 20 in H_2O (a), d-Tween in D_2O (b) and h-Tween in D_2O (c) micelles alone (black), micelles in the presence of saturation amounts of 4-CHOL (red) and ADRENO (blue) at 2.0 wt %.

The values of the model-fitted parameters are listed in Table 4.19. Though the amounts of steroids solubilised in the micelles are not enough to cause a change in the shape of the micelles there is evidence of their increasing sphericity in the presence of 4-CHOL and ADRENO. The core radius shows no difference upon addition of steroids while

the shell thickness decreases slightly when ADRENO is solubilised in the micelle present at a Tween 20 concentration of 3.5 wt%.

From the solubilisation studies (section 2.1), it was found that the molar ratios for 4-CHOL and ADRENO were 1 per 5 and 50 molecules of Tween 20, respectively, and these findings are consistent with the calculated aggregation numbers given in Table 4.19. These differences in solubilisation capacity, however, do not lead to any significant change in the shape of the Tween 20 micelles.

Since the chain deuterated Tween 20 was not available for these studies, the scattering length density value of the hydrocarbon chain region was not adjusted. However, the fitted scattering length densities of the deuterated micelle shell region did not change upon addition of saturating amounts of the steroids. It is reasonable to predict, therefore, that the locus of solubilisation of 4-CHOL in Tween 20 micelles was in the tail region. The location of solubilisation of ADRENO, however, cannot be determined.

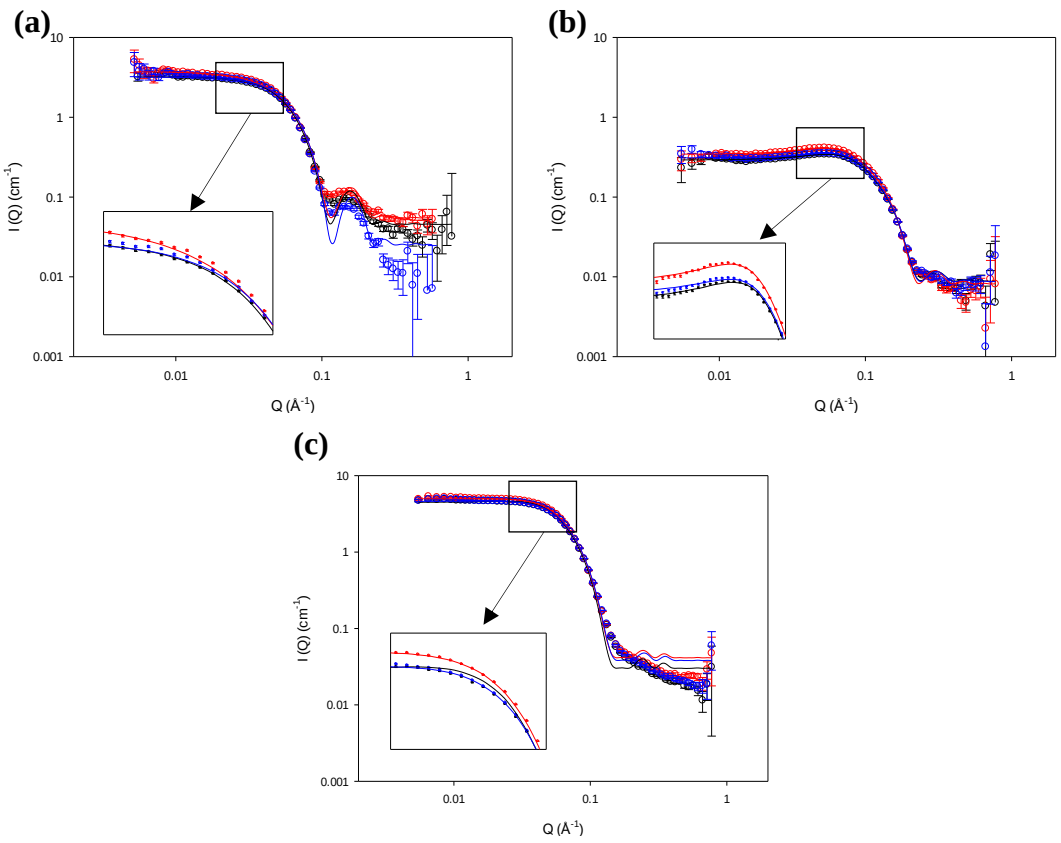

Figure 4. 27 SANS profiles for d-Tween 20 in H_2O (a), d-Tween 20 in D_2O (b) and h-Tween 20 (c) in D_2O micelles alone (black), micelles in the presence of saturation amounts of 4-CHOL (red) and ADRENO (blue) at 3.5 wt %.

Table 4. 19 Values of model fitted parameters for 2 wt% and 3.5 wt% Tween 20 micelles in the presence of steroids.

Steroids	Contrast	R_1 (Å)	x	R_3 (Å)	δ (Å)	V_m (Å^3)	SAA N_{agg}	Steroids N_{agg}	S_{core} (Å^2)	A_{core} (Å^2)	S_m (Å^2)	A_m (Å^2)
4-CHOL	2% Drop	16.0	1.12	17.9	19.5	197537	53	10	3477	66	16411	312
	2% Shell	16.0	1.12	17.9	19.5	30345	53	10	3477	66	16411	312
	2% Core	16.0	1.12	17.9	19.5	197537	53	10	3477	66	16411	312
ADRENO	2% Drop	16.0	1.12	17.1	19.5	197537	54	1	3477	64	16411	302
	2% Shell	16.0	1.12	17.1	19.5	32613	54	1	3477	64	16411	302
	2% Core	16.0	1.12	17.1	19.5	197537	54	1	3477	64	16411	302

Steroids	Contrast	R_1 (Å)	x	R_3 (Å)	δ (Å)	V_m ($Å^3$)	SAA N_{agg}	Steroids N_{agg}	S_{core} ($Å^2$)	A_{core} ($Å^2$)	S_m ($Å^2$)	A_m ($Å^2$)
4-CHOL	3.5% Drop	16.0	1.07	17.9	19.2	188503	50	10	3368	67	15902	317
	3.5% Shell	16.0	1.07	17.9	19.2	30377	50	10	3368	67	15902	317
	3.5% Core	16.0	1.07	17.9	19.2	188503	50	10	3368	67	15902	317
ADRENO	3.5% Drop	16.0	1.02	16.3	18.9	179365	49	1	3251	66	15381	312
	3.5% Shell	16.0	1.02	16.3	18.9	30371	49	1	3251	66	15381	312
	3.5% Core	16.0	1.02	16.3	18.9	179365	49	1	3251	66	15381	312

Fitting parameters include the core equatorial radius (R_1), core axial radius (R_3), core axial ratio (x), shell thickness (δ), micelle volume (V_m), micelle and steroids aggregation number (SAA N_{agg} and steroids N_{agg}), surface area for hydrocarbon chain (S_{core}) and whole micelle (S_m) and the corresponding the area per molecule (A_{core} and A_m). Uncertainty for R_1, x, δ, N_{agg}, S and A = ± 0.3, ± 0.03, ± 0.3, ± 7, ± 250, and ± 1 respectively.

Aggregates behaviour of Brij 35 micelles

SANS profiles are shown in Figure 4.28 for Brij 35 micelles only in the drop SANS contrast as deuterated Brij 35 was not available. As expected, the scattering intensity is seen to increase with increasing surfactant concentration but very surprisingly there is an interaction peak seen at Q = 0.06 $Å^{-1}$ and this becomes more pronounced as the surfactant concentration is increased. In model-fitting these SANS data, however, the hard sphere structure factor (HS S(Q)) was still used because physically sensible models could not be fitted assuming the presence of charge on the micelles.

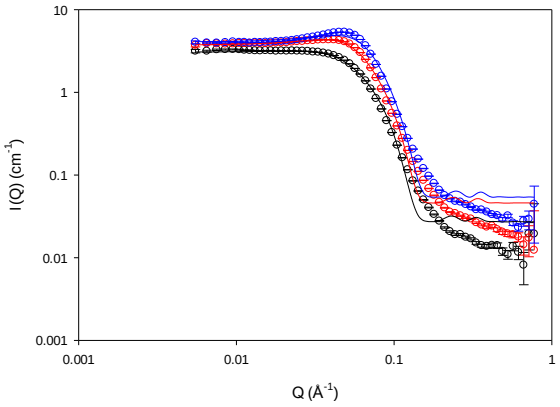

Figure 4. 28 SANS profiles and model fits (solid line) for 2 wt % (black), 3.5 wt % (red) and 5 wt% (blue) h_{25}Brij 35 in D_2O

The Brij 35 micelles were found to be prolate ellipsoidal with a core radius at 16.7 Å (Table 4.20). With increasing concentration, the micelles were found to become more spherical, with x decreasing from 1.2 to 1. The increase in surfactant concentration also led to a decrease in micelle volume by 5% and 19% at concentrations of 2 wt% and 5 wt%, respectively.

Tummino and Gafni [200] studied the aggregation number of Brij 35 micelles using steady-state fluorescence quenching. They found that for 1.2 wt% Brij 35 at 30 ^oC, the micelles had an aggregation number of 53 ± 3. In later SANS studies carried out by Borbély, the aggregate structure of Brij 35 micelles was determined at different temperatures for concentrations ranging from 0.5 wt% to 20 wt% [201]. Borbély proposed that at low concentrations, the micelles could be modelled as a polydisperse spherical core with tethered polymer chains on the surface. Studied at 20 ^oC, the micelles were shown to have a core radius of 18 ± 0.5 Å, with aggregation numbers of 45.7 ± 0.8 at a concentration of 2.5 wt% and 47.5 ± 1.6 at 5 wt%. Borbély also

explained that the core radius of the micelles was longer than the fully extended length of a C_{12} chain because of the intrusion of hydrated poly (ethylene oxide) moieties into the micelle alkyl chain region. At temperatures above 20 ^{o}C, the micelles are found to be larger, while the core radius increases only slightly. In the studies presented here the model used in describing the Brij 35 micelles is simpler than the one used by Borbély, but it is still considered satisfactory.

Preu et al. have also reported studies of Brij 35 micelles using SANS and they too employ an ellipsoidal core/shell model to describe their geometry as a function of concentration [202]. These workers found aggregation numbers of 42, 42 and 44 for surfactant concentrations of 1 wt%, 4 wt% and 6 wt%, respectively, and the micelles formed were shown in all cases to be prolate ellipsoidal. The surfactant head groups were modelled as having 7 water molecules per ethylene oxide unit and the micelle shell thickness was quoted at 33 Å. In the present study, there were determined to be only 2 H_2O per ethylene oxide unit and the shell thickness of the micelle was found to be much thinner, at 19 Å. These parameter values, however, agree with those reported by Saaka [87].

Table 4. 20 Values of model fitted parameters for 2 wt%, 3.5 and 5 wt% Brij 35 micelles.

Concentration	R_1 (Å)	x	R_3 (Å)	δ (Å)	V_m ($Å^3$)	SAA N_{agg}	S_{core} ($Å^2$)	A_{core} ($Å^2$)	S_m ($Å^2$)	A_m ($Å^2$)
2 wt%	16.7	1.24	20.7	19.0	211984	68	4077	60	17227	252
3.5 wt%	16.7	1.15	19.2	18.6	196508	63	3860	61	16359	258
5 wt%	16.7	1.01	16.9	18.0	175858	56	3528	63	15180	272

Fitting parameters include the core equatorial radius (R_1), core axial radius (R_3), core axial ratio (x), shell thickness (δ), micelle volume (V_m), micelle aggregation number (SAA N_{agg}), surface area for hydrocarbon chain (S_{core}) and whole micelle (S_m) and the corresponding areas per molecule (A_{core} and A_m). Uncertainty for R_1, x, δ, N_{agg}, S and A = ± 0.3, ± 0.03, ± 0.3, ± 7, ± 250, and ± 1 respectively.

Brij 35 micelles in the presence of steroids

Figure 4.29 presents the SANS profiles and the model-fitted curves for Brij 35 micelles in the absence and presence of 4-CHOL and ADRENO. In each contrast, there is no obvious change in the scattering intensities nor in the shapes of the curves. This suggests that the presence of the solubilised steroids does not perturb the structure of the Brij 35 micelles.

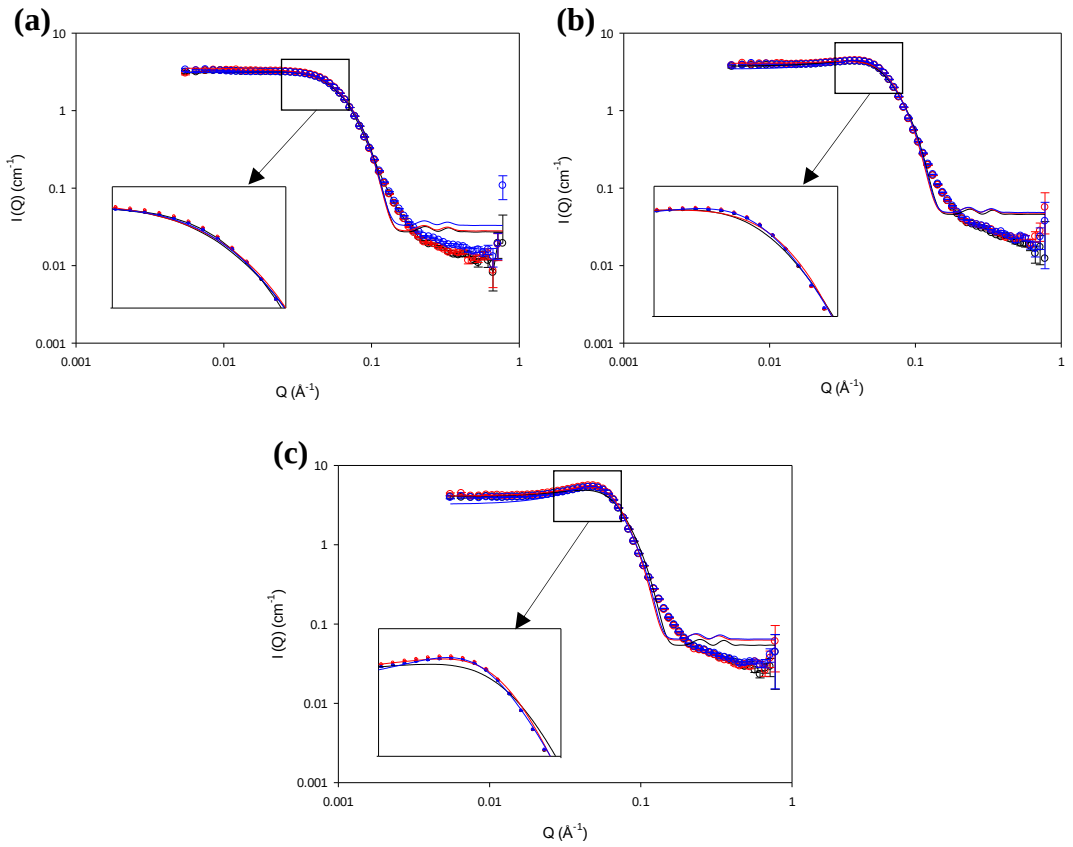

Figure 4. 29 SANS profiles and model fits (solid line) for 2 wt% (a), 3.5 wt% (b) and 5 wt% (c) of h_{25}Brij in D_2O in the absence (black) and in the presence of 4-CHOL (red) and ADRENO (blue).

This inference was confirmed by the values obtained for the model-fitted parameters (Table 4.21). The volumes of the micelles were increased by less than 5% upon the addition of 4-CHOL and ADRENO, and x increased by ~10% in the presence of the steroids.

It was not possible from the SANS model-fitting to determine with any confidence whether there were changes in the micelle shell and core regions of the Brij 35 micelles caused by the addition of the 4-CHOL and ADRENO because of the similarity in the scattering length densities for the protiated head group and alkyl chain of the

surfactant. Given also that there is also only 1 molecule of steroid solubilised per micelle, it is thus impossible to determine their locus of solubilisation within the Brij 35 micelles.

Table 4. 21 Values of model fitted parameters for 2 wt%, 3.5 wt% and 5 wt% Brij 35 micelles in the presence of steroids.

Steroids	Concentration	R_1 (Å)	x	R_3 (Å)	δ (Å)	V_m (Å^3)	SAA N_{agg}	Steroids N_{agg}	S_{core} (Å^2)	A_{core} (Å^2)	S_m (Å^2)	A_m (Å^2)
4-CHOL	2 wt%	16.7	1.33	22.2	19.4	227149	73	1	4297	59	18067	248
	3.5 wt%	16.7	1.33	22.2	19.4	227149	73	1	4297	59	18067	248
	5 wt%	16.7	1.30	21.7	19.3	222630	72	1	4224	59	17816	249
ADRENO	2 wt%	16.7	1.31	21.9	19.3	223536	72	1	4248	59	17868	248
	3.5 wt%	16.7	1.23	20.5	19.0	211092	68	1	4053	60	17176	253
	5 wt%	16.7	1.20	20.0	18.8	205033	66	1	3980	60	16839	255

Fitting parameters include the core equatorial radius (R_1), core axial radius (R_3), core axial ratio (x), shell thickness (δ), micelle volume (V_m), micelle and steroids aggregation number (SAA N_{agg} and steroids N_{agg}), surface area for hydrocarbon chain (S_{core}) and whole micelle (S_m) and the corresponding the area per molecule (A_{core} and A_m). Uncertainty for R_1, x, δ, N_{agg}, S and A = ± 0.3, ± 0.03, ± 0.3, ± 7, ± 250, and ± 1 respectively.

4.4.4 The structure of dodecyl sulfate surfactant micelles in the presence of steroids as a function of time

The neutron reflectivity studies of the surfactant monolayers showed that the time taken for the dodecyl sulfate surfactant monolayers to reach equilibrium when in the presence of 4-cholesten-3-one (4-CHOL) was very much longer than for the monolayers formed in the presence of saturation amounts of adrenosterone (ADRENO). It was hypothesised, therefore, that the time required for the dodecyl sulfate micelles to reach equilibrium in the presence of 4-CHOL would be longer than that required in the presence of ADRENO. In order to test this hypothesis, further SANS studies were performed to determine the effect of time on the dodecyl sulfate surfactant micelle dispersions in the presence and absence of the two steroids.

SANS data were obtained using LOQ and only the drop (h_{25}SAA in D_2O) contrast was measured for each sample. As expected, there were no differences apparent in the SANS profiles recorded for the fresh surfactant micelle solutions in the absence of steroids and those recorded for the samples stored for 14 days, and this was the case regardless of the surfactant concentration and counterion (Appendix C). It is thus concluded that the dodecyl sulfate micelles are stable in solution even over a period of two weeks.

The same observation was made for dodecyl sulfate micelles in the presence of ADRENO (Appendix C). There was no difference seen in any of the SANS profiles recorded beyond 6 hours and through to 14 days, suggesting that the amount of ADRENO solubilised within the micelles reaches a maximum at ≤ 6 hours.

In order to monitor the kinetics of formation of the 4-CHOL/SAA micelles, the SANS measurements for each system were recorded at 6 hours, 12 hours, 1 day, 2 days, 3 days, 5 days, 7 days, 9 days, 11 days, 14 days and 16 days. As shown in Figure 4.30, it can be confirmed that, unlike ADRENO, the time for the 4-CHOL/SAA systems to reach equilibrium is much longer than 6 hours. When comparing the SANS profiles of the micellar solutions in the presence of 4-CHOL collected after 6 hours, 1 day and 7 days, the interaction peak is seen to shift to the left and the scattering intensity is seen to increase, while the shape of profile shows no significant change. It can be deduced, therefore, that the SAA micelles become larger as the amount of 4-CHOL

solubilised within the micelles increases over time. The SANS data were fitted by using the same method for anionic surfactant micelles and the values of the model-fitted parameters are shown in Table 4.22.

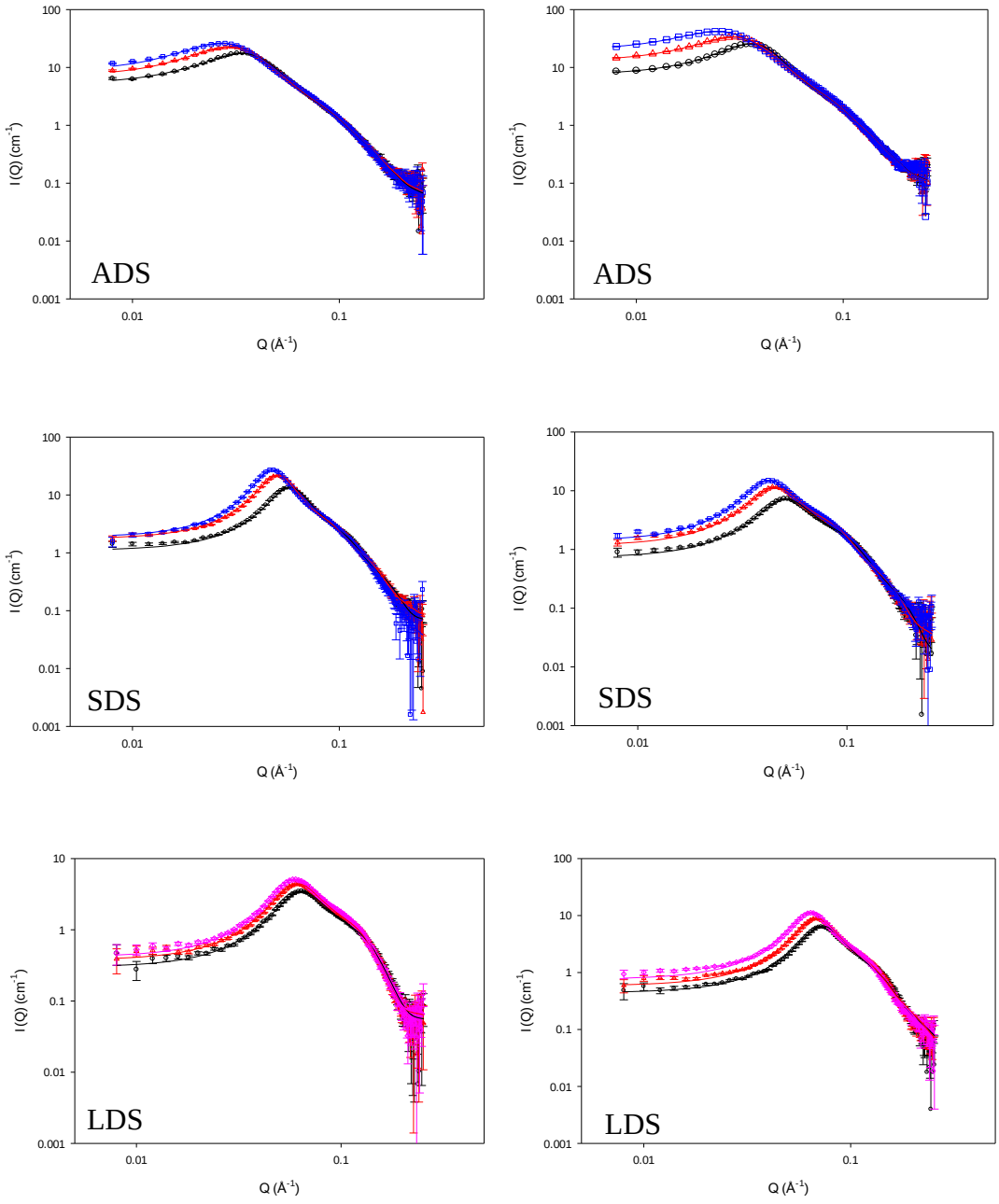

Figure 4. 30 SANS profiles and model fits (solid line) of dodecyl sulfate micelles in the presence of 4-CHOL at surfactant concentration 3 wt% (left column) and 5 wt%(right column) ○: 6 hours, Δ:1 day, ◊: 5 days, □: 7 days

For the ADS and SDS micelles in the presence of 4-CHOL, the fitted parameters show that equilibrium is achieved after 7 days, while for the 4-CHOL/LDS system the

equilibrium time is found to be ca. 5 days. There is no evidence to suggest a relation between the speed of equilibration and the surfactant concentration.

Table 4. 22 Values of model fitted parameters for dodecyl sulfate surfactant micelles in the presence of 4-cholesten-3-one.

Surfactant concentration	Time	R_1 (Å)	x	R_3 (Å)	δ (Å)	V_m ($Å^3$)	Z	SAA N_{agg}	Steroids N_{agg}	S_{core} ($Å^2$)	A_{core} ($Å^2$)	S_m ($Å^2$)	A_m ($Å^2$)
ADS 3 wt%	6 hours	61.1	0.25	15.3	4.2	347850	15	454	120	30244	67	37826	83
	1 day	61.9	0.25	15.5	4.2	361255	18	472	125	31062	66	38826	82
	7 days	62.0	0.25	15.5	4.2	362807	21	474	126	31165	66	38942	82
	16 days	62.0	0.25	15.5	4.2	362807	21	474	126	31165	66	38942	82
ADS 5 wt%	6 hours	68.6	0.21	14.2	4.3	410825	19	532	141	35587	67	43487	82
	1 day	68.8	0.21	14.2	4.3	414347	21	536	142	35759	67	43736	82
	7 days	69.0	0.21	14.3	4.3	418023	23	541	143	35971	66	44000	81
	16 days	69.0	0.21	14.3	4.3	418023	23	541	143	35971	66	44000	81

Surfactant concentration	Time	R_1 (Å)	x	R_3 (Å)	δ (Å)	V_m (Å^3)	Z	SAA N_{agg}	Steroids N_{agg}	S_{core} (Å^2)	A_{core} (Å^2)	S_m (Å^2)	A_m (Å^2)
SDS 3 wt%	6 hours	33.5	0.41	13.7	3.7	101064	25	114	37	11879	104	16474	144
	1 day	38.4	0.39	15.0	4.2	145336	32	164	53	15184	93	21061	129
	7 days	42.0	0.39	16.4	4.5	189114	35	214	69	18318	85	25341	118
	16 days	42.0	0.39	16.4	4.5	189114	35	214	69	18318	85	25341	118
SDS 5 wt%	6 hours	35.8	0.42	15.0	4.0	126308	24	143	46	13938	98	19386	136
	1 day	43.7	0.36	15.7	4.5	196889	30	223	72	18714	84	25704	115
	7 days	44.56	0.36	16.0	4.6	208956	35	236	77	19489	82	26796	113
	16 days	44.56	0.36	16.0	4.6	208956	35	236	77	19489	82	26796	113

Surfactant concentration	Time	R_1 (Å)	x	R_3 (Å)	δ (Å)	V_m (Å^3)	Z	SAA N_{agg}	Steroids N_{agg}	S_{core} (Å^2)	A_{core} (Å^2)	S_m (Å^2)	A_m (Å^2)
	6 hours	35.8	0.42	15.0	4.0	60746	22	67	16	13938	208	19386	289
LDS	1 day	43.7	0.36	15.7	4.5	72906	24	80	19	18714	233	25704	320
3 wt%	5 days	44.6	0.36	16.0	4.6	77421	26	85	20	19489	228	26796	314
	16 days	44.6	0.36	16.0	4.6	77421	26	85	20	19489	228	26796	314
	6 hours	27.0	0.49	13.1	4.4	71929	20	79	18	8751	110	13570	171
LDS	1 day	29.2	0.46	13.4	4.6	86171	22	95	22	9781	103	15176	160
5 wt%	5 days	31.6	0.46	14.5	5.0	109149	24	120	28	11577	96	17941	149
	16 days	31.8	0.46	14.6	5.0	111426	25	123	29	11748	96	18206	148

Fitting parameters include the core equatorial radius (R_1), core axial radius (R_3), core axial ratio (x), shell thickness (δ), micelle volume (V_m), micelle charge (Z), micelle and steroids aggregation number (SAA N_{agg} and steroids N_{agg}), surface area for hydrocarbon chain (S_{core}) and whole micelle (S_m) and the corresponding the area per molecule (A_{core} and A_m). Uncertainty for R_1, x, δ, N_{agg}, S and A = ± 0.3, ± 0.03, ± 0.3, ± 7, ± 250, and ± 1 respectively.

According to Table 4.22, the micelle core equatorial radius gets larger with time. The core axial radii in all cases are less than one, indicating that the micelles are oblate in shape and become flatter with time. The change in x with time is more pronounced for the 4-CHOL/SDS and 4-CHOL/LDS systems than for the 4-CHOL/ADS system. As expected, the size of the micelles in the presence of 4-CHOL also increases with time, as too do the aggregation numbers of the surfactant and steroids.

It is interesting to note too that when comparing the extent of the increased size of micelles among SDS, LDS and ADS systems, the size of the ADS micelles in the presence of 4-CHOL only increases by less than 5% between 6 hours after saturating and reaching the equilibrium, while the growth rate of 4-CHOL/SDS micelles is the highest.

To further study the properties of the dodecyl sulfate micelles in the presence of steroids at different times following their preparation, the concentrations of 4-CHOL and ADRENO in each micellar solution were determined using UV/VIS spectroscopy.

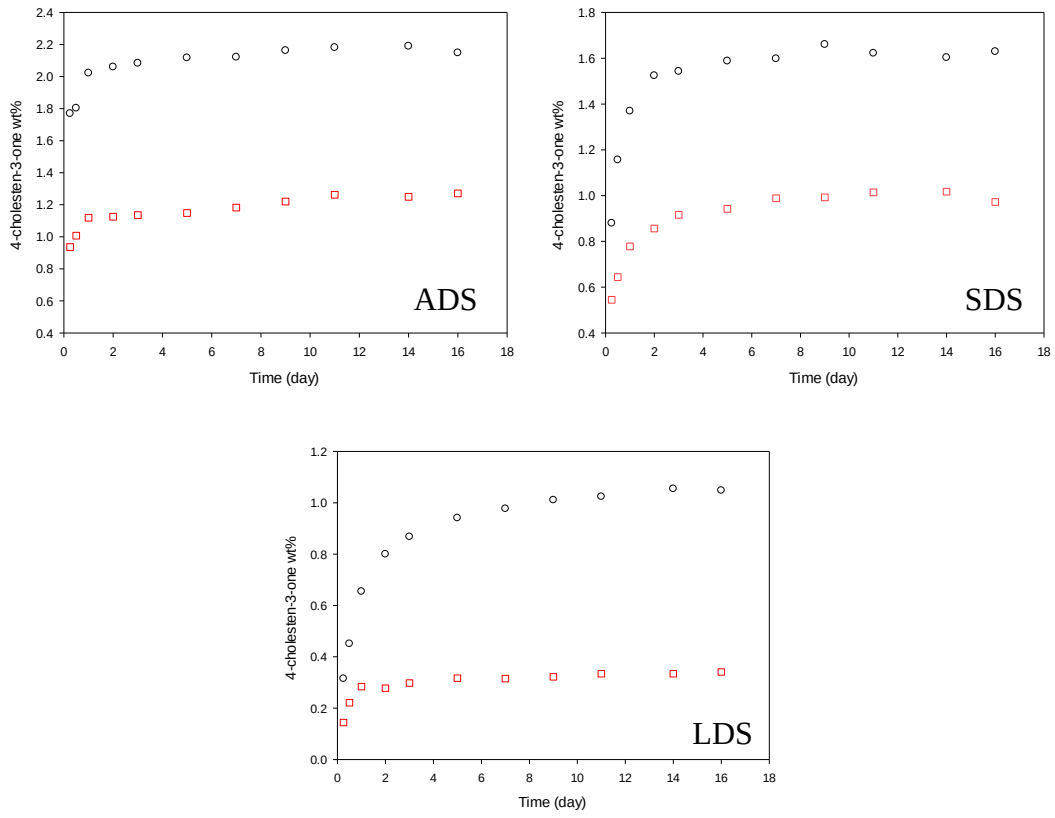

Figure 4. 31 Concentration of 4-cholesten-3-one in micellar solutions (at surfactant concentration □: 3 wt%, ○: 5 wt%)

***No error bar included due to the single sample measured each time in SANS**

From Figure 4.31, it is clear that the concentration of 4-CHOL in the micellar solutions increases until equilibrium is reached. The time taken to reach equilibrium follows the order: ADS < SDS ≈ LDS.

It should be noted that the solubilisation capacity of LDS for 4-CHOL is much lower than that of SDS and ADS, and so the increase in 4-CHOL in the LDS micelles may not be detected because of the limited sensitivity of the SANS measurements performed here.

4.5 Conclusions

The micelles formed by nine different C_{12} chain surfactants (SAA), each with a different type of polar head group, were investigated using small angle neutron scattering (SANS), to probe the composition of the micelles in the presence and absence of the steroids, 4-cholesten-3-one (4-CHOL) and adrenosterone (ADRENO). The SANS studies were performed using the three different isotopic contrasts of d_{25}SAA in H_2O (the core contrast), d_{25}SAA in D_2O (the shell contrast) and h_{25}SAA in H_2O (the drop contrast). The three SANS profiles measured for each system were modelled individually until a consistent set of parameters describing the detailed structure of the micelles was obtained. The micelles were modelled as core-shell ellipsoids for which the core equatorial radius (R_1), core axial ratio (x) and aggregation number (N_{agg}) were determined.

The structures of the micelles formed by the anionic surfactants SDS, ADS and LDS were different from one another, testifying to the influence of the counterions on the surfactant aggregation behaviour. In all cases, however, the micelles formed were prolate ellipsoidal and became more elongated with increased surfactant concentration. The ADS micelles were much larger micelles than those formed by SDS and LDS but they were found to have a much thinner shell. The charge on these anionic micelles (modelled with a Hayter-Penfold structure factor) followed the order ADS < SDS < LDS.

The addition of 4-CHOL caused a change in shape of the anionic surfactant micelles from prolate ellipsoidal to oblate and, as found for the steroid-free micelles, these tended to become flatter with increased surfactant concentration. In contrast, the addition of ADRENO caused no significant change in structure of the anionic surfactant micelles, and the ADRENO-saturated SDS micelles were found to be spherical rather than ellipsoidal. The locus of solubilisation of the steroids in the anionic surfactant micelles was confirmed as the micelle core region as evidenced by the fitted scattering length density for the micelle core obtained in model-fitting the SANS profiles for the core and shell contrasts.

By comparison with the ionic surfactant micelles, the changes in micelle structure caused by the additional steroids in the zwitterionic or non-ionic surfactant systems

were very much smaller. This can be explained by the much lower solubilisation capacities of these surfactants for the steroids (as determined through the solubilisation studies; section 2.1). It is interesting to note here though that in some of these systems, increasing surfactant concentration led to the micelles becoming more spherical while in other cases the micelles tended to be more elongated with increased surfactant concentration.

The SANS studies detailed here clearly show that the charge and hydration of a surfactant's polar head group can significantly affect the level of steroid solubilisation. Electrostatic interactions between charged head groups modulate the packing of surfactant molecules within a micelle and so change the volumes of the core and shell. Hydrogen bond interactions between the solubilised steroid and the surfactant head groups will influence the orientation of the steroid within the micelle and thereby affect how the steroid inserts into the aggregate.

SANS studies of the dodecyl sulfate/steroid micelles performed as a function of time showed that the ADRENO/SAA system reached equilibrium after 6 hours, while the 4-CHOL/dodecyl sulfate micellar systems required 5 – 7 days to reach equilibrium. It was also found that although the shape and size of the 4-CHOL/SAA micelles showed little change over time, the amount of 4-CHOL that was solubilised within the micelles nevertheless showed a small but progressive increase over time.

Chapter 5

Conclusions and future prospects

5.1 Conclusions

The solubilisation of drugs within surfactant micelles has long been considered as a means by which to facilitate the formulation and delivery of drugs that have poor aqueous solubility. Unfortunately, however, for any given drug and any given micellar surfactant, it is not yet possible to predict with any certainty either the amount of drug that can be solubilised inside the micelle or its locus of solubilisation.

In the work reported here the aim was to clarify the link between the structures of surfactant molecules and the micelles they form in aqueous solution, and then to determine how these influence the level and manner of solubilisation of two poorly water-soluble drug-like compounds, 4-cholesten-3-one (4-CHOL) and adrenosterone (ADRENO). A range of C_{12}-chain surfactants with varying head group were used to solubilise the two steroids, and the physical-chemical properties of the surfactant micelles were determined in their presence and absence.

On the basis of the collected findings from these various studies, the following general conclusions are drawn:

- *A priori, the solubilisation of solutes within surfactant micelles will be affected by the shape of the micelles, and this in turn will be influenced by the surfactant molecular interfacial surface area.*

From the SANS studies performed here, it is seen that the ionic surfactants occupy relatively lower interfacial molecular surface areas in their micelles compared with the zwitterionic and non-ionic surfactants (*viz.*, 60 – 80 $Å^2$ *vs.* ~90 $Å^2$ and 250 – 300 $Å^2$, respectively), and (from the solubilisation studies performed) it is found that the anionic surfactants, SDS and DTAB, accordingly solubilise the highest amounts of 4-

CHOL and ADRENO, and the non-ionic surfactants, Brij-35 and Tween 20, solubilise the least.

- *A priori, the solubilisation of solutes within a given type of surfactant micelles will be affected by the size of the micelles, with the expectation that larger volume micelles are likely to incorporate higher levels of solute*.

The SANS studies of the anionic surfactant micelles provide some support for this assertion, in that at low surfactant concentrations (3 wt% and 5 wt%) the SDS micelles solubilise less than the ADS micelles, the latter having a larger volume than the former. The opposite trend is seen, however, at the higher surfactant concentrations (> 10 wt%), and it is also noted from the SANS studies, that the solubilisation of 4-CHOL and ADRENO leads to changes in the sizes and shapes of the surfactant micelles.

- *Solutes that have extensive apolar molecular surface areas are most likely to insert into the hydrocarbon chains layer of a surfactant monolayer, and are most likely to be solubilised in the hydrophobic core of a surfactant micelle.*

The locus of solubilisation of 4-CHOL and ADRENO in the C_{12}-chain surfactants was made by determining the structures of the surfactant monolayers at the air-water interface using neutron reflectivity (NR), and in the surfactant micelles in bulk solution using small angle neutron scattering (SANS). It was shown that 4-CHOL and ADRENO inserted into the hydrocarbon layer of the C_{12}-chain surfactants monolayers and into the micelle cores – and this was regardless of the nature of the surfactant head group. Such findings accord with the generally non-polar nature of the two steroids (Figure 5.1) and given that these two molecules have quite different shapes, polar surface areas, and amphiphilicities (Figure 5.1), it is easy to see why 4-CHOL is solubilised within the surfactant C_{12}-chains to a greater extent than ADRENO.

- *The findings from neutron reflectivity studies of a solute's interactions with a surfactant monolayer formed at the air-water interface might reasonably be assumed to give clues as to the solubilisation of the solute within the surfactant micelles.*

For the ionic surfactants (SDS, ADS, LDS and DTAB), the level of 4-CHOL and ADRENO solubilised within the surfactant monolayers (determined through the monolayer neutron reflectivity studies) is found to correlate with the level of

solubilisation of the steroids seen in the corresponding micelles (determined through the SANS studies), but this appears not to be true for the zwitterionic surfactants (DPC and DDAO) (Figure 5.2). It would seem, therefore, that caution should be exercised when using the findings from studies of a drug's interactions with surfactant monolayers to extrapolate its interactions with aggregates in the bulk.

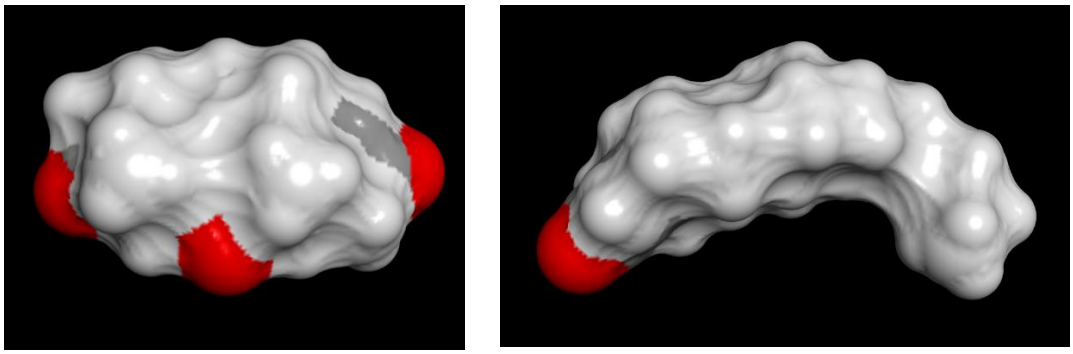

Figure 5. 1 Space-filling models of adrenosterone (left) and 4-cholesten-3-one (right), generated using Accelrys Discovery Studio 4.0. The molecular surface associated with oxygen atoms is coloured red; all other surface is shown in grey.

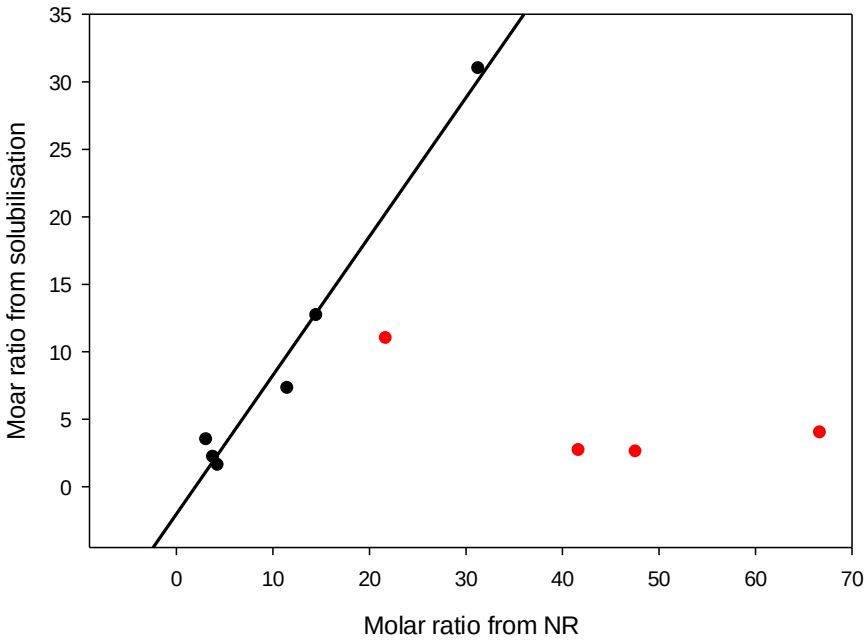

Figure 5. 2 The molar ratio obtained from solubilisation (y axis) and NR (x axis) respectively (black: ionic surfactants; red: zwitterionic surfactants)

- *Non-polar solutes that are solubilised in the core of a surfactant micelle are unlikely to be well-solubilised if the surfactant carries a polar head group that is heavily hydrated (since this will hinder its insertion into the micelle core).*

This assertion is supported by the findings from the SANS studies reported here, wherein it is seen that the heavily hydrated non-ionic surfactants, Brij 35 and Tween 20, have extremely low solubilisation capacities for the non-polar solutes, 4-CHOL and ADRENO, while the ionic and zwitterionic surfactants – that have head groups that are much less heavily hydrated – have higher solubilisation capacities for these steroids.

- *Electrostatic interactions between the head groups of surfactants will modulate the packing of the molecules within the micelle and as a consequence will change the volumes of the micelle core and shell, and these changes in turn will affect the level of solubilisation of solutes.*

The solubilisation measurements and SANS studies performed here show clearly that there are marked differences in the levels of steroid solubilisation between ionic, zwitterionic and non-ionic surfactants, and these differences can in part be attributed to ion-dipole interactions between the charged and zwitterionic surfactant headgroups and the surrounding water molecules.

- *Hydrogen bond interactions between a solute and the head group of the solubilising surfactant are likely to influence the orientation of the solute within the micelle and will thus affect how the solute inserts into the aggregate.*

None of the experiments performed and reported here provide information to allow this hypothesis to be tested because the analytical modelling of the reflectivity and SANS data cannot furnish details of the orientation of solutes within a surfactant monolayer or micelle.

- *The solubilisation capacity of non-ionic surfactant is much lower than that of ionic surfactants.*

Micelle-forming surfactants will generally disrupt the structure and integrity of biological membranes and because of this they can be irritant when applied to the skin and can be toxic when ingested. The usefulness of a surfactant as an aid to the formulation of a poorly water soluble drug will thus depend not only upon its

solubilisation capacity but also on its relative toxicity. While non-ionic surfactants are not electrically charged and show minimal toxicity, their solubilisation capacities – as shown here in the solubilisation and SANS studies – are much lower than found for ionic and zwitterionic surfactants. The solubilisation capacities of the ionic surfactants are shown to be significantly greater than the non-ionic surfactants, but their toxic effects make them less ideal in drug solubilisation.

- *The time needed for solutes to reach equilibrium when inserting into surfactant monolayers or when solubilised in micellar solutions will depend on the nature/structure of the solute.*

For the solubilisation of ADRENO, the NR studies performed here show that the time needed to reach equilibrium is of the order of minutes when the surfactant is organised as a monolayer at the air-water interface, and from the SANS studies performed here the equilibration time is shown to be of the order of 6 hours when the steroid inserts into the surfactant micelles. The solubilisation of 4-CHOL in the dodecyl sulfate surfactant monolayers and micelles takes much longer to reach equilibrium than does ADRENO – the equilibration time for the monolayers being around 12 hours and for the micelles, 5 – 7 days. For the various other surfactants studied here, the equilibration times for solubilisation of the 4-CHOL and ADRENO are much shorter and more similar.

The studies here thus show that the equilibration times not vary according to the nature of the solute but also according to the nature of the surfactant. Moreover, while there have been some studies reported previously in which it has been noted that the transfer rate of drugs into surfactant micelles depends on the nature of the micelle [203-205], there are *no* reports of systems that exhibit equilibrium times as long as those observed here.

5.2 Future prospects

- In all of the different C_{12}-chain surfactant micelles studied here, 4-cholesten-3-one was solubilised to a far greater extent than adrenosterone. These two steroids have a similar molecular weight but different topography and amphiphilicity (Figure 5.1). It would be interesting to carry out solubilisation

studies for other poorly water-soluble steroids which show other, perhaps more significant, variations in structure. Such studies might include, for example, cholesterol – which has a hydroxyl at C3, or campesterol which has a hydroxyl at C3 and a dimethylheptyl chain at C17.

It should also be noted here, however, that the modelling of both the neutron reflectivity data obtained for surfactant monolayers and the SANS data obtained for surfactant micelles would benefit greatly from having an additional isotopic contrast provided through the use of a *perdeuterated or selectively deuterated steroid*. With the additional isotopic contrasts so provided, it would then be possible more clearly to define the locus of steroid solubilisation.

- The locus of surfactant solubilisation of 4-CHOL and ADRENO were made here using the neutron contrast variation afforded through the use of D_2O/H_2O mixtures and protiated and chain deuterated surfactants. The contrasts used, however, did not allow the interaction of the two steroids with the hydrophilic head groups of the surfactant micelles to be explored. With the additional isotopic contrast(s) which would be afforded with the availability and use of *head group deuterated* surfactants, it would be much easier to determine the extent to which the steroid molecules inserted into the surfactant monolayers and micelles.
- The details of solute orientation and solute-surfactant interatomic interactions in surfactant micelles – which are difficult to determine unambiguously simply by analytic modelling of SANS data – could be explored using full atom molecular dynamics simulations.
- The long equilibration times seen for the insertion of 4-CHOL into SDS, LDS and ADS monolayers and for the solubilisation of this steroid in the micelles formed by these surfactants is speculated to be due to the water inserted between the surfactant head groups hindering the entry of the 4-CHOL molecules. In truth, however, none of the various experiments performed here allow the structural basis of these long equilibration times to be determined, and there are no other studies reported where similarly long equilibrium times have been seen. Further studies are thus needed to explain this phenomenon and these studies would ideally explore the behaviour of other types of anionic

surfactant (such as sulfonates and gluconates), and make use of head group deuterated surfactants and/or deuterated steroids to probe the mechanism of the solubilisation process in detail.

A systematic and comprehensive study of a wide range of surfactants with two different solutes was performed here. With an improved understanding of the relationship between surfactant and solute molecular structure and its influence on the locus of a drug's solubilisation within a surfactant micelle, it might be hoped that we would then be better able to make a quantitative prediction of the level of drug solubilised in a specific micelle system and so be better able to select/design surfactants to speed up the drug formulation process. The studies performed here go only part of the way towards achieving these ends and much more work is needed before the process of formulating poorly water soluble drugs using surfactant micelles can be made truly rational.

Appendices

Appendix A Supplementary solubilisation, viscometry and densitometry results

Table A. 1 Amount of 4-cholesten-3-one (wt%) solubilised in aqueous solutions of surfactant micelles at ambient temperature

Surfactant. concentration wt%	SDS	ADS	LDS	DTAB	DPC	DDAPS	DDAO	Tween 20	Brij 35
2.5	0.52 ± 0.04	1.02 ± 0.01	0.27 ± 0.06	0.11 ± 0.01	0.09 ± 0.00	0.10 ± 0.00	0.19 ± 0.01	0.16 ± 0.00	0.01 ± 0.00
5	1.62 ± 0.25	2.36 ± 0.07	1.23 ± 0.03	0.19 ± 0.00	0.11 ± 0.01	0.22 ± 0.00	0.37 ± 0.01	0.30 ± 0.00	0.03 ± 0.00
7.5	2.76 ± 0.15	3.10 ± 0.13	1.72 ± 0.21	0.33 ± 0.03	0.17 ± 0.02	0.35 ± 0.01	0.61 ± 0.02	0.45 ± 0.02	0.05 ± 0.00
10	3.94 ± 0.10	4.03 ± 0.22	2.87 ± 0.20	0.51 ± 0.06	0.19 ± 0.01	0.48 ± 0.03	0.78 ± 0.02	0.60 ± 0.01	0.07 ± 0.00
12.5	4.85 ± 0.25	4.89 ± 0.33	3.88 ± 0.87	0.74 ± 0.03	0.27 ± 0.01	0.63 ± 0.04	0.94 ± 0.01	0.74 ± 0.02	0.08 ± 0.00
15	5.97 ± 0.37	5.97 ± 0.41	4.50 ± 0.55	1.04 ± 0.08	0.35 ± 0.02	0.73 ± 0.03	1.13 ± 0.02	0.85 ± 0.02	0.10 ± 0.00

Table A. 2 Amount of adrenosterone (wt%) solubilised in aqueous solutions of surfactant micelles at ambient temperature

Surfactant concentration wt%	SDS	ADS	LDS	DTAB	DPC	DDAPS	DDAO	TWEEN	BRIJ	SACR
2.5	0.43 ± 0.01	0.28 ± 0.01	0.33 ± 0.01	0.16 ± 0.00	0.07 ± 0.00	0.12 ± 0.00	0.13 ± 0.00	0.02 ± 0.00	0.02 ± 0.00	0.10 ± 0.00
5	0.73 ± 0.07	0.47 ± 0.03	0.62 ± 0.01	0.29 ± 0.01	0.13 ± 0.00	0.22 ± 0.00	0.19 ± 0.02	0.04 ± 0.00	0.03 ± 0.00	0.15 ± 0.00
7.5	0.99 ± 0.02	0.61 ± 0.04	0.86 ± 0.02	0.36 ± 0.03	0.18 ± 0.01	0.31 ± 0.01	0.25 ± 0.02	0.05 ± 0.00	0.04 ± 0.00	0.20 ± 0.00
10	1.18 ± 0.05	0.72 ± 0.04	1.04 ± 0.01	0.47 ± 0.02	0.23 ± 0.00	0.41 ± 0.02	0.30 ± 0.02	0.06 ± 0.00	0.05 ± 0.00	0.23 ± 0.01
12.5	1.40 ± 0.11	0.80 ± 0.01	1.25 ± 0.04	0.55 ± 0.03	0.28 ± 0.00	0.50 ± 0.02	0.36 ± 0.02	0.07 ± 0.00	0.06 ± 0.00	0.25 ± 0.01
15	1.67 ± 0.14	0.99 ± 0.06	1.39 ± 0.01	0.60 ± 0.02	0.34 ± 0.01	0.59 ± 0.01	0.39 ± 0.04	0.08 ± 0.00	0.06 ± 0.00	0.28 ± 0.00

Table A. 3 The reduced and inherent viscosity of SDS micellar solution at 25 ± 0.1 ºC

SDS Concentration wt%	Reduced viscosity	Inherent viscosity
5.0	4.44 ± 0.02	4.02 ± 0.01
4.5	4.34 ± 0.00	3.97 ± 0.00
4.0	4.26 ± 0.04	3.95 ± 0.03
3.5	4.17 ± 0.05	3.92 ± 0.05
3.0	4.09 ± 0.02	3.87 ± 0.02

Table A. 4 The reduced and inherent viscosity of DTAB micellar solution at 25 ± 0.1 ºC

DTAB Concentration wt%	Reduced viscosity	Inherent viscosity
5.0	3.64 ± 0.00	3.35 ± 0.00
4.5	3.58 ± 0.00	3.32 ± 0.00
4.0	3.52 ± 0.00	3.29 ± 0.00
3.5	3.47 ± 0.00	3.28 ± 0.00
3.0	3.42 ± 0.00	3.25 ± 0.00

Table A. 5 The reduced and inherent viscosity of DDAO micellar solution at 25 ± 0.1 ºC

DDAO Concentration wt%	Reduced viscosity	Inherent viscosity
5.0	5.31 ± 0.00	4.71 ± 0.00
4.5	5.18 ± 0.00	4.66 ± 0.00
4.0	5.06 ± 0.00	4.60 ± 0.00
3.5	4.92 ± 0.00	4.54 ± 0.00
3.0	4.78 ± 0.00	4.47 ± 0.00

Table A. 6 The reduced and inherent viscosity of DDAPS micellar solution at 25 ± 0.1 ºC

DDAPS Concentration wt%	Reduced viscosity	Inherent viscosity
5.0	4.24 ± 0.00	3.85 ± 0.00
3.8	3.96 ± 0.00	3.70 ± 0.00
3.0	3.79 ± 0.00	3.59 ± 0.00
2.5	3.66 ± 0.00	3.50 ± 0.00
2.2	3.58 ± 0.01	3.45 ± 0.00

Table A. 7 The reduced and inherent viscosity of Brij 35 micellar solution at 25 ± 0.1 ºC

Brij 35 Concentration wt%	Reduced viscosity	Inherent viscosity
10.0	22.30 ± 0.00	11.72 ± 0.00
6.7	14.27 ± 0.22	10.03 ± 0.11
5.0	12.74 ± 0.05	9.85 ± 0.03
4.0	11.58 ± 0.20	9.52 ± 0.13
3.3	10.98 ± 0.02	9.36 ± 0.01

Table A. 8 The reduced and inherent viscosity of SDS micellar solution in the presence of 4-cholesten-4-one at 25 ± 0.1 ºC

SDS Concentration wt%	Reduced viscosity	Inherent viscosity
5.0	7.26 ± 0.02	6.20 ± 0.02
4.5	6.97 ± 0.00	6.06 ± 0.00
4.0	6.70 ± 0.00	5.93 ± 0.00
3.5	6.45 ± 0.00	5.81 ± 0.00
3.0	6.20 ± 0.00	5.68 ± 0.00

Table A. 9 The reduced and inherent viscosity of SDS micellar solution in the presence of adrenosterone at 25 ± 0.1 ºC

SDS concentration wt%	Reduced viscosity	Inherent viscosity
5.0	4.93 ± 0.01	4.41 ± 0.01
4.5	4.79 ± 0.02	4.34 ± 0.01
4.0	4.68 ± 0.02	4.29 ± 0.02
3.5	4.58 ± 0.00	4.24 ± 0.00
3.0	4.47 ± 0.00	4.19 ± 0.00

Table A. 10 The reduced and inherent viscosity of DTAB micellar solution in the presence of 4-cholesten-4-one at 25 ± 0.1 ºC

DTAB concentration wt%	Reduced viscosity	Inherent viscosity
5.0	3.75 ± 0.02	3.44 ± 0.01
4.5	3.69 ± 0.00	3.42 ± 0.00
4.0	3.66 ± 0.05	3.42 ± 0.04
3.5	3.60 ± 0.01	3.39 ± 0.01
3.0	3.57 ± 0.02	3.39 ± 0.01

Table A. 11 The reduced and inherent viscosity of DTAB micellar solution in the presence of adrenosterone at 25 ± 0.1 ºC

DTAB concentration wt%	Reduced viscosity	Inherent viscosity
5.0	3.92 ± 0.04	3.58 ± 0.03
4.5	3.87 ± 0.00	3.57 ± 0.00
4.0	3.81 ± 0.01	3.55 ± 0.00
3.5	3.80 ± 0.04	3.57 ± 0.04
3.0	3.71 ± 0.01	3.51 ± 0.01

Table A. 12 The reduced and inherent viscosity of DDAPS micellar solution in the presence of 4-cholesten-4-one at 25 ± 0.1 ºC

DDAPS concentration wt%	Reduced viscosity	Inherent viscosity
5.0	4.47 ± 0.01	4.04 ± 0.01
3.8	4.29 ± 0.06	3.98 ± 0.06
3.0	4.10 ± 0.06	3.87 ± 0.06
2.5	4.00 ± 0.07	3.81 ± 0.07
2.2	3.96 ± 0.09	3.79 ± 0.08

Table A. 13 The reduced and inherent viscosity of DDAPS micellar solution in the presence of adrenosterone at 25 ± 0.1 ºC

DDAPS concentration wt%	Reduced viscosity	Inherent viscosity
5.0	4.41 ± 0.01	4.00 ± 0.00
3.8	4.21 ± 0.04	3.91 ± 0.03
3.0	4.07 ± 0.00	3.84 ± 0.00
2.5	3.95 ± 0.10	3.77 ± 0.09
2.2	3.97 ± 0.00	3.81 ± 0.00

Table A. 14 The intrinsic viscosity [η], density of solvent ρ_0, partial specific volume $\bar{\nu}_1$ and density of solute ρ_1

Surfactant	[η] (mL/g)	ρ_0 (g/mL)	$\bar{\nu}_1$ (cm^3/g)	ρ_1 (g/mL)
SDS	3.64	0.9999	0.867	1.1533
SDS + 4-cholesten-3-one	4.76	0.9999	0.863	1.1589
DTAB	3.10	0.9979	0.927	1.0790
DTAB + 4-cholesten-3-one	3.30	0.9986	0.922	1.0847

Appendix B Supplementary NR results

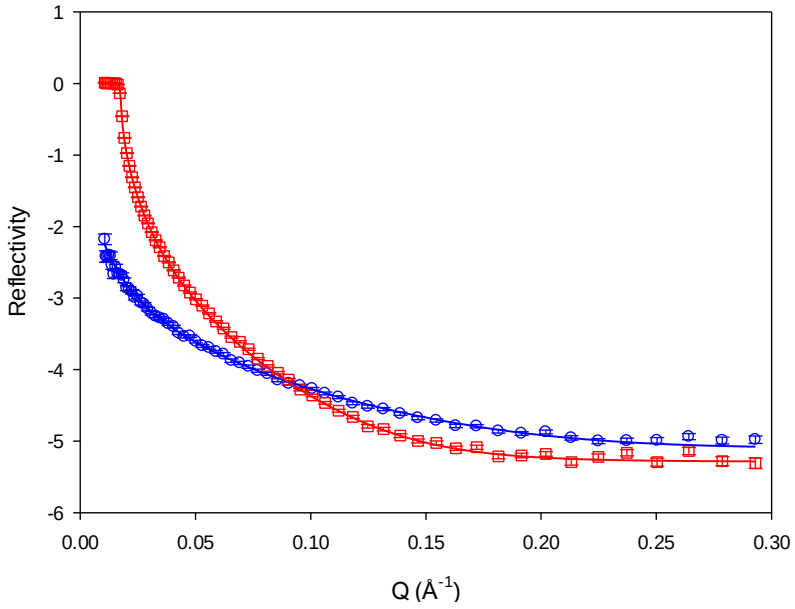

Figure B. 1 NR profile for monolayer of d_{25}-SDS in ACMW (blue) and D_2O (red) in the presence of 4-CHOL at 2 x CMC using Model 1.

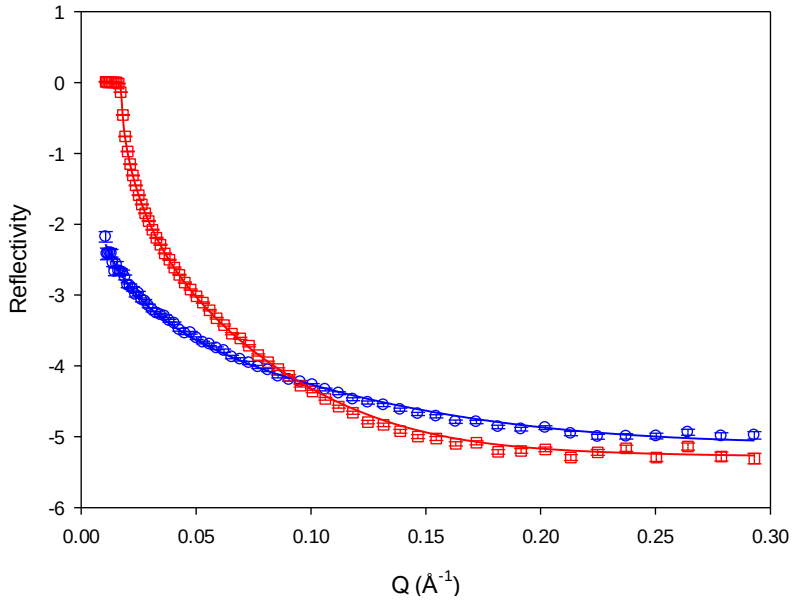

Figure B. 2 NR profile for monolayer of d_{25}-SDS in ACMW (blue) and D_2O (red) in the presence of 4-CHOL at 2 x CMC using Model 2.

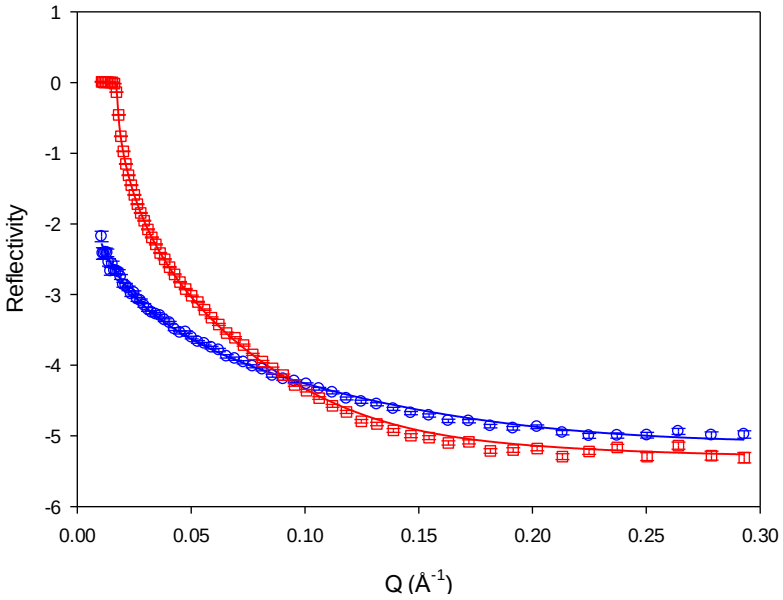

Figure B. 3 NR profile for monolayer of d_{25}-SDS in ACMW (blue) and D_2O (red) in the presence of 4-CHOL at 2 x CMC using Model 3.

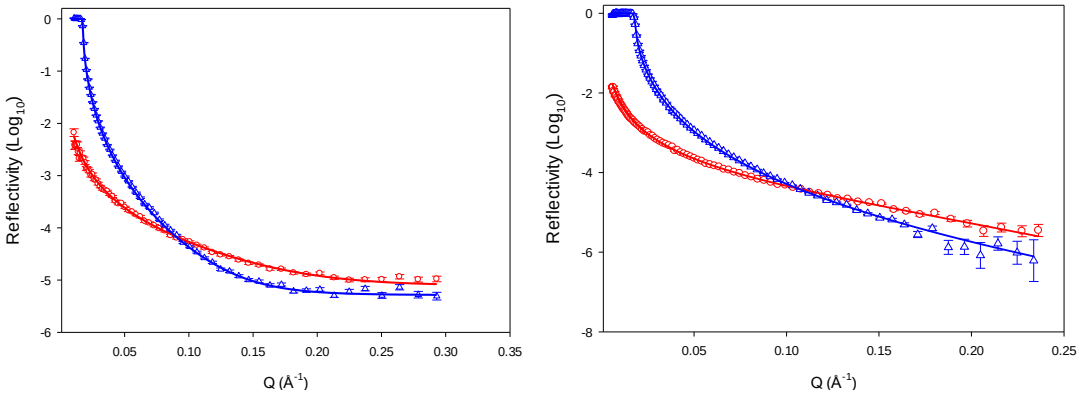

Figure B. 4 NR profile for monolayer of d_{25}-SDS in ACMW (red) and D_2O (blue) in the presence of 4-CHOL (left) and ADRENO (right).

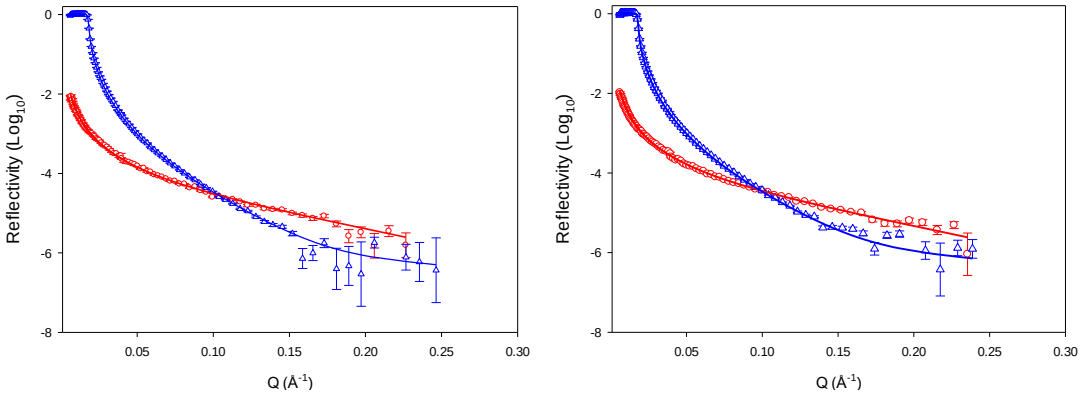

Figure B. 5 NR profile for monolayer of d_{25}-DTAB in ACMW (red) and D_2O (blue) in the presence of 4-CHOL (left) and ADRENO (right).

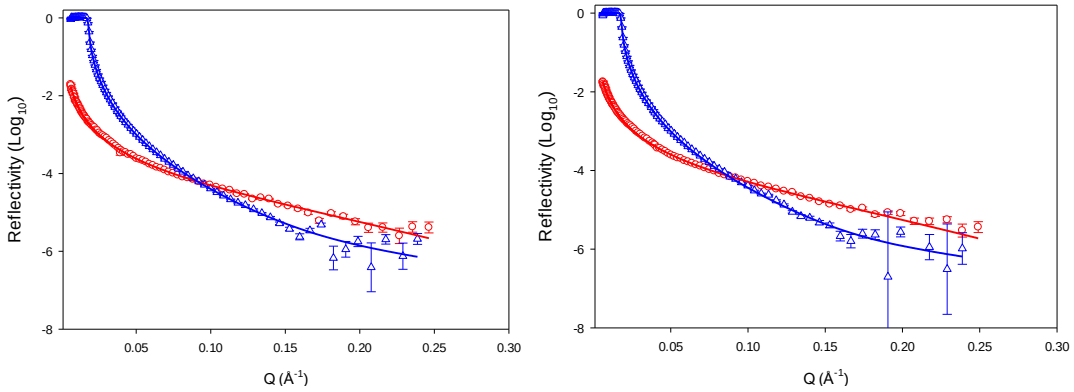

Figure B. 6 NR profile for monolayer of d_{25}-DDAO in ACMW (red) and D_2O (blue) in the presence of 4-CHOL (left) and ADRENO (right).

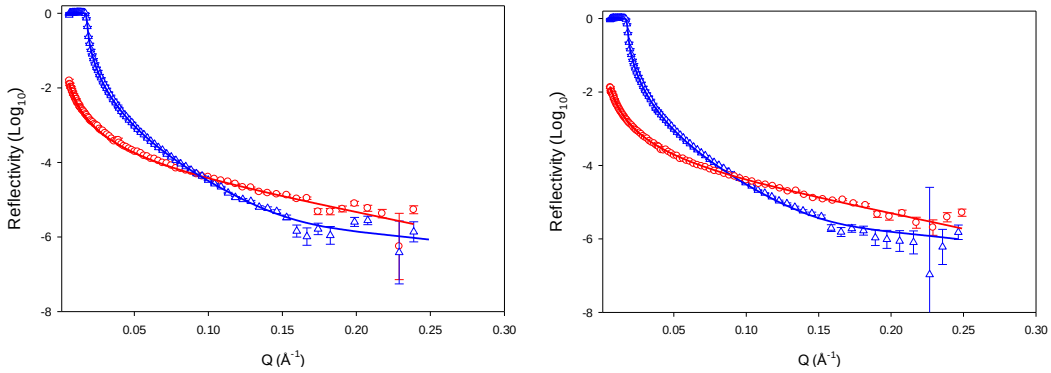

Figure B. 7 NR profile for monolayer of d_{25}-DDAPS in ACMW (red) and D_2O (blue) in the presence of 4-CHOL (left) and ADRENO (right).

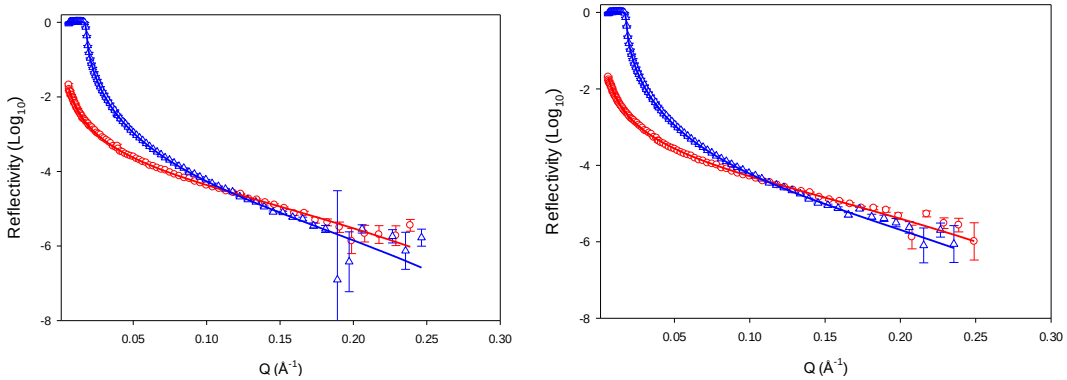

Figure B. 8 NR profile for monolayer of d_{25}-DPC in ACMW (red) and D_2O (blue) in the presence of 4-CHOL (left) and ADRENO (right).

Table B. 1 χ^2 values obtained for modelling of the NR profile of surfactant at the air-water interface in the presence of 4-CHOL at 2 x CMC using model 1, 2 and 3.

Fitting model	SDS	DTAB	DDAO	DDAPS	DPC
1	91.2	10.7	15.7	14.5	12.4
2	40.6	12.5	16.8	8.7	19.6
3	10.4	12.6	24.4	14.0	31

Table B. 2 χ^2 values obtained for modelling of the NR profile of surfactant at the air-water interface in the presence of ADRENO at 2 x CMC using model 1, 2 and 3.

Fitting model	SDS	DTAB	DDAO	DDAPS	DPC
1	6.5	12.7	18.2	14.4	9.5
2	7.1	11.7	22.5	14.4	17.5
3	8.8	6.6	33.3	14.2	21.5

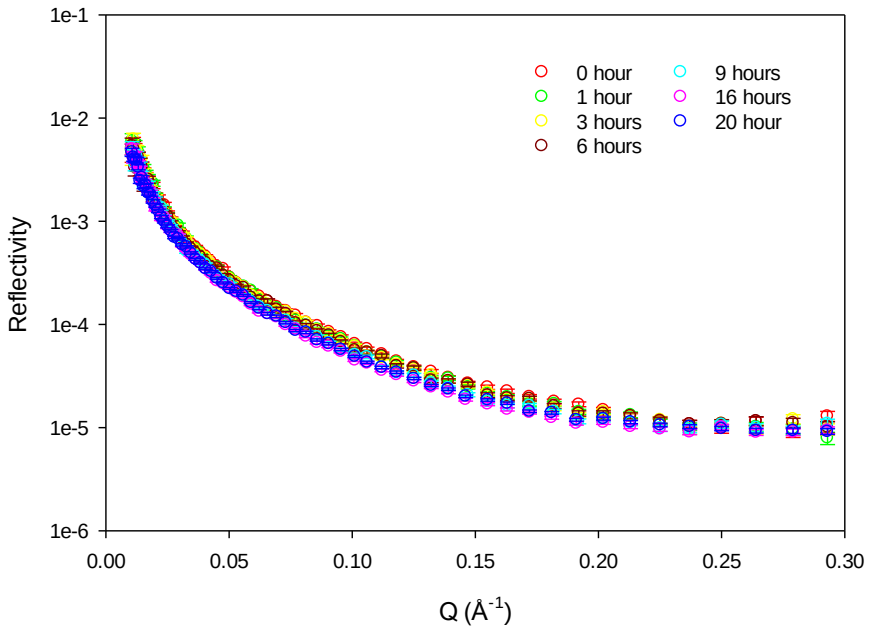

Figure B. 9 NR profile for d_{25}-SDS in ACMW in the presence of 4-CHOL at 1.5 x CMC.

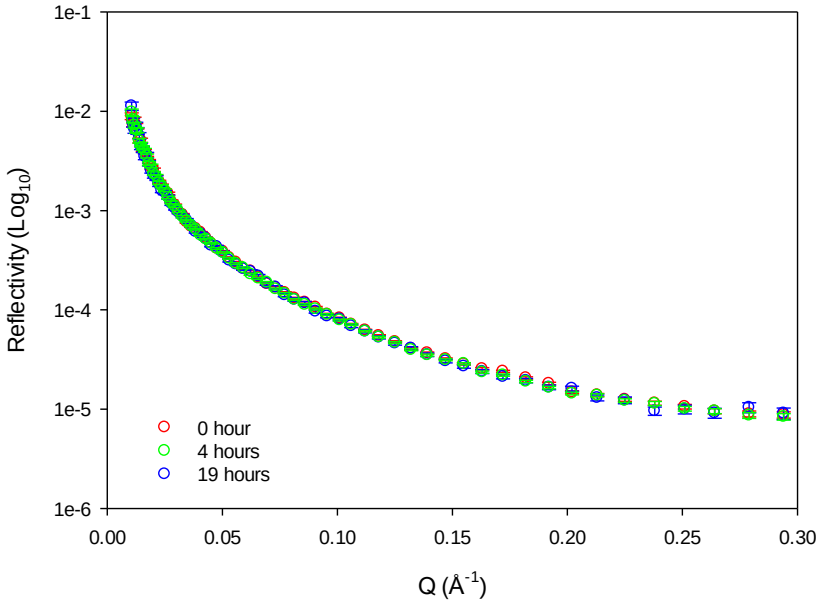

Figure B. 10 NR profile for d_{25}-DDAO in ACMW in the presence of 4-CHOL.

Appendix C Supplementary SANS results

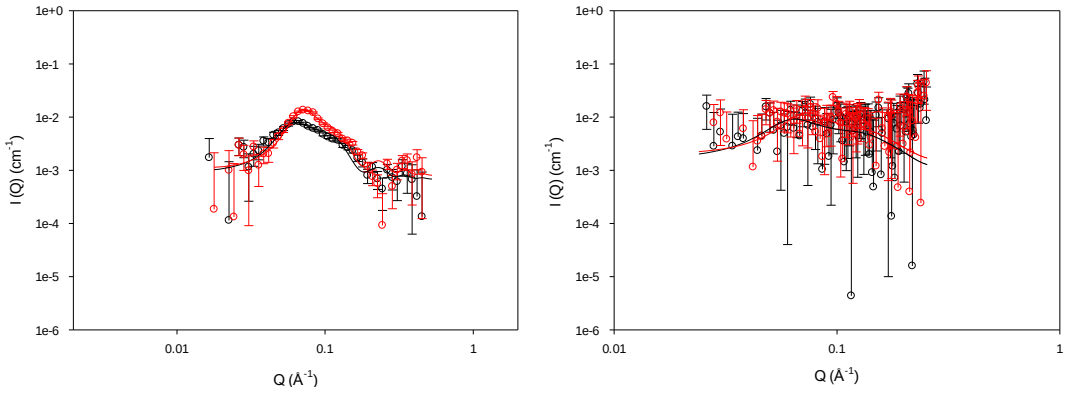

Figure C. 1 SANS profiles of 3 wt% (black) and 5 wt% (red) for d_{25} SDS in D_2O obtained from SANS 2D (left) and LOQ (right).

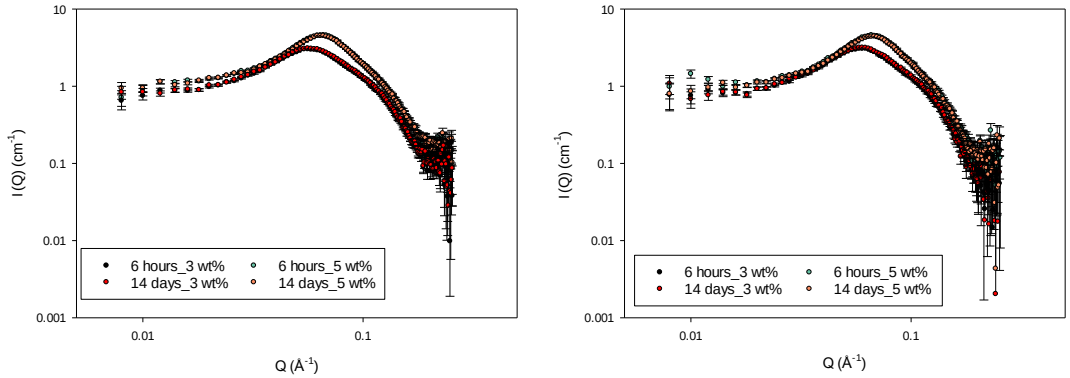

Figure C. 2 SANS profiles for h_{25}-ADS in D_2O in the absence (left) and presence (right) of ADRENO.

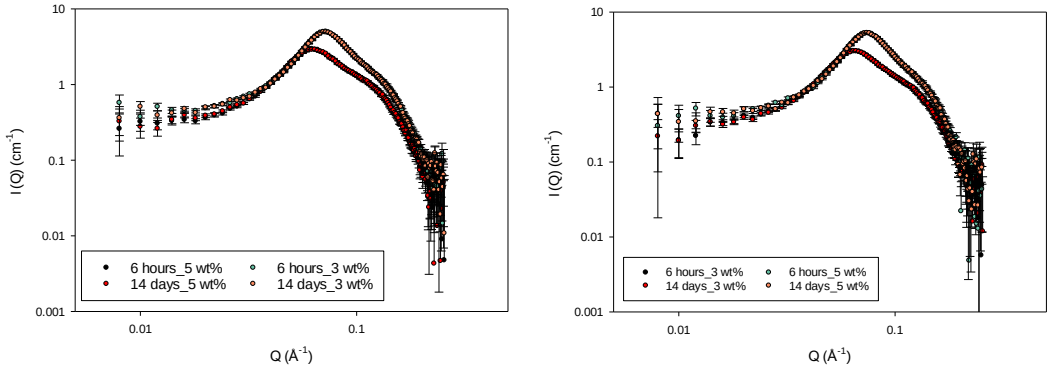

Figure C. 3 SANS profiles for h_{25}-SDS in D_2O in the absence (left) and presence (right) of ADRENO

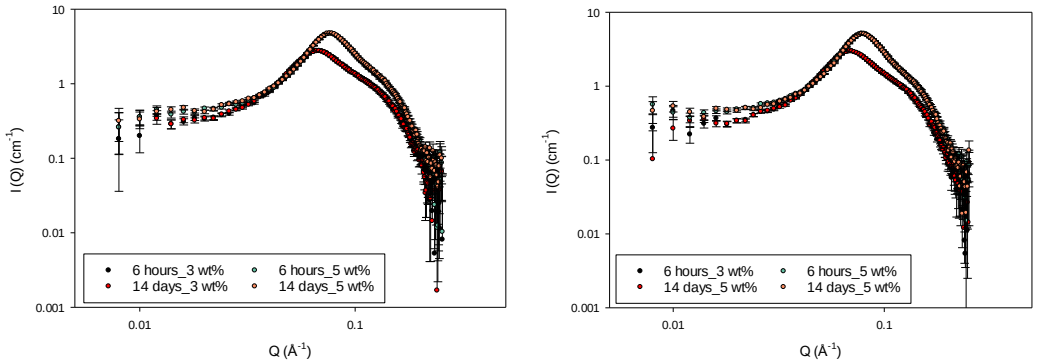

Figure C. 4 SANS profiles for h_{25}-LDS in D_2O in the absence (left) and presence (right) of ADRENO

References

1. Liu, G., et al., *Patient preferences for oral versus intravenous palliative chemotherapy.* Journal of Clinical Oncology, 1997. **15**(1): p. 110-115.
2. Borner, M., et al., *Patient preference and pharmacokinetics of oral modulated UFT versus intravenous fluorouracil and leucovorin: a randomised crossover trial in advanced colorectal cancer.* European Journal of Cancer, 2002. **38**(3): p. 349-358.
3. Loos, U., et al., *Pharmacokinetics of oral and intravenous rifampicin during chronic administration.* Klinische Wochenschrift, 1985. **63**(23): p. 1205-1211.
4. Homeida, M., L. Jackson, and C. Roberts, *Decreased first-pass metabolism of labetalol in chronic liver disease.* Br Med J, 1978. **2**(6144): p. 1048-1050.
5. Shoskes, J.J., M.K. Wilson, and M.L. Spinner, *Pharmacology of testosterone replacement therapy preparations.* Translational Andrology and Urology, 2016. **5**(6): p. 834.
6. Martinez, M.N. and G.L. Amidon, *A mechanistic approach to understanding the factors affecting drug absorption: a review of fundamentals.* The Journal of Clinical Pharmacology, 2002. **42**(6): p. 620-643.
7. Pouton, C.W., *Formulation of poorly water-soluble drugs for oral administration: physicochemical and physiological issues and the lipid formulation classification system.* European Journal of Pharmaceutical Sciences, 2006. **29**(3-4): p. 278-287.
8. Hörter, D. and J.B. Dressman, *Influence of physicochemical properties on dissolution of drugs in the gastrointestinal tract.* Advanced Drug Delivery Reviews, 2001. **46**(1-3): p. 75-87.
9. Ku, M.S. and W. Dulin, *A biopharmaceutical classification-based Right-First-Time formulation approach to reduce human pharmacokinetic variability and project cycle time from First-In-Human to clinical Proof-Of-Concept.* Pharmaceutical Development and Technology, 2012. **17**(3): p. 285-302.
10. Takagi, T., et al., *A provisional biopharmaceutical classification of the top 200 oral drug products in the United States, Great Britain, Spain, and Japan.* Molecular Pharmaceutics, 2006. **3**(6): p. 631-643.
11. Göke, K., et al., *Novel strategies for the formulation and processing of poorly water-soluble drugs.* European Journal of Pharmaceutics and Biopharmaceutics, 2018. **126**: p. 40-56.
12. Hetal, T., P. Bindesh, and T. Sneha, *A review on techniques for oral bioavailability enhancement of drugs.* Health, 2010. **4**(3): p. 203-223.
13. Allam, A.N., S. El Gamal, and V. Naggar, *Bioavailability: A pharmaceutical review.* Int J Novel Drug Deliv Tech, 2011. **1**(1): p. 77-93.
14. Gomez-Orellana, I., *Strategies to improve oral drug bioavailability.* Expert opinion on drug delivery, 2005. **2**(3): p. 419-433.
15. Organization, W.H., *The international pharmacopoeia*. 2006: World Health Organization.
16. Williams, H.D., et al., *Strategies to Address Low Drug Solubility in Discovery and Development.* Pharmacological Reviews, 2013. **65**(1): p. 315-499.

17. Van Eerdenbrugh, B., G. Van den Mooter, and P. Augustijns, *Top-down production of drug nanocrystals: nanosuspension stabilization, miniaturization and transformation into solid products.* International Journal of Pharmaceutics, 2008. **364**(1): p. 64-75.

18. Wiedmann, T.S. and A. Naqwi, *Pharmaceutical salts: Theory, use in solid dosage forms and in situ preparation in an aerosol.* Asian Journal of Pharmaceutical Sciences, 2016. **11**(6): p. 722-734.

19. Hanafy, N., M. El-Kemary, and S. Leporatti, *Micelles structure development as a strategy to improve smart cancer therapy.* Cancers, 2018. **10**(7): p. 238.

20. Verma, G. and P. Hassan, *Self assembled materials: design strategies and drug delivery perspectives.* Physical Chemistry Chemical Physics, 2013. **15**(40): p. 17016-17028.

21. Lombardo, D., et al., *Amphiphiles self-assembly: basic concepts and future perspectives of supramolecular approaches.* Advances in Condensed Matter Physics, 2015. **2015**.

22. Attwood, D. and A.T. Florence, *Surfactant systems: their chemistry, pharmacy and biology*. 1983: Chapman and Hall.

23. Mukerjee, P. and K.J. Mysels, *Critical micelle concentrations of aqueous surfactant systems*. 1971, National Standard Reference Data System.

24. Presto, W.C. and W. Preston, *Some correlating principles of detergent action.* The Journal of Physical Chemistry, 1948. **52**(1): p. 84-97.

25. Lomax, E.G., *Amphoteric surfactants*. Vol. 59. 1996: CRC Press.

26. Chevalier, Y., F. Melis, and J.P. Dalbiez, *Structure of zwitterionic surfactant micelles: micellar size and intermicellar interactions.* The Journal of Physical Chemistry, 1992. **96**(21): p. 8614-8619.

27. Chevalier, Y., L. Germanaud, and P. Le Perchec, *Micellar properties of zwitterionic phosphobetaine amphiphiles in aqueous solution: Influence of the intercharge distance.* Colloid and Polymer Science, 1988. **266**(5): p. 441-448.

28. Herrmann, K.W., *Micellar properties of some zwitterionic surfactants.* Journal of Colloid and Interface Science, 1966. **22**(4): p. 352-359.

29. Fendler, J.H. and E.J. Fendler, *Catalysis in Micellar and Macromolecular Systems*. 1975, New York: Academic Press.

30. Yokoyama, M., *Block copolymers as drug carriers.* Critical Reviews in Therapeutic Drug Carrier Systems, 1992. **9**(3-4): p. 213-248.

31. Sharma, N.K., M. Singh, and A. Bhattarai, *Hydrophobic study of increasing alkyl chain length of platinum surfactant complexes: synthesis, characterization, micellization, thermodynamics, thermogravimetrics and surface morphology.* RSC Advances, 2016. **6**(93): p. 90607-90623.

32. Shinoda, K., T. Yamaguchi, and R. Hori, *The surface tension and the critical micelle concentration in aqueous solution of β-D-alkyl glucosides and their mixtures.* Bulletin of the Chemical Society of Japan, 1961. **34**(2): p. 237-241.

33. Barry, B. and G. Russell, *Prediction of micellar molecular weights and thermodynamics of micellization of mixtures of alkyltrimethylammonium salts.* Journal of Colloid and Interface Science, 1972. **40**(2): p. 174-194.

34. Arnason, T. and P. Elworthy, *Effects of structural variations of non‐ionic surfactants on micellar properties and solubilization: surfactants containing very long*

hydrocarbon chains. Journal of Pharmacy and Pharmacology, 1981. **33**(1): p. 141-144.

35. Oliver, R.C., et al., *Dependence of micelle size and shape on detergent alkyl chain length and head group.* PloS one, 2013. **8**(5): p. e62488.
36. Tanford, C., *Micelle shape and size.* The Journal of Physical Chemistry, 1972. **76**(21): p. 3020-3024.
37. Mukerjee, P., *The nature of the association equilibria and hydrophobic bonding in aqueous solutions of association colloids.* Advances in Colloid and Interface Science, 1967. **1**(3): p. 242-275.
38. Eastoe, J. and T. Cosgrove, *Colloid science: principles, methods and applications*. 2005, Blackwell publishing: Cambridge, MA.
39. Winterborn, I.K., *The modifying effects of cetyltrimethylam-monium bromide on the rates of base catalysed hydrolysis of simple carboxylic acid esters*. 1972, University of Bath: U.K.
40. Florence, A.T. and D. Attwood, *Physicochemical principles of pharmacy: In manufacture, formulation and clinical use*. 2015: Pharmaceutical press.
41. Chen, L.J., S.Y. Lin, and C.C. Huang, *Effect of hydrophobic chain length of surfactants on enthalpy− entropy compensation of micellization.* The Journal of Physical Chemistry B, 1998. **102**(22): p. 4350-4356.
42. Stigter, D., *Micelle formation by ionic surfactants. II. Specificity of head groups, micelle structure*. The Journal of Physical Chemistry, 1974. **78**(24): p. 2480-2485.
43. Klevens, H.B., *Structure and aggregation in dilate solution of surface active agents.* Journal of the American Oil Chemists' Society, 1953. **30**(2): p. 74-80.
44. Anacker, E.W., R.D. Geer, and E.H. Eylar, *Dependence of micelle aggregation number on polar head structure. I. Light scattering by aqueous solutions of decylammonium salts and related surfactants.* The Journal of Physical Chemistry, 1971. **75**(3): p. 369-374.
45. Rosen, M.J. and J.T. Kunjappu, *Surfactants and interfacial phenomena*. 2012: John Wiley & Sons.
46. Mohajeri, E. and G.D. Noudeh, *Effect of temperature on the critical micelle concentration and micellization thermodynamic of nonionic surfactants: polyoxyethylene sorbitan fatty acid esters.* Journal of Chemistry, 2012. **9**(4): p. 2268-2274.
47. Tori, K. and T. Nakagawa, *Colloid chemical properties of ampholytic surfactants.* Kolloid-Zeitschrift und Zeitschrift für Polymere, 1963. **187**(1): p. 44-51.
48. Stearns, R.S., et al., *Solubilization by Solutions of Long‐Chain Colloidal Electrolytes.* The Journal of Chemical Physics, 1947. **15**(7): p. 496-507.
49. Hsieh, C.M., *Investigations of Pharmaceutical Oil-in-water (o/w) Microemulsions as Drug Delivery Systems*. 2010, University of London.
50. Vinarov, Z., P. Dobreva, and S. Tcholakova, *Effect of surfactant molecular structure on Progesterone solubilization.* Journal of Drug Delivery Science and Technology, 2018. **43**: p. 44-49.
51. Arnason, T. and P. Elworthy, *Effects of structural variations of non‐ionic surfactants on micellar properties and solubilization: surfactants based on erucyl and behenyl (C22) alcohols.* Journal of Pharmacy and Pharmacology, 1980. **32**(1): p. 381-385.

52. Kolthoff, I.M. and W. Stricks, *Solubilization of dimethiylaminoazobenzene in solutions of detergents. I. The effect of temperature on the solubilization and upon the critical concentration.* The Journal of Physical Chemistry, 1948. **52**(6): p. 915-941.

53. Vinarov, Z., et al., *Micellar solubilization of poorly water-soluble drugs: effect of surfactant and solubilizate molecular structure.* Drug Development and Industrial Pharmacy, 2018. **44**(4): p. 677-686.

54. Alkhamis, K.A., H. Allaboun, and W.a.Y. Al‐Momani, *Study of the solubilization of gliclazide by aqueous micellar solutions.* Journal of Pharmaceutical Sciences, 2003. **92**(4): p. 839-846.

55. Jacobs, P.T. and E.W. Anacker, *The role of polar head structure in dye solubilization by cationic surfactants.* Journal of Colloid and Interface Science, 1973. **43**(1): p. 105-112.

56. Jacobs, P.T. and E.W. Anacker, *The effect of hydroxyl functionality in the polar head on surfactant aggregation number and dye solubilization efficiency.* Journal of Colloid and Interface Science, 1976. **56**(2): p. 255-261.

57. Kim, J.-H., M.M. Domach, and R.D. Tilton, *Effect of electrolytes on the pyrene solubilization capacity of dodecyl sulfate micelles.* Langmuir, 2000. **16**(26): p. 10037-10043.

58. Saito, S., *Solubilization properties of polymer-surfactant complexes.* Journal of Colloid and Interface Science, 1967. **24**(2): p. 227-234.

59. Jones, F., *The Solubility and Solubilisation of Disperse Dyes.* Journal of the Society of Dyers and Colourists, 1984. **100**(2): p. 66-72.

60. McBain, J.W. and P.H. Richards, *Solubilization of Insoluble Organic Liquids by Detergents.* Industrial & Engineering Chemistry, 1946. **38**(6): p. 642-646.

61. Harkins, W.D., *A cylindrical model for the small soap micelle.* The Journal of Chemical Physics, 1948. **16**(2): p. 156-157.

62. Nakagawa, T. and K. Tori, *Solubilization of long chain alkyl compounds by a non-ionic surfactant, and clouding formation observed in such systems.* Kolloid-Zeitschrift, 1960. **168**(2): p. 132-139.

63. Gale, M.M. and L. Saunders, *The solubilisation of steroids by lysophosphatidylcholine. Testosterone, estradiol and their 17α-ethinyl derivations.* Biochimica et Biophysica Acta (BBA)-Lipids and Lipid Metabolism, 1971. **248**(3): p. 466-470.

64. Bates, T.R., M. Gibaldi, and J.L. Kanig, *Solubilizing properties of bile salt solutions II. Effect of inorganic electrolyte, lipids, and a mixed bile salt system on solubilization of glutethimide, griseofulvin, and hexestrol.* Journal of Pharmaceutical Sciences, 1966. **55**(9): p. 901-906.

65. Barry, B.W. and D.E. Eini, *Solubilization of hydrocortisone, dexamethasone, testosterone and progesterone by long‐chain polyoxyethylene surfactants.* Journal of Pharmacy and Pharmacology, 1976. **28**(3): p. 210-218.

66. Savjani, K.T., A.K. Gajjar, and J.K. Savjani, *Drug solubility: importance and enhancement techniques.* International Scholarly Research Notices: Pharmaceutics, 2012. **2012**.

67. Allen, C., D. Maysinger, and A. Eisenberg, *Nano-engineering block copolymer aggregates for drug delivery.* Colloids and Surfaces B: Biointerfaces, 1999. **16**(1-4): p. 3-27.

68. Torchilin, V.P., *Structure and design of polymeric surfactant-based drug delivery systems.* Journal of Controlled Release, 2001. **73**(2-3): p. 137-172.

69. Vimalson, D.C., *Techniques to enhance solubility of hydrophobic drugs: an overview.* Asian Journal of Pharmaceutics, 2016. **10**(2).

70. Feng, S.X., *Studies on drug solubilization mechanism in simple micelle systems*. 2009, University of Kentucky.

71. Ekwall, P. and L. Sjöblom, *Solubilisation of steroid hormones by association colloids.* Acta Chemica Scandinavica, 1949. **3**: p. 1179-0080.

72. Guttman, D.E., et al., *Solubilization of anti‐inflammatory steroids by aqueous solutions of Triton WR‐1339.* Journal of Pharmaceutical Sciences, 1961. **50**(4): p. 305-307.

73. Thakkar, A.L. and P.B. Kuehn, *Solubilization of some steroids in aqueous solutions of a steroidal nonionic surfactant.* Journal of Pharmaceutical Sciences, 1969. **58**(7): p. 850-852.

74. Thakkar, A.L. and N.A. Hall, *Micellar solubilization of testosterone I. In aqueous solutions of polysorbates.* Journal of Pharmaceutical Sciences, 1967. **56**(9): p. 1121-1125.

75. Thakkar, A.L. and N.A. Hall, *Micellar solubilization of testosterone II. In Aqueous Solutions of Some Ionic Surfactants.* Journal of Pharmaceutical Sciences, 1968. **57**(8): p. 1394-1398.

76. Ong, J.T. and E. Manoukian, *Micellar solubilization of timobesone acetate in aqueous and aqueous propylene glycol solutions of nonionic surfactants.* Pharmaceutical Research, 1988. **5**(11): p. 704-708.

77. Guo, Y.P. and Y.Y. Hu, *Solubilization of moderately hydrophobic 17α-ethinylestradiol by mono- and di-rhamnolipid solutions.* Colloids and Surfaces A: Physicochemical and Engineering Aspects, 2014. **445**: p. 12-20.

78. Vinarov, Z., et al., *Micellar solubilization of poorly water-soluble drugs: effect of surfactant and solubilizate molecular structure.* Drug Development and Industrial Pharmacy, 2018. **44**(4): p. 677-686.

79. Alvarez-Núñez, F.A. and S.H. Yalkowsky, *Relationship between Polysorbate 80 solubilization descriptors and octanol–water partition coefficients of drugs.* International Journal of Pharmaceutics, 2000. **200**(2): p. 217-222.

80. Ismail, A.A., M.W. Gouda, and M.M. Motawi, *Micellar solubilization of barbiturates I: Solubilities of certain barbiturates in polysorbates of varying hydrophobic chain length.* Journal of Pharmaceutical Sciences, 1970. **59**(2): p. 220-224.

81. Rangel-Yagui, C.O., A. Pessoa Jr, and L.C. Tavares, *Micellar solubilization of drugs.* Journal of Pharmacy and Pharmaceutical Sciences, 2005. **8**(2): p. 147-163.

82. Duangjit, S., et al., *Role of the charge, carbon chain length, and content of surfactant on the skin penetration of meloxicam-loaded liposomes.* International Journal of Nanomedicine, 2014. **9**: p. 2005.

83. *Virtual Computational Chemistry Laboratory (VCCLAB)*. Available from: http://www.vcclab.org/

84. Lawrence, M.J. and F. Devínsky, *The solubilising capacity of a series of non-aromatic amine oxide surfactants.* Journal of Pharmacy and Pharmacology, 1988. **40**: p. 124.

85. Satra, C., M. Thomas, and M.J. Lawrence, *The solubility of testosterone propionate in oil-in-water microemulsions.* Journal of Pharmacy and Pharmacology, 1995. **47**(12): p. 1126-1126.

86. Qu, G., et al., *Structural properties of N-dodecyl-N,N-dimethyl-3-ammonio-1-propane-sulfonate micelle in water by molecular dynamics simulation.* Journal of Dispersion Science and Technology, 2017. **38**(12): p. 1792-1797.

87. Saaka, Y., et al., *Effect of surfactant head group on drug solubilisation*. 2016, King's College London.

88. Ghosh, P., *Surface Tension.* NPTEL– Chemical Engineering – Interfacial Engineering, 2009: p. 1-24.

89. Somasundaran, P., *Encyclopedia of surface and colloid science*. Vol. 2. 2006: CRC press.

90. Drelich, J., C. Fang, and C. White, *Measurement of interfacial tension in fluid-fluid systems.* Encyclopedia of Surface and Colloid Science, 2002. **3**: p. 3158-3163.

91. Kalyanasundaram, K. and J.K. Thomas, *Environmental effects on vibronic band intensities in pyrene monomer fluorescence and their application in studies of micellar systems.* Journal of the American Chemical Society, 1977. **99**(7): p. 2039-2044.

92. Ruiz, C.C., *A photophysical study of the urea effect on micellar properties of sodium dodecylsulfate aqueous solutions.* Colloid and Polymer Science, 1995. **273**(11): p. 1033-1040.

93. McLachlan, A.A. and D.G. Marangoni, *Interactions between zwitterionic and conventional anionic and cationic surfactants.* Journal of Colloid and Interface Science, 2006. **295**(1): p. 243-248.

94. Mysels, K.J., *Surface tension of solutions of pure sodium dodecyl sulfate.* Langmuir, 1986. **2**(4): p. 423-428.

95. Lu, J.R., et al., *Adsorption of dodecyl sulfate surfactants with monovalent metal counterions at the air-water interface studied by neutron reflection and surface tension.* Journal of colloid and interface science, 1993. **158**(2): p. 303-316.

96. Gnezdilov, O.I., et al., *Self-Diffusion of Ionic Surfactants and Counterions in Premicellar and Micellar Solutions of Sodium, Lithium and Cesium Dodecyl Sulfates as Studied by NMR-Diffusometry.* Applied Magnetic Resonance, 2011. **40**(1): p. 91-103.

97. Kim, H.U. and K.H. Lim, *Sizes and structures of micelles of cationic octadecyl trimethyl ammonium chloride and anionic ammonium dodecyl sulfate surfactants in aqueous solutions.* Bulletin of the Korean Chemical Society, 2004. **25**(3): p. 382-388.

98. Kang, K.H., H.-U. Kim, and K.-H. Lim, *Effect of temperature on critical micelle concentration and thermodynamic potentials of micellization of anionic ammonium dodecyl sulfate and cationic octadecyl trimethyl ammonium chloride.* Colloids and Surfaces A: Physicochemical and Engineering Aspects, 2001. **189**(1-3): p. 113-121.

99. Kang, K.H., et al., *Mixed micellization of anionic ammonium dodecyl sulfate and cationic octadecyl trimethyl ammonium chloride.* Bulletin-Korean Chemical Society, 2001. **22**(9): p. 1009-1014.

100. Zieliński, R., et al., *Effect of temperature on micelle formation in aqueous solutions of alkyltrimethylammonium bromides.* Journal of Colloid and Interface Science, 1989. **129**(1): p. 175-184.

101. Suárez, M.J. and V. Mosquera, *Mixed micelles of n-alkyltrimethylammonium bromides: influence of alkyl chain length.* Physical Chemistry Chemical Physics, 1999. **1**(15): p. 3583-3587.

102. Amin-Alami, A., N. Kamenka, and S. Partyuka, *Interfacial properties of zwitterionic surfactants: N-dodecylbetaine.* Thermochimica Acta, 1987. **122**(1): p. 171-179.

103. Manzo, G., et al., *Characterization of sodium dodecylsulphate and dodecylphosphocholine mixed micelles through NMR and dynamic light scattering.* Magnetic Resonance in Chemistry, 2013. **51**(3): p. 176-183.

104. Sikorska, E., et al., *Thermodynamics, size, and dynamics of zwitterionic dodecylphosphocholine and anionic sodium dodecyl sulfate mixed micelles.* Journal of Thermal Analysis and Calorimetry, 2016. **123**(1): p. 511-523.

105. Varade, D., et al., *Micellar behavior of mixtures of sodium dodecyl sulfate and dodecyldimethylamine oxide in aqueous solutions.* Colloids and Surfaces A: Physicochemical and Engineering Aspects, 2005. **259**(1-3): p. 103-109.

106. Kakitani, M., T. Imae, and M. Furusaka, *Investigation of mixed micelles of dodecyldimethylamine oxide and sodium dodecyl sulfate by SANS: Shape, size, charge, and interaction.* The Journal of Physical Chemistry, 1995. **99**(43): p. 16018-16023.

107. Vargaftik, N., B. Volkov, and L. Voljak, *International tables of the surface tension of water.* Journal of Physical and Chemical Reference Data, 1983. **12**(3): p. 817-820.

108. Princen, H.M., *Capillary phenomena in assemblies of parallel cylinders: I. Capillary rise between two cylinders.* Journal of Colloid and Interface Science, 1969. **30**(1): p. 69-75.

109. Gibbs, J.W., *The scientific papers of J. Willard Gibbs*. Vol. 1. 1906: Longmans, Green and Company.

110. Miles, G.D. and L. Shedlovsky, *Minima in Surface Tension–Concentration Curves of Solutions of Sodium Alcohol Sulfates.* The journal of physical chemistry, 1944. **48**(1): p. 57-62.

111. *Anionic and non-ionic surface active agents – Determination of the critical micellization concentration – Method by measuring surface tension with a plate, stirrup or ring*. 1980: Geneva: International Organization for Standardization.

112. Volkov, A.G., S. Paula, and D. Deamer, *Two mechanisms of permeation of small neutral molecules and hydrated ions across phospholipid bilayers.* Bioelectrochemistry and Bioenergetics, 1997. **42**(2): p. 153-160.

113. Menger, F.M., L. Shi, and S.A.A. Rizvi, *Additional support for a revised Gibbs analysis.* Langmuir, 2009. **26**(3): p. 1588-1589.

114. Menger, F.M. and S.A.A. Rizvi, *Relationship between surface tension and surface coverage.* Langmuir, 2011. **27**(23): p. 13975-13977.

115. Xu, H., et al., *Limitations in the application of the Gibbs equation to anionic surfactants at the air/water surface: sodium dodecylsulfate and sodium dodecylmonooxyethylenesulfate above and below the CMC.* Langmuir, 2013. **29**(30): p. 9335-9351.

116. Li, P.X., et al., *Application of the Gibbs equation to the adsorption of nonionic surfactants and polymers at the air–water interface: comparison with surface excesses determined directly using neutron reflectivity.* Langmuir, 2013. **29**(30): p. 9324-9334.

117. Li, P.X., R.K. Thomas, and J. Penfold, *Limitations in the use of surface tension and the Gibbs equation to determine surface excesses of cationic surfactants.* Langmuir, 2014. **30**(23): p. 6739-6747.

118. Lyttle, D., et al., *Structure of a dodecyltrimethylammonium bromide layer at the air/water interface determined by neutron reflection: comparison of the monolayer structure of cationic surfactants with different chain lengths.* Langmuir, 1995. **11**(3): p. 1001-1008.

119. Huggins, M.L., *The viscosity of dilute solutions of long-chain molecules. IV. Dependence on concentration.* Journal of the American Chemical Society, 1942. **64**(11): p. 2716-2718.

120. Kraemer, E.O., *Molecular weights of celluloses and cellulose derivates.* Industrial & Engineering Chemistry, 1938. **30**(10): p. 1200-1203.

121. Amelia, R., J.C. Tomic, and W.F. Nirode, *The determination of the solubility parameter (δ) and the Mark-Houwink constants (K & α) of food grade Polyvinyl Acetate (PVAc).* Journal of Polymer and Biopolymer Physics Chemistry, 2014. **2**(4): p. 67-72.

122. Masuelli, M., *Hydrodynamic Parameters of Strelitzia Gum.* Colloids and Interfaces, 2018. **2**(4): p. 45.

123. Pamies, R., et al., *Determination of intrinsic viscosities of macromolecules and nanoparticles. Comparison of single-point and dilution procedures.* Colloid and Polymer Science, 2008. **286**(11): p. 1223-1231.

124. Charlier, Q., et al., *Solution viscosity–molar mass relationships for poly (butylene succinate) and discussion on molar mass analysis.* Express Polymer Letters, 2015. **9**(5).

125. Marani, D., J. Hjelm, and M. Wandel, *Use of intrinsic viscosity for evaluation of polymer-solvent affinity.* Annu Trans Nord Rheol Soc, 2013. **21**: p. 255-261.

126. Einstein, A., *Eine neue bestimmung der moleküldimensionen.* Annalen der Physik, 1906. **324**(2): p. 289-306.

127. Einstein, A., *Berichtigung zu meiner Arbeit:„Eine neue Bestimmung der Moleküldimensionen"* . Annalen der Physik, 1911. **339**(3): p. 591-592.

128. Oncley, J., *Evidence from physical chemistry regarding the size and shape of protein molecules from ultra-centrifugation, diffusion, viscosity, dielectric dispersion, and double refraction of flow.* Annals of the New York Academy of Sciences, 1941. **41**(2): p. 121-150.

129. Polson, A., *Determination of Particle Weight and Shape from Diffusion and Viscosity Data.* Nature, 1936. **137**(3470): p. 740.

130. Simha, R., *Effect of concentration on the viscosity of dilute solutions.* Transactions of the New York Academy of Sciences, 1949. **11**: p. 96.

131. Simha, R., *The influence of Brownian movement on the viscosity of solutions.* The Journal of Physical Chemistry, 1940. **44**(1): p. 25-34.

132. Tokiwa, F. and K. Ohki, *Micellar properties of a series of sodium dodecylpolyoxyethylene sulfates from hydrodynamics data.* The Journal of Physical Chemistry, 1967. **71**(5): p. 1343-1348.

133. Soni, S.S., et al., *Surface Activity, SANS, and Viscosity Studies in Aqueous Solutions of Oxyethylene and Oxybutylene Di- and Triblock Copolymers.* The Journal of Physical Chemistry B, 2002. **106**(50): p. 13069-13077.

134. Khan, A., et al., *Surface tension, density and viscosity studies on the associative behaviour of oxyethylene-oxybutylene diblock copolymers in water at different temperatures.* International Journal of Organic Chemistry, 2012. **2**(1): p. 82-92.

135. Durchschlag, H. and P. Zipper, *Calculation of the partial volume of organic compounds and polymers*, in *Progress in Colloid and Polymer Science*. 1994, Springer. p. 20-39.

136. Parker, R.A. and S.P. Wasik, *On the Electroviscous Effect in Dilute Aqueous Solutions of Ionic Detergents.* The Journal of Physical Chemistry, 1958. **62**(8): p. 967-969.

137. Ogino, K. and M. Abe, *Mixed surfactant systems*. 1992: CRC Press.

138. Weast, R.C., M.J. Astle, and W.H. Beyer, *CRC handbook of chemistry and physics*. Vol. 69. 1988: CRC press Boca Raton, FL.

139. Elworthy, P., *The increasingly clever micelle.* Journal of Pharmacy and Pharmacology, 1997. **49**(6): p. xi-xxiii.

140. Courchene, W., *Micellar properties from hydrodynamic data.* The Journal of Physical Chemistry, 1964. **68**(7): p. 1870-1874.

141. Barlow, D.J., et al., *Small-angle neutron-scattering studies on the nature of the incorporation of polar oils into aggregates of N, N-dimethyldodecylamine-N-oxide.* Langmuir, 2000. **16**(26): p. 10398-10403.

142. McBain, J.W., Y. Kawakami, and H. Lucas, *The ultrafiltration of soap solutions.* Journal of the American Chemical Society, 1933. **55**(7): p. 2762-2769.

143. Long, J.A., B.M. Rankin, and D. Ben-Amotz, *Micelle structure and hydrophobic hydration.* Journal of the American Chemical Society, 2015. **137**(33): p. 10809-10815.

144. Svens, B. and B. Rosenholm, *An investigation of the size and structure of the micelles in sodium octanoate solutions by small-angle X-ray scattering.* Journal of Colloid and Interface Science, 1973. **44**(3): p. 495-504.

145. Lindman, B., et al., *Some aspects on the hydration of surfactant micelles.* Pure and Applied Chemistry, 1980. **52**(5): p. 1307-1315.

146. Griffiths, P.C., et al., *A small-angle neutron scattering study of biologically relevant mixed surfactant micelles comprising 1, 2-diheptanoyl-sn-phosphatidylcholine and sodium dodecyl sulfate or dodecyltrimethylammonium bromide.* Soft Matter, 2005. **1**(2): p. 152-159.

147. Lorenz, C.D., et al., *Molecular dynamics simulations of the interfacial and structural properties of dimethyldodecylamine-N-oxide micelles.* Langmuir, 2010. **27**(2): p. 546-553.

148. La Mesa, C., et al., *Phase diagram of the binary system water-(dodecyldimethylammonio) propanesulfonate.* Langmuir, 1990. **6**(4): p. 728-731.

149. Tanford, C., Y. Nozaki, and M.F. Rohde, *Size and shape of globular micelles formed in aqueous solution by n-alkyl polyoxyethylene ethers.* The Journal of Physical Chemistry, 1977. **81**(16): p. 1555-1560.

150. Shikata, T., M. Okuzono, and N. Sugimoto, *Temperature-dependent hydration/dehydration behavior of poly (ethylene oxide) s in aqueous solution.* Macromolecules, 2013. **46**(5): p. 1956-1961.

151. Allen, D.T., et al., *Specific effects of monovalent counterions on the structural and interfacial properties of dodecyl sulfate monolayers.* Physical Chemistry Chemical Physics, 2016. **18**(44): p. 30394-30406.

152. Scheraga, H.A. and L. Mandelkern, *Consideration of the hydrodynamic properties of proteins1, 2.* Journal of the American Chemical Society, 1953. **75**(1): p. 179-184.

153. Harding, S.E., *The intrinsic viscosity of biological macromolecules. Progress in measurement, interpretation and application to structure in dilute solution.* Progress in Biophysics and Molecular Biology, 1997. **68**(2): p. 207-262.

154. Lu, J.R., R.K. Thomas, and J. Penfold, *Surfactant layers at the air/water interface: structure and composition.* Advances in Colloid and Interface Science, 2000. **84**(1-3): p. 143-304.

155. Penfold, J., et al., *Adsorption of mixed cationic and nonionic surfactants at the hydrophilic silicon surface from aqueous solution: The effect of solution composition and concentration.* Langmuir, 2000. **16**(23): p. 8879-8883.

156. Domínguez, H., *Self-aggregation of the SDS surfactant at a solid− liquid interface.* The Journal of Physical Chemistry B, 2007. **111**(16): p. 4054-4059.

157. Staples, E., J. Penfold, and I. Tucker, *Adsorption of Mixed Surfactants at the Oil− Water Interface.* The Journal of Physical Chemistry B, 2000. **104**(3): p. 606-614.

158. Penfold, J., et al., *Adsorption of mixed anionic and nonionic surfactants at the hydrophilic silicon surface.* Langmuir, 2002. **18**(15): p. 5755-5760.

159. Thomas, R.K. and J. Penfold, *Neutron and X-ray reflectometry of interfacial systems in colloid and polymer chemistry.* Current Opinion in Colloid and Interface Science, 1996. **1**(1): p. 23-33.

160. Lu, J., et al., *Direct determination by neutron reflection of the penetration of water into surfactant layers at the air/water interface.* Langmuir, 1992. **8**(7): p. 1837-1844.

161. Born, M. and E. Wolf, *Principles of Optics, 334*. 1970: Pergamon Press, Oxford.

162. Nelson, A., *Co-refinement of multiple-contrast neutron/X-ray reflectivity data using MOTOFIT.* Journal of applied crystallography, 2006. **39**(2): p. 273-276.

163. Campbell, R.A., et al., *Structure of surfactant and phospholipid monolayers at the air/water interface modeled from neutron reflectivity data.* Journal of Colloid and Interface Science, 2018. **531**: p. 98-108.

164. Fullagar, W.K., S.A. Holt, and I.R. Gentle, *Structure of SP-B/DPPC mixed films studied by neutron reflectometry.* Biophysical Journal, 2008. **95**(10): p. 4829-36.

165. Yanez Arteta, M., R.A. Campbell, and T. Nylander, *Adsorption of Mixtures of Poly (amidoamine) Dendrimers and Sodium Dodecyl Sulfate at the Air–Water Interface.* Langmuir, 2014. **30**(20): p. 5817-5828.

166. Lu, J., X. Zhao, and M. Yaseen, *Biomimetic amphiphiles: Biosurfactants.* Current Opinion in Colloid & Interface Science, 2007. **12**(2): p. 60-67.

167. Qu, G., et al., *Molecular Dynamics Study ofN-Dodecyl-N,N-Dimethyl-3-Ammonio-1-Propanesulfonate Mono-Layer Adsorbed at the Air/Water Interface.* Journal of Dispersion Science and Technology, 2015. **37**(8): p. 1067-1075.

168. Eastoe, J. and J.S. Dalton, *Dynamic surface tension and adsorption mechanisms of surfactants at the air–water interface.* Advances in Colloid and Interface Science, 2000. **85**(2-3): p. 103-144.

169. Saaka, Y., et al., *Towards optimised drug delivery: structure and composition of testosterone enanthate in sodium dodecyl sulfate monolayers.* Soft Matter, 2018. **14**(16): p. 3135-3150.

170. Pecora, R., *Dynamic light scattering: applications of photon correlation spectroscopy*. 2013: Springer Science & Business Media.

171. Langenbucher, G., *Small-Angle X-ray Scattering for Pharmaceutical Applications.* Pharmaceutical Technology, 2010. **34**: p. s32-s37.

172. Di Cola, E., I. Grillo, and S. Ristori, *Small angle X-ray and neutron scattering: powerful tools for studying the structure of drug-loaded liposomes.* Pharmaceutics, 2016. **8**(2): p. 10.

173. Chen, S.-H., *Small angle neutron scattering studies of the structure and interaction in micellar and microemulsion systems.* Annual Review of Physical Chemistry, 1986. **37**(1): p. 351-399.

174. Mehan, S., et al., *Small-angle neutron scattering study of structure and interaction of nanoparticle, protein, and surfactant complexes.* Langmuir, 2013. **29**(36): p. 11290-11299.

175. Ashkar, R., et al., *Neutron scattering in the biological sciences: progress and prospects.* Acta Crystallographica Section D: Structural Biology, 2018. **74**(12): p. 1129-1168.

176. Bahadur, J., et al., *Small-angle and ultrasmall-angle neutron scattering (SANS/USANS) study of New Albany Shale: a treatise on microporosity.* Energy & Fuels, 2015. **29**(2): p. 567-576.

177. Putra, E.G.R. and A. Patriati. *Structural and phase transition changes of sodium dodecyl sulfate micellar solution in alcohols probed by small-angle neutron scattering (SANS).* in *AIP Conference Proceedings*. 2015. AIP Publishing.

178. Pethrick, R.A. and J. Dawkins, *Modern techniques for polymer characterisation*. 1999: J. Wiley.

179. Heenan, R., et al., *COLETTE users' guide*. 1989, Rutherford Appleton Laboratory.

180. King, S.M. and R.K. Heenan, *Using COLETTE*. 1995, Rutherford Appleton Laboratory.

181. Hayter, J. and J. Penfold, *Determination of micelle structure and charge by neutron small-angle scattering.* Colloid and Polymer Science, 1983. **261**(12): p. 1022-1030.

182. Rodenas, E., et al., *Physical properties of dodecyltrimethylammonium bromide (DTAB) micelles in aqueous solution and their behavior as the reaction medium.* Langmuir, 1994. **10**(7): p. 2088-2094.

183. Aswal, V. and P. Goyal, *Mixed micelles of alkyltrimethylammonium halides a small-angle neutron-scattering study.* Physica B: Condensed Matter, 1998. **245**(1): p. 73-80.

184. Caponetti, E., D. Chillura-Martino, and L. Pedone, *Partitioning of macrocyclic compounds in a cationic and an anionic micellar solution: A small-angle neutron scattering study*. Langmuir, 2004. **20**(10): p. 3854-3862.

185. Hassan, P., G. Fritz, and E.W. Kaler, *Small angle neutron scattering study of sodium dodecyl sulfate micellar growth driven by addition of a hydrotropic salt.* Journal of Colloid and Interface Science, 2003. **257**(1): p. 154-162.

186. Bergström, L.M. and V.M. Garamus, *Geometrical shape of micelles formed by cationic dimeric surfactants determined with small-angle neutron scattering.* Langmuir, 2012. **28**(25): p. 9311-9321.

187. Liu, Y., et al., *Structure and Interaction of lithium dodecyl sulfate micelles in the presence of Li-specific macrocyclic cage: a study by SANS.* The Journal of Physical Chemistry, 1994. **98**(40): p. 10208-10215.

188. Bendedouch, D., S.H. Chen, and W. Koehler, *Structure of ionic micelles from small angle neutron scattering*. The Journal of Physical Chemistry, 1983. **87**(1): p. 153-159.

189. Li, N., R.K. Thomas, and A.R. Rennie, *Effect of pH, surface charge and counter-ions on the adsorption of sodium dodecyl sulfate to the sapphire/solution interface*. Journal of Colloid and Interface Science, 2012. **378**(1): p. 152-158.

190. Kang, K.-H. and K.-H. Lim, *A SANS study for structural transition of micelles of cationic octadecyl trimethyl ammonium chloride and anionic ammonium dodecyl sulfate surfactants in aqueous solutions.* Colloids and Surfaces A: Physicochemical and Engineering Aspects, 2011. **391**(1-3): p. 69-79.

191. Vass, S., et al., *Ambiguity in determining the shape of alkali alkyl sulfate micelles from small-angle scattering data.* Langmuir, 2008. **24**(2): p. 408-417.

192. Tcacenco, C.M., R. Zana, and B.L. Bales, *Effect of the nature of the counterion on the properties of anionic surfactants. 5. Self-association behavior and micellar properties of ammonium dodecyl sulfate.* The Journal of Physical Chemistry B, 2005. **109**(33): p. 15997-16004.

193. Ullah, I., M.K. Baloch, and I. Ullah, *Apparent solubility of ibuprofen in dimethyl dodecyl ammonium-propane sulfonate, DDAPS, micelles, DDAPS/butanol mixtures and in oil-in-water microemulsions stabilized by DDAPS.* Journal of Solution Chemistry, 2013. **42**(3): p. 657-665.

194. Masudo, T. and T. Okada, *Potentiometric and chromatographic evaluation of ion uptake by zwitterionic micelles.* Physical Chemistry Chemical Physics, 1999. **1**(15): p. 3577-3582.

195. Pambou, E., et al., *Structural features of micelles of zwitterionic dodecyl-phosphocholine (C12PC) surfactants studied by small-angle neutron scattering.* Langmuir, 2015. **31**(36): p. 9781-9789.

196. Wymore, T., X. Gao, and T. Wong, *Molecular dynamics simulation of the structure and dynamics of a dodecylphosphocholine micelle in aqueous solution.* Journal of Molecular Structure, 1999. **485**: p. 195-210.

197. Tieleman, D., D. Van der Spoel, and H. Berendsen, *Molecular dynamics simulations of dodecylphosphocholine micelles at three different aggregate sizes: micellar structure and chain relaxation.* The Journal of Physical Chemistry B, 2000. **104**(27): p. 6380-6388.

198. Ullah, I., M.K. Baloch, and G.F. Durrani, *Solubility of nonsteroidal anti-inflammatory drugs (NSAIDs) in aqueous solutions of non-ionic surfactants.* Journal of Solution Chemistry, 2011. **40**(7): p. 1341.

199. Penfold, J., et al., *Adsorption at air–water and oil–water interfaces and self-assembly in aqueous solution of ethoxylated polysorbate nonionic surfactants.* Langmuir, 2015. **31**(10): p. 3003-3011.

200. Tummino, P.J. and A. Gafni, *Determination of the aggregation number of detergent micelles using steady-state fluorescence quenching.* Biophysical Journal, 1993. **64**(5): p. 1580-1587.

201. Borbély, S., *Aggregate structure in aqueous solutions of Brij-35 nonionic surfactant studied by small-angle neutron scattering.* Langmuir, 2000. **16**(13): p. 5540-5545.

202. Preu, H., et al., *Small angle neutron scattering of D_2O–Brij 35 and D_2O–alcohol–Brij 35 solutions and their modelling using the Percus–Yevick integral equation.* Physical Chemistry Chemical Physics, 1999. **1**(14): p. 3321-3329.

203. Turco Liveri, Maria Liria, et al. *Peculiar mechanism of solubilization of a sparingly water soluble drug into polymeric micelles. Kinetic and equilibrium studies.* The Journal of Physical Chemistry *B* 116.16 (2012): 5037-5046.

204. Xiarchos, Ioannis, and Danae Doulia. "*Effect of nonionic surfactants on the solubilization of alachlor*." Journal of hazardous materials 136.3 (2006): 882-888.

205. Mall, S., G. Buckton, and D. A. Rawlins. "*Slower dissolution rates of sulphamerazine in aqueous sodium dodecyl sulphate solutions than in water*." International journal of pharmaceutics131.1 (1996): 41-46.